

Identification of the Molecular
Mechanisms underlying the
Gastrointestinal Toxicity of the
Immunosuppressants Mycophenolate
Mofetil and Enteric-coated
Mycophenolate Sodium using a
Proteo-Metabolomic Approach

Dissertation
zur Erlangung des Grades eines
Doktors der Naturwissenschaften
- Dr. rer. nat. -

vorgelegt im Fachbereich Biologie/Chemie
der Universität Bremen von

Svenja Heischmann

Bremen
Mai 2013

Universität Bremen
University of Colorado

Tag des Promotionskolloquiums: 11. Juni 2013

1. Gutachter: Prof. Dr. Dieter Leibfritz
2. Gutachter: Prof. Dr. Uwe Christians

a

Für meine Eltern

Danksagung/Acknowledgements

Mein besonderer Dank gilt Herrn Prof. Dr. Dieter Leibfritz und Herrn Prof. Dr. Uwe Christians für die Ermöglichung dieser Arbeit, die interessante Themenstellung, ihre Ratschläge und Unterstützung.

Den Mitarbeitern der Arbeitsgruppe Leibfritz danke ich, wie schon in Zeiten meiner Diplomarbeit, für ihre Hilfe und Freundschaft. Insbesondere danke ich Herrn Johannes Stelten für seine Hilfe bei den NMR-Experimenten und Erklärungen, die sehr zu einem besseren Verständnis der Methode beitrugen. Bei Herrn Dr. Wieland Willker möchte ich mich für die Hilfe bei den 2D-NMR-Messungen bedanken.

Ich möchte mich bei meinen Eltern und meiner Schwester für ihre Unterstützung während meines gesamten Studiums und der Dissertation bedanken. Ebenfalls danke ich meinen Freunden, insbesondere Herrn Dr. Daniel Krause und Frau Rabea Riedel, für ihre Unterstützung.

Thanks to all my colleagues from the workgroup Christians for their help and advice. I especially thank Björn Schniedewind for his help with the MS-based studies, his time, and patience.

I especially would like to thank Dr. Chris Rivard for his continuous assistance, time, and excellent advice, which helped me a lot in terms of western blot analysis, other molecular biology methods, and to become a better scientist.

I also thank Dr. Monika Dzieciatkowska and Dr. Kirk Hansen from the proteomics core for their guidance and help with the proteomics experiments, without which a big part of this thesis would not have been possible.

Contents

Danksagung/Acknowledgements	i
Abbreviations	vii
Zusammenfassung	1
Summary	7
1 Introduction	13
1.1 Immunosuppression and mycophenolic acid	13
1.1.1 History and success of MPA	13
1.1.2 The two formulations of MPA	14
1.1.3 Benefits and adverse effects of MPA and their consequences .	14
1.1.4 Pharmacodynamic properties: Mechanism of immunosuppression	16
1.1.5 Pharmacokinetic properties	20
1.2 The GI tract and GI toxicity of MPA	24
1.2.1 Impact of MPA GI side effects	24
1.2.2 Parts, functions, and features of the GI tract	25
1.2.3 Mechanisms and modulation of intestinal inflammation and repair	28
1.3 Hypothesis, aims of the study, and research strategies	31
1.3.1 LS180 cell culture model and its qualification	31
1.3.2 Biomarkers, proteomics, and metabolomics	32
2 Results and Discussion	35
2.1 Determination of cell culture treatment conditions	35
2.1.1 Drug treatment	35
2.1.2 Guanosine treatment	36

Contents

2.2	Validation of the LS180 cell culture model	36
2.2.1	Dependency of protein expression on passage number of LS180 cells	38
2.2.2	Influence of MPA treatment on expression levels of enzymes involved in MPA metabolism in LS180 cells	39
2.3	Cytotoxicity of MPA	47
2.3.1	Necrotic potential of MPA	47
2.3.2	Apoptotic potential of MPA	49
2.4	Antiproliferative properties	53
2.4.1	Influence of exogenous guanosine on proliferation of different cell types during MPA treatment	56
2.5	Effects on nucleotide levels and energy charge	66
2.5.1	Nucleotide levels and energy charge after single doses of drugs without exogenous guanosine	67
2.5.2	Influence of exogenous guanosine on nucleotide levels and energy charge	70
2.5.3	Influence of MPA treatment on Na ⁺ -K ⁺ -ATPase expression levels	72
2.5.4	Influence of MPA treatment on cAMP and cGMP levels	80
2.6	HPLC-MS method development and preliminary studies for method validation	85
2.6.1	HPLC-MS method development	85
2.6.2	Preliminary studies prior to HPLC-MS method validation	88
2.7	Investigation of proteome alterations in LS180 cells after MPA treatment	91
2.7.1	SILAC	91
2.7.2	Identification of protein targets using an anti-MPA/AcMPAG antibody	128
2.8	Metabolome analysis in LS180 cells after MPA treatment	137
2.8.1	Quantitative ¹ H NMR spectroscopy of hydrophilic cell extracts	138
2.8.2	Quantitative ¹³ C NMR spectroscopy of cell extracts	143
2.8.3	Quantitative ¹ H NMR spectroscopy of lipid extracts	150
2.8.4	¹ H- ¹³ C HSQC NMR spectroscopy of hydrophilic and lipophilic cell extracts	155
2.9	<i>In vitro</i> gut inflammation model	157
2.9.1	Evaluation of cell monolayer integration	160
2.9.2	Cytokine release from RAW 264.7 cells	160

2.9.3	mRNA levels of IL-8 and SERT in LS180 cells	164
2.9.4	Evaluation of the LS180-RAW 264.7 coculture model	164
2.10	Summary discussion, conclusions, and perspectives	165
3	Materials and Methods	169
3.1	Cell cultures and incubation conditions	169
3.1.1	Experimental conditions and drug treatment	170
3.2	Cell proliferation, cell viability, and other assays	170
3.2.1	Doubling time	170
3.2.2	CyQUANT NF Cell Proliferation Assays	170
3.2.3	LDH assays	171
3.2.4	Caspase-3 western blots	171
3.2.5	cAMP/cGMP assays	171
3.3	Protein determination	172
3.4	Extraction methods	172
3.5	Molecular biology methods	174
3.5.1	Western blot analysis	174
3.5.2	QPCR	176
3.6	NMR analysis	177
3.6.1	Processing of cell extracts, media, and pellets	177
3.6.2	Acquisition and processing parameters of NMR spectra	177
3.6.3	Quantitative analysis of NMR spectra	179
3.7	Measurement of high-energy phosphate levels	182
3.8	HPLC-MS assay development	183
3.8.1	HPLC-MS conditions	183
3.8.2	Stability experiments	184
3.9	Proteomics	184
3.9.1	Labeling of LS180 cells for SILAC experiments	184
3.9.2	IP using an anti-MPA/AcMPAG antibody	184
3.10	<i>In vitro</i> gut inflammation model	190
3.10.1	Cultivation of LS180 cells on cell culture inserts and TEER measurements	190
3.10.2	Treatment of RAW 264.7 cells	190
3.10.3	Preparation of cell culture media for western blot analysis	191
3.11	Statistics	191
	List of Figures	193

Contents

List of Tables	201
Bibliography	203
4 Appendix	243

Abbreviations

Gene symbols and abbreviations of proteins as used in tables are not listed, unless they are used in the text.

Amino acid abbreviations are based on International Union of Pure and Applied Chemistry (IUPAC) nomenclature.

aa	amino acid (used only in terms of protein sequences)
ACAA2	acetyl-CoA acyltransferase
ACAT2	acetyl-CoA acetyltransferase
Acetyl (Protein N-term)	N- α -acetylation
AcMPAG	mycophenolic acid acyl glucuronide
AcMPA-GS	mycophenolic acid acyl glucoside
ACN	acetonitrile
ACSL5	long-chain acyl-CoA synthetase 5
ACTB	actin, cytoplasmic 1
ADP	adenosine diphosphate
AEBSF	4-(2-aminoethyl) benzenesulfonyl fluoride hydrochloride
AEC	adenylate energy charge
AK3	GTP:AMP phosphotransferase, mitochondrial (adenylate kinase 3)
AMP	adenosine monophosphate
ANOVA	one-way analysis of variance
ANXA1	annexin A1
AOX	peroxisomal acyl-CoA oxidase 1
Asn	asparagine
ATCC	American Type Culture Collection
ATP	adenosine triphosphate
AUC	area under the curve/integral of the concentration-time curve
AZA	azathioprine
α -ETF	electron-transfer-flavoprotein
BCRP	breast cancer resistance protein
BSA	bovine serum albumin
CAD	collisionally activated dissociation
cAMP	cyclic adenosine monophosphate
cDNA	complementary deoxyribonucleic acid
CDP	cytidine diphosphate
CE	collision energy
CEG	cytidylate energy charge
cGMP	cyclic guanosine monophosphate
C_{max}	maximum concentration a drug reaches after administration prior to administration of a second dose
CMP	cytidine monophosphate
CoA	coenzyme A
CTP	cytidine triphosphate
CXP	collision cell exit potential

Abbreviations

CYP	cytochrome P450 oxidase
dATP	deoxyadenosine triphosphate
DAVID	database for annotation, visualization, and integrated discovery
DBAF	dibutylammonium formate
dGTP	deoxyguanosine triphosphate
DLD	dihydrolipoamide dehydrogenase
DMSO	dimethyl sulfoxide
DNA	deoxyribonucleic acid
DM-MPA	6-O-desmethyl mycophenolic acid
DM-MPA-4G	desmethyl mycophenolic acid-4-O-phenyl glucuronide
DM-MPA-6G	desmethyl mycophenolic acid-6-O-phenyl glucuronide
DP	declustering potential
DTT	dithiothreitol
EASE	expression analysis systematic explorer
EC-MPS	enteric-coated mycophenolate sodium
EDTA	ethylenediaminetetraacetic acid
EF-Tu	elongation factor Tu/P43
E_{Lac}	^{13}C enrichments in C3 of lactate
ELISA	enzyme-linked immunosorbent assay
ER	endoplasmatic reticulum
ESI	electrospray ionization
FA	formic acid
FABP1	fatty acid-binding protein 1
FAD	flavin adenine dinucleotide
FBS	fetal bovine serum
FDR	false discovery rate
GDP	guanosine diphosphate
GEC	guanylate energy charge
GeLC	gel-based liquid chromatography
GI	gastrointestinal
Gln \rightarrow pyro-Glu	cyclization of N-terminal glutamine residues to pyro-glutamic acid
Glx	glutamine and glutamate
GMP	guanosine monophosphate
GO	gene ontology
GTP	guanosine triphosphate
HGPRT	hypoxanthine-guanine phosphoribosyltransferase
HPLC	high performance liquid chromatography
HPRD	Human Protein Reference Database
HRP	horseradish peroxidase
HSA	human serum albumin
HSQC	heteronuclear single quantum coherence
I	peak area (intensity, e.g. $I(^{13}\text{C-Lac})$): peak area of the [$3-^{13}\text{C}$]lactate signal from ^{13}C spectra)
IAA	iodoacetamide
IBD	inflammatory bowel disorder
IL	interleukin
IC_{50}	half maximal inhibitory concentration
IMP	inosine monophosphate
IMPDH	inosine monophosphate dehydrogenase
INF- γ	interferon- γ
IP	immunoprecipitation
IUPAC	International Union of Pure and Applied Chemistry
KEGG	Kyoto Encyclopedia of Genes and Genomes
LDH	lactate dehydrogenase
MDR1	multidrug resistance protein 1
MMF	mycophenolate mofetil
MPA	mycophenolic acid

MPAG	phenolic mycophenolic acid glucuronide
MRM	multiple reaction monitoring
mRNA	messenger ribonucleic acid
MRP	multidrug resistance-associated protein
MS	mass spectrometry
MTT	3-(4,5-dimethylthiazol-2-yl)-2,5-diphenyltetrazolium bromide
MUFA	monounsaturated fatty acids
n.a.	natural abundance
NAD ⁺	nicotinamide adenine dinucleotide, oxidized
NADH	nicotinamide adenine dinucleotide, reduced
NADP ⁺	nicotinamide adenine dinucleotide phosphate, oxidized
NADPH	nicotinamide adenine dinucleotide phosphate, reduced
NEC	nucleotide energy charge
NMR	nuclear magnetic resonance
NTP	nucleotide triphosphate
NOE	Nuclear Overhauser Enhancement
OATP	organic anion-transportin peptide
Oxidation (M)	methionine oxidation
PANTHER	protein analysis through evolutionary relationships
PCA	perchloric acid
PIgR	polymeric immunoglobulin receptor
PK	pharmacokinetic
PPAR	peroxisome proliferator-activated receptor
PRPP	5-phosphoribosyl-1-pyrophosphate
PtdCho	phosphatidylcholine
PUFA	polyunsaturated fatty acids
PXR	pregnane X receptor
QPCR	quantitative polymerase chain reaction
REG-4	regenerating islet-derived protein 4
Ribose 5P	ribose 5-phosphate
RNA	ribonucleic acid
SCS- α	succinyl-CoA ligase [ADP/GDP-forming] subunit α
SILAC	stable isotopic labeling by amino acids in cell culture
SLC12A2	solute carrier family 12 member 2
S/N	signal/noise
TCA	tricarboxylic acid
TFP	trifunctional enzyme subunit α
TLR	toll-like receptor
T_{max}	time of maximal concentration after administration
TBS	Tris-buffered saline
TTBS	Tris-buffered saline with 0.1% Tween-20
TNF- α	tumor necrosis factor- α
TUBA1C	tubulin α -1C chain
TUBA4A	tubulin α -4A chain
TUBB	tubulin β chain
TUBB4A	tubulin β -4A chain
UBC	polyubiquitin-C, cleaved into ubiquitin
UDP	uridine diphosphate
UEC	uridylylate energy charge
UGT	5'-uridine diphosphate glucuronosyltransferase
UMP	uridine monophosphate
UTP	uridine triphosphate
VLCAD	very long-chain specific acyl-CoA dehydrogenase
XMP	xanthosine monophosphate
ZO-1	tight junction protein ZO-1
14-3-3 θ	14-3-3 protein θ

Zusammenfassung

Das Ziel dieser Arbeit war es mit Hilfe eines Zellkulturmodells, basierend auf der humanen Colonkrebszelllinie LS180, und einer Kombination von Methoden der Proteom- und Metabolomanalyse sowie der Molekularbiologie, die molekularen Mechanismen für die gastrointestinale (gastrointestinal, GI) Toxizität der Mycophenolsäure (mycophenolic acid, MPA) aufzuklären.

Im ersten Schritt wurde das Zellkultursystem validiert. Hierbei wurde die Stabilität von wichtigen Transportern und pharmakametabolisierenden Enzymen über 13 Passagen durch Westernblotanalyse bestätigt. Außerdem wurde sichergestellt, dass die zu untersuchenden Pharmaka in den getesteten Konzentrationen nicht zelltoxisch waren. Insgesamt wurde bestätigt, dass LS180-Zellen ein geeignetes Modell sind, um die molekularen Gründe für MPA-induzierte GI Nebenwirkungen aufzuzeigen. In Kombination mit Metabolom- und Proteomanalysen durch nukleare magnetische Resonanz (nuclear magnetic resonance, NMR)- und Massenspektrometrie (mass spectrometry, MS)-Messungen, die eine schnelle und umfassende analytische Strategie darstellen, Veränderungen in biochemischen Stoffwechselwegen und Toxizitätsmechanismen aufzuklären, bildete diese schnell wachsende und einfach zu handhabende Zelllinie eine optimale Grundlage für unsere NMR- und MS-basierten Experimente.

Anfangs wurden die Effekte von MPA, des MPA-Derivats Mycophenolat Mofetil (mycophenolate mofetil, MMF), des MMF-Esterrests 4-(2-Hydroxyethyl)morpholin und MPA in Kombination mit 4-(2-Hydroxyethyl)morpholin auf LS180-Zellen untersucht. Das Zellkulturmodell wurde in Hinsicht auf Anreicherung des Zellkulturmediums mit fötalem Kälberserum und Guanosin (um MPA-induzierte Effekte aufzuheben) und auf die Auswirkungen auf Zellebensfähigkeit und Proliferation weiter untersucht, um optimale und physiologisch sinnvolle Bedingungen für die folgenden Experimente sicherzustellen. MPAs antiproliferativer Effekt konnte durch Zugabe von Guanosin zum Zellkulturmedium rückgängig gemacht werden, jedoch lediglich über einen Zeitraum von 72 Stunden. Da sich das Epithel des Magen-Darm-Trakts

Zusammenfassung

alle 3-5 Tage vollständig erneuert, wurden die Effekte über 5 Tage beobachtet, wobei sich ein signifikanter Einbruch der Proliferation ($p < 0.001$) nach 5 Tagen Inkubationszeit zeigte. Die Effekte der Guanosinzugabe wurden mit Hilfe zweier anderer Zelllinien kreuzvalidiert.

Messung von Nukleotidkonzentrationen und Nukleotidenergieniveaus mittels Hochleistungsflüssigkeitschromatographie (high performance liquid chromatography, HPLC)-MS in LS180-Zellen nach Behandlung mit MPA mit und ohne Guanosinbeigabe zeigte eine gravierende Verarmung der LS180-Zellen an Guanosinnukleotiden. Trotz Anreicherung und wiederholter Dosierung der Zellen mit der maximalen Guanosinkonzentration ($1000\mu\text{M}$) waren Guanosinmono-, Guanosindi- und Guanosintriphosphatniveaus auf etwa 40% der Kontrollwerte gesenkt ($p < 0.001$). Erhöhte Uridin- und Cytidinnukleotidkonzentrationen, verursacht durch die Verarmung an Guanosinnukleotiden, waren ebenfalls nicht durch Zugabe von Guanosin zu normalisieren. Dieses Ungleichgewicht könnte beispielsweise Einfluss auf den Glykosylierungsstatus von Proteinen haben, wie er auch später in den Proteomanalysen sichtbar wurde. Intrazelluläre Konzentrationen von zyklischem Adenosinmonophosphat und zyklischem Guanosinmonophosphat waren jedoch nicht betroffen, wie durch Enzymimmuntests sichergestellt wurde.

Um intrazelluläre Medikamenten- und Metabolitenkonzentrationen und Konzentrationen in LS180-Zellkulturmedien messen zu können, wurde eine HPLC-MS-Methode für MPA, MMF und ihre Metabolite entwickelt. Der Versuch, diesen Assay zu validieren, scheiterte an Matrixeffekten, die die Analytstabilitäten, vor allem der Metabolite, gravierend beeinträchtigten. Diese Effekte wurden bis jetzt noch nicht in der Literatur beschrieben. Da diese Matrixeffekte höchstwahrscheinlich von der Anwesenheit und Konzentration von bestimmten Serumproteinen und dem pH-Wert der Probe abhängen, könnte unsere Beobachtung ebenfalls eine Relevanz für die Messung klinischer Blut- und Urinproben haben.

Proteomanalyse von LS180-Zellen nach MPA-Behandlung durch stabile Isotopenmarkierung durch Aminosäuren in Zellkultur (stable isotope labeling by amino acids in cell culture, SILAC) und gelbasierte Flüssigkeitschromatographie (GeLC)-MS zeigte, dass die Expression von 35 Proteinen signifikant verändert war. Datenanalyse mit Hilfe verschiedener online-Programme und Datenbanken zeigte, dass insbesondere Proteine des Lipidmetabolismus und strukturelle Proteine, die an der Bildung von Gap Junctions beteiligt sind und damit die epitheliale Integrität garantieren,

betroffen waren. Ebenso waren Prozesse, die guanosinnukleotidabhängig sind, signifikant beeinträchtigt. Die Kreuzvalidierung von schon publizierten Daten (Rattenmodell und humane Zelllinien ohne Krebsursprung) mit den MPA-induzierten Proteomveränderungen in LS180-Zellen war erfolgreich und bestätigte nochmals die Eignung von LS180-Zellen als Modell. Weitere Datenanalyse, die auf der Bildung von Proteinnetzwerken basiert und für die verschiedene Datenbanken verwendet wurden, deutete auf eine Beeinträchtigung weiterer Proteine hin, die jedoch durch Westernblotanalysen widerlegt wurde. Teilweise uneinheitliche Ergebnisse von MS- und Westernblotanalysen ließen auf MPA-induzierte Veränderungen von post-translationalen Modifikationen schließen, insbesondere da bekannt ist, dass MPA die Glykosylierung von Proteinen beeinträchtigt und Glykoproteinsynthese Uridin- und Cytidintriphosphat abhängig ist.

Die direkte Identifizierung von Proteintargets durch kovalente Modifikation der Proteine durch MPA und MPA-Metabolite, insbesondere durch das Mycophenolsäure--acylglucuronid (mycophenolic acid acyl glucuronide, AcMPAG), mit Hilfe eines anti-MPA/AcMPAG-Antikörpers schlug fehl, obwohl der Ansatz ausreichend validiert worden war und in der Literatur bekannt ist. Während in der Literatur nur Proteinmodifikationen durch AcMPAG in Betracht gezogen wurden, wurden hier auch andere mögliche Addukte berücksichtigt, die über ähnliches Toxizitätspotential wie AcMPAG-Addukte verfügen könnten.

Metabolomanalyse durch ^1H -NMR-Messungen bestätigte Veränderungen im Lipidmetabolismus, wie sie auch schon in der Proteomanalyse gesehen wurden. MPA steigerte die Synthese von Cholesterol, freien Fettsäuren und Phosphatidylcholin. Ungleichgewichte in Konzentrationen dieser wichtigen Membranbestandteile könnte eine Beeinträchtigung der intestinalen Barrierefunktion zur Folge haben.

Keine Beeinträchtigung des Kohlenhydratmetabolismus war messbar. Versuche mit markierter Glukose und ^{13}C -NMR-Messungen zeigten keine Änderungen in oxidativem versus anaplerotischem Glukosestoffwechsel, lediglich ein Trend zu einem gesteigerten oxidativen Metabolismus war sichtbar (statistisch nicht signifikant). Diese Daten decken sich weitgehend mit den Ergebnissen aus den zuvor beschriebenen Proteomicsexperimenten. Die krebsartige Natur der LS180-Zellen und eine veränderte Metabolisierung von Glukose, auf den die 1D- und 2D-NMR-Daten hinweisen, spiegelten sich in unseren Daten wahrscheinlich wieder.

Ein *in vitro*-Darmentzündungsmodell aus LS180- und RAW 264.7-Zellen wurde ba-

Zusammenfassung

sierend auf einem schon existierenden Modell aus Caco-2- und RAW 264.7-Zellen entwickelt, um Entzündungsreaktionen, die möglicherweise durch MPA und/oder die Metabolite ausgelöst werden, zu untersuchen. Das Modell basierte auf der Freisetzung von Zytokinen von RAW 264.7-Zellen durch Stimuli wie Medikamente oder Lipopolysaccharid. Für MPA und die MPA-Metabolite wurde keine Zytokinfreisetzung gemessen, während die positive Kontrolle eine starke Reaktion hervorrief. Da die Testsubstanzen keine Zytokinfreisetzung von RAW 264.7-Zellen auslösten, wurden keine Folgeexperimente ausgeführt. Mit geringfügigen Änderungen, z.B. Kocultivierung beider Zelltypen in der selben Zellkulturschale, könnte dieses andernfalls vielversprechende Modell weitere Einsichten in die Toxizitätsmechanismen von MPA geben.

Zusammenfassend beweisen unsere Studien die Eignung des LS180-Zellkulturmodells und zeigen sogar Vorzüge gegenüber den oft verwendeten Caco-2-Zellen auf.

MPA beeinträchtigte insbesondere nukleotidabhängige Prozesse, die Expression struktureller Proteine, sowie den Fettsäure- und Lipidmetabolismus in LS180-Zellen. Diesen Ergebnissen nach, kann die GI Toxizität zum Teil einer eingeschränkten Barrierefunktion des durch MPA kompromittierten Epitheliums zugeschrieben werden, wie auch veränderten Konzentrationen an essentiellen Proteinen und Membranbestandteilen. Unsere Studien berücksichtigen darüber hinaus wichtige Aspekte der Validierung von Modellsystemen und Assays. Ein umfassender Einblick in die Mechanismen MPAs molekularer Toxizität konnte mit Hilfe der vielfältigen Methoden, die im Rahmen dieser Arbeit zum Einsatz kamen, gewonnen werden.

In Abbildung 0.1 sind die hier vorgeschlagenen Toxizitätsmechanismen von MPA in Abhängigkeit voneinander und die verwendeten Methoden dargestellt.

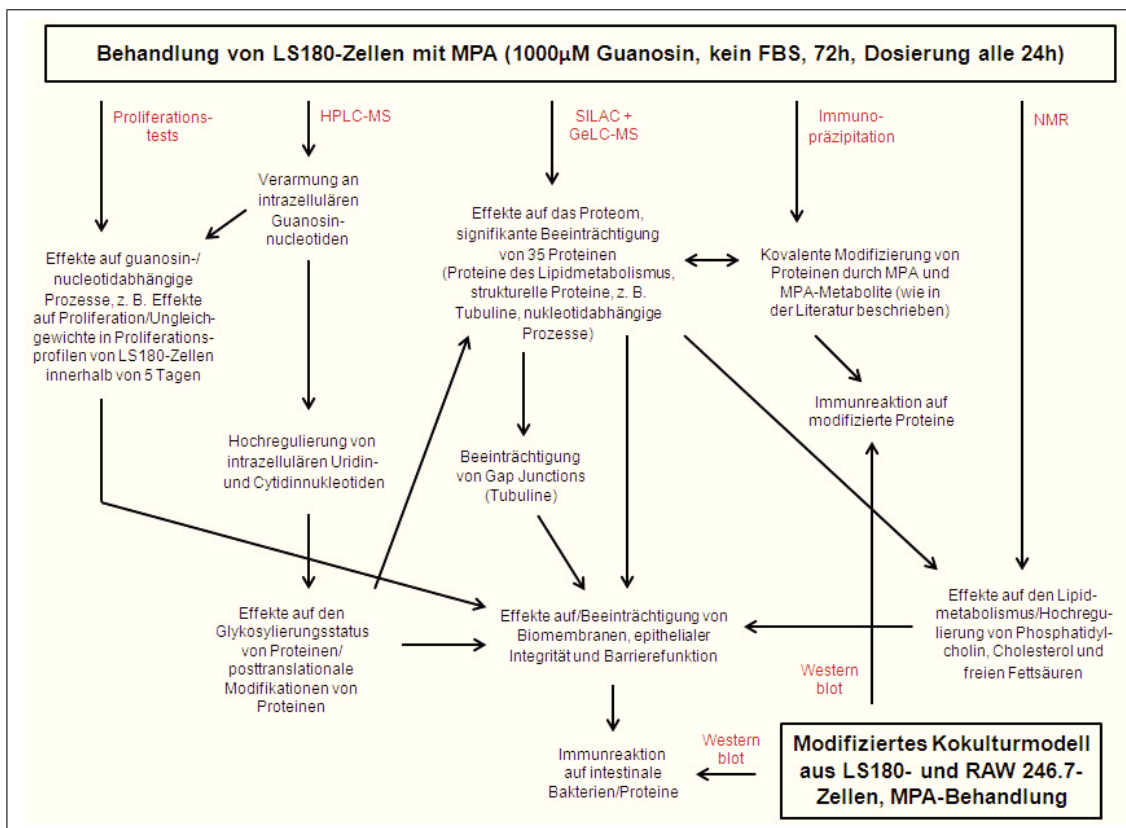


Abb. 0.1: Vorgeschlagene Mechanismen der GI Toxizität von MPA aufgeklärt durch das LS180-Zellkulturmodell in Kombination mit den verwendeten Methoden. Die erwähnten MPA-abhängigen Effekte wurden mit Hilfe des LS180-Zellkulturmodells erklärt mit Ausnahme von "Kovalente Modifizierung von Proteinen durch MPA und MPA-Metabolite". Dieses Experiment lieferte keine sinnvollen Ergebnisse, jedoch wurden kovalente Proteinmodifikationen zuvor in der Literatur beschrieben. Das LS180-RAW 264.7-Kokulturmodell, wie es von uns eingesetzt wurde, zeigte keine Immunreaktion gegen MPA oder MPA-Metabolite. Ein modifiziertes Kokulturmodell, wie es in späteren Abschnitten diskutiert wird, könnte Informationen hinsichtlich Immunreaktionen gegen modifizierte Proteine liefern. FBS: fötales Kälberserum (fetal bovine serum), GeLC: gelbasierte Flüssigkeitschromatographie, HPLC: Hochleistungsflüssigkeitschromatographie (high performance liquid chromatography), MPA: Mycophenolsäure (mycophenolic acid), MS: Massenspektrometrie (mass spectrometry), NMR: nucleare magnetische Resonanz (nuclear magnetic resonance), SILAC: stabile Isotopenmarkierung durch Aminosäuren in Zellkultur (stable isotopic labeling by amino acids in cell culture).

Summary

The objective of this thesis was the elucidation of the molecular mechanisms of the gastrointestinal (GI) toxicity of mycophenolic acid (MPA) using a cell culture model based on the human colon cancer cell line LS180 and a combination of methods of proteome and metabolome analysis as well as molecular biology methods.

In a first step the cell culture system was validated. The stability of important transporters and drug-metabolizing enzymes was ensured by western blot analysis over 13 passages. It also was assured that the test drugs did not show cytotoxicity within the tested concentration ranges. Overall it was confirmed that LS180 cells are an appropriate model to clarify the molecular mechanisms of MPA-induced GI side effects. In combination with proteome and metabolome analyses by nuclear magnetic resonance (NMR) and mass spectrometry (MS) measurements, which provide a fast and comprehensive approach to explain changes in metabolic pathways and mechanisms of toxicity, this fast-growing and easily manageable cell line constituted an optimal basis for our NMR- and MS-based studies.

The effects of MPA, the MPA-derivative mycophenolate mofetil (MMF), the MMF ester residue 4-(2-hydroxyethyl)morpholine, and MPA in combination with 4-(2-hydroxyethyl)morpholine on LS180 cells were examined. The cell culture model was further investigated in terms of supplementation of the cell culture medium with fetal bovine serum and guanosine (to reverse MPA-induced effects) and the effects on cell viability and proliferation to guarantee optimal and physiologically reasonable conditions for the following experiments. MPA's antiproliferative effects were reversed by supplementation of the cell culture medium with guanosine, but only over a period of 72 hours. Since the epithelium of the GI tract is renewed every 3-5 days, the effects were monitored over 5 days whereupon a significant decrease in proliferation appeared after 5 days of incubation ($p < 0.001$). The effects of guanosine supplementation were cross-validated with two other cell lines.

Measurement of nucleotide concentrations and nucleotide energy levels using high

Summary

performance liquid chromatography (HPLC)-MS in LS180 cells after MPA treatment with and without guanosine supplementation resulted in marked depletion of guanosine nucleotides in LS180 cells. Despite supplementation and redosing of cells with the maximal guanosine concentration ($1000\mu\text{M}$) levels of guanosine mono-, di-, and triphosphates decreased to about 40% of control values ($p < 0.001$). Elevated uridine and cytidine nucleotide concentrations, triggered by the depletion of guanosine nucleotides, were not reversible by supplementation with guanosine either. These imbalances could influence the glycosylation status of proteins as it was apparent in later conducted proteome analyses. On the other hand intracellular concentrations of cyclic adenosine monophosphate and cyclic guanosine monophosphate were not affected as evaluated by enzyme-linked immunosorbent assays.

To measure intracellular drug and metabolite concentrations and concentrations in LS180 cell culture media, an HPLC-MS assay for MPA, MMF, and their metabolites was developed. The attempt to validate this assay failed due to matrix effects which severely compromised analyte stabilities, especially the stability of the metabolites. These effects had not been described in the literature before. Since these matrix effects very likely depended on the presence and concentration of certain serum proteins and a sample's pH value, our observations might be relevant for the measurement of clinical blood and urine samples.

Proteome analysis of LS180 cells after MPA treatment by stable isotopic labeling by amino acids in cell culture (SILAC) and gel-based liquid chromatography (GeLC)-MS showed that the expression of 35 proteins was significantly affected. Data analysis using several online programs and databases revealed that especially proteins of lipid metabolism, structural proteins that are involved in the formation of gap junctions and guarantee epithelial integrity, are compromised. Cross-validation of already published data (rat model and human cell lines of non-cancerous origin) with MPA-induced proteome changes in LS180 cells was successful and again confirmed the applicability of LS180 cells as model system. Further data analysis, which was based on the construction of protein networks and for which different databases were used, pointed towards disturbance of additional proteins. Partly inconsistent results of MS and western blot analyses indicated MPA-induced changes of post-translational modifications, especially since MPA is known to affect the glycosylation of proteins and glycoprotein synthesis is dependent on uridine and cytidine triphosphate.

The direct identification of covalent modification of proteins by MPA and MPA metabolites, especially by the mycophenolic acid acyl glucuronide (AcMPAG) metabolite, using an anti-MPA/AcMPAG antibody failed although the approach had been thoroughly validated and is known throughout the literature. While in the literature only protein modifications by AcMPAG are considered, here other possible adducts, that should exhibit a similar potential of toxicity as AcMPAG adducts, were taken into account as well.

Metabolome analysis by ^1H NMR measurements confirmed changes in lipid metabolism as they were seen in proteome analyses before. MPA increased the synthesis of cholesterol, free fatty acids, and phosphatidylcholine. Imbalances in concentrations of these important membrane constituents could compromise intestinal barrier function.

No impairment of carbohydrate metabolism was measureable. Experiments with marked glucose and ^{13}C NMR measurements did not show changes in oxidative versus anaerobic glucose metabolism, just a trend towards increased oxidative metabolism was observed (not statistically significant). These data corresponded to the results of the previously described proteomics experiments. The cancerous nature of LS180 cells and a changed glucose metabolism, which is indicated by 1D and 2D NMR data, is most likely reflected in our data.

An *in vitro* gut inflammation model based on LS180 and RAW 264.7 cells was developed by modification of an already existing model of Caco-2 and RAW 264.7 cells to include inflammatory processes possibly triggered by MPA and/or MPA metabolites. The model is based on the liberation of cytokines from RAW 264.7 cells by stimuli such as drugs or lipopolysaccharide. No release of cytokines was seen for MPA and MPA metabolites, whereas the positive control triggered a strong reaction. Since the test compounds did not cause cytokine release from RAW 264.7 cells, no further experiments were conducted. With marginal changes, e.g. coculture of both cell types in the same cell culture dish, this otherwise promising model could provide further insight in MPA's mechanisms of toxicity.

Overall our studies demonstrated the applicability of the LS180 cell culture model and even show advantages over the often used Caco-2 cells.

MPA especially compromised nucleotide-dependent processes, the expression of structural proteins, as well as fatty acid and lipid metabolism in LS180 cells. According to these results, MPA's GI toxicity is partly attributable to an impaired barrier

Summary

function of the MPA-compromised epithelium, but also to changed concentrations of essential proteins and membrane components. Moreover, our studies considered important aspects in terms of the validation of model systems and assays. Comprehensive insight in the mechanisms of MPA's molecular toxicity was gained by the multifaceted methods used within the scope of this thesis.

In Figure 0.2 the proposed molecular mechanisms of MPA's toxicity are summarized in context of the used methods.

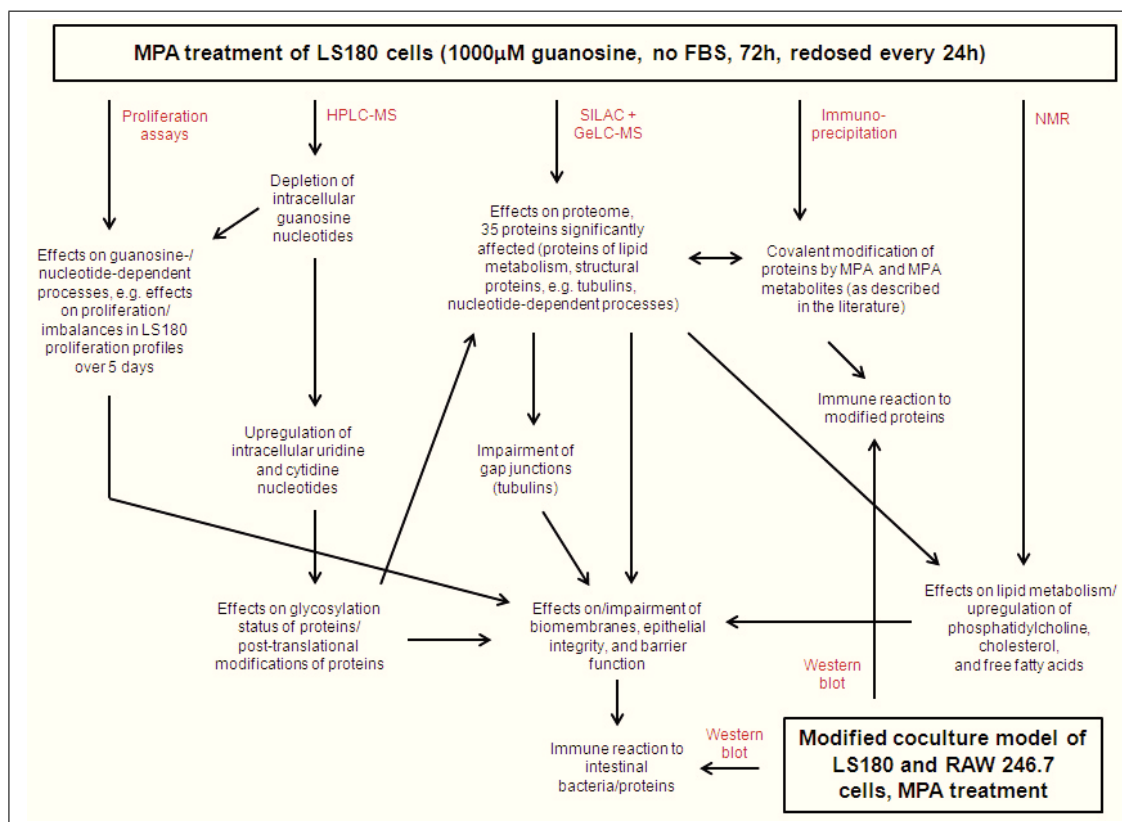


Fig. 0.2: Proposed molecular mechanisms of MPA's GI toxicity elucidated using the LS180 cell culture model and various methods. *The listed MPA-dependent effects were determined using the LS180 cell culture model except for "Covalent modification of proteins by MPA and MPA metabolites". This experiment did not yield analyzable results, but covalent modifications of proteins have been described in the literature before. The LS180-RAW 264.7 cell coculture model as it was used by us did not show immune reactions to MPA or MPA metabolites. A modified coculture model as discussed in later sections could provide information about immune reactions to modified proteins and/or intra- and extracellular parameters. FBS: fetal bovine serum, GeLC: gel-based liquid chromatography, HPLC: high performance liquid chromatography, MPA: mycophenolic acid, MS: mass spectrometry, NMR: nuclear magnetic resonance, SILAC: stable isotopic labeling by amino acids in cell culture.*

1 Introduction

1.1 Immunosuppression and mycophenolic acid

Over 25,000 organ transplants are performed annually in the United States of America with another 100,000 patients waiting for a transplant [1, 2]. To minimize the discrepancy between demand and supply, the improvement of transplantation outcomes is fundamental.

Any immunosuppressive treatment, crucial for graft maintenance, needs to be balanced between drug efficacy and tolerability [1, 3]. Nowadays a broad range of immunosuppressive drugs are available to customize regimens. Most commonly used are steroids, calcineurin inhibitors such as cyclosporine and tacrolimus, mammalian target of rapamycin inhibitors such as sirolimus (rapamycin), and other agents, e.g. antiproliferatives such as mycophenolic acid (MPA). Most regimens feature MPA in combination with calcineurin inhibitors and steroids due to diminished major side effects despite well maintained immunosuppression [4].

1.1.1 History and success of MPA

MPA was discovered as a product of different *Penicillium* species and first extracted from *Penicillium stoloniferum* in the 1890's by Bartolomeo Gosio [5, 6]. Within the following decades it was found to have antiviral, antifungal [7], and antineoplastic [8, 9] effects and became the first comprehensively characterized antibiotic in history. Another valuable property of MPA is its immunosuppressive nature [10].

Until the end of the 20th century the antiproliferative drug of choice in combination therapies was 6-mercaptopurine, which was primarily marketed as its prodrug azathioprine (AZA) [11]. The preference for AZA as an antiproliferative lapsed when findings in animal models of transplantation [12–16] and first clinical trials around 1990 [16–19] led to the approval of mycophenolate mofetil (MMF), the morpholinoethyl ester prodrug and first formulation of MPA for kidney transplantation in 1995. Within a few years, MMF became the most frequently used antiproliferative agent in immunosuppressive drug regimens for kidney, pancreas, liver, and heart

1 Introduction

transplantation [20]. Today, instead of AZA, MMF is commonly administered in transplant regimens combined with cyclosporine and corticosteroids [4, 11, 21, 22], exhibiting superior performance and safety profiles [23, 24].

1.1.2 The two formulations of MPA

Currently MPA is available in two formulations [25]. The conventional mycophenolate mofetil (MMF, CellCept[®], International Union of Pure and Applied Chemistry (IUPAC) name: 2-(morpholine-4-yl)ethyl(4E)-6-(4-hydroxy-6-methoxy-7-methyl-3-oxo-1,3-dihydro-2-benzofuran-5-yl)-4-methylhex-4-enoate; Roche Pharmaceuticals, Basel, Switzerland; approved in 1995 [20]) is immediately released after drug intake. The alternate, tentatively advanced formulation enteric-coated mycophenolate sodium (EC-MPS, myfortic[®], sodium salt of (4E)-6-(4-hydroxy-6-methoxy-7-methyl-3-oxo-1,3-dihydro-2-benzofuran-5-yl)-4-methylhex-4-enoic acid; Novartis Pharma AG, Basel, Switzerland; approved in 2005 [21]) delays the release of the pharmacologically active component MPA until more distal portions of the small intestine to diminish upper gastrointestinal (GI) side effects. Structures, sum formulas, and molecular weights of MPA, EC-MPS, MMF, and the ester moiety 4-(2-hydroxyethyl)morpholine (subsequently called morpholinoethanol) are shown in Figure 1.1.

1.1.3 Benefits and adverse effects of MPA and their consequences

Amongst other reasons for the success of MPA is that it neither possesses cardiovascular nor renal toxicity [4, 20, 25]. The former is of major interest considering that the main cause of death in renal transplant patients is of cardiovascular origin, the latter taking into account that calcineurin inhibitor adverse effects (especially renal toxicity) contribute to chronic allograft dysfunction and potentially graft loss.

Additional benefits are a lack of diabetogenic potential due to the fact that MPA is mainly metabolized by glucuronidation [20], superiority to AZA in diminishing incidence and severity of acute rejection episodes, which are a main reason for graft loss during the first year after kidney and heart transplantation [26, 27], as well as reduced dyslipidemia, improved wound healing [28, 29], and increased patient and graft survival as long-term benefits [30, 31]. Another favorable attribute of MPA immunosuppression is the possibility of reduction or withdrawal of the combination drugs (cyclosporine and corticosteroids) [32].

1.1 Immunosuppression and mycophenolic acid

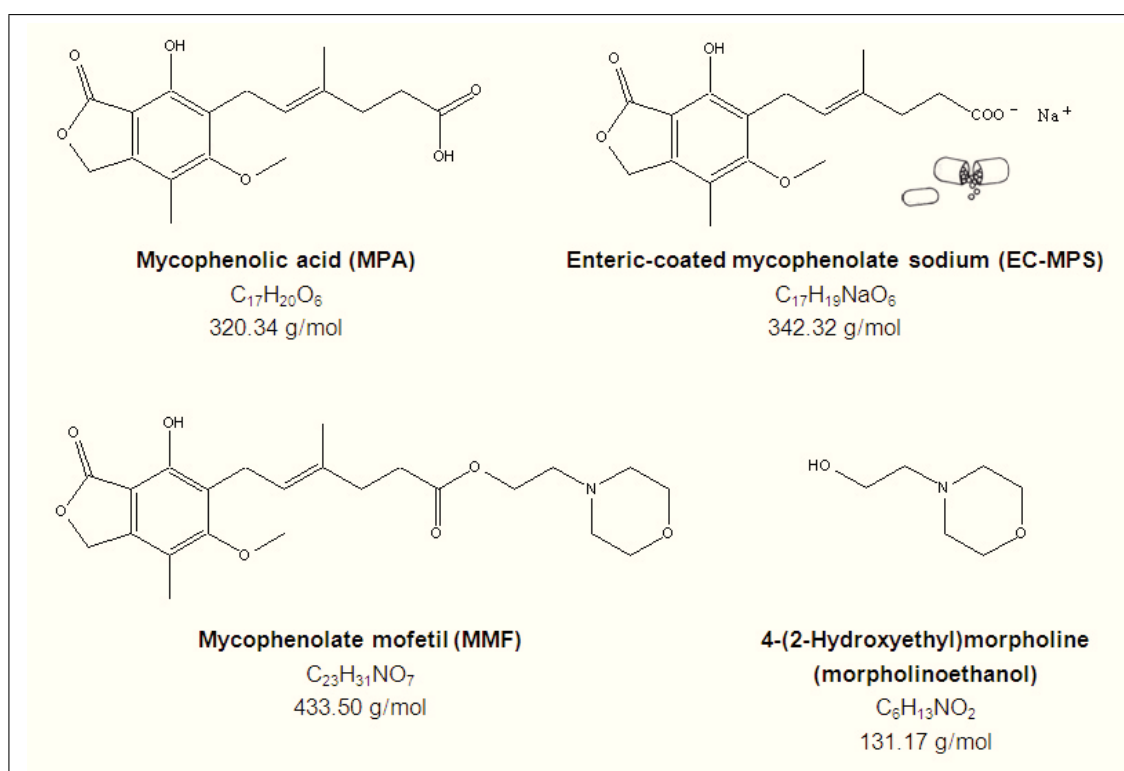


Fig. 1.1: Chemical structures, sum formulas, and molecular weights of mycophenolic acid, enteric-coated mycophenolate sodium, mycophenolate mofetil, and 4-(2-hydroxyethyl)morpholine.

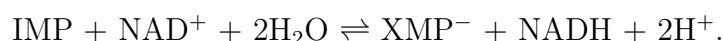
1 Introduction

The main concern about MPA typically is GI intolerance which tends to be more severe than GI side effects occurring in patients on other immunosuppressive drug regimens [20, 25, 33–35]. These, yet not fully elucidated disorders, are mainly attributed to MPA itself, MPA’s acyl glucuronide metabolite (AcMPAG), and impaired immunity under immunosuppressive therapy. Other very common side effects associated with MPA therapy resemble those of AZA such as hematologic disorders, e.g. anemia, thrombocytopenia, leucopenia, and malignancy [25, 34, 36, 37].

1.1.4 Pharmacodynamic properties: Mechanism of immunosuppression

Inosine monophosphate dehydrogenase inhibition

The enzyme inosine monophosphate dehydrogenase (IMPDH, EC 1.1.1.205) catalyzes the nicotinamide adenine dinucleotide (NAD)-dependent oxidation of inosine 5'-monophosphate (IMP) to xanthosine 5'-monophosphate (XMP) and reduced nicotinamide adenine dinucleotide (NADH):



A cross-linked position in metabolism makes IMPDH a popular target for several classes of drugs, i.e. for anticancer (tiazofurin), antiviral (ribavirin, thiazole-4-carboxamide adenine dinucleotide), and immunosuppressive (MPA, mizorbine) therapy [38, 39]. IMPDH can either be inhibited by modification of the substrate site (ribavirin, mizorbin) or NAD-binding site (MPA, thiazole-4-carboxamide adenine dinucleotide).

MPA is a non-competitive reversible non-nucleoside inhibitor of IMPDH, the rate-limiting enzyme in the *de novo* pathway of purine synthesis [4, 20, 40]. In most cell types a salvage pathway is utilized for purine synthesis additionally to the *de novo* pathway to replenish purine pools. Lymphocytes, in contrast to other cells, are almost fully dependent on purine *de novo* generation [41]. Unrestrained *de novo* synthesis of purines as precursors for building blocks of deoxyribonucleic acid (DNA) is therefore critical for lymphocyte proliferation [4, 40].

Pathways of guanosine nucleotide synthesis

Studies of genetic defects elucidated the above described lymphocyte-specific condition and suggested immunomodulatory potential [16, 22, 42, 43]. Children suffering

1.1 Immunosuppression and mycophenolic acid

from Lesch-Nyhan syndrome, a deficiency in hypoxanthine-guanine phosphoribosyl-transferase (HGPRT, E.C. 2.4.2.8, enzyme of the salvage pathway), show mental defects while having normal numbers of T and B lymphocytes and a properly working immune system. The salvage pathway and HGPRT seemed to be crucial for brain cell development and function, while lymphocytes seemed to be unaffected and therefore independent of the salvage pathway. Adenosine deaminase deficiency on the other hand leads to a decrease in number and function of T and B lymphocytes, but neither brain function nor numbers of neutrophils, erythrocytes, or platelets are affected. Since brain and other cell types are capable of *de novo* guanosine synthesis their proliferation is, unlike lymphocyte proliferation, unaffected.

Pathways of adenosine and guanosine nucleotide (purine nucleotide) biosynthesis are explained in Figure 1.2. Key substrate for the generation of purine as well as pyrimidine nucleotides is phosphoribosyl pyrophosphat (PRPP) which is synthesized from ribose 5-phosphate (Ribose 5P) from the pentose phosphate pathway and adenosine triphosphate (ATP) [42, 43]. Several steps lead to IMP, which can either be transformed to adenosine monophosphate (AMP) or guanosine monophosphate (GMP). GMP is generated by *de novo* (blue arrows in Figure 1.2) or salvage (green arrows) synthesis. *De novo* GMP is formed by conversion of IMP to XMP; intermediates of the salvage pathway are hypoxanthine, xanthine, and guanine. MPA inhibits IMPDH and shuts down the *de novo* route of GMP synthesis, thereby depleting the GMP pool of lymphocytes selectively and suppressing responses to antigenic or mitogenic stimulation. Shortly, MPA immunotherapy leads to a lack of key substrates for DNA and ribonucleic acid (RNA) synthesis (absence of GMP leading to a shortage of guanosine triphosphate (GTP) and deoxyguanosine triphosphate (dGTP)) as it occurs in the case of genetic mutations in adenosine deaminase-deficient individuals (absence of AMP leading to a shortage of ATP and deoxyadenosine triphosphate (dATP)).

1 Introduction

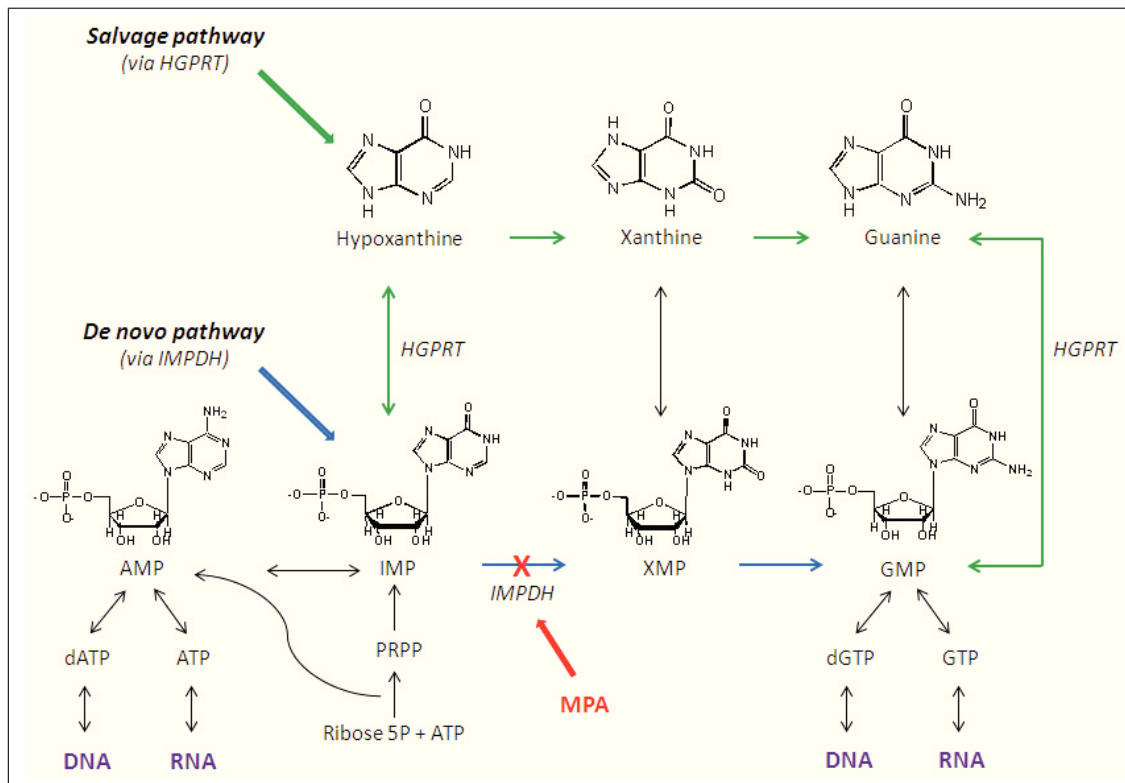


Fig. 1.2: Pathways of purine biosynthesis and immunosuppressive mechanism of MPA. MPA antagonizes IMPDH and therefore the de novo pathway of purine synthesis. Lymphocytes do not feature the salvage pathway which makes them strongly dependent on GMP production via IMPDH for synthesis of deoxyribonucleic acid (DNA) and ribonucleic acid (RNA) and susceptible for inhibition of cell proliferation by MPA. AMP: adenosine monophosphate, ATP: adenosine triphosphate, dATP: deoxyadenosine triphosphate, dGTP: deoxyguanosine triphosphate, GMP: guanosine monophosphate, GTP: guanosine triphosphate, HGPRT: hypoxanthine-guanine phosphoribosyltransferase, IMP: inosine 5'-monophosphate, IMPDH: inosine monophosphate dehydrogenase, MPA: mycophenolic acid, PRPP: phosphoribosyl pyrophosphate, Ribose 5P: ribose 5-phosphate, XMP: xanthosine 5'-monophosphate. Adapted from [20, 44, 45], modified.

Additional advantages of MPA's mechanism of immunosuppression

Throughout the literature, many minor immunosuppressive actions of MPA in addition to the main effect of IMPDH inhibition are described [20, 42, 43, 46]. A few examples are listed below.

- **Allosteric regulation of other key enzymes**

Blocking of IMPDH manipulates the nucleotide-dependent allosteric regulation of PRPP synthetase ($\text{Ribose 5P} + \text{ATP} \rightleftharpoons \text{PRPP} + \text{AMP}$) and ribonucleotide reductase ($\text{deoxyguanosine triphosphate} + \text{H}^+ + \text{reduced nicotinamide adenine dinucleotide phosphate (NADPH)} \rightleftharpoons \text{deoxyguanosine triphosphate} + \text{nicotinamide adenine dinucleotide phosphate (NADP}^+\text{)}$), e.g. $\text{guanosine diphosphate (GDP)} \rightleftharpoons \text{deoxyguanosine diphosphate}$, $\text{adenosine diphosphate (ADP)} \rightleftharpoons \text{deoxyadenosine diphosphate}$) in lymphocytes [43, 47]. While PRPP synthetase is inhibited by AMP and ADP, activation occurs by high levels of GMP, GDP, and GTP. Ribonucleotide reductase activity is impaired by dATP, but dGTP on the other hand stimulates the enzyme and results in ADP reduction. High abundance of adenosine nucleotides and/or low abundance of guanosine ribonucleotides lowers PRPP levels by inhibiting PRPP synthetase. High levels of dATP and/or low levels of dGTP inhibit ribonucleotide reductase, depleting deoxyribonucleotide triphosphate pools and DNA synthesis. While guanosine and deoxyguanosine nucleotides stimulate lymphocyte proliferation, high levels of adenosine and deoxyadenosine nucleotides inhibit proliferation. This ensures inhibition of DNA synthesis after the initial depletion of guanosine pools by IMPDH inhibition by MPA.

- **Isoforms of IMPDH**

Two different isoforms of IMPDH exist [40, 43, 48, 49]. MPA acts on human IMPDH isoform II with about four times greater specificity than on isoform I [40]. Type II IMPDH is strongly upregulated in stimulated lymphocytes [50], which collaterally increases MPA's antiproliferative effects and suppression of clonal expansion of T and B cells.

- **Inhibition of glycosylation and expression of adhesion molecules**

A lack of GTP diminishes fucose and mannose transfer to glycoproteins [42]. As glycosylation of adhesion molecules is pivotal for the attachment of leukocytes (integrin-mediated sticking through selectins) to the endothelium, recruitment of lymphocytes and monocytes into areas of inflammation/graft rejection is inhibited [42, 43, 46].

1.1.5 Pharmacokinetic properties

The main site of MPA metabolism is the liver [20], but organs such as the kidney and intestine contribute significantly and play an important role in drug degradation and transformation [4, 42, 51].

Differences in pharmacokinetic properties of formulations

MMF's solubility in water at neutral pH is low ($43\mu\text{g}/\text{mL}$ at pH 7.4) [52], but it increases with decrease of pH ($4.27\text{mg}/\text{mL}$ at pH 3.6). Orally administered MMF is dissolved in the stomach at pH values of 1-3 (Fig. 1.6). In the stomach and even in oral/pregastric regions of the digestive tract, esterases acting on aromatic and aliphatic ester bonds are ubiquitous [53–56]. Carboxylesterases convert MMF to MPA (Fig. 1.3) and morpholinoethanol [57]. MMF is rapidly de-esterified in the stomach [58] and MPA is absorbed partly in the stomach and partly in the proximal small intestine [59]. Orally administered MMF is also absorbed by the wall of the GI tract directly and is intracellularly hydrolyzed by esterases in tissue and plasma to MPA and morpholinoethanol [57].

The alternative formulation EC-MPS offers an enteric coating that dissolves at pH values > 5.5 (Fig. 1.3), as it is present in the small intestine [59] (Fig. 1.6). Release of MPA is thereby delayed until entry and disintegration of the EC-MPS capsule in the duodenum. The gavage of MPA as a salt enhances solubility and absorption compared to administration as an acid.

In the past it was assumed that pharmacokinetic (PK) properties differ only slightly between the two MPA formulations [3, 25]. The aberrant metabolism was thought to primarily be due to a delayed release of the pharmacologically active component MPA resulting in a delayed T_{max} (time of maximal concentration after administration, 1 hour for MMF [20] versus 2-3 hours for EC-MPS [60]). Formulations were considered equivalent [3, 20, 25] as studies showed that MMF yields a bioavailability of MPA of 94% [20, 61]. More recent and more diligent publications deny bioequivalence of MMF and EC-MPS mainly because of severely diverging concentration-time profiles [60, 62]. Formulations should, due to differences in multiple PK parameters, not be considered equivalent as agreed on in a consensus meeting about MPA therapeutic drug monitoring held in 2008 [60]. In addition the comparison of PK proper-

ties of formulations is hindered by a lack of information on EC-MPS metabolism and disposition, while PK attributes of MMF have been studied extensively for different types of transplants, healthy controls, adults and pediatric patients [20, 60, 63, 64].

General PK characteristics of MPA

Uptake of a wide variety of substrates is mediated by organic anion-transporting polypeptides (OATPs), which are encoded by solute carrier organic anion transporter genes. Hepatocellular and intestinal uptake of MPA is promoted by OATP1B1 (formerly OATP2), OATP1B3, and OATP2B1 located in the basolateral cell membrane [65] as depicted for an intestinal cell in Figure 1.4. Intracellularly MPA is extensively metabolized by glucuronidation by 5'-uridine diphosphate glucuronosyltransferase (UGT) enzymes (Fig. 1.3) imbedded in the membrane of the endoplasmic reticulum (ER) [20, 66] (Fig. 1.4). About 80% of the drug is converted to its major metabolite, the phenolic mycophenolic acid glucuronide (MPAG, β -D-glucuronide, 7-O-glucuronide; for labeling routine in the MPA molecule please see comments in Section 2.7.2), which reaches its C_{max} (maximum concentration a drug reaches after administration prior to administration of a second dose) about 1 hour after the MPA C_{max} and is pharmacologically inactive [20, 67]. MPAG is mainly generated by UGT isoforms UGT1A8, UGT1A9, and UGT1A10 (phase II enzymes), of which UGT1A8 and UGT1A10 are only expressed in the GI tract. The minor glucuronide metabolite AcMPAG constitutes about 10% of the MPA-AUC₀₋₁₂ (area under the curve/integral of the concentration-time curve over 12h after drug administration), peaks 1 hour after the MPA C_{max} as well, but is pharmacologically active and adds to the immunosuppressive potential of MPA. UGT2B7 is almost entirely responsible for AcMPAG formation and to a smaller extent also UGT1A8.

In addition the two glucuronides two glucoside metabolites, a phenolic (MPA-GS, 7-O-glucoside; for labeling routine in the MPA molecule please see comments in Section 2.7.2) and an acyl glucoside (AcMPA-GS), have been identified [51, 68]. MPA-GS constitutes about 10% of the AUC of the respective MPA-AUC, while AcMPA-GS is only prominent in trace amounts and cannot be determined due to detection limits of the methods used [20]. The glucoside metabolites are formed by phase II transformation via UGT enzymes as well (Fig. 1.3).

Other minor metabolites of unclear clinical significance include 6-O-desmethyl-MPA (DM-MPA, formerly named M-3; 12h-AUC of 0.3-2.8% of 12h-MPA-AUC) and two related glucuronides, DM-MPA-6-O-phenyl glucuronide (DM-MPA-6G, 0.6-3.5%) and DM-MPA-4-O-phenyl glucuronide (DM-MPA-4G, 0.4-1.1%) [69]. DM-MPA is produced by cytochrome P450 oxidase (CYP, phase I enzymes) isoforms CYP3A4

1 Introduction

and CYP3A5 and possibly to a minor extent by CYP2C8 (Fig. 1.3) [69]. CYP enzymes are located in the membrane of the ER (Fig. 1.4) [70].

After uptake and possibly conjugation inside a hepatocyte or intestinal cell (or another metabolizing tissue, e.g. the placenta), MPA and conjugates can be excreted into bile or back into the intestinal lumen (enterohepatic recirculation) or the blood stream respectively (Fig. 1.4). Export is mediated by efflux pumps, namely multidrug resistance-associated protein (MRP) 1 and 2, multidrug resistance protein 1 (MDR1, also known as P-glycoprotein/P-gp), and breast cancer resistance protein (BCRP) [65, 71]. Glucuronides can enzymatically and non-enzymatically be hydrolysed back to MPA and glucuronic acid [20].

More than 90% of an MPA dose (mainly in form of MPAG) can be recovered from urine (active tubular secretion) within 3 days [20, 67]. While MPA and the above described metabolites have been detected in urine in minor amounts, MMF has never been found. 5.5% of a given MMF dose can be recovered in the feces. The ester moiety released by de-esterification of MMF is metabolized as well and almost completely excreted in urine within 1 day [20].

Inter- and inpatient variability in MPA exposure is striking and, as commonly seen in PK profiles of drugs, multiple parameters such as renal function, coadministered drugs (for MPA especially cyclosporine) [21, 72], albumin levels, genetic factors, meal times, or disease can affect all elements of MPA metabolism, e.g. absorption, enterohepatic circulation, metabolite formation, and bioavailability [20, 21]. Major efforts have been undertaken to clarify the role of genetic polymorphisms in enzymes involved in MPA metabolism [20].

In terms of MPA GI toxicity, it should be mentioned that effects on MPA metabolism by food ingestion have been found to be minor, as plasma MPA-AUC of fed and fasted state are equivalent [73]. If taken with food, T_{max} is delayed by 1 hour [34, 67]. Although C_{max} is significantly decreased [34, 67], no adjustment of intake or dosage is required [67].

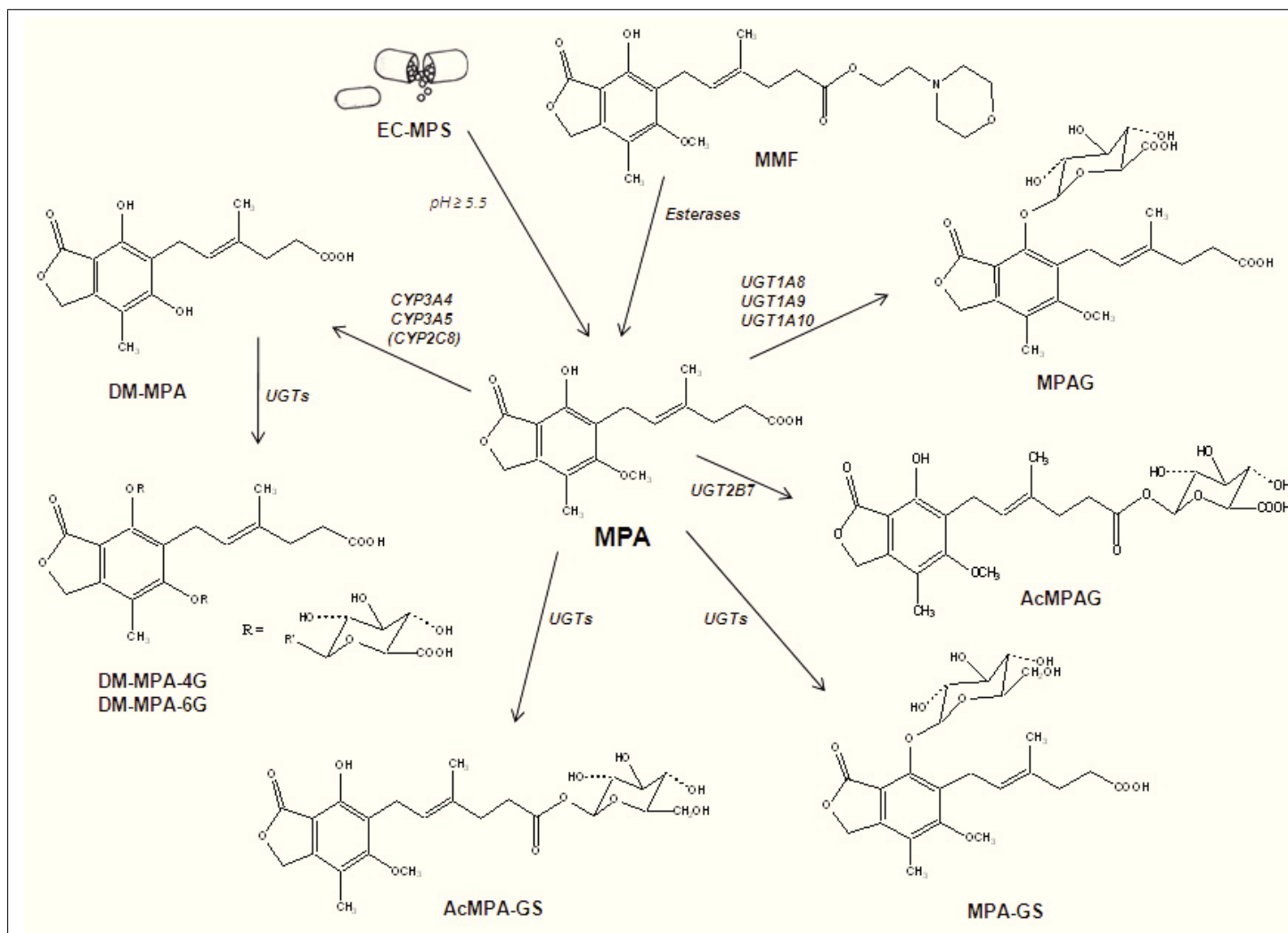


Fig. 1.3: Metabolism of EC-MPS and MMF. Location of named enzymes in the GI tract wall is shown in Figure 1.4. AcMPAG: mycophenolic acid acyl glucuronide, CYP: cytochrome P 450 oxidases, DM-MPA: 6-O-desmethyl mycophenolic acid, DM-MPA-4/6G: 6-O-desmethyl mycophenolic acid-4/6-O-phenyl glucuronide, EC-MPS: enteric-coated mycophenolate sodium, MMF: mycophenolate mofetil, MPA: mycophenolic acid, MPAG: mycophenolic acid glucuronide, UGT: 5'-uridine diphosphate glucuronosyltransferase.

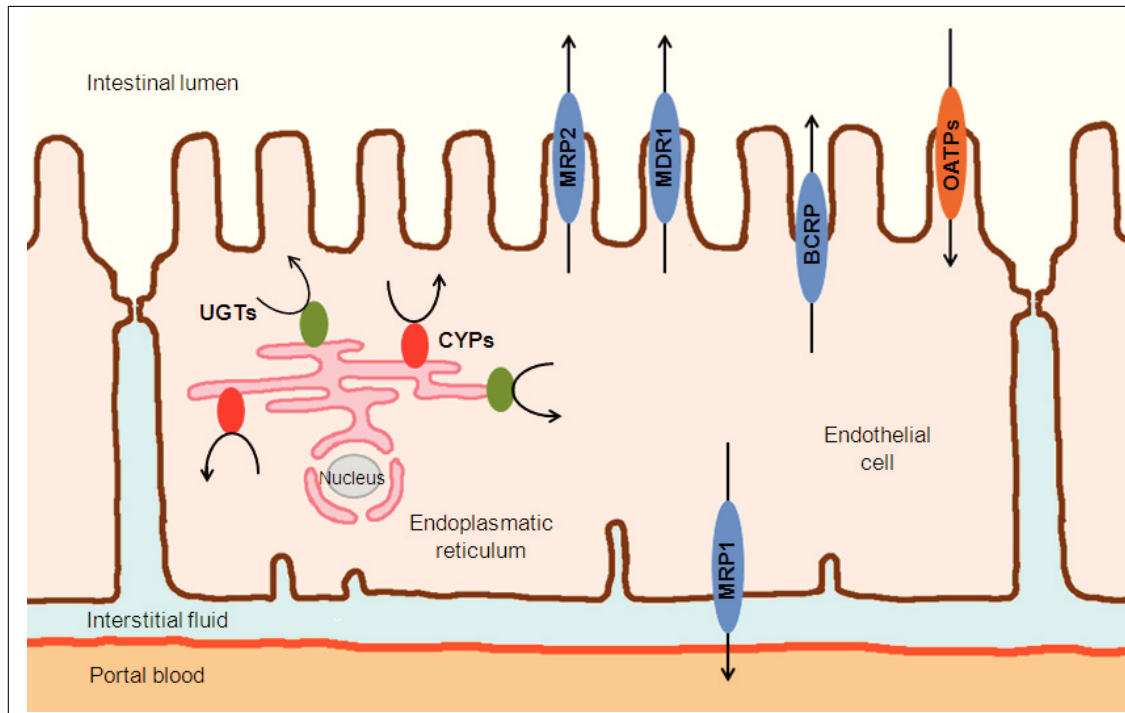


Fig. 1.4: MPA disposition. *Metabolic transformations of MPA to MPA metabolites catalyzed by the named enzymes is depicted in Figure 1.3. BCRP: breast cancer resistance protein, CYPs: cytochrome P 450 oxidases, MDR1: multidrug resistance protein 1, MRP1/2: multidrug resistance-associated protein 1/2, UGTs: 5'-uridine diphosphate glucuronosyltransferases.*

1.2 The GI tract and GI toxicity of MPA

1.2.1 Impact of MPA GI side effects

GI intolerability is the main reason for an MMF/EC-MPS dose change or even discontinuation [33, 35, 74–77]. Over 50% of renal transplant patients were found to be subject to these adjustments [77]. Consequences negatively affect short- and long-term graft outcomes due to suboptimal dosing (risk of underdosing to avoid GI symptoms or withdrawal) as can be clearly seen when correlating incidences of graft loss, GI symptoms, and MMF dose reduction/discontinuation (Fig. 1.5) [77].

As GI symptoms vary widely in terms of nature and severity, as well as the patient's perception of wellness and constraints in daily life [35], assessment of GI symptom burden is difficult [25]. Insufficient comparability among studies and differences in assessment of data are other pitfalls in clinical trials trying to clarify the clinical impact of MPA GI toxicity [25, 35].

Another important factor in reviewing MPA GI toxicity is the financial distress that is placed on healthcare systems by MPA due to GI complications (e.g. hospitalization in 20% of patients) and subsequent actions such as dose reduction or discontinuation [75].

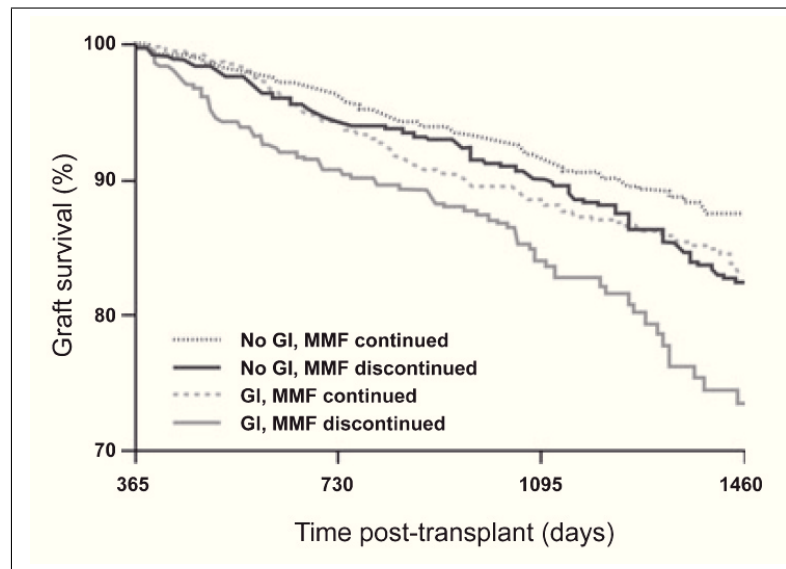


Fig. 1.5: Correlation of GI events, MMF discontinuation, and graft survival. Graft survival over 3 years in patients with or without gastrointestinal complications (GI) after the first year dependent on as to whether MMF was continued or discontinued. Graft survival was significantly lower in the “GI/MMF discontinued” group (70.2%, $p < 0.0001$) and the “GI/MMF continued” group (83%, $p = 0.001$) versus patients without GI complications in whom MMF was continued (87.1%). Graft survival was 82.3% in the group with GI complications who continued MMF ($p = 0.091\%$). Graph and caption taken from [35] and [77], unmodified.

1.2.2 Parts, functions, and features of the GI tract

The GI tract consists of the mouth, pharynx (most parts), esophagus, stomach, small intestine, and large intestine [78, 79] (Fig. 1.6). Associated digestive organs are teeth, tongue, salivary glands, liver, gallbladder, and pancreas. Since it is the goal to discuss MPA’s intestinal side effects, this section focuses on the physiology of the small and large intestine.

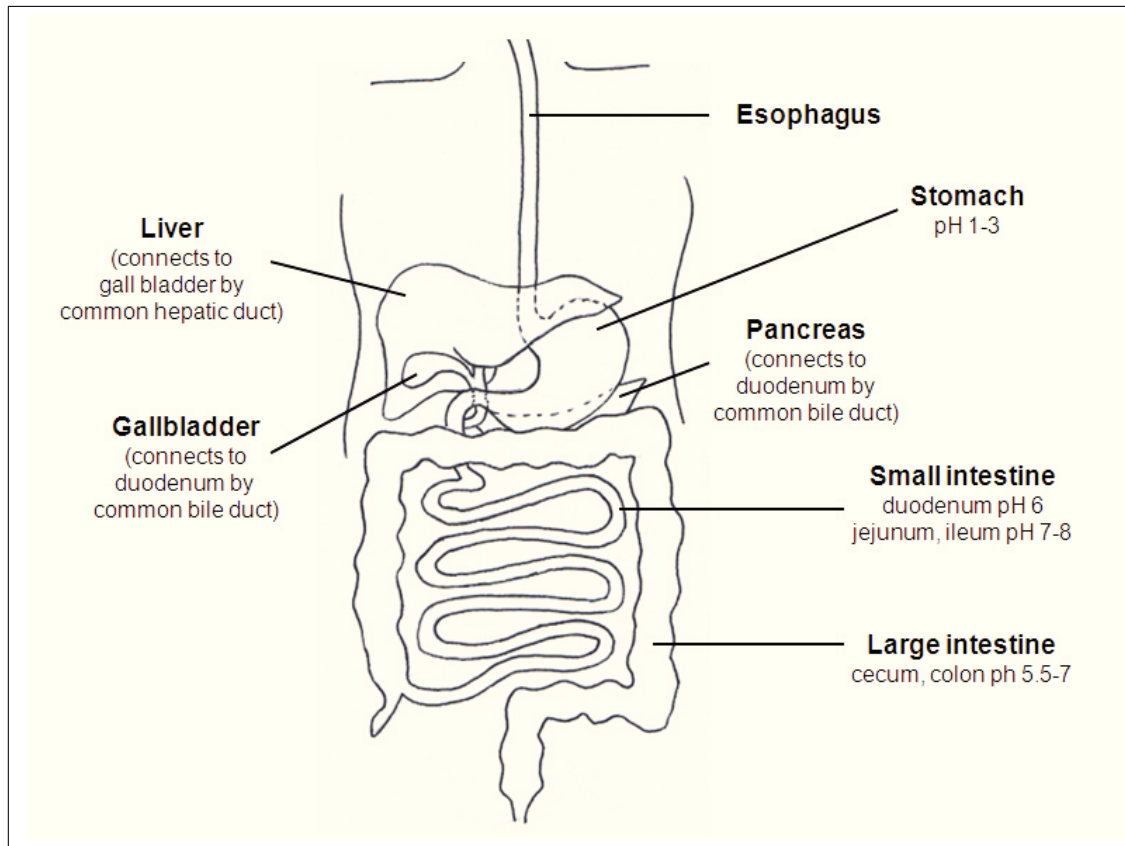


Fig. 1.6: GI tract and supporting organs. *pH values are given for the stomach and portions of the small and large intestine [78–80]. Liver, gallbladder, and pancreas connect to the GI tract. They assist in the digestive process and influence drug metabolism and disposition. Drawing adapted from [81], modified.*

The small intestine

The small intestine is divided into the duodenum, jejunum, and ileum [80, 82] (Fig. 1.6). Absorption mainly takes place in the first portion of the small intestine, the duodenum. Pancreatic and mucosal enzymes break down food components/(pro)drugs for absorption. The products of this process include monosaccharides, amino acids, di- and tripeptides, monoacylglycerols, free fatty acids, vitamins, water, and/or drugs. To be absorbed, material has to pass the mucus layer of the intestine, the epithelium, the *lamina propria*, and the endothelial cells of the capillaries to reach the blood stream [82]. Products reach the liver via the portal vein where they are metabolized further and distributed or excreted.

As depicted in Figure 1.7 the intestinal tube is made up of the tunica serosa, a coat of longitudinal muscle fibers, the myenteric plexus (Auerbach's plexus), a coat

1.2 The GI tract and GI toxicity of MPA

of circular muscle fibers, the *submucous plexus* (Meissner's plexus), the *muscularis mucosa* and the *lamina propria* covered by epithelial cells (Fig. 1.7). Nerves, blood vessels, and lymph vessels span the layers of the small intestine. Kercking's folds, villi, and enterocytic microvilli (brush border) increase the intestinal surface by 300-1600 times.

Enterocytes are responsible for absorption of nutrients and drugs [78, 80]. Inbetween the enterocytes goblet cells secrete mucus to protect and lubricate. Undifferentiated cells in the intestinal glands (crypts of Lieberkuehn) differentiate into villous cells, mucous cells, endocrine and paracrine cells, and immune cells. From the crypts of Lieberkuehn the epithelium of the small intestine is continuously replaced every 3-5 days.

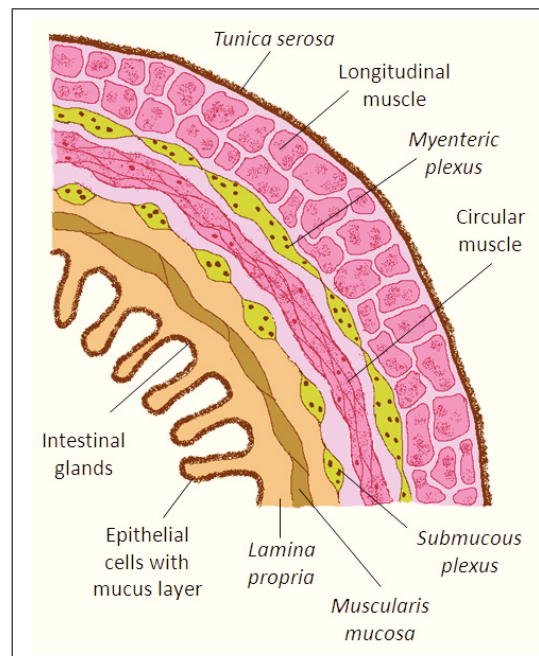


Fig. 1.7: Structure of the small intestine. Drawing adapted from [80], modified.

The large intestine

The large intestine consists of the cecum, colon, and rectum [78, 80] (Fig. 1.6). The main functions include storage of intestinal contents and the absorption of water and electrolytes. Water removal reduces the volume of digestive matter significantly, playing a pivotal role in fluid balance e.g. the development of diarrhea.

Another feature of the large intestine worth mentioning is its bacterial colonization, which is more pronounced than in upper regions of the intestine due to the low pH of

1 Introduction

the stomach acting as a barrier against pathogens (upper small intestine $0-10^4$ /mL, ileum 10^6 /mL, large intestine up to 10^{12} /mL) [83].

1.2.3 Mechanisms and modulation of intestinal inflammation and repair

Similarity of Crohn's disease and MPA GI side effects

Crohn's disease is a chronic inflammation of the gut wall provoked by an inadequate immune response to the commensal microflora [84] and is among the main types of inflammatory bowel disorders (IBD) [85, 86]. Genetic, immunologic, and environmental factors contribute to IBD pathogenesis. MPA GI adverse events generally manifest as Crohn's disease-like enterocolitis (inflammation of the small intestine and the colon) [34, 42, 58, 75, 77]. Diarrhea, abdominal pain, mucosal changes such as ulcers, and submucosal inflammation are some of the frequently occurring characteristics of MPA GI toxicity that are seen in Crohn's disease as well [84]. Crohn's disease can affect all areas of the GI tract but is most commonly located in the terminal ileum [84]. As MPA GI side effects show a pattern very similar to Crohn's disease.

Mucosal epithelial barrier and flora

The alimentary tract possesses remarkable potential to maintain and restore integrity of the mucosal epithelial barrier despite aggressive conditions such as the presence of low pH values, proteolytic enzymes, and noxious substances within the intestinal lumen [87, 88]. Injury to the mucosa/epithelium is frequently occurring even under physiologic conditions (e.g. diet, disease, GI flora, proteases). Fast regeneration is guaranteed by a network of factors involving epithelial restitution (cell migration), proliferation, differentiation, regulatory peptides (growth factors and cytokines), non-peptide molecules (e.g. phospholipids, short-chain fatty acids, adenine nucleotides, trace elements) [87], and other key mediators (nitric oxide, polyamides, eicosanoids) [89].

The bacterial content of the small and large intestine accounts for up to 10^6 and 10^{12} bacteria/mL, respectively [80, 83]. In healthy individuals a viscous mucus layer spanning the epithelium eliminates contact of epithelial cells and these bacteria [83]. Patrolling leukocytes within the layer and probiotic strains growing on the outside offer additional protection of the mucosa. Only in case of a defective mucus layer and compromised mucus barrier function, like in IBD, inflammatory responses occur due

to bacterial (polymicrobial) invasion of the epithelium. The reasons for chronically compromised barrier function in IBD is not known. Factors such as lifestyle, diet, use of detergents and emulsifiers, genetic background etc. seem to influence disease development and progression [83].

Immunological factors of Crohn's disease

Crohn's disease results from an inappropriate immune response of the mucosa to the gut flora [84]. Genetic predisposition and factors that have not been fully determined nor understood have to coincide. Occurrence of intestinal lesions in Crohn's disease can be explained as results of a broadly accepted inflammatory cascade shown in detail in Figure 1.8. Damage of the epithelium allows paracellular transit of bacterial antigens and gut contents to reach the *lamina propria* (1 in Figure 1.8). Macrophages present antigens to T cells, which become activated and start to release pro-inflammatory cytokines (2). Even without passage, bacteria can be caught by dendritic cells through intracellular spaces or toll-like receptors (TLRs) expressed on epithelial cells (3) and lead to activation of T cells (polarization into Th1 and Th17 cells, 4). Different cytokines are involved in the pathogenesis of Crohn's disease among them interferon- γ (INF- γ ; production of interleukin (IL)-12 by macrophages, activation of T cells by IL-12). Neutrophils are recruited by TLRs interacting with luminal antigens and IL-8, which is secreted by the epithelium after stimulation by IL-17 (5). Activated macrophages secrete tumor necrosis factor- α (TNF- α), leading to upregulation of adhesion molecules, aiding more immune cells to access the area of inflammation from the blood vessels (6) and formation of fistulae by overproduction of matrix metalloproteinases (7). TNF- α can also damage the epithelium directly inducing de-epithelization and ulceration (7).

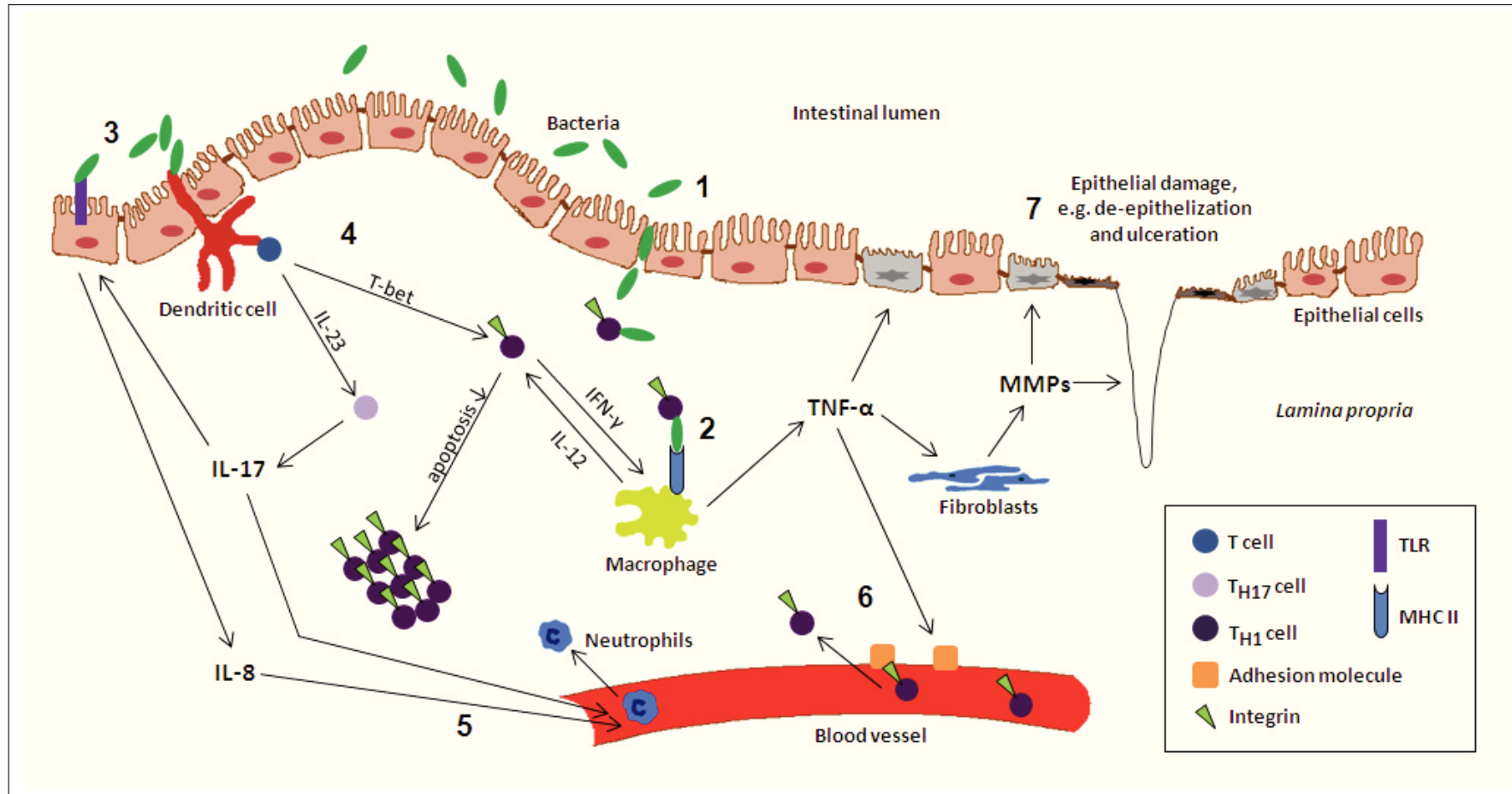


Fig. 1.8: Immune response of the mucosa to the gut flora. *IFN- γ* : interferon- γ , *IL*: interleukin, *MHC*: major histocompatibility complex, *MMPs*: matrix metalloproteinases, *TLR*: toll-like receptor, *TNF- α* : tumor necrosis factor- α , numbers are explained in the text. Drawing adapted from [84], modified.

1.3 Hypothesis, aims of the study, and research strategies

It is hypothesized that MPA promotes GI inflammation by disrupting the GI barrier and allowing bacterial toxins and proteins to penetrate the mucosa as described in Section 1.2.3 in the context of the pathogenesis of Crohn's disease. Luminal and/or intracellular proteins might additionally get covalently modified by MPA and/or MPA metabolites and act as immunogens.

Objectives of the present study were

1. assessment of the potential of LS180 cells as a model for studies on MPA/MMF GI toxicity concerning protein expression and stability of expression over passage numbers,
2. assessment of time- and dose-dependent effects of MPA on the metabolome and proteome of colonic epithelial cells (LS180 cells),
3. assessment of direct toxic effects of MPA and MPA metabolites (especially AcMPAG) on colonic epithelial cells,
4. determination of inflammatory parameters involved in MPA GI toxicity and their direct effects on colonic epithelial cells.

1.3.1 LS180 cell culture model and its qualification

LS180 colonic epithelial cells (adenocarcinoma) were chosen as a model over Caco-2 cells, which is the most commonly used colon carcinoma cell line to study GI drug metabolism and effects [90]. Although LS180 cells are not well characterized [91] they feature expression of pregnane X receptor (PXR) [91, 92], which induces drug metabolizers (CYP3A4) [91] and transporters (MDR1) [91]. Caco-2 cells on the other hand are PXR-deficient [91, 92]. LS180 cells, likewise the Caco-2 cell line [93, 94] express mucin genes [95], which make it possible to include drug treatment effects on certain traits of the GI tract's mucus layer, e.g. epithelial barrier integrity, in LS180 studies if necessary.

Since toxicity of AcMPAG was a central question of this study and LS180 cells turned out to provide a stable and high content of AcMPAG-producing UGT2B7 (Sec. 2.2.1), this cell line was used to investigate MPA-induced effects on cell function and metabolism in detail.

1.3.2 Biomarkers, proteomics, and metabolomics

A biomarker is “a characteristic that is objectively measured and evaluated as an indicator of normal biological processes, pathogenic processes, or pharmacologic response to therapeutic intervention” [96, 97]. For this study a proteo-metabolomic profiling strategy was employed which is generally used for the search of biomarkers to identify disease processes. Within the last decade non-targeted screening technologies and tools in the fields of genetic profiling (transcriptomics), protein profiling (proteomics), and biochemical profiling (metabolomics) have developed rapidly [97, 98]. A combination of these tools was used to gain insight into mechanisms of GI toxicity of MPA on a systematic and comprehensive basis.

While metabolomics is defined as “the quantitative measurement of the time-related multi-parametric metabolic response of living systems to pathophysiological stimuli or genetic modification” [99] proteomics relates to the response of the proteome i.e. “the systematic analysis of all the proteins in any defined biologic compartment” [100] (Fig. 1.9). Metabolic profiling mainly employs techniques such as nuclear magnetic resonance (NMR) spectroscopy and mass spectrometry (MS) [101], proteomic studies usually rely on MS-dependent approaches [100] followed by confirmation of results by immunoblotting [97]. Poor correlation of transcriptomic data and actual changes on the metabolite and/or protein level promotes examination of metabolome and proteome directly without relying on assumptions of transferability of changes determined on the messenger ribonucleic acid (mRNA) level to the metabolite/protein level.

NMR-based studies also provide the possibility to use labeled tracers to examine abnormal metabolic fluxes induced by e.g. drug treatment, toxins, or disease state [102, 103]. Concentrations of small molecule metabolites, lipids, phosphates, and isotopomers can be assessed and provide clues on impairment of metabolic pathways, severeness of medical conditions, mechanisms of toxicity, and related questions. Another advantage of NMR spectroscopy is its non-invasiveness.

MS-based studies on the other hand allow for higher throughput than NMR measurements or RNA micro array tools. MS is also superior in terms of sensitivity than NMR spectroscopy [97]. Scanning the entire metabolome and proteome of a given organism for drug-induced changes is an immense undertaking which has been made possible by improvements in biological MS and bioinformatics over the last 20 years.

1.3 Hypothesis, aims of the study, and research strategies

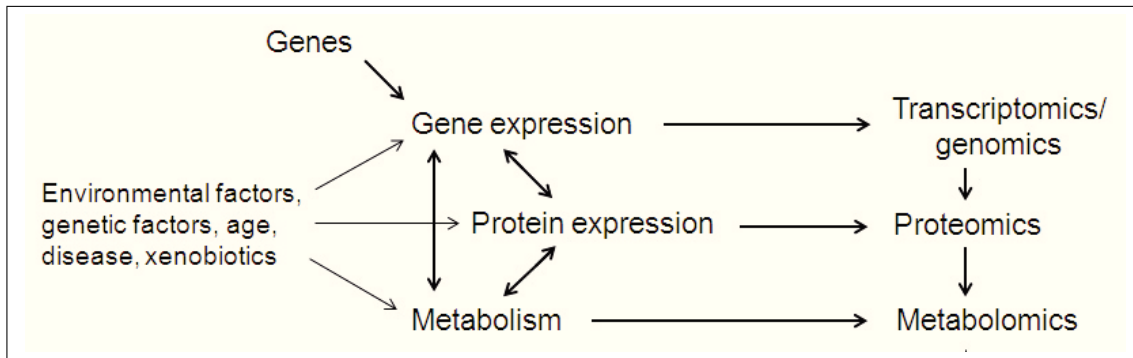


Fig. 1.9: Relationship between transcriptomics (genomics), proteomics, and metabolomics. Adapted from [97], modified.

2 Results and Discussion

2.1 Determination of cell culture treatment conditions

2.1.1 Drug treatment

Oral dosing of drugs is likely to create high local concentrations of the administered compound in the gut lumen [104]. Therefore LS180 cells were treated with compound concentrations from $0.01\mu\text{M}$ up to $250\mu\text{M}$. Considering that 1-1.5g of MPA are given twice daily, dependent on the formulation, even much higher concentrations may occur locally for certain periods of time ($1\text{g MPA/L} = 3.1217\text{mM} = 3121.7\mu\text{M}$, $M_{MPA} = 320.34\text{g/mol}$). While an MMF tablet is likely to dissolve in the stomach already and to release less concentrated MMF suspension into the duodenum, the enteric coating of an EC-MPS capsule dissolves rapidly in the small intestine (Sec. 1.1.5), releases its contents and exposes the epithelium to a high amount of MPA. Due to limited solubility of MMF and MPA in the cell culture medium when spiked from more concentrated stocks in dimethyl sulfoxide (DMSO), $250\mu\text{M}$ was chosen to be the maximum concentration used in most experiments.

For experiments initially conducted, LS180 cell cultures were treated not only with MPA but with MMF, MPA + morpholinoethanol (in combination), and morpholinoethanol as well to cover for all possible variations of drug-induced effects. Neither the metabolic capacity of LS180 cells for MPA and associated compounds was known nor was literature available for differences in metabolism/toxicity of compounds, i.e. MPA versus MMF, in cell culture.

Although tertiary amines are often used as prodrugs to increase a drug's water solubility [105, 106] the morpholinoethanol moiety of MMF seems to be rarely used as most literature on morpholinoethanol prodrugs refers to MMF/MPA. Morpholinoethanol and MPA + morpholinoethanol were therefore included in first experiments, i.e. proliferation assays (Sec. 2.4) and measurements of intracellular nucleotide levels (Sec. 2.5).

2 Results and Discussion

Since the effects on LS180 cells induced by MPA, MMF, and MPA + morpholinoethanol showed consistently the same profiles and no effects on LS180 cells were seen after morpholinoethanol treatment, only MPA treatment was pursued to gain insight into MPA-related mechanisms of toxicity.

Due to very limited stability of the AcMPAG metabolite described in the literature [107], especially under cell culture conditions (37°C, neutral pH, long incubation times up to 72h; please see Section 2.6 for further explanation and preliminary stability studies), in most experiments AcMPAG was not tested directly. Assessment of effects of AcMPAG was a major aim of this study, so that sufficient formation of AcMPAG by LS180 cells was essential. Since LS180 cells were proven to provide a high and stable amount of the UGT2B7 enzyme, via which AcMPAG is formed, incubation of cells was restricted to incubation with MPA.

The MPAG metabolite is universally described as non-toxic [60, 108] (the possibility of covalent modifications of proteins by MPAG is discussed at the end of Section 2.7.2). As MPAG is very polar and only crosses cell membranes erratically no experiments were conducted applying MPAG directly in cell cultures.

2.1.2 Guanosine treatment

After assessment of the first data such as IC₅₀ values (Sec. 2.4) and nucleotide levels (Sec. 2.5) in LS180 cells, the LS180 cell culture model for elucidation of MPA GI toxicity was promoted in terms of mimicking physiological conditions by addition of guanosine to the culture medium. Epithelial cells within the GI tract are known to import nucleotides from the intestinal lumen [109, 110]. Thus, effects of MPA linked to guanosine nucleotide depletion and cell cycle arrest can be reversed by exogenous guanosine [109, 110]. After determination of the most appropriate guanosine concentration, most experiments were conducted by addition of 1000µM guanosine to culture media.

2.2 Validation of the LS180 cell culture model

Human cell lines are a popular model to study *in vitro* biotransformation and transport of drugs [111], especially since it is difficult to discriminate between liver and extrahepatic tissue contribution *in vivo* [112]. For screening of intestinal metabolism, commercially available colon carcinoma cell lines are widely used besides other cell intact systems (e.g. biopsies, precision-cut slices) and subcellular fractions (e.g. mi-

chromosomes) [112, 113].

Human Caco-2 cells are the most commonly used cells to study intestinal drug metabolism and effects [90], followed by LS180 cells [112]. Both cell lines are human colon adenocarcinoma-derived.

Caco-2 cells polarize and differentiate until they form a monolayer with tight junctions and are considered the more physiological model, especially for drug transport and absorption studies [112, 113]. On the other hand expression levels of important drug-metabolizing enzymes and drug transporters differ extremely between Caco-2 cells and the *in vivo* situation present in the small intestine and colon (e.g. low levels for CYP3A4, other CYP enzymes, and MDR1), so that transfection is required to justify the use of Caco-2 cells for prediction of drug metabolism [90, 112, 114]. Low levels [113] or absence [115] of nuclear PXR, which is important for induction of enzymes of low abundance such as MDR1 and CYP3A4, is reported as well [116]. Another significant issue with Caco-2 cells is inter- and intra-laboratory reproducibility [112]. Expression levels of drug-metabolizing enzymes and drug transporters inbetween passage numbers [112, 117] and during cultivation [112, 118] are highly unstable (e.g. 4-fold increase in CYP3A4 expression levels inbetween low and high passage numbers [112, 117]). The long culture time of about 20 days until confluency and morphological and functional differentiation, as well as deficiency of a mucus layer of Caco-2 cells are drawbacks of an otherwise simple and extensively used model for drug screening.

LS180 cells are not as extensively characterized in terms of expression of drug-metabolizing enzymes and drug transporters as Caco-2 cells [112, 113], but some characterization has been published [91, 92, 95, 111–113, 115]. While expression levels of enzymes as CYP3A4 and MDR1 seem to be similar in LS180 and Caco-2 cells, BCRP expression is lower [112]. Overall there seem to be certain advantages and disadvantages for each of the two popular culture models looking at metabolic capacities and comparability to the *in vivo* situation. A very prominent aspect of choice for the appropriate cell culture system was the fact that only the LS180 line offers PXR expression [112, 113] and provides the potential to upregulate/induce expression of important enzymes by PXR as it occurs *in vivo* [113, 116].

It needs to be kept in mind that LS180 as well as Caco-2 cells are of cancerous origin and reveal certain characteristics of cancer tissue such as over/underexpression of certain proteins and a deviant metabolism [113, 119] (Sec. 2.8.2). A major concern is the overexpression of export pumps and metabolizing enzymes in cancer cells establishing drug resistance or at least diminished metabolism of drugs and endogenous compounds [113, 120].

Other intestinal cell lines such as Caco-2 TC7 (Caco-2 cells that have been exposed to methotrexate) or (non-cancerous) lines from the small intestine such as IEC-6 (rat duodenum), IEC-18 (rat ileum), HUTU 80 (human duodenum), HCT 8 (human ileum/cecum), and FHS 74 (human fetal small intestine) have been used as well [112, 121]. All of these cell lines lack one or more crucial characteristic to guarantee general applicability. While insufficient/contradictory biochemical characterization in only a few published studies seems to be an ubiquitous problem, deficiency of important metabolizers and transporters (for IEC-6, IEC-18, HUTU 80, and HCT 8 cells) constituted another criterion for not considering these cell lines for the present study.

Based on a comprehensive literature review, LS180 cells seemed the best model for achieving our study aims. Thus, the first step was a validation of the LS180 cell model to confirm that it can be considered adequate.

2.2.1 Dependency of protein expression on passage number of LS180 cells

Although LS180 cells are well characterized concerning the expression of enzymes/mRNA of enzymes linked to the metabolism of xenobiotics [113, 122–124], enzyme stability over a certain amount of passage numbers has never been assessed for this cell line. In terms of MPA metabolizing enzymes, LS180 cells have been described to provide mRNA and protein expression of all involved UGTs, CYPs, and transporters as well as PXR [113, 122–124].

To ensure LS180 cells are suitable for the studies of MPA transport and metabolism, cells were characterized in terms of the expression of MPA-metabolizing enzymes (UGT1A7/8/9/10, UGT2B7, CYP3A4/5), import transporters (OATP1B1, OATP1B3, OATP2B1), export pumps (MRP1/2, MDR1, BCRP) as well as PXR and IMPDH isoforms 1 and 2, by western blot.

LS180 cells (American Type Culture Collection, ATCC) of unknown passage number N were subcultured and were extracted in passage numbers N+7, N+11, N+15, and N+19 (subsequently referred to as passage numbers 7, 11, 15, and 19) and subjected to western blot or quantitative polymerase chain reaction (QPCR) analysis. Western blots and the expression levels of MPA metabolizing enzymes are shown in Figure 2.1 and Figure 2.2, respectively. Expression levels of MPA transporting enzymes and pharmacodynamic target proteins of MPA are shown in Figure 2.3 - Figure 2.6. UGT1A8 stability could not be assured directly, but mRNA levels be-

tween passages were compared. For BCRP neither enzyme nor mRNA stability could be ensured, due to unsatisfying results in western blots (lack of an appropriate antibody) and QPCR data (most likely due to not optimally designed primers). Since all other enzymes were stable over passage numbers, BCRP content was assumed to be stable over checked passages as well and not investigated further.

Cell proliferation assays for MPA, MMF, MPA + morpholinoethanol, and morpholinoethanol were carried out using cells in passage numbers 7 and 23, respectively, to ensure that no apparent alterations in drug metabolism in LS180 cells occur due to age of the cell culture (data for passage number 7 shown in Figure 2.14 in Section 2.4, data for passage number 23 not shown). Proliferation of cells of low passages compared to high passages did not show profound differences.

Stabilities of cell lines over passage numbers has often been evaluated, but is not always a routine procedure to validate a cell culture model. While certain cell lines are characterized over a long period of time/multiple passage numbers (e.g. up to 150 [126]), others (especially primary cultures) can only be surveyed for shorter periods (e.g. 10 or even less passage numbers [127]). Here, LS180 cells were evaluated over 12 passages to establish stability for the experiments performed. The relatively short time of evaluation of 12 passages makes it difficult to compare results to Caco-2 cells. Passage numbers termed “high” and “low” generally span a longer time frame (with passage numbers around 30 typically considered low, around 100 high [112, 128]). Changes occurring in Caco-2 cells over time affect cell morphology [112, 128], as well as diffusion characteristics and most problematic for studies on drug transport and drug metabolism, transporters, and other enzymes expressed in the brush border [128]. Their faster proliferation rate (Sec. 3.2.1), time until confluency of the culture (about 3 days for LS180 cells versus about 20 days for Caco-2 cells after subcultivation), and less distinct morphological and functional differentiation during cultivation [112], makes it easier to maintain homogeneity of LS180 than of Caco-2 cells during experiments.

2.2.2 Influence of MPA treatment on expression levels of enzymes involved in MPA metabolism in LS180 cells

A standard parameter of evaluating a drug’s properties in terms of absorption, distribution, metabolism, and excretion *in vivo* involves screening of the drug’s impact on transporters and conjugating enzymes as drug-induced changes can significantly

2 Results and Discussion

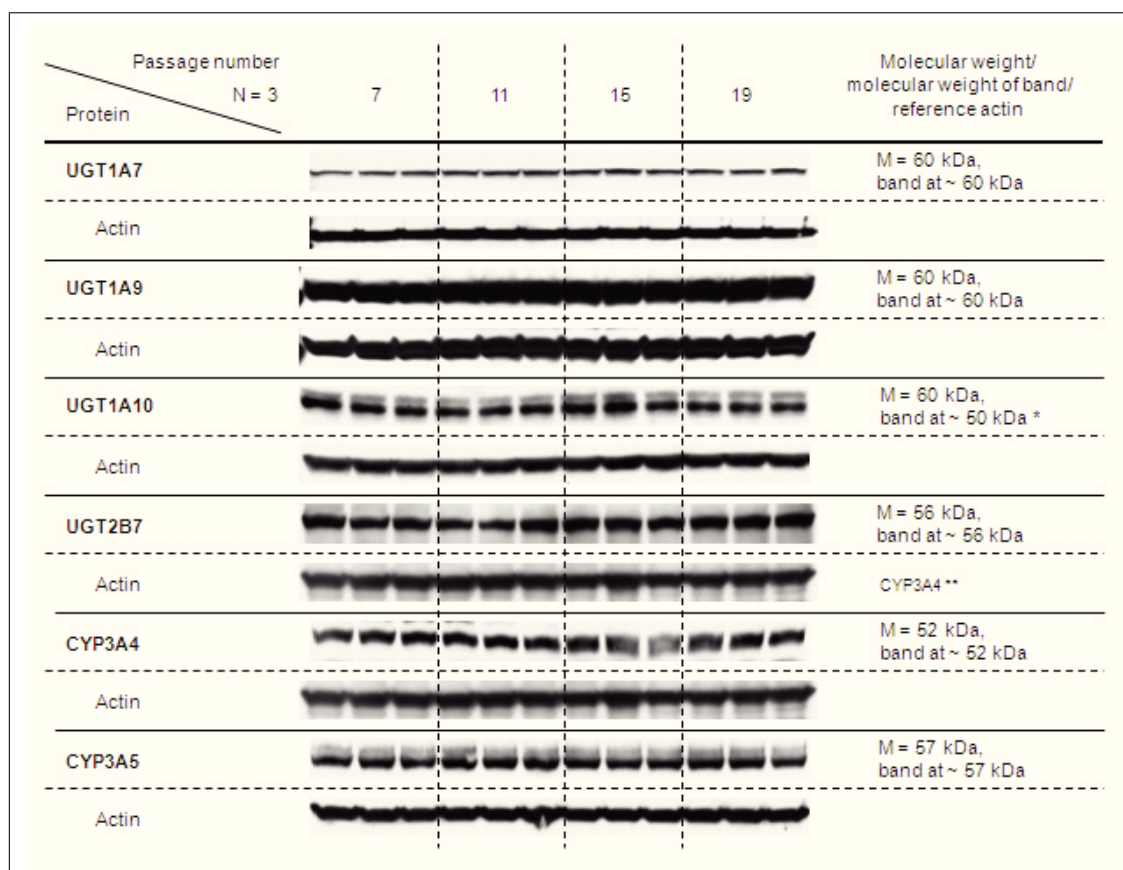


Fig. 2.1: Western blots for determination of expression levels of MPA-metabolizing enzymes in LS180 cells in passages 7, 11, 15, and 19. Bands are shown with their respective β -actin bands (N=3). Relative intensities as determined by densitometry analysis normalized based on β -actin are shown in Figure 2.2. M: molecular weight, *: difference between actual and predicted band size probably due to post-translational modifications, post-translational cleavage, splice variants, relative charge or multimerization [125], **: due to cutting/stripping of the membrane the same β -actin band served for the normalization of multiple proteins.

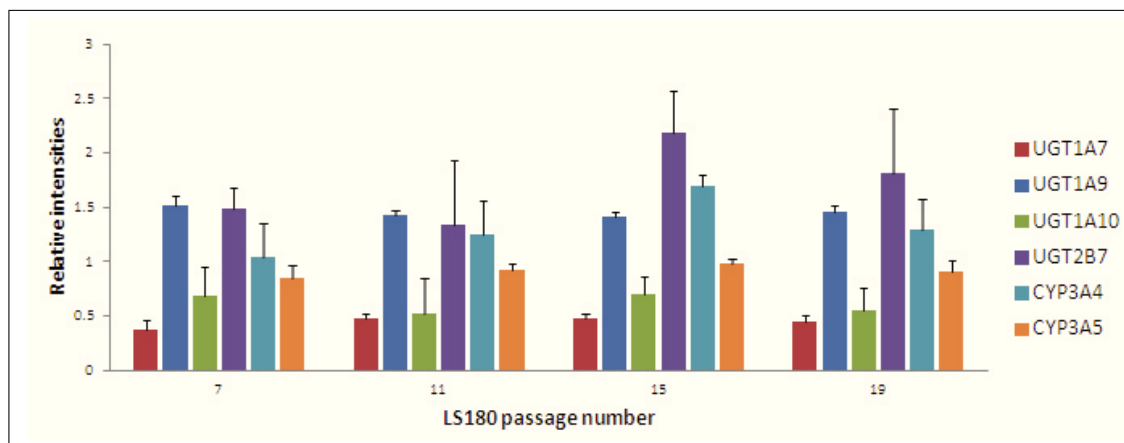


Fig. 2.2: Expression levels of MPA-metabolizing enzymes in LS180 cells in passages 7, 11, 15, and 19 as determined by densitometry analysis. Intensities were normalized based on β -actin ($N=3$). Western blots with their respective β -actin bands are shown in Figure 2.1. No statistically significant differences in expression levels were found among passage numbers as determined using one-way ANOVA in combination with Scheffe's *post – hoc* test.

change PK properties, efficacy, and toxicity [129].

LS180 cells were treated with increasing concentrations of MPA as described in Section 2.1.1 in detail. As the here presented induction studies were performed at the beginning of the project, for these experiments cell culture media were not supplemented with guanosine.

Western blots (not shown) of LS180 lysates were performed after 24h of MPA treatment for drug-metabolizing enzymes directly involved in MPA metabolism (UGT1A7/9/10, CYP3A4/5, except for UGT1A8), efflux pumps (MRP1/2, MDR1, except BCRP), and IMPDH isoform 1 and 2.

Expression levels did not change significantly after 24h of MPA treatment, although many xenobiotics frequently induce proteins necessary for their detoxification in normal and especially in cancer tissue [130]. After 24h a trend towards increased IMPDH2 expression ($p=0.192$) was observed. As IMPDH1 is prevalent in most normal tissues, IMPDH2 is predominant and constantly upregulated in neoplastic and fast replicating tissue [40]. The trend towards overexpression of isoform 2 might be attributable to the cancerous nature of LS180 cells or guanosine nucleotide depletion which has been reported to lead to upregulation of IMPDH gene expression [131, 132].

2 Results and Discussion

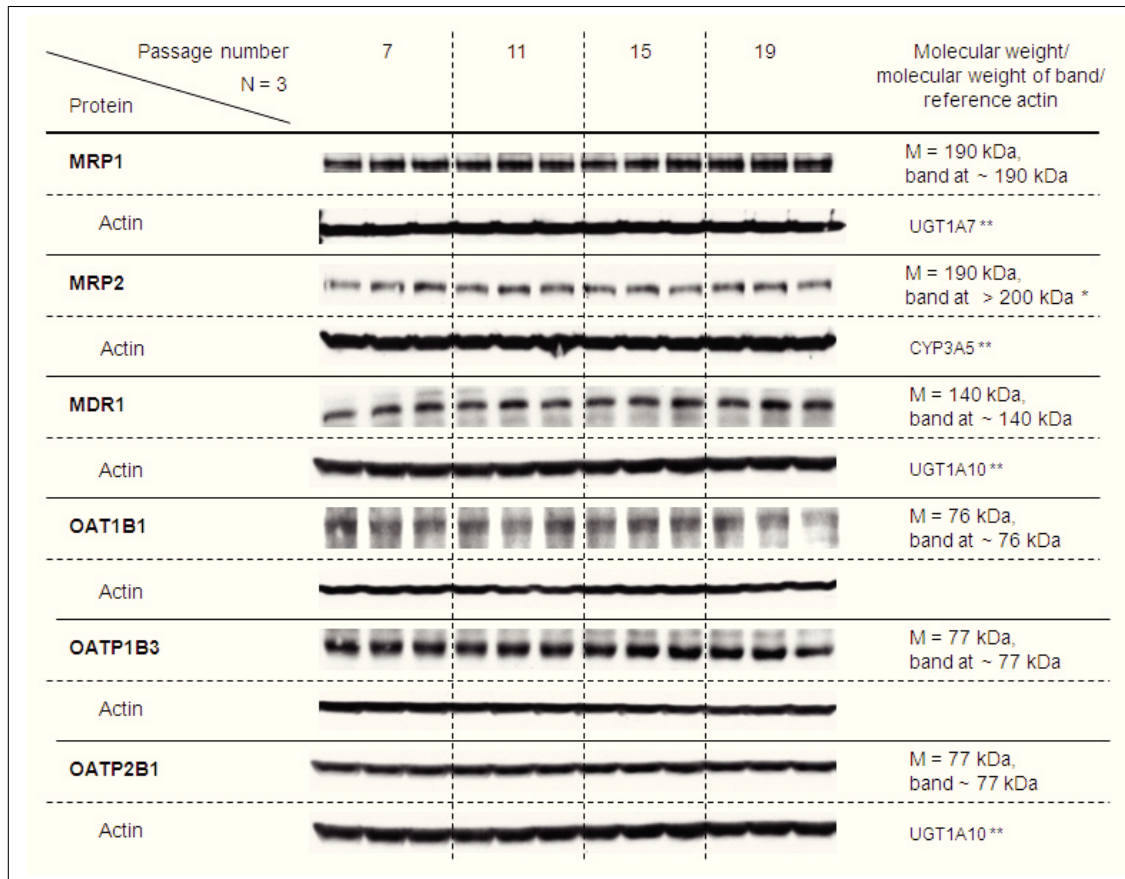


Fig. 2.3: Western blots for determination of expression levels of transporters of potential relevance for MPA in LS180 cells in passages 7, 11, 15, and 19. Bands are shown with their respective β -actin bands (N=3). Relative intensities as determined by densitometry analysis normalized based on β -actin are shown in Figure 2.4. M: molecular weight, *: difference between actual and predicted band size probably due to post-translational modifications, post-translational cleavage, splice variants, relative charge or multimerization [125], **: due to cutting/stripping of the membrane the same β -actin band served for the normalization of multiple proteins.

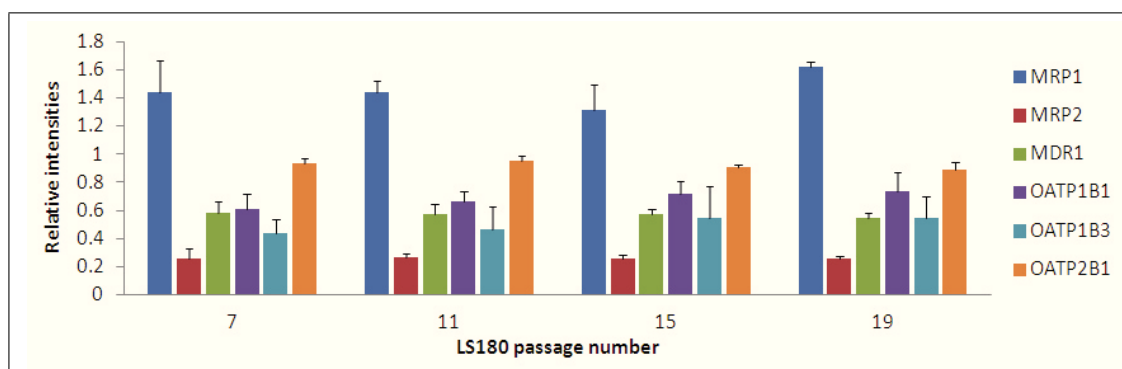


Fig. 2.4: Expression levels of transporters of potential relevance for MPA in LS180 cells in passages 7, 11, 15, and 19 as determined by densitometry analysis. Intensities were normalized based on β -actin ($N=3$). Western blots with their respective β -actin bands are shown in Figure 2.1. No statistically significant differences in expression levels were found among passage numbers as determined using one-way ANOVA in combination with Scheffe's *post – hoc* test.

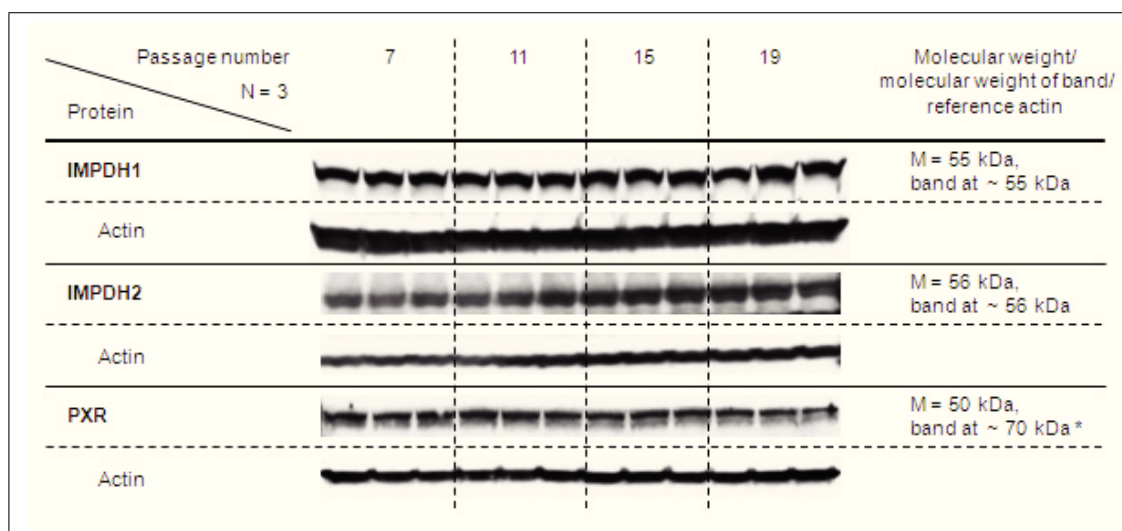


Fig. 2.5: Western blots for determination of expression levels of pharmacodynamic target proteins of MPA in LS180 cells in passages 7, 11, 15, and 19. Bands are shown with their respective β -actin bands ($N=3$). Relative intensities as determined by densitometry analysis normalized to β -actin are shown in Figure 2.6. M: molecular weight, *: difference between actual and predicted band size probably due to post-translational modifications, post-translational cleavage, splice variants, relative charge or multimerization [125].

2 Results and Discussion

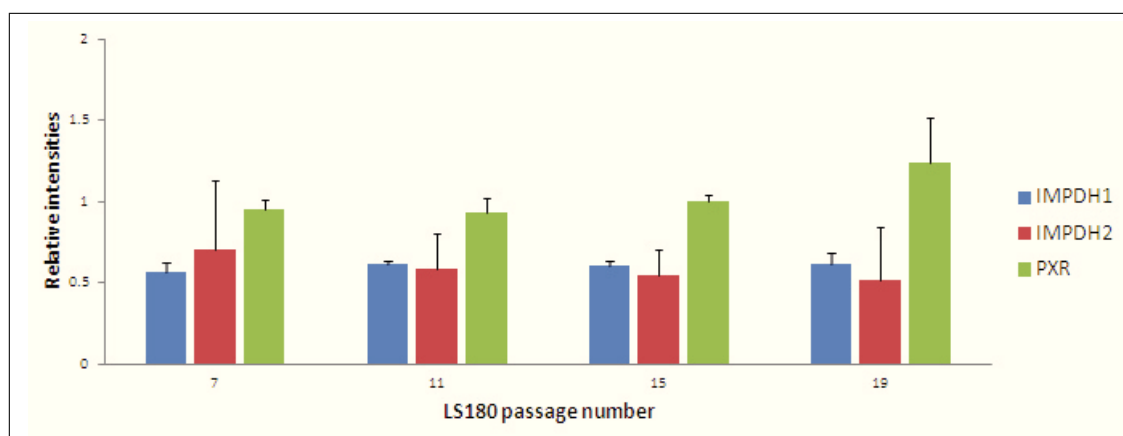


Fig. 2.6: Expression levels of pharmacodynamic target proteins of MPA in LS180 cells in passages 7, 11, 15, and 19 as determined by densitometry analysis. Intensities were normalized based on β -actin ($N=3$). Western blots with their respective β -actin bands are shown in Figure 2.1. No statistically significant differences in expression levels were found among passage numbers for the studied target proteins as determined using one-way ANOVA in combination with Scheffe's *post – hoc* test.

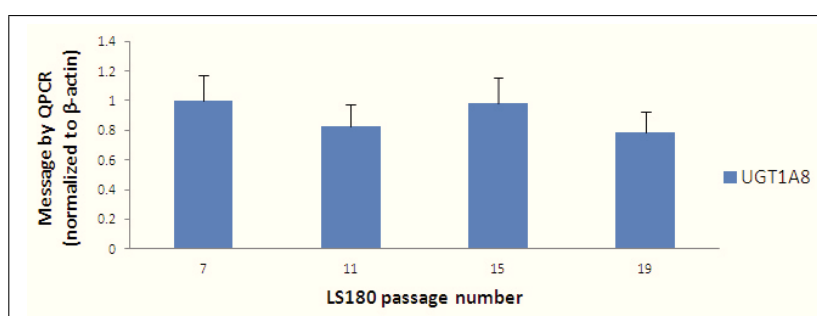


Fig. 2.7: Change in UGT1A8 message in LS180 cells in passages 7, 11, 15, and 19. Message measured using QPCR was normalized based on β -actin ($N=3$). No statistically significant differences in mRNA levels were found among passages for UGT1A8 as determined using one-way ANOVA in combination with Scheffe's *post – hoc* test.

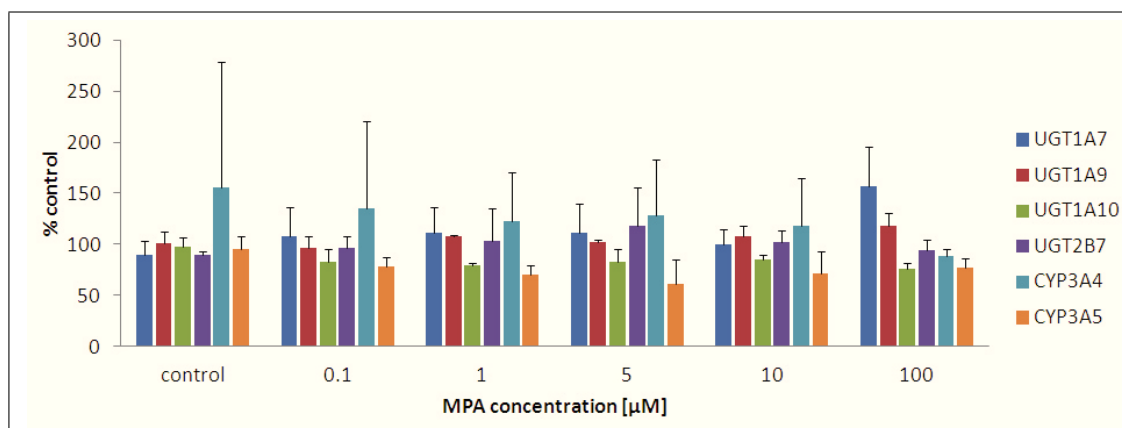


Fig. 2.8: Expression levels of MPA-metabolizing enzymes in LS180 cells after 24h of MPA treatment as determined by densitometry analysis. Intensities were normalized based on β -actin ($N=3$). Western blots with their respective β -actin bands are not shown. There were no statistically significant differences in expression levels of the studied MPA-metabolizing enzymes after 24h of MPA treatment as determined using one-way ANOVA in combination with Scheffe's post – hoc test.

Additional western blots (not shown) were performed after 72h treatment (single dose of MPA) for efflux transporters such as MRP1/2 and MDR1 that are known to be frequently upregulated in tissues exposed to xenobiotics (such as drugs or toxins). After 72h MDR1 expression was significantly upregulated by almost 3.5-fold after treatment with single doses of $100\mu\text{M}$ and $250\mu\text{M}$ MPA ($334.0 \pm 59.0\%$ and $343.6 \pm 33.6\%$) and a gradual increase could be seen for smaller doses as shown in Figure 2.10. No such changes were found for MRP1 or MRP2.

A marked upregulation of MDR1 protein expression or mRNA expression can be seen often in epithelial *in vitro* models treated with MDR1 substrates [104, 130]. An upregulation in LS180 cells has been observed before in the presence of many other drugs such as rifampicin, phenobarbital, clotrimazole, reserpine, and isosafrole before potentially decreasing their intracellular residence time [130, 133]. Upregulation of MDR1 is also commonly observed *in vivo* [134], in other *in vitro* models, as well as PK computational models [135].

In conclusion, LS180 cells are stable over the tested passage numbers including all drug-metabolizing enzymes, drug transporters, and pharmacodynamic target proteins relevant for the present study. Based on these results and the literature on

2 Results and Discussion

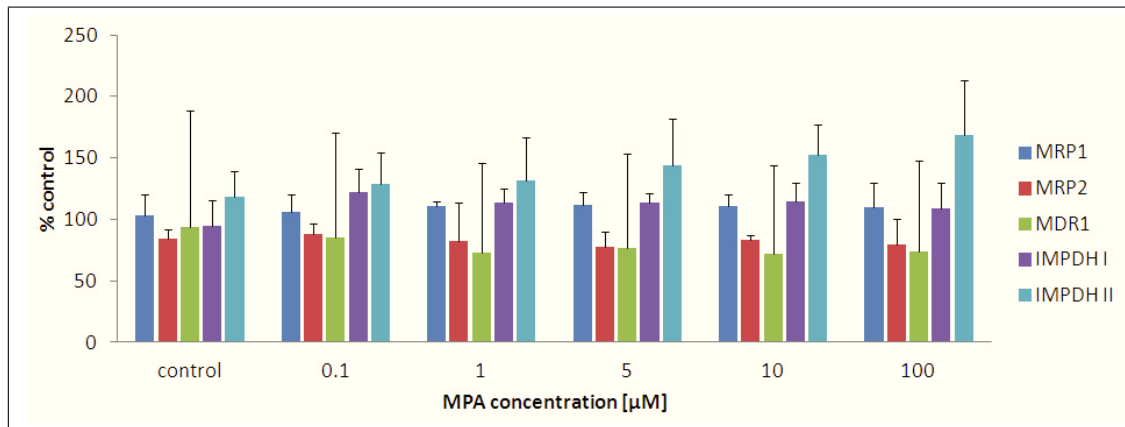


Fig. 2.9: Expression levels of MPA efflux transporters and IMPDH isoform 1 and 2 in LS180 cells after 24h of MPA treatment as determined by densitometry analysis. Intensities were normalized based on β -actin ($N=3$). Western blots with their respective β -actin bands are not shown. There were no statistically significant differences in expression levels of the studied transporters after 24h of MPA treatment as determined using one-way ANOVA in combination with Scheffe's post – hoc test.

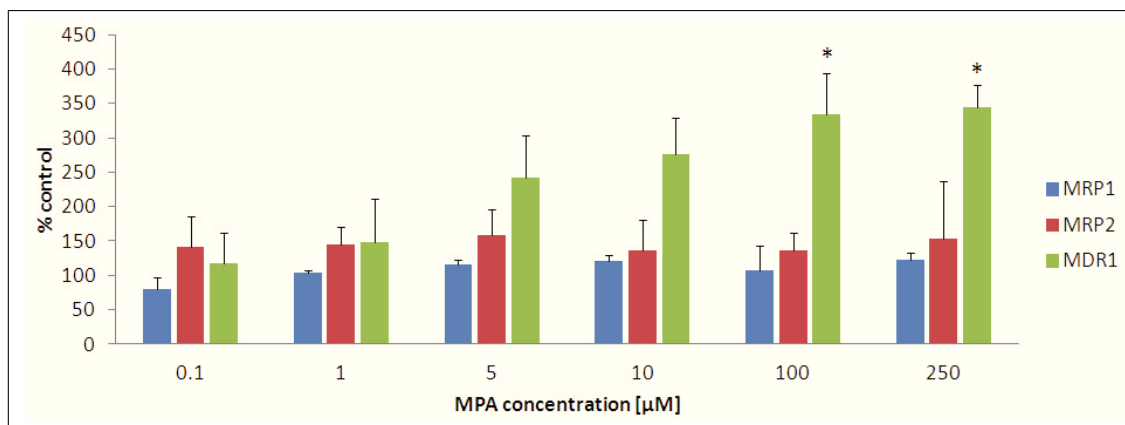


Fig. 2.10: Expression levels of MPA efflux transporters MRP1, MRP2, and MDR1 in LS180 cells after 72h of MPA treatment as determined by densitometry analysis. Intensities were normalized based on β -actin ($N=3$). Western blots with their respective β -actin bands are not shown. Differences in expression levels of the studied transporters after 24h of MPA treatment were determined using one-way ANOVA in combination with Scheffe's post – hoc test with *: $p<0.05$).

LS180 cells, these cells were considered a valid model to study MPA metabolism and toxicity over the passages tested.

2.3 Cytotoxicity of MPA

Incubating cells with a compound that possibly has cytotoxic properties, two different mechanisms of cell death can occur [136, 137]. Necrosis, the “accidental” cell death is defined by alterations in plasma membrane permeability, i.e. spontaneous cell lysis and extrusion of intracellular compounds. Apoptosis, the “normal” cell death removes unwanted or old cells in a controlled way.

To rule out major cytotoxic effects of the MPA concentrations used the necrotic and apoptotic potential of MPA on LS180 cells was determined individually.

2.3.1 Necrotic potential of MPA

During necrosis cell damage and lysis occur. The soluble enzyme lactate dehydrogenase (LDH) is released from the cytosol into the cell culture medium. LDH activity measurement can be used to indicate the amount of necrosis in a cell culture [138].

To determine necrotic effects of MPA on LS180 cells were incubated with 0.01, 0.1, 0.5, 1, 5, 10, 50, 100, and 250 μ M MPA. Assays were carried out for 24h, 48h, and 72h for comparison with cell proliferation assays (described in Section 2.4 and Section 3.2.2) and to provide the opportunity to adjust proliferation assay data in case of cytotoxic potential of MPA. For one set of cytotoxicity assays, cells were not redosed for potentially released LDH to accumulate in the cell culture media for 24h, 48h, and 72h, respectively. A second set of assays was run for which cells were redosed every 24h to test if a second/third dose puts additional stress on LS180 cells as measured by LDH leakage. For this set values represent the amount of LDH that leaked into the cell culture supernatants in the time period from 24h to 48h after the second dose of MPA after 24h (48h redosed) and in the time period from 48h to 72h after the third dose of MPA after 48h (72h redosed). Results calculated as percentages of controls (% control in figures/graphs) are shown in Figure 2.11 for the five different experiments.

Cell numbers were not compromised by morpholinoethanol in the CyQUANT NF Cell Proliferation Assays (Sec. 2.4), which would have revealed cytotoxic properties of morpholinoethanol. Thus, no further cytotoxicity assay was run for this com-

2 Results and Discussion

pound. For the same reason no cytotoxicity assays were run for MMF and MPA + morpholinoethanol as their proliferation profiles matched the profile of MPA.

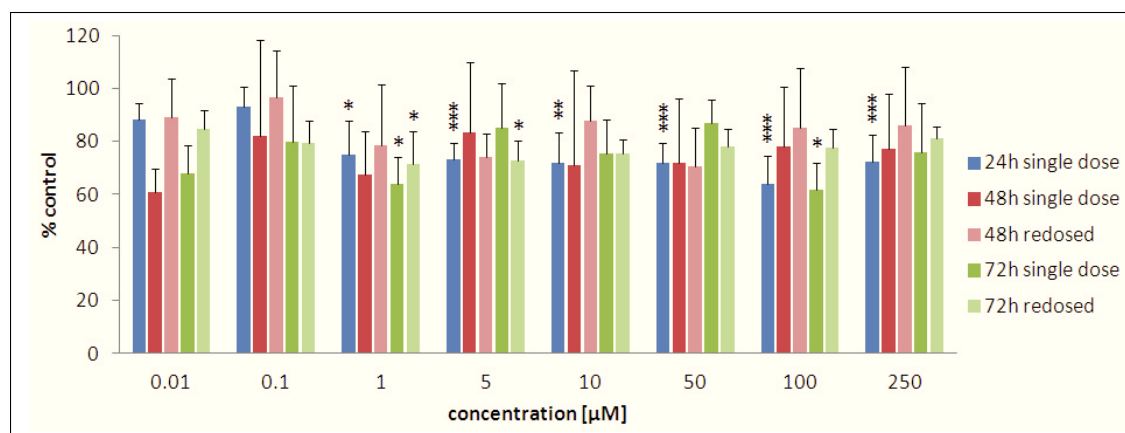


Fig. 2.11: LDH activity in cell culture media of LS180 cells after treatment with a single dose and multiple doses of MPA for 24h, 48h (single dose and redosed every 24h), and 72h (single dose and redosed every 24h). Values are given as means of % of controls with standard deviations ($N=6$). Significance was determined using one-way ANOVA combined with Scheffe's *post-hoc* test with *: $p<0.05$; **: $p<0.005$; ***: $p<0.001$ versus controls. Values were calculated from LDH activities and normalized to fluorescence intensities (cell numbers) as measured using the CyQUANT NF Cell Proliferation Assay.

As shown in Figure 2.11 LDH activity values in culture media of LS180 cells were $<100\%$ of values of controls for all MPA concentrations in all five experiments, although LDH activities were normalized to cell content per well measured by the CyQUANT NF Cell Proliferation Assay. Assays were run without addition of fetal bovine serum (FBS) to the culture media to avoid interference since FBS contains LDH. Withdrawal of FBS is generally used to growth arrest cultured cells [139]. LDH activities ranged from 7mU/mL (controls) to 3mU/mL for 24h assays and assays that were redosed every 24h, while values ranged from 28mU/mL to 18mU/mL for 48h and 72h for single dose assays. Proliferation rates were widely unaffected due to growth arresting LS180 cells by FBS withdrawal. Only in case of the redosed 72h assays, proliferation rates dropped from $100\pm 3.5\%$ (controls) to $91.4\pm 4.6\%$ ($250\mu\text{M}$ MPA, not statistically significant versus controls).

The decreased LDH activities in LS180 culture media after MPA treatment with low and high concentrations are most likely caused by growth inhibition via IMPDH inhibition by MPA (cells get arrested in the S phase of the cell cycle [140]). Control cells, without IMPDH inhibitor, keep multiplying with a demand for nutrients usu-

ally provided by addition of 10% FBS to the culture media. Although withdrawal of FBS is widely used for growth arresting, a slight increase of necrosis due to FBS withdrawal cannot be ruled out completely. It was not possible to assess the effects of FBS withdrawal on LS180 cells using this specific cell culture assay due to the interference of FBS with the assay. No changes between different MPA concentrations, especially in comparison with changes occurring between controls and low MPA concentrations, were seen. Thus, MPA does not seem to induce necrosis in LS180 cells within the time and dose ranges used for subsequent experiments. This was further confirmed by the fact that no dead cells/cell debris were observed in the culture media at any time throughout the experiments.

Dependent on species, tissue, cell type, exposure time, and dose *in vitro* data on MPA cytotoxicity (and effects generally) differ widely. Another fact complicating comparison of the present data with the current literature is the limited amount of research and publications on MPA and MPA toxicity in cultured cells. Concentrations used in most studies were within or slightly above the therapeutic range of MPA (up to $10\mu\text{M}$) [109, 110, 139, 141]. Concentrations as high as expected in the vicinity of mucosa cells and tested in our studies are relatively rarely described. While in many studies significantly decreased cell survival can be seen with fairly low concentrations of MPA, addition of guanosine to the cell culture media reverses effects of MPA and MPA's cytotoxic effects that can be attributed to depletion of guanosine nucleotides [109, 110]. Guanosine depletion due to MPA obviously has a less fatal effect on LS180 cells than on other cell types. This might be partly attributable to LS180 cells not being primary cells as no cytotoxic effects were seen in other immortalized cell lines before [141, 142]. Changes in metabolism and drug transport due to the cancerous origin of LS180 cells (p53 inactivation in cancers and MDR1 overexpression as described in Sec. 2.2.2 leading to selective drug resistance) could be a reason as well [143]. Kaczmarek et al. also did not find any evidence for cytotoxic effects of MPA at concentrations as high as $250\mu\text{g/mL}$ ($=780\mu\text{M}$) in another human epithelial cell line (human retinal pigment epithelial cells, ARPE19) after 24h and 72h incubation using the 3-(4,5-dimethylthiazol-2-yl)-2,5-diphenyltetrazolium bromide (MTT) assay to test antiproliferative and cytotoxic effects of MPA [142].

2.3.2 Apoptotic potential of MPA

Cleavage of caspase-3 is crucial in programmed cell death (apoptosis) and activated p17 and p12 fragments resulting from cleavage of caspase-3 show induction of apoptosis [144]. Western blots using a caspase-3 antibody detecting full length caspase-3

2 Results and Discussion

of 35kDa and the 17kDa and 19kDa fragments were employed to assess apoptotic properties of MPA on LS180 cells.

LS180 cell lysates from previously performed experiments of cultures incubated with increasing concentrations of MPA (0.1, 1, 5, 10, 100, 250 μ M MPA and controls incubated with 0.5% DMSO) and 1000 μ M guanosine and no FBS for 3h, 24h, and 72h (redosed every 24h) were used for caspase-3 western blots. These conditions were chosen after evaluation of the LS180 cell culture model in terms of addition of guanosine, redosing with MPA and guanosine, and MPA as described in the previous section. Additional lysates of cultures treated with 500 μ M and 1000 μ M MPA (control incubated with 2% DMSO) were prepared for the 3h incubation to also test high local concentrations potentially occurring for short time periods in the duodenum after administration of EC-MPS.

Caspase-3 western blots are shown in Figure 2.12 and the corresponding densitometry analysis is shown in Figure 2.13. After incubation with MPA for 3h only full length caspase-3 was present in LS180 lysates (Fig. 2.13). The amount of caspase-3 covered about 100% of the values of controls for all samples even for concentrations of 500 μ M and 1000 μ M MPA. After 24h and 72h p17 and p12 fragments of caspase-3 were visible in western blots. For cleavage of caspase-3 occurring in controls as well as in treated samples, relative intensities were expressed as % of controls. Ratios of cleaved to total (cleaved + uncleaved) caspase-3 are presented as well (also shown as % of controls).

None of the changes in uncleaved or cleaved caspase-3 levels or ratios of cleaved to total caspase-3 reached statistical significance. All values were elevated (full length and cleaved caspase-3 as well as the ratio uncleaved/total caspase-3; except for 10 μ M MPA 72h cleaved and uncleaved/total caspase-3 which were <100% of control values) with peak values around 150% of controls for MPA concentrations in the medium range (for cleaved and uncleaved/total caspase-3 after 24h and 27h treatment). 3h values for full length caspase-3 ranged from 100 \pm 2.1% and 100 \pm 15.8% for controls (0.05% and 2% DMSO, respectively) to 112.0 \pm 15.1% for 1000 μ M MPA. Although no statistically significant change was found, a trend towards increased expression of full length caspase-3 can be seen after 3h incubation with MPA. This trend was observed after 24h and 72h as well, but less pronounced. Very distinct trends towards increases in cleaved caspase-3 levels were detected for 17kDa and 19kDa fragments after 24h and 72h (Fig. 2.12).

As for data on MPA-induced necrosis, almost no literature can be found for MPA-induced apoptosis in human intestinal cell lines. No data on LS180 or Caco-2 cells is available. Findings in examined cell lines (often lymphocytes [145] or other blood cells [146], that are dependent on *de novo* guanosine synthesis and cannot utilize exogenous guanosine as efficiently as other cell types) differ widely and are hard to compare to findings in the LS180 cell model.

Many publications report induction of apoptosis by MPA *in vitro* in cells of non-cancerous [145, 146] and cancerous origin, e.g. neuroblastoma [147, 148] and leukemia cells [149]. The common cause of induction seems to be guanosine nucleotide depletion [148, 149]. Very few publications are available that report no apoptotic potential of MPA [150] (article in Chinese, only abstract in English).

The lack of MPA-induced apoptosis can be caused by multiple factors or by an interplay of factors. LS180 cells were supplemented with 1000 μ M guanosine, which is often neglected in *in vitro* experiments [148, 149]. Although intracellular nucleotide concentrations in LS180 cells are unbalanced despite supplementation with 1000 μ M guanosine of the growth medium (please see Section 2.5.2), 1000 μ M guanosine may have had an ameliorating effect on the induction of apoptosis. FBS depletion of the culture media most likely had no effect on LS180 cells treated with MPA, as described and depicted in Section 2.3.1. Another reason might be the cancerous origin of LS180 cells. Overexpression of MDR1 leading to multidrug resistance (already described in Section 2.2.2 and Section 2.3.1), which was specifically shown for LS180 cells treated with a single dose of MPA for 72h (Sec. 2.2.2), could diminish apoptotic potential of MPA in LS180 cells. Overexpression of OATP1B3, with increases up to 100-fold in colorectal cancers [120], may have antiapoptotic effects due to altered p53-dependent pathways [120] and could enhance cell survival as well. Additionally an antiapoptotic effect of PXR was found in human colon cancer cells as well as normal mouse colon epithelium, which may occur in LS180 cells as well [151].

Cytotoxicity tests showed very little to no cytotoxic effects of MPA concentrations up to 250 μ M (in case of short term apoptosis studies even up to 1000 μ M) on LS180 cells under the different conditions tested (no use of FBS, no necrosis even without supplementation with exogenous guanosine, no significant apoptosis/cleavage of caspase-3 compared to controls with 1000 μ M exogenous guanosine).

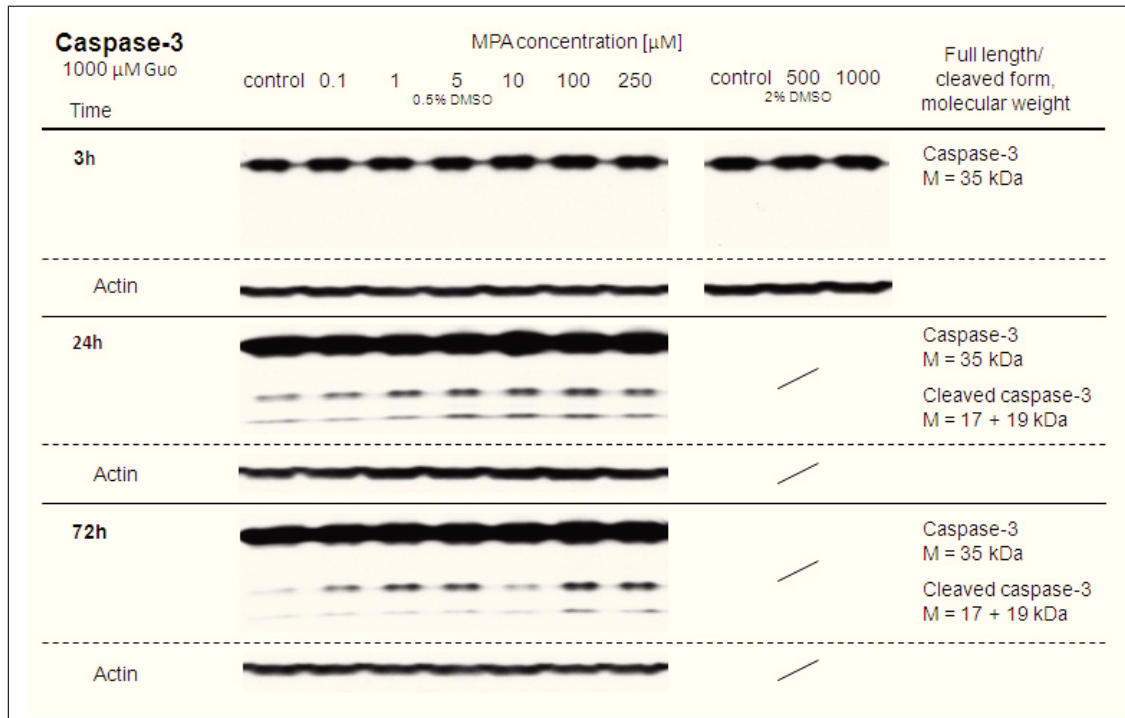


Fig. 2.12: Western blots for determination of expression levels of caspase-3 and levels of cleaved caspase-3 in LS180 cells after treatment with increasing concentrations of MPA and 1000 μ M guanosine for 3h (8 MPA concentrations), 24h, and 72h (6 MPA concentrations). Caspase-3 gave a band at 35kDa, cleaved caspase-3 gave bands at 17kDa and 19kDa. Bands are shown with their respective β -actin bands (N=3). Relative intensities as determined by densitometry analysis were normalized based on β -actin and calculated as % of controls are shown in Figure 2.13.

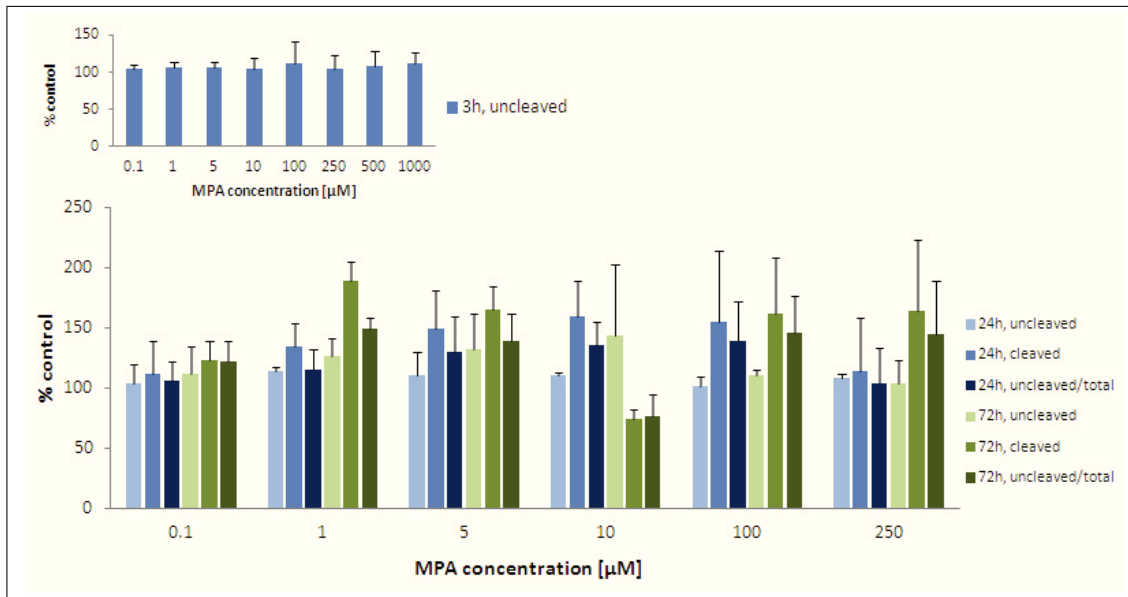


Fig. 2.13: Expression levels of caspase-3 and levels of cleaved caspase-3 in LS180 cells after treatment with increasing concentrations of MPA and 1000 μM guanosine for 3h (8 MPA concentrations), 24h, and 72h (6 MPA concentrations) as assessed using densitometry of western blots. Values are given as means of % of controls of relative intensities as determined by densitometry analysis normalized based on β -actin for uncleaved caspase-3 (35 kDa), cleaved caspase-3 (sum of intensities of bands at 17 and 19 kDa), and the ratio of uncleaved to total caspase-3 (sum of intensities of bands at 17, 19, and 35 kDa) ($N=3$). Western blots with their respective β -actin bands are shown in Figure 2.12. No statistically significant differences in caspase-3 expression levels versus controls were found in LS180 cells after treatment with increasing concentrations of MPA and supplementation with 1000 μM guanosine for 3h, 24h, and 72h as determined using one-way ANOVA in combination with Scheffe's *post – hoc* test.

2.4 Antiproliferative properties

Cell proliferation of LS180 cells exposed to increasing concentrations of MPA, MMF, MPA + morpholinoethanol, and morpholinoethanol was measured using CyQUANT NF Cell Proliferation Assays. This assay relies on a fluorescent dye that binds to cellular DNA, the amount of which is closely related to cell number, and allows to assess proliferation rates by measuring fluorescence intensities.

Since the CyQUANT NF Cell Proliferation Assay estimates cell numbers by measuring DNA content of a sample, it identifies impairment of cell populations caused

2 Results and Discussion

by cell proliferation inhibition as well as cytotoxicity. A contribution of necrosis or apoptosis to decreases in cell numbers, that may be caused by MPA's antiproliferative properties, was evaluated and widely ruled out by LDH assays and measurement of caspase-3 and cleaved caspase-3 levels (Sec. 2.3). The assay outcome should therefore depend on cell proliferation exclusively.

LS180 cells were incubated with MPA, MMF, MPA + morpholinoethanol, and morpholinoethanol at concentrations of 0, 0.01, 0.1, 0.5, 1, 5, 10, 50, 100, and 250 μ M. Two sets (single dose and redosed every 24h) were run for 48h and 72h incubations. Incubation times of at least 48h were chosen for first experiments to reliably allow for detecting differences in data for LS180 cell proliferation rates (doubling time of 51.1 ± 2.7 hours for LS180 cells, Sec. 3.2.1). Fluorescence readings were calculated as % of controls.

Data for single dose studies are shown in Figure 2.14. Data for studies in which cells were redosed every 24h are shown in Section 2.4.1 for cells treated with and without exogenous guanosine and MPA (Fig. 2.16).

Since decreases in cell proliferation occurred during exposure to MPA, MMF, MPA + morpholinoethanol (discussed below) while morpholinoethanol treatment alone did not show any significant effects, data shown in Figure 2.16 in Section 2.4.1 were collected for MPA treatment only.

Figure 2.14 shows significant decreases in cell proliferation after a single dose of MPA, MMF, and MPA + morpholinoethanol for concentrations $\geq 1\mu$ M after 48h (all p-values > 0.001). After 72h, drug concentrations $\geq 5\mu$ M significantly decreased proliferation, while 1μ M drug concentrations did not affect proliferation. This shift might result from glucuronidation/metabolism of MPA/MMF as it often occurs for many drugs in tumor cells (one mechanism of drug resistance) [152] and from LS180 cells adapting to MPA exposure (Sec. 2.2.2).

Half maximal inhibitory concentration (IC_{50}) values were calculated for incubation of LS180 cells for 48h and 72h with single doses of MPA, MMF, and MPA + morpholinoethanol. IC_{50} values ranged around 2μ M, with IC_{50} (MPA, 48h, single dose) = 2.59μ M, IC_{50} (MMF, 48h, single dose) = 1.15μ M, IC_{50} (MPA + morpholinoethanol, 48h, single dose) = 2.44μ M, IC_{50} (MPA, 72h, single dose) = 1.73μ M, IC_{50} (MMF, 72h, single dose) = 2.13μ M, and IC_{50} (MPA + morpholinoethanol) = 1.24μ M. For 24h incubations (Sec. 2.4.1) an IC_{50} (MPA, 24h) = 2.25μ M was determined, as well as values for redosed cell cultures for 48h and 72h incubations of IC_{50} (MPA, 48h, redosed) = 2.28μ M and IC_{50} (MPA, 72h, redosed) = 4.40μ M.

Comparing IC_{50} values for LS180 cells for different incubation times after single MPA doses, no apparent changes in values were observed. An increase in IC_{50} val-

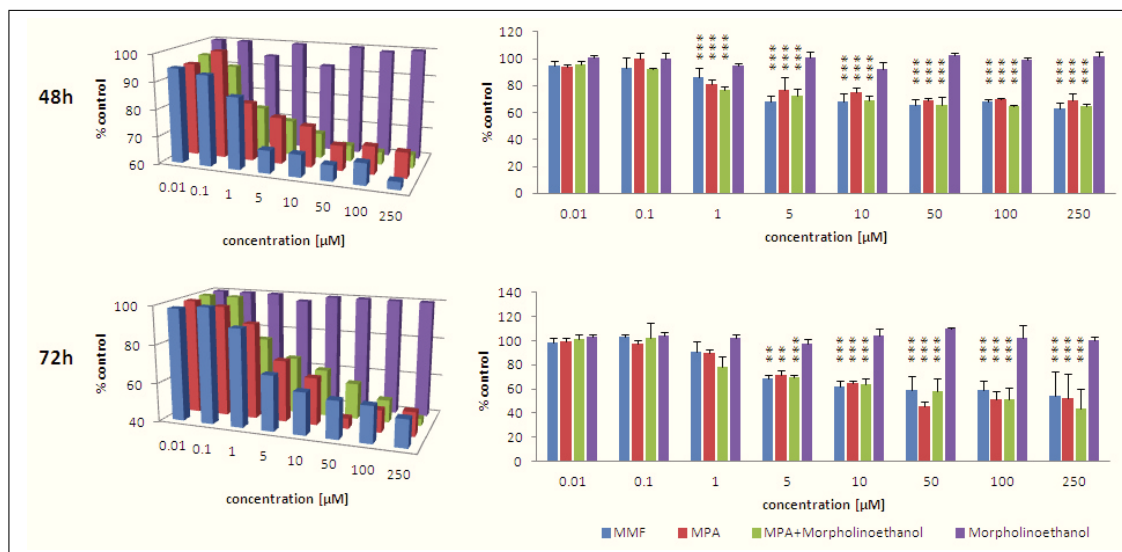


Fig. 2.14: Effects of drug treatment (single dose) on LS180 cell proliferation after 48h and 72h. Values are given as means of % of controls ($N=6$). Values were calculated from fluorescence intensities using the CyQUANT NF Cell Proliferation Assay. Due to the 96-well plate format of the assay, a set of controls was run for each drug individually. Significance was determined using one-way ANOVA combined with Scheffe's post – hoc test with *: $p < 0.05$; **: $p < 0.005$; ***: $p < 0.001$ versus controls.

ues could have been expected due to the increasing drug inactivation over time due to glucuronidation/metabolism of the parent drug as already mentioned above [152]. While after single MPA doses the IC_{50} doses after different incubation periods were consistent, after repeat doses and 72h incubation, the IC_{50} values approximately doubled to $4.4\mu\text{M}$. This about 2-fold higher IC_{50} value may be due to LS180 cells adapting to MPA as mechanism of drug resistance (described above and in Sec. 2.2.2). Overexpression of enzymes and transporters linked to MPA metabolism, i.e. MRP1 (significantly upregulated after 72h of MPA treatment, Fig. 2.10), as well as of enzymes linked to pharmacodynamics of MPA, i.e. IMPDH 2 (trend towards upregulation after only 24h of MPA treatment, Fig. 2.9), in LS180 cells was observed and is discussed in context of these studies in Section 2.2.2 already. Slight differences in experimental conditions (most likely cell density at the start of the experiment) and conditions during the experiment (media renewal ensuring optimal growth conditions for cells) may also contribute to the increase of the IC_{50} values for cells treated with repeated doses of MPA over 72h.

The necessity to redose for sufficient guanosine supplementation of the media for follow-up experiments, the shift in proliferation profiles as shown in Figure 2.14,

2 Results and Discussion

and redosing being the more physiologic approach, led us to the use of a repeated dosing strategy with MPA and guanosine in subsequent experiments (Sec. 2.1.2).

Comparing the above findings to the currently available literature, it is ambiguous that MPA depletes intracellular GTP and exerts its antiproliferative effects in a strongly cell type-specific manner [153]. Lymphocytes respond to MPA *in vitro* with IC_{50} values of proliferation inhibition of less than $0.1\mu\text{M}$ while cells such as fibroblast or endothelial cells are less sensitive or unaffected by concentrations in this concentration range (IC_{50} values $\approx 0.6\mu\text{M}$) [42, 43]. Evaluating effects of MPA on the proliferation of different cancer cell lines for a duration of 48h, Franklin et al. reported differences in IC_{50} values inbetween cell lines as well, although the examined lines had a cancerous origin in common [152]. While EMT6 (murine mammary carcinoma) cells exhibited an IC_{50} for proliferation inhibition of $0.24\mu\text{M}$ MPA, HeLa (human cervical carcinoma) cells showed an IC_{50} of $0.80\mu\text{M}$ MPA, and HT29 (human colorectal carcinoma) cells an IC_{50} of $12.9\mu\text{M}$ MPA. Yalowitz et al. found an even higher IC_{50} of $21\mu\text{M}$ MPA for growth inhibition of HT29 cells by MPA [154]. The IC_{50} values found in LS180 cells ($\approx 2\mu\text{M}$ MPA) correspond to the high IC_{50} values for HT29 cells and the low values for EMT6 and HeLa, which are all human cancer cell lines. Especially values for HT29 show that even very high IC_{50} values for human colon adenocarcinomas are reasonable. Proliferation rates (and therefore utilization of nucleotides) such as a doubling time of 1 day for HT29 cells in presence of FBS [155], about 1 day for HeLa cells [156], and about 2 days for LS180 cells (Sec. 3.2.1) do not seem to be directly affected by MPA exposure. Probable reasons are cell type-dependent characteristics such as differences in utilization of pathways of nucleotide synthesis (Sec. 1.1.4) as well as preconditions (Sec. 2.2.1) and adaptation (Sec. 2.2.2).

2.4.1 Influence of exogenous guanosine on proliferation of different cell types during MPA treatment

The influence of exogenous guanosine on MPA's antiproliferative properties was assessed for different time periods in LS180 cells and subsequently in two additional cell types using the CyQUANT NF Cell Proliferation Assay as described above (Sec. 2.4). For these experiments cells were redosed with MPA and guanosine every 24h to ensure sufficient availability of guanosine and to avoid insufficient exposure to the parent drug due to drug inactivation by glucuronidation/metabolism.

RAW 264.7 and CCD-18Co cells were employed as controls to check and verify changes in proliferation patterns seen in LS180 cells, which are grade II tumor cells and therefore bear abnormalities in metabolism (Sec. 2.2 and Sec. 2.8.2). Taken higher proliferation rates/shorter doubling times of RAW 264.7 and CCD-18Co cells into account (Sec. 3.2.1) and therefore eventually higher demand of guanosine, assays determining effects of MPA and only 100 μ M guanosine were not carried out for these cells types. As no cytotoxicity assays were conducted for these cells, contribution of cell death cannot be fully ruled out in these studies. Arguing against the occurrence of necrosis in these two cell types is that no dead cells were observed during the experiments.

Influence of exogenous guanosine on LS180 cells

LS180 cell proliferation under MPA and guanosine (0, 100, 200, 400 and 1000 μ M) treatment was tested for 24h, 48h, 72h, and 5 days (5 days for 1000 μ M guanosine only).

Figure 2.15 shows effects of treatment in LS180 cells within the first 72h. After 24h LS180 cell proliferation was diminished for cells grown in culture medium containing 0 μ M and 100 μ M guanosine for MPA concentrations $\geq 5\mu$ M. Almost the same changes were present for 48h and 72h (no changes for 100 μ M guanosine, but 200 μ M guanosine) treatment. 1000 μ M guanosine antagonized the negative effects on proliferation by MPA even at higher MPA concentrations. Compared to assays without guanosine substitution this included higher proliferation rates for cells treated with 100 μ M MPA after 24h, 100 and 250 μ M MPA after 48h, and 10, 50, and 100 μ M MPA after 72h.

Data shown in Figure 2.15 (arranged based on increasing guanosine concentrations) is shown again in Figure 2.16, this time with data sorted based on incubation time (for 0, 100, 200, and 400 μ M guanosine) and Figure 2.17 (for 1000 μ M guanosine).

Influence of exogenous guanosine on RAW 264.7 cells

Due to the relatively high proliferation rate of the murine macrophage cell line RAW 264.7 (Sec. 3.2.1) proliferation assay duration was limited to 72h to guarantee uncompromised proliferation of controls and treatment groups.

In Figure 2.18 RAW 264.7 data is sorted based on increasing guanosine concentrations for 24h, 48h, and 72h. Significantly impaired cell growth was seen after 24h and 48h only for RAW 264.7 cells grown in medium without guanosine and MPA

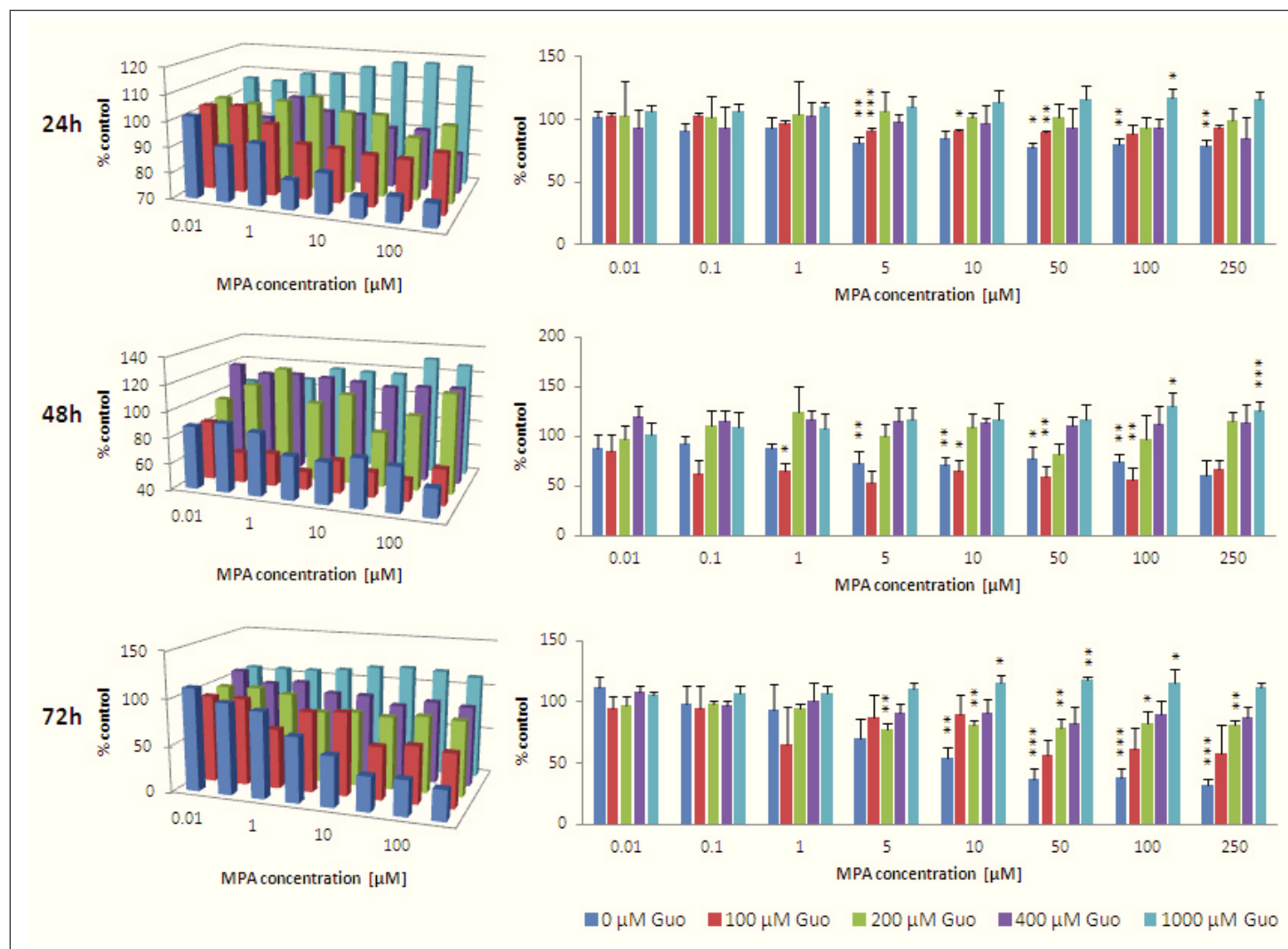


Fig. 2.15: Effects on LS180 cell proliferation after 24h, 48h, and 72h of MPA treatment and supplementation with 100, 200, 400, and 1000 μM guanosine (redosed every 24h). Values are given as means of % of controls ($N=6$). Significance was determined using one-way ANOVA combined with Scheffe's *post-hoc* test with *: $p < 0.05$; **: $p < 0.005$; *: $p < 0.001$ versus controls. Values were calculated from fluorescence intensities using the CyQUANT NF Cell Proliferation Assay. Due to the 96-well plate format of the assay a set of controls was run for each guanosine concentration individually.**

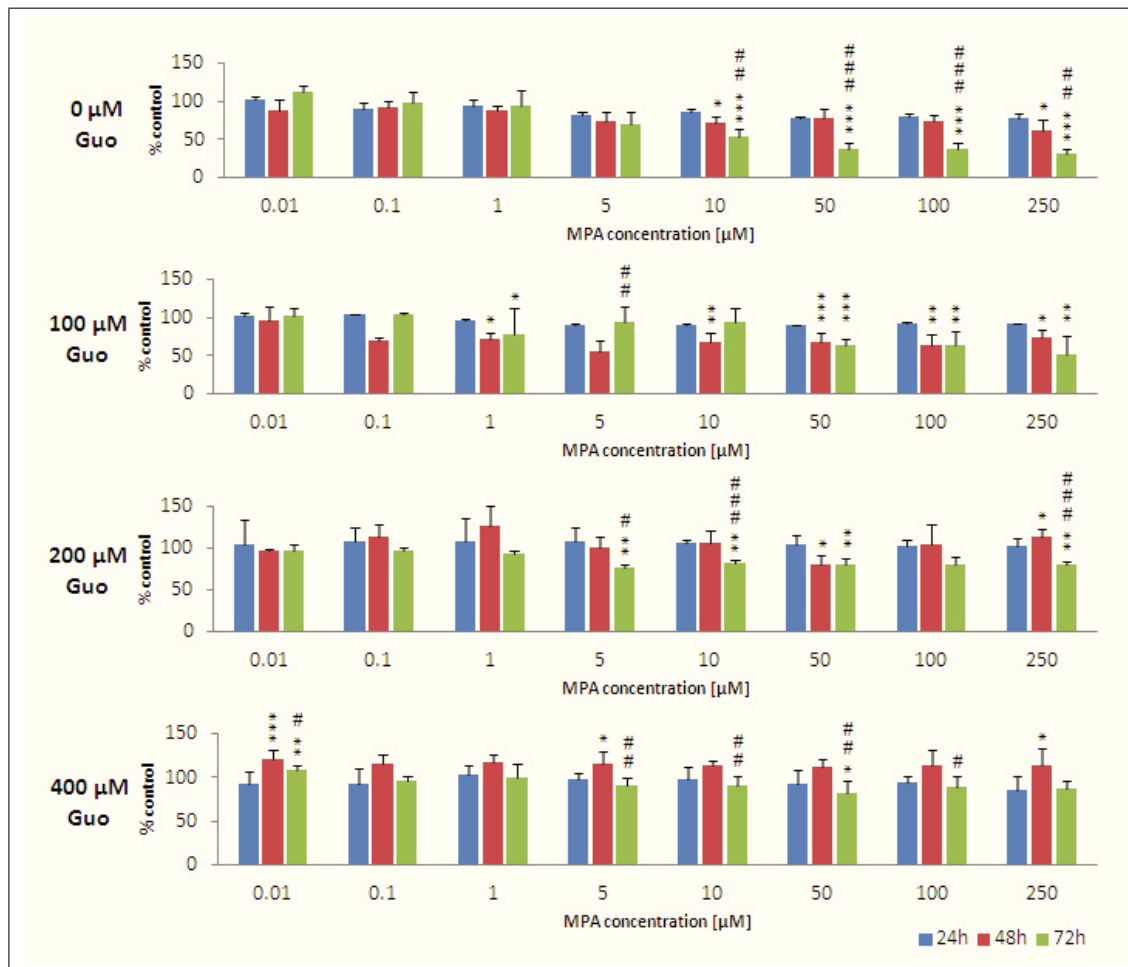


Fig. 2.16: Effects on LS180 cell proliferation after 24h, 48h, and 72h of MPA treatment and supplementation with 0, 100, 200, and 400 μM guanosine (re-dosed every 24h). Values are given as means of % of controls ($N=6$). Significance was determined using one-way ANOVA combined with Scheffe's post – hoc test with */ #: $p<0.05$; **/ ##: $p<0.005$; ***/ ###: $p<0.001$ versus controls; *: significance versus 24h values, #: significance versus 48h values of same MPA concentration. Values were calculated from fluorescence intensities using the CyQUANT NF Cell Proliferation Assay. Due to the 96-well plate format of the assay a set of controls was run for each guanosine concentration individually.

2 Results and Discussion

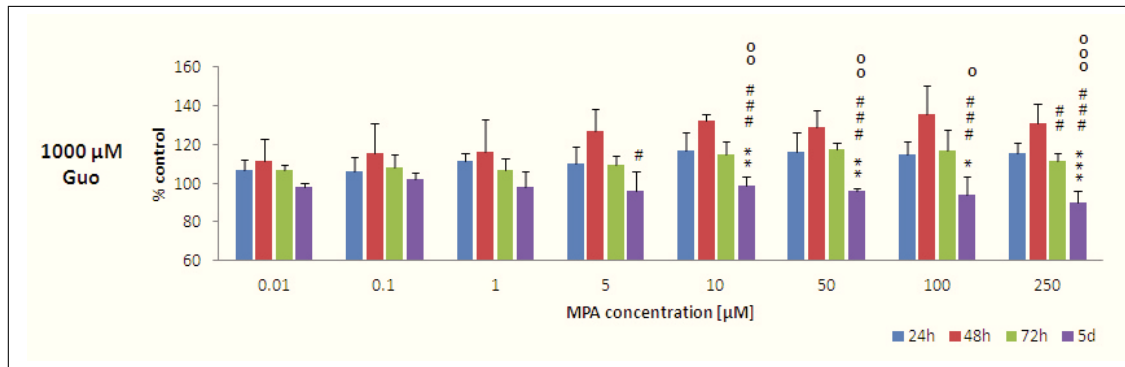


Fig. 2.17: Effects on LS180 cell proliferation after 24h, 48h, 72h, and 5d of MPA treatment and supplementation with 1000 μM guanosine (redosed every 24h). Values are given as means of % of controls ($N=6$). Significance was determined using one-way ANOVA combined with Scheffe's post – hoc test with */ #/ o: $p < 0.05$; **/ ##/ oo: $p < 0.005$; ***/ ###/ ooo: $p < 0.001$ versus controls; *: significance versus 24h values, #: significance versus 48h values of same MPA concentration, o: significance versus 72h values of same MPA concentration. Values were calculated from fluorescence intensities measured by a fluorescence microplate reader using the CyQUANT NF Cell Proliferation Assay. Due to the 96-well plate format of the assay a set of controls was run for each guanosine concentration individually.

concentrations $\geq 5 \mu\text{M}$. In most cases guanosine substitution $\geq 200 \mu\text{M}$ was sufficient to return proliferation rates back to normal as compared to controls. A comparison of effects of MPA treatment and insufficient guanosine levels as shown in the first graph in Figure 2.19 ($0 \mu\text{M}$ guanosine) shows significantly lower cell numbers (calculated as % of controls) after 24h and 48h/72h of treatment.

Figure 2.19 shows the time course of RAW 264.7 proliferation changes over 72h after supplementation with 0 (controls), 200, 400, and $1000 \mu\text{M}$ guanosine. Supplementation of cell culture media with 200, 400, and $1000 \mu\text{M}$ guanosine reversed the effects of MPA (except for significant decreases for concentrations of $400 \mu\text{M}$ guanosine and $10\text{-}100 \mu\text{M}$ MPA). Starting at $5 \mu\text{M}$ MPA depleted RAW 264.7 cell numbers for cells grown in $200 \mu\text{M}$ guanosine-containing medium after 48h ($p < 0.001$ for MPA concentrations $\geq 5 \mu\text{M}$ for 48h values versus 72h values). These changes were less pronounced but still significant for cells exposed to higher guanosine concentrations. For $400 \mu\text{M}$ guanosine-treated cells p-values ranged between 0.05 and 0.01 for MPA doses between $5 \mu\text{M}$ and $100 \mu\text{M}$. There did not seem to be further improvement over supplementation with $400 \mu\text{M}$ guanosine as the effects of supplementation with $1000 \mu\text{M}$ showed similar results.

2.4 Antiproliferative properties

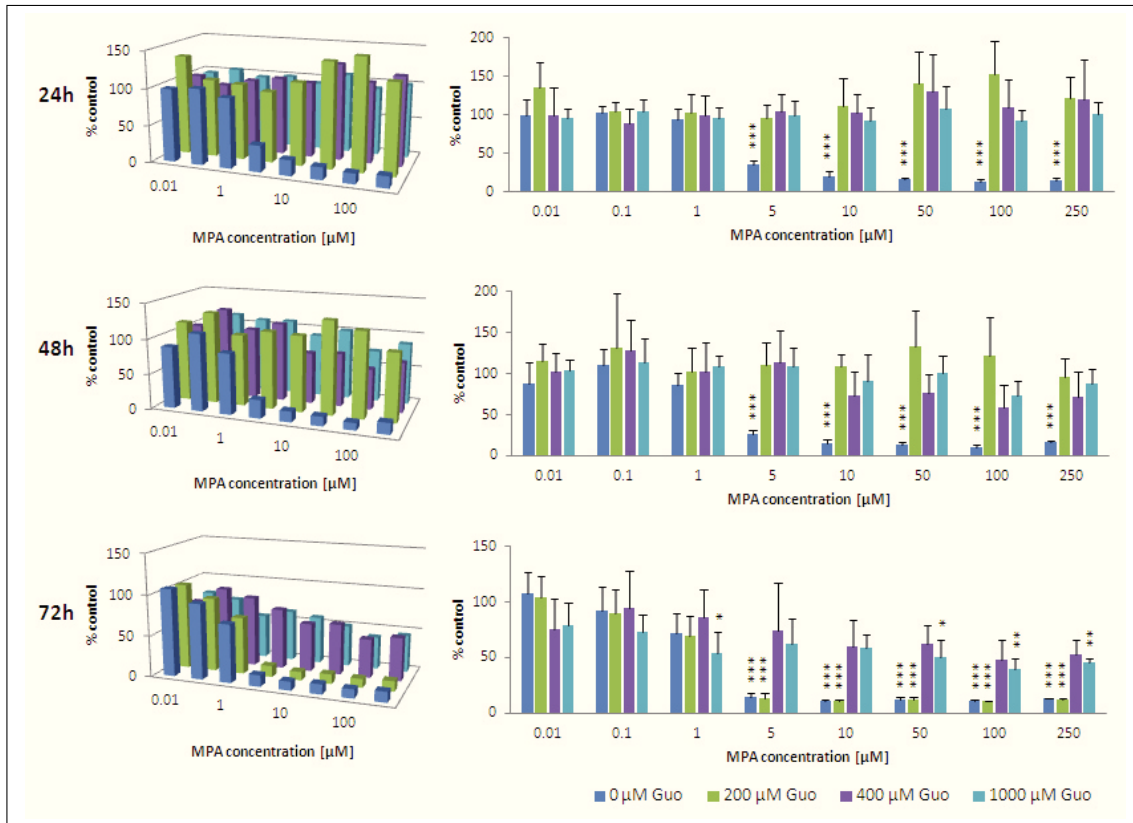


Fig. 2.18: Effects on RAW 264.7 cell proliferation after 24h, 48h, and 72h of MPA treatment and supplementation with 0, 200, 400, and 1000 μM guanosine (redosed every 24h). Values are given as means of % of controls ($N=6$). Significance was determined using one-way ANOVA combined with Scheffe's post – hoc test with *: $p<0.05$; **: $p<0.005$; ***: $p<0.001$ versus controls. Values were calculated from fluorescence intensities using the CyQUANT NF Cell Proliferation Assay. Due to the 96-well plate format of the assay a set of controls was run for each guanosine concentration individually.

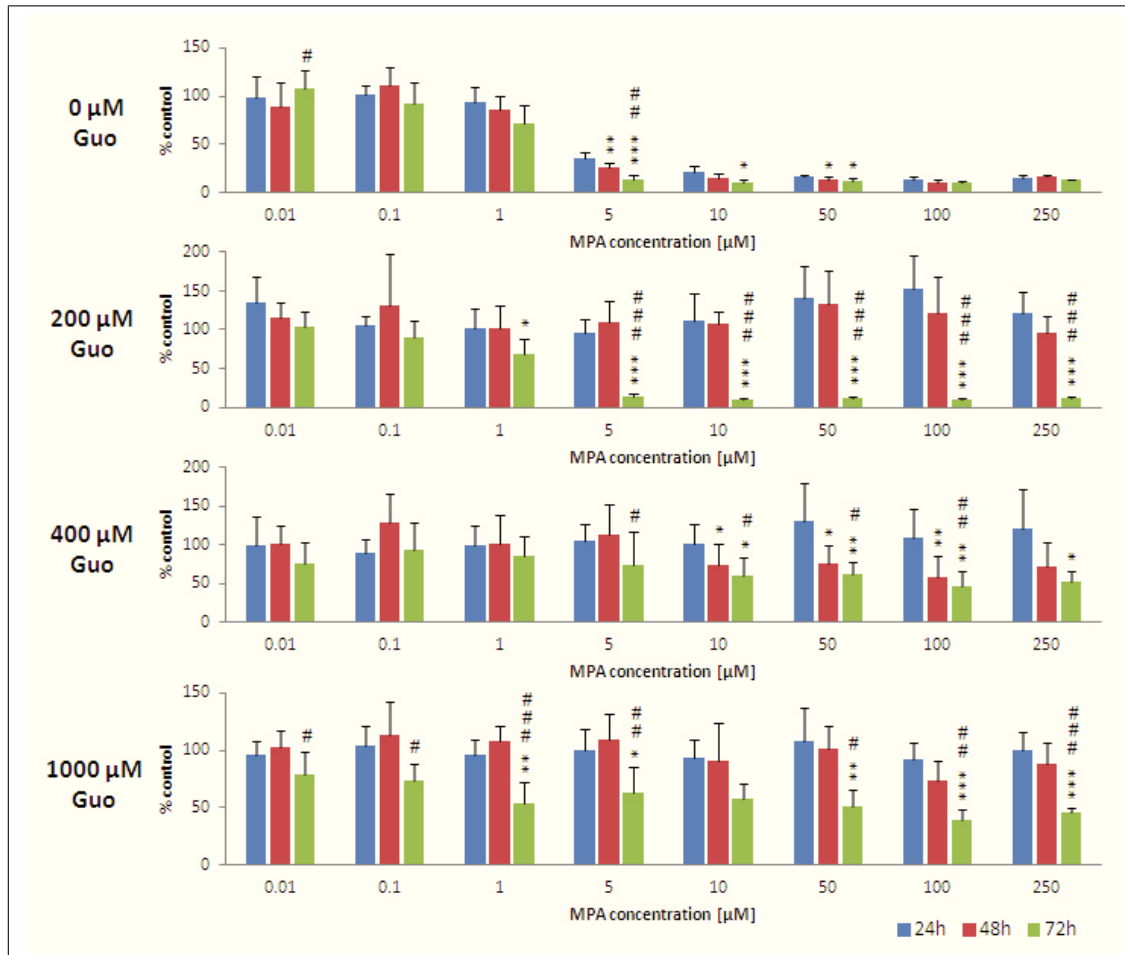


Fig. 2.19: Effects on RAW 264.7 cell proliferation after 24h, 48h, and 72h of MPA treatment and supplementation with 0, 200, 400, and 1000 μM guanosine (redosed every 24h). Values are given as means of % of controls (N=6). Significance was determined using one-way ANOVA combined with Scheffe's *post – hoc* test with */ #: $p < 0.05$; **/ ##: $p < 0.005$; ***/ ###: $p < 0.001$ versus controls; *: significance versus 24h values of same MPA concentration, #: significance versus 48h values of same MPA concentration. Values were calculated from fluorescence intensities using the CyQUANT NF Cell Proliferation Assay. Due to the 96-well plate format of the assay a set of controls was run for each guanosine concentration individually.

Influence of exogenous guanosine on CCD-18Co cells

CCD-18Co cells turned out to be more resistant to MPA-induced changes in proliferation under treatment with exogenous guanosine than LS180 and RAW 264.7 cells. To follow growth profiles over a longer period of time assays were run for 24h, 48h, 72h, and additionally for 5 days after guanosine supplementation with 0 (controls), 200, 400, and 1000 μ M.

Figure 2.20 shows CCD-18Co cell proliferation with data sorted based on concentrations of exogenous guanosine. After 24h only a trend towards lower cell numbers under higher doses of MPA was seen for 0 μ M guanosine (250 μ M MPA: 90.8 \pm 19.6% of control values), while in comparison after 24h statistically significant changes occurred already for LS180 cells with $p < 0.01$ versus controls and $p < 0.001$ versus controls for RAW 264.7 cells. For concentrations of 200-1000 μ M guanosine, pronounced trends towards elevated proliferation of CCD-18Co cells under increasing doses of MPA were detected (250 μ M MPA: 135.1 \pm 26.7% of control values for 200 μ M guanosine, 138.1 \pm 27.6% of control values for 400 μ M guanosine, 120.6 \pm 34.6% of control values for 1000 μ M guanosine; please see 3D graph in Figure 2.20). Significant decreases in proliferation without guanosine supplementation was found after 48h with significance levels increasing with incubation time. Significant decreases in CCD-18Co cell numbers under guanosine treatment occurred after 5 days for 400 μ M guanosine for 100 μ M and 250 μ M MPA.

Time courses of growth profiles of CCD-18Co cells are shown in Figure 2.21. Without guanosine supplementation, MPA reduced CCD-18Co cell numbers after 48h for MPA concentrations $\geq 1\mu$ M and after 72h already for MPA concentrations $\geq 0.01\mu$ M, which was also the lowest concentration used. Significant decreases in cell numbers were seen for all MPA concentrations starting at 0.01 μ M when incubated for 48h or 72h as well. No changes were detected when cells were incubated without guanosine supplementation for more than 72h.

Supplementation with 200 μ M and 400 μ M guanosine did not prevent reduction in cell numbers after 5 days of treatment with 100 μ M MPA (200 μ M and 400 μ M guanosine) and 250 μ M MPA (400 μ M guanosine). Neither trends nor significant changes were found in time-dependent proliferation patterns for CCD-18Co cells exposed to 1000 μ M guanosine at any of the MPA concentrations tested.

2 Results and Discussion

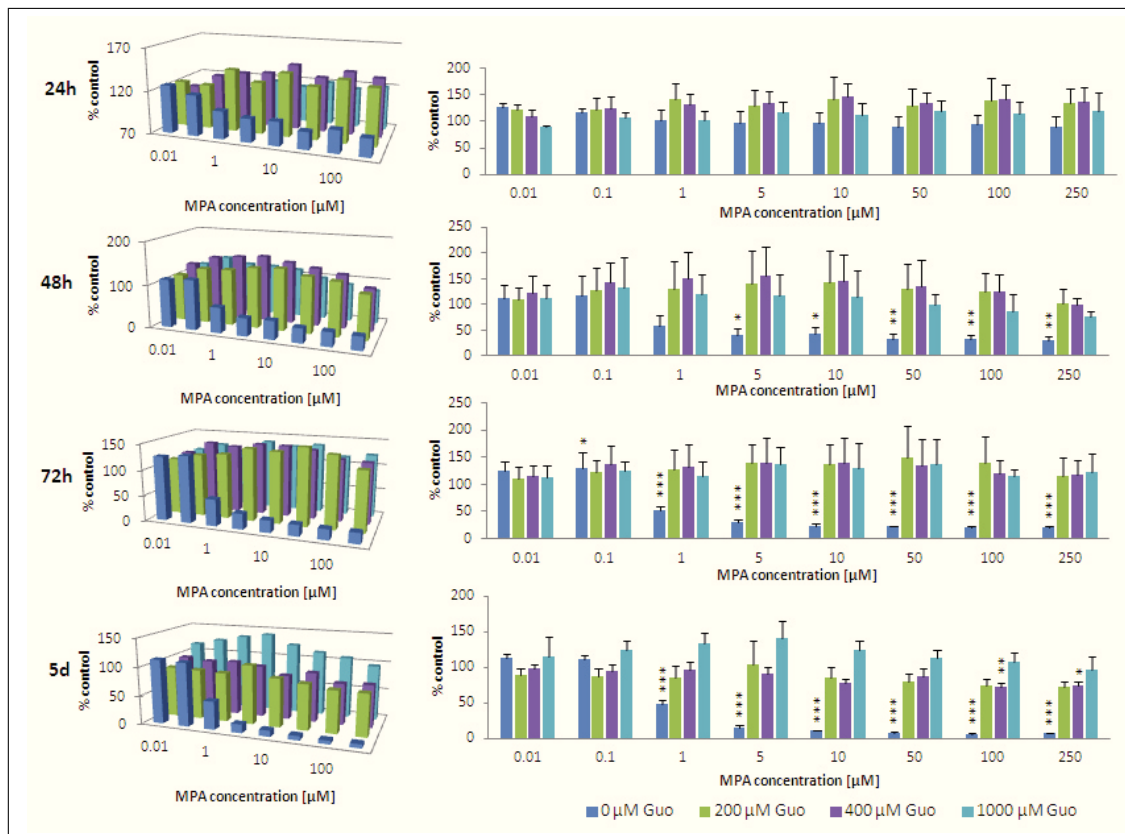


Fig. 2.20: Effects on CCD-18Co cell proliferation after 24h, 48h, 72h, and 5d of MPA treatment and supplementation with 0, 200, 400, and 1000 μ M guanosine (redosed every 24h). Values are given as means of % of controls ($N=6$). Significance was determined using one-way ANOVA combined with Scheffe's *post – hoc* test with *: $p<0.05$; **: $p<0.01$; *: $p<0.001$ versus controls. Values were calculated from fluorescence intensities using the CyQUANT NF Cell Proliferation Assay. Due to the 96-well plate format of the assay a set of controls was run for each guanosine concentration individually.**

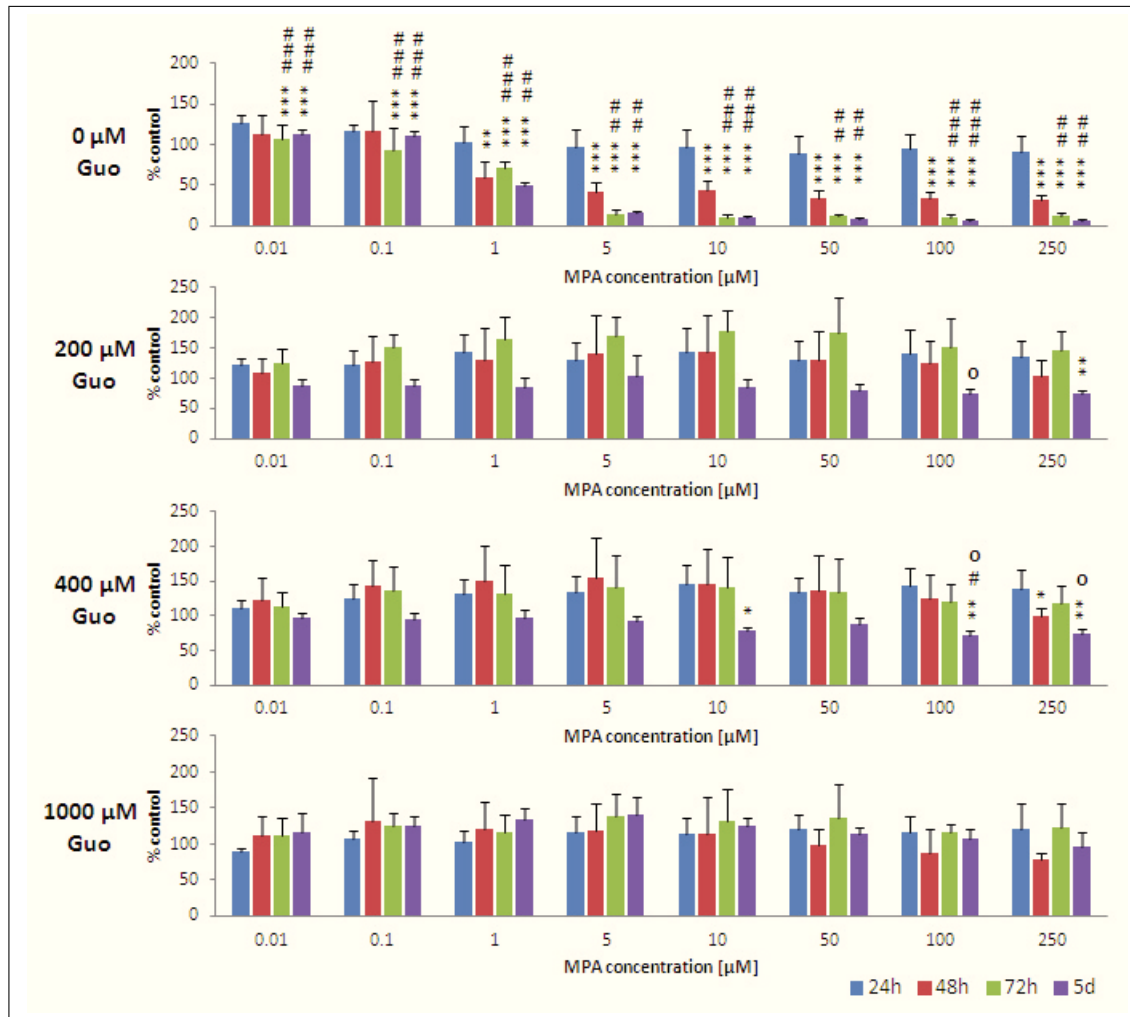


Fig. 2.21: Effects on CCD-18Co cell proliferation after 24h, 48h, 72h and 5d of MPA treatment and supplementation with 0, 200, 400, and 1000 μM guanosine (redosed every 24h). Values are given as means of % of controls ($N=6$). Significance was determined using one-way ANOVA combined with Scheffe's *post-hoc* test with */ #/ \circ : $p < 0.05$; **/ ##/ $\circ\circ$: $p < 0.005$; ***/ ###/ $\circ\circ\circ$: $p < 0.001$ versus controls; *: significance versus 24h values, #: significance versus 48h values of same MPA concentration, \circ : significance versus 72h values of same MPA concentration. Values were calculated from fluorescence intensities using the CyQUANT NF Cell Proliferation Assay. Due to the 96-well plate format of the assay a set of controls was run for each guanosine concentration individually.

The literature supports that most negative MPA effects on cell proliferation, function, and metabolism can be antagonized by supplementation with guanosine [43, 110, 157]. While reversal of certain effects, e.g. the MPA-mediated negative effect on the expression of certain proteins is not established [157], effects such as intra- and

extracellular levels of signaling molecules and LDH [110] as well as DNA synthesis can generally be restored to normal [43, 110, 157] or sometimes even supranormal levels [157].

Restoration of proliferation to normal as well as even supranormal levels, as it was described before [157] was seen. Looking at proliferation profiles over time for cells in differently supplemented media has not been described in the literature yet. Decreases in the capacity to utilize exogenous guanosine as seen in the three examined cell types occurring after distinct incubation times leads to the question how the divergent epithelial cell types, especially stem cells, constituting the intestinal barrier along the crypt-villus axis [158, 159] are affected. If intestinal barrier function was compromised by these disturbances, Crohn's disease-like patterns of inflammation would result as they are seen in transplant patients receiving an MPA-based immunosuppressive drug regimen (Sec. 1.2.3).

2.5 Effects on nucleotide levels and energy charge

Nucleotides (nucleoside mono-, di-, and triphosphates) are high-energy phosphates that are essential for a multitude of biochemical processes within cells [131, 148, 160]. They determine a cell's energy state, serve as coenzymes and as intermediates in anabolic and catabolic pathways, and they are the building blocks of nucleic acids constituting DNA (deoxyribonucleotides) and RNA (ribonucleotides) (Sec. 1.1.4, Fig. 1.2). Cyclic nucleotides, especially cyclic adenosine monophosphate (cAMP) and cyclic guanosine monophosphate (cGMP), serve as second messengers influencing metabolism, gene transcription, cell morphology, and signal transduction amongst many other crucial cellular actions [161]. Redox cofactors such as NAD^+ , NADP^+ , and flavin adenine dinucleotide (FAD) are inevitable for maintaining functions such as cellular respiration, oxidative phosphorylation, lipid synthesis, gluconeogenesis, post-translational modifications of proteins, and many others [78, 80].

Concentrations of high-energy phosphates (ATP, ADP, AMP, GTP, GDP, GMP, UTP, UDP, UMP, CTP, CDP, CMP) as well as NAD^+ , NADP^+ , and FAD in extracts of drug-treated LS180 cell were assessed to investigate the influence of MPA and its derivatives on nucleotide levels in LS180 cells in detail. Dependent on the experiment cells were or were not supplemented with guanosine. After drug incubation cells were extracted with perchloric acid (PCA) and a quantitative high performance liquid chromatography (HPLC)-MS assay developed by Klawitter et al. was used to measure nucleotide concentrations [160].

2.5.1 Nucleotide levels and energy charge after single doses of drugs without exogenous guanosine

To obtain concentration-dependent profiles and for comparison of drugs and drug combinations, LS180 cells were incubated 12h, 24h, and 48h, respectively, with single doses of drugs (MPA, MMF, MPA + morpholinoethanol, and morpholinoethanol) at increasing concentrations (0.01, 0.05, 0.1, 0.5, 1, 5, 10, 50, 100, and 250 μ M) or 0.05% DMSO for controls (N=4). As this was one of the first experiments performed, cells were neither redosed nor were cell culture media supplemented with guanosine. Nucleotide levels were measured quantitatively [160], normalized to amounts of protein per sample and calculated as % of controls. The adenylate energy charge (AEC) of treated LS180 cells was calculated according to the formula by Atkinson: $AEC = (ATP + 0.5*ADP)/(AMP + ADP + ATP)$ [162]. Respective energy charge values for guanine (GEC), uridine (UEG), and cytidine (CEG) nucleotides were calculated using the respective concentrations of nucleotide triphosphates (NTPs), nucleotide diphosphates (NDPs), and nucleotide monophosphates (NMPs). The corresponding equations are based on the equation for a general nucleotide energy charge (NEC): $NEC = (NTP + 0.5*NDP)/(NMP + NDP + NTP)$ [163].

Graphs of levels of nucleotide tri-, di-, and monophosphates (ATP, ADP, AMP, GTP, GDP, GMP, UTP, UDP, UMP, CTP, CDP, CMP) as well as of redox cofactors (FAD, NAD⁺, NADP⁺) and NECs (AEC, GEC, UEC, CEC) in LS180 cells after 12h, 24h, and 48h incubations with MPA, MMF, MPA + morpholinoethanol, and morpholinoethanol are shown calculated as % of controls in the appendix (Fig. 4.1 - Fig. 4.19).

Nucleotide ratios in LS180 cells were in normal ranges when compared to published data on physiological nucleotide concentrations in predominantly mammalian cell lines and fluids [164]. Traut et al. found the following average concentrations for the four NTPs: ATP: 3152 \pm 1698 μ M, GTP: 468 \pm 224 μ M, UTP: 567 \pm 460 μ M, CTP: 278 \pm 242 μ M, with concentrations being elevated 1.2-5-fold in tumor cells compared to normal cells [164]. As values are given in μ M it is hard to compare Traut's values directly to our values due to the procedure used to measure nucleotides in our samples: After reconstitution of lyophilized cell extracts of LS180 cells in 500 μ L HPLC grade H₂O, 1:20 dilution, and measurement using HPLC-MS, absolute amounts of compounds were calculated and normalized to protein contents of samples (unit:

Table 2.1: Influence of MPA, MMF, and MPA + morpholinoethanol (ME) on nucleotide levels and energy charge. Statistically significant changes ($\uparrow\downarrow$, number of displayed arrows reflects the most significant change within one treatment group of increasing drug concentrations versus controls) and trends ($\uparrow\downarrow$, not statistically significant) in compound concentrations versus controls are summarized, $p < 0.05$: \uparrow/\downarrow , $p < 0.01$: $\uparrow\uparrow/\downarrow\downarrow$, $p < 0.001$: $\uparrow\uparrow\uparrow/\downarrow\downarrow\downarrow$.

	MPA			MMF			MPA+ME		
	12h	24h	48h	12h	24h	48h	12h	24h	48h
ATP	-	\downarrow	$\uparrow\uparrow\uparrow$	-	-	$\uparrow\uparrow\uparrow$	-	\downarrow	-
ADP	-	-	$\uparrow\uparrow\uparrow$	-	-	$\uparrow\uparrow$	-	-	-
AMP	-	-	-	-	-	-	-	-	-
GTP	$\downarrow\downarrow\downarrow$	$\downarrow\downarrow\downarrow$	$\downarrow\downarrow\downarrow$	$\downarrow\downarrow\downarrow$	$\downarrow\downarrow\downarrow$	$\downarrow\downarrow$	$\downarrow\downarrow\downarrow$	$\downarrow\downarrow\downarrow$	\downarrow
GDP	$\downarrow\downarrow\downarrow$	$\downarrow\downarrow\downarrow$	-	$\downarrow\downarrow\downarrow$	$\downarrow\downarrow\downarrow$	-	$\downarrow\downarrow\downarrow$	$\downarrow\downarrow\downarrow$	-
GMP	$\downarrow\downarrow\downarrow$	$\downarrow\downarrow\downarrow$	-	$\downarrow\downarrow\downarrow$	$\downarrow\downarrow\downarrow$	-	$\downarrow\downarrow\downarrow$	$\downarrow\downarrow\downarrow$	-
UTP	$\uparrow\uparrow\uparrow$	$\uparrow\uparrow\uparrow$	$\uparrow\uparrow\uparrow$	$\uparrow\uparrow\uparrow$	$\uparrow\uparrow\uparrow$	$\uparrow\uparrow\uparrow$	$\uparrow\uparrow\uparrow$	$\uparrow\uparrow\uparrow$	$\uparrow\uparrow$
UDP	$\uparrow\uparrow\uparrow$	$\uparrow\uparrow\uparrow$	$\uparrow\uparrow\uparrow$	$\uparrow\uparrow\uparrow$	$\uparrow\uparrow\uparrow$	$\uparrow\uparrow\uparrow$	$\uparrow\uparrow\uparrow$	$\uparrow\uparrow\uparrow$	\uparrow
UMP	$\uparrow\uparrow\uparrow$	$\uparrow\uparrow\uparrow$	$\uparrow\uparrow\uparrow$	$\uparrow\uparrow\uparrow$	$\uparrow\uparrow\uparrow$	$\uparrow\uparrow\uparrow$	$\uparrow\uparrow\uparrow$	$\uparrow\uparrow\uparrow$	\uparrow
CTP	$\uparrow\uparrow\uparrow$	$\uparrow\uparrow$	$\uparrow\uparrow\uparrow$	$\uparrow\uparrow\uparrow$	$\uparrow\uparrow\uparrow$	$\uparrow\uparrow\uparrow$	$\uparrow\uparrow\uparrow$	$\uparrow\uparrow\uparrow$	-
CDP	$\uparrow\uparrow\uparrow$	$\uparrow\uparrow\uparrow$	$\uparrow\uparrow\uparrow$	$\uparrow\uparrow\uparrow$	$\uparrow\uparrow\uparrow$	$\uparrow\uparrow\uparrow$	$\uparrow\uparrow\uparrow$	$\uparrow\uparrow\uparrow$	\uparrow
CMP	$\uparrow\uparrow\uparrow$	$\uparrow\uparrow\uparrow$	$\uparrow\uparrow\uparrow$	$\uparrow\uparrow\uparrow$	$\uparrow\uparrow\uparrow$	$\uparrow\uparrow\uparrow$	$\uparrow\uparrow\uparrow$	$\uparrow\uparrow\uparrow$	\uparrow
NAD ⁺	-	-	$\uparrow\uparrow\uparrow$	-	-	$\uparrow\uparrow$	-	$\uparrow\uparrow$	-
NADP ⁺	-	-	$\uparrow\uparrow\uparrow$	\uparrow	-	$\uparrow\uparrow\uparrow$	\uparrow	-	-
FAD	-	-	$\uparrow\uparrow\uparrow$	-	-	\uparrow	-	-	\uparrow
AEC	-	-	-	-	-	-	-	-	-
GEC	$\downarrow\downarrow\downarrow$	-	-	$\downarrow\downarrow\downarrow$	-	-	$\downarrow\downarrow\downarrow$	-	-
UEC	-	-	-	-	-	-	-	-	-
CEC	-	-	-	-	-	-	-	-	-

2.5 Effects on nucleotide levels and energy charge

nmol/mg protein). Results are given as % of control NTP values (nmol/mg protein). Representative examples of values for 72h cell extracts of LS180 cells not supplemented with exogenous guanosine (control, 72h, 0 μ M guanosine) are as follows: ATP: 3308.0 \pm 172.8nmol/mg protein, GTP: 1448.8 \pm 133.9nmol/mg protein, UTP: 447.4 \pm 18.8nmol/mg protein, CTP: 2278.5 \pm 95.7nmol/mg protein. The amount of UTP seems relatively low compared to values for ATP, GTP, and CTP, but is still reasonable when taking the high standard deviation found for UTP as reported by Traut into account [164]. The same applies for CTP values which seem fairly high even for a cancer cell line.

Overall nucleotide levels were not affected differently for MPA, MMF, or MPA + morpholinoethanol and responses of LS180 cells showed closely matching profiles. Adenosine nucleotide levels (Fig. 4.1 - Fig. 4.3) were largely unaffected after 12h, 24h, and 48h after single doses of drugs with exemption of a few elevated ATP and ADP values after 48h (Fig. 4.1 and Fig. 4.2). Relative high-energy phosphate concentrations were found for MPA and MMF in the range of 5-250 μ M, but also for 5 μ M morpholinoethanol. These surprising elevations after 48h are likely to be a stress response of LS180 cells after 48h of drug treatment (elevation only for higher concentrations) and no exchange of culture media. Depletion of nutrients in culture media seems to be a reason especially since imbalances in other nucleotide levels are balanced after 48h compared to 12h and 24h. The AEC did not change for any compound/compound combination after 12h, 24h, or 48h of treatment with a single dose (Fig. 4.16).

Guanosine nucleotide levels (Fig. 4.4 - Fig. 4.6) were significantly reduced starting at MPA concentrations of 0.5 μ M after 12h and 24h. After 48h only GTP levels were still significantly affected at higher MPA concentrations. The amelioration of MPA-induced effects between 24h and 48h is most likely due to drug metabolism (Sec. 2.2.2). Figure 4.5 and Figure 4.6 show significantly decreased values with $p < 0.001$ for all concentrations $> 1\mu$ M after 12h and 24h with no significant decreases being obvious after 48h anymore. This pattern also occurs in the case of uridine and cytidine nucleotides. The GEC is significantly affected after 12h for concentrations $> 1\mu$ M (except for morpholinoethanol), with imbalances evened out after 24h already.

Pyrimidine (uridine and cytidine) nucleotides were significantly higher for MPA, MMF, and MPA + morpholinoethanol than for the controls at all time points assessed starting at drug doses of 5 μ M (Fig. 4.7 - Fig. 4.12). This upregulation of pyrimidine nucleotides is most likely caused by increased PRPP concentrations due

2 Results and Discussion

to IMPDH inhibition by MPA [165], as PRPP is used in the synthesis of purines as well as synthesis of uridine nucleotides, which are substrates for cytidine nucleotides [166].

The rate of phosphorylation of the respective nucleotide did not seem to have influence on synthesis suppressing/elevating effects since mono-, di-, and trinucleotides were equally affected for guanosine, uridine, and cytidine.

Concentrations of NAD^+ , NADP^+ , and FAD were found changed (Fig. 4.13, Fig. 4.14, and Fig. 4.15, respectively).

The results discussed above are summarized in Table 2.1 (morpholinoethanol is not listed in this summary, as incubation with morpholinoethanol did not induce any significant changes in measured compounds).

Imbalances of nucleotide/ribonucleotide pools with increased synthesis of certain uridine and cytidine nucleotides/ribonucleotides were observed in the 1970ies and 80ies already [167, 168]. Studies of the biological effects of inhibition of guanosine nucleotide synthesis by MPA in cultured cells such as murine neuroblastoma cells [167], murine leukemia L1210 cells [168], human umbilical vein endothelial cells [169], and murine sarcoma 180 cells [170] showed similar effects as seen here in LS180 cells. To mention in this context is a randomized PK study of MPA that did not show significant effects of MPA on intracellular pools of deoxytriphosphates of cytidine and guanosine in HIV-1-infected patients on MMF therapy compared to non-MMF patients [171].

In Section 2.5.2 MPA's effects on nucleotide levels in guanosine-supplemented LS180 cells are discussed in detail in the context of a more physiological experiment not sacrificing the availability of exogenous guanosine.

2.5.2 Influence of exogenous guanosine on nucleotide levels and energy charge

To reassess effects of perturbations of cellular guanosine nucleotide levels in the presence of exogenous guanosine, LS180 cells were incubated with 0, 0.1, 5, 100, and $250\mu\text{M}$ MPA in the presence of 0, 200, and $1000\mu\text{M}$ guanosine for 24h and 72h (redosed every 24h), extracted with PCA, and high-energy phosphate concentrations were measured using HPLC-MS.

Effects of the incubation conditions on adenosine, guanosine, uridine, and cytidine

2.5 Effects on nucleotide levels and energy charge

nucleotide levels are shown in Figure 2.22 - Figure 2.25, effects on NAD^+ , NADP^+ , and FAD levels are shown in Figure 2.26, energy charges of all nucleotides are shown in Figure 2.27. Effects of MPA and exogenous guanosine treatment on all measured intracellular compounds in LS180 cells are summarized in Table 2.2.

While adenosine concentrations were relatively unaffected by a single dose of MPA (Sec. 2.5.1, Fig. 4.1 - Fig. 4.3), redosing of cells every 24h led to depletion of ATP, ADP, and AMP to levels of $40.7 \pm 8.3\%$ of controls, $25.2 \pm 4.2\%$ of controls, and $9.4 \pm 4.5\%$ of controls, respectively (without guanosine supplementation, $250\mu\text{M}$ MPA; Fig. 2.22). Adenosine nucleotide levels were largely restored by supplementation with $200\mu\text{M}$ and $1000\mu\text{M}$ guanosine.

Guanosine nucleotides were significantly lower for MPA concentrations $\geq 5\mu\text{M}$ for all guanosine concentrations applied for 24h and 72h (Fig. 2.23). Even for LS180 cells treated with $1000\mu\text{M}$ exogenous guanosine GTP, GDP, and GMP levels ranged around 30% of controls only. As described in Section 2.4.1 (Fig. 2.15), LS180 cell proliferation was restored by $1000\mu\text{M}$ and drastically improved by $200\mu\text{M}$ and $400\mu\text{M}$ guanosine. Restoration of proliferation rates does not reflect intracellular guanosine nucleotide levels as nucleotide levels only slightly improved in the presence of high guanosine concentrations but levels could neither be restored completely nor be elevated to control levels.

Addition of guanosine antagonized the changes of UMP and UDP levels after 72h that occurred without $200\mu\text{M}$ and $1000\mu\text{M}$ guanosine (Fig. 2.24). UTP levels on the other hand were significantly higher for MPA concentrations $\geq 5\mu\text{M}$ in the presence of $200\mu\text{M}$ and $1000\mu\text{M}$ guanosine ($127.6 \pm 8.3\%$ of controls and $199.8 \pm 12.3\%$ of controls for $250\mu\text{M}$ MPA after 24h and 72h).

Changes of cytidine nucleotide levels were reversed by supplementation with guanosine in most cases. The few slightly elevated values (GTP: $100\mu\text{M}$ MPA, $200\mu\text{M}$ and $1000\mu\text{M}$ guanosine; GMP: $100\mu\text{M}$ MPA, $1000\mu\text{M}$ guanosine) suggested imbalances in cytidine nucleotide levels in LS180 cells despite of/due to heavy guanosine supplementation of the cell culture media.

Disturbances in NAD^+ , NADP^+ , and FAD, which mainly occurred after 72h for higher MPA concentrations in the absence of guanosine supplementation, were similar to control levels during supplementation with guanosine.

After 24h the GEC was significantly decreased ($74.9 \pm 4.2\%$ of controls, i.e. 0.499 ± 0.005 for controls versus 0.374 ± 0.021 for $250\mu\text{M}$ MPA) in LS180 cells without guanosine supplementation. The other NECs did not show any differences versus controls after 24h (Fig. 2.27). After 72h treatment changes occurred in AEC, GEC,

2 Results and Discussion

and CEC without guanosine supplementation (AEC: $115.9 \pm 1.0\%$ of controls, i.e. 0.760 ± 0.018 for controls versus 0.862 ± 0.041 for $250\mu\text{M}$ MPA; GEC: $135.3 \pm 5.5\%$ of controls, i.e. 0.502 ± 0.028 for controls versus 0.681 ± 0.024 for $250\mu\text{M}$ MPA; CEC: $83.7 \pm 2.9\%$ of controls, i.e. 0.503 ± 0.030 for controls versus 0.422 ± 0.014 for $250\mu\text{M}$ MPA). The increase in UEC values after 72h of treatment with $250\mu\text{M}$ MPA and $1000\mu\text{M}$ guanosine to $125.3 \pm 5.0\%$ of controls (i.e. 0.503 ± 0.041 for controls versus 0.630 ± 0.025 for $250\mu\text{M}$ MPA, $p > 0.05$) in consideration of imbalances in pyrimidine nucleotide levels even under guanosine supplementation described above is remarkable due to the magnitude and significance of metabolic roles of uridine and cytosine nucleotides. GDP-, UDP-, and CDP-linked intermediates are involved in e.g. lipid and protein glycosylation and membrane synthesis [166, 172]. Our findings concerning nucleotide concentrations in LS180 cells during MPA and guanosine treatment will be discussed further in later sections, i.e. Section 2.7 and Section 2.8 describing MPA-induced proteome and metabolome alterations in LS180 cells.

Again, MPA concentrations used in the literature were in lower ranges (e.g. $0.1\mu\text{M}$ - $5\mu\text{M}$ [165], $10\mu\text{M}$ [170]) than in our studies, accordingly guanosine concentrations necessary to reverse MPA-induced effects typically ranged around $50\mu\text{M}$ - $100\mu\text{M}$ [165, 170].

2.5.3 Influence of MPA treatment on Na^+ - K^+ -ATPase expression levels

Na^+ - K^+ -ATPase (sodium pump) is a membrane-bound enzyme that regulates Na^+ and K^+ gradients across plasma membranes in mammalian cells [173]. ATP is hydrolyzed to ADP and P_i and drives the movement of ions against their concentration gradients. The enzyme plays a role in many essential cellular functions such as maintaining cytoplasmic Na^+ concentrations which regulate cell volume, cytoplasmic pH and Ca^{2+} concentrations (through Na^+/H^+ and $\text{Na}^+/\text{Ca}^{2+}$ exchangers), and secondary transport processes (Na^+ -dependent glucose and amino acid transport). Since water and Na^+ absorption are dependent on each other, Na^+ - K^+ -ATPase is crucial to water absorption in the intestine and closely linked to the pathophysiology of diarrhea [173, 174], which is one of MPA's most prominent side effects (Sec. 1.2.3).

Although ATP and AEC levels were only affected by MPA as long as cell culture

2.5 Effects on nucleotide levels and energy charge

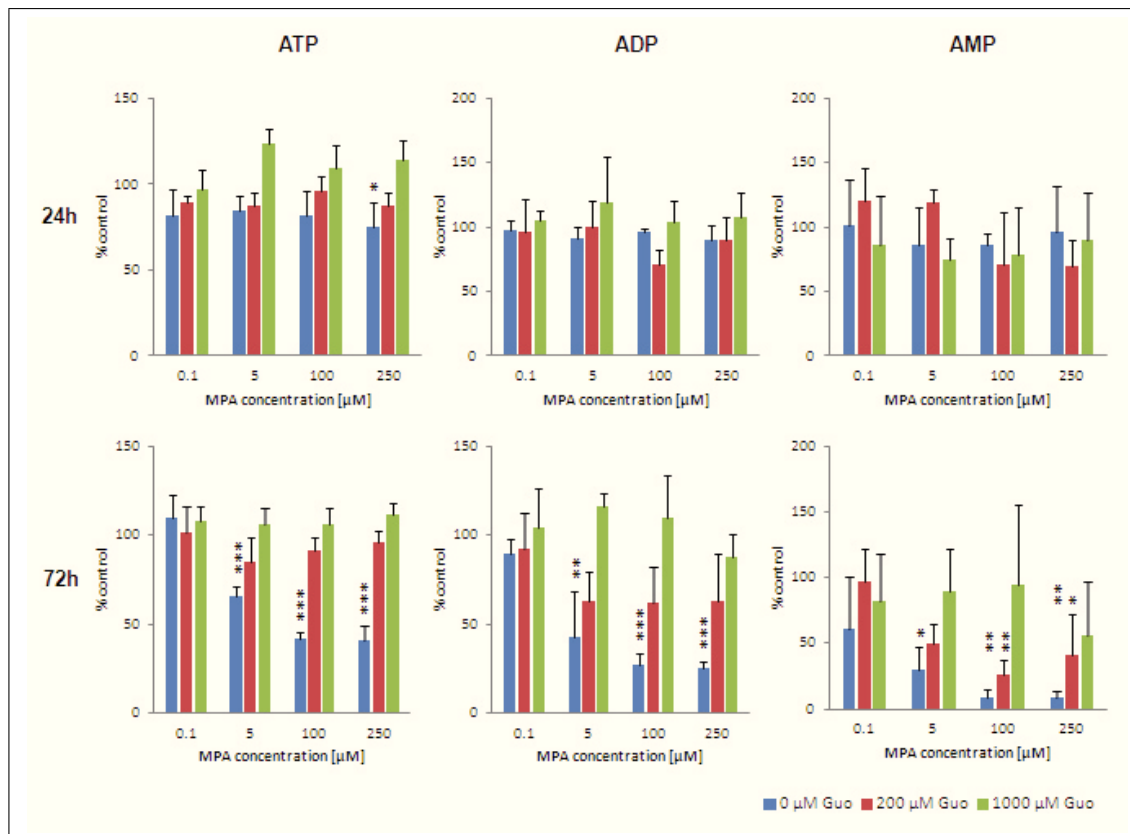


Fig. 2.22: Adenosine nucleotide levels of LS180 cells after 24h and 72h (redosed every 24h) of treatment with MPA and guanosine. Values are given as means of % of controls ($N=4$). Significance was determined using one-way ANOVA combined with Scheffe's post – hoc test with *: $p<0.05$; **: $p<0.005$; ***: $p<0.001$ versus controls.

2 Results and Discussion

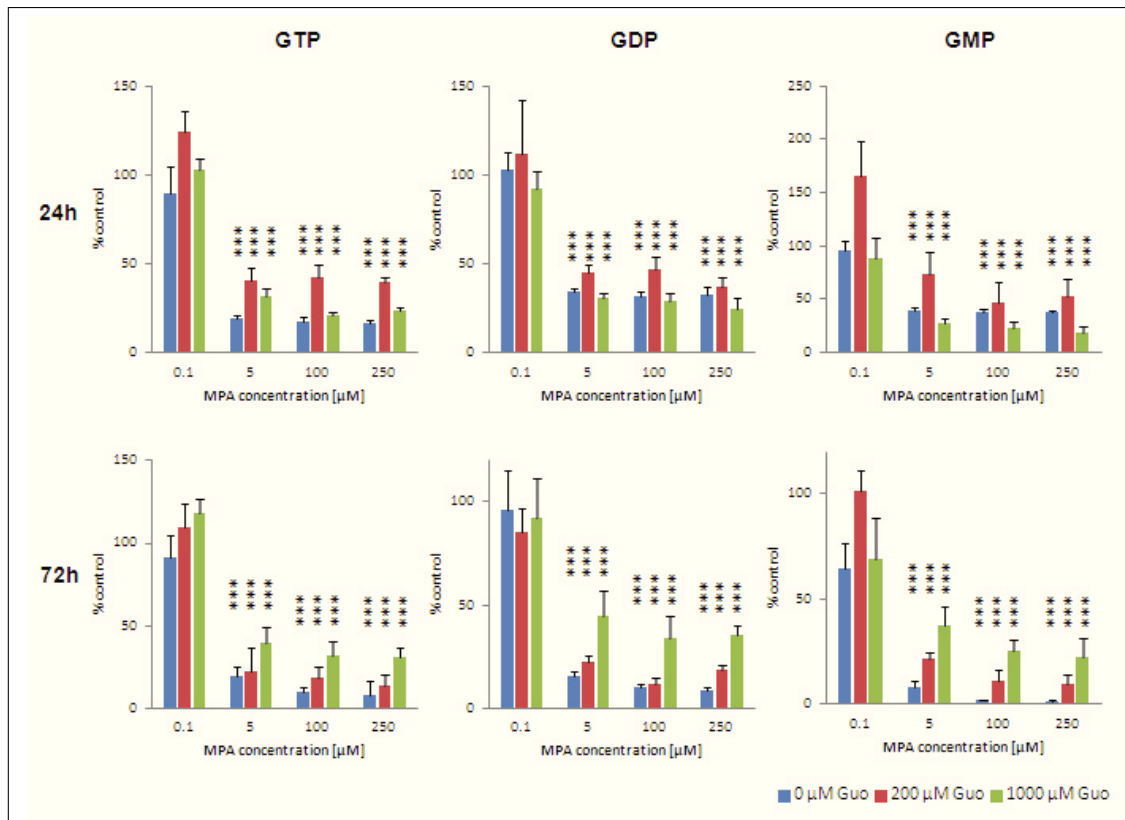


Fig. 2.23: Guanosine nucleotide levels of LS180 cells after 24h and 72h (redosed every 24h) of treatment with MPA and guanosine. Values are given as means of % of controls ($N=4$). Significance was determined using one-way ANOVA combined with Scheffe's *post – hoc* test with *: $p<0.05$; **: $p<0.005$; ***: $p<0.001$ versus controls.

2.5 Effects on nucleotide levels and energy charge

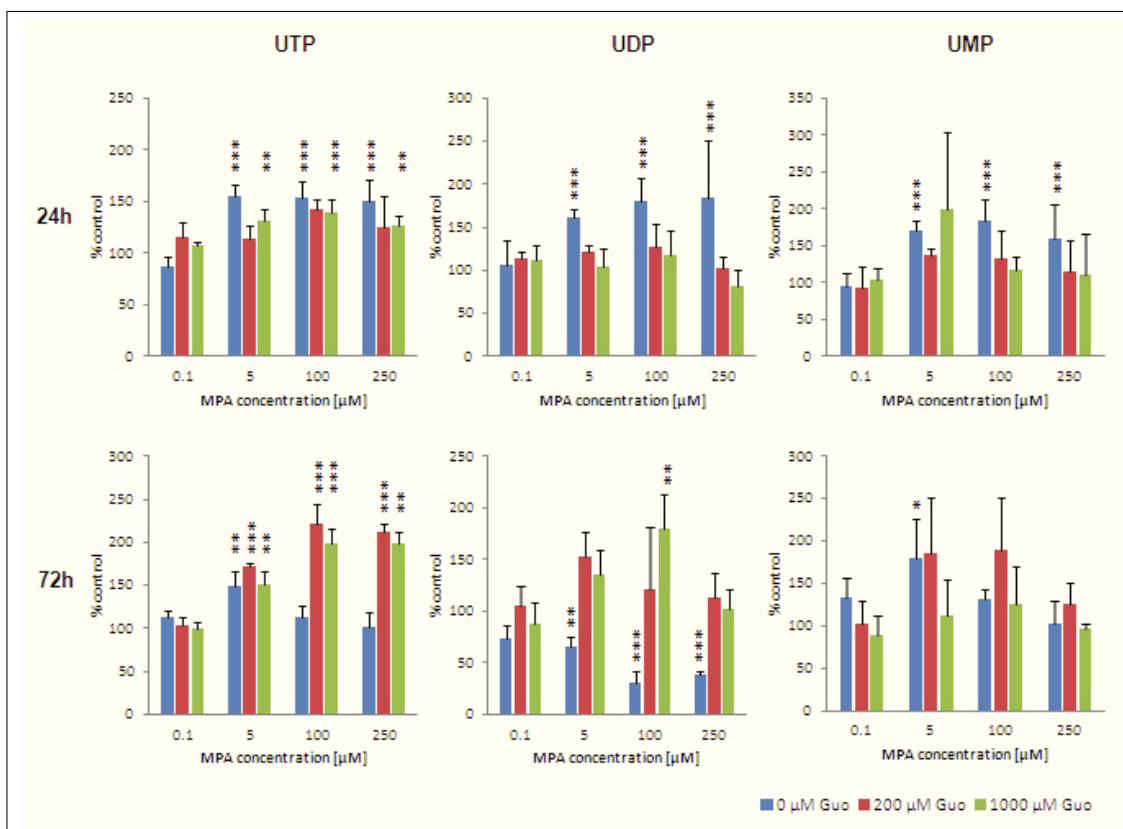


Fig. 2.24: Uridine nucleotide levels of LS180 cells after 24h and 72h (redosed every 24h) of treatment with MPA and guanosine. Values are given as means of % of controls ($N=4$). Significance was determined using one-way ANOVA combined with Scheffe's post – hoc test with *: $p<0.05$; **: $p<0.005$; ***: $p<0.001$ versus controls.

2 Results and Discussion

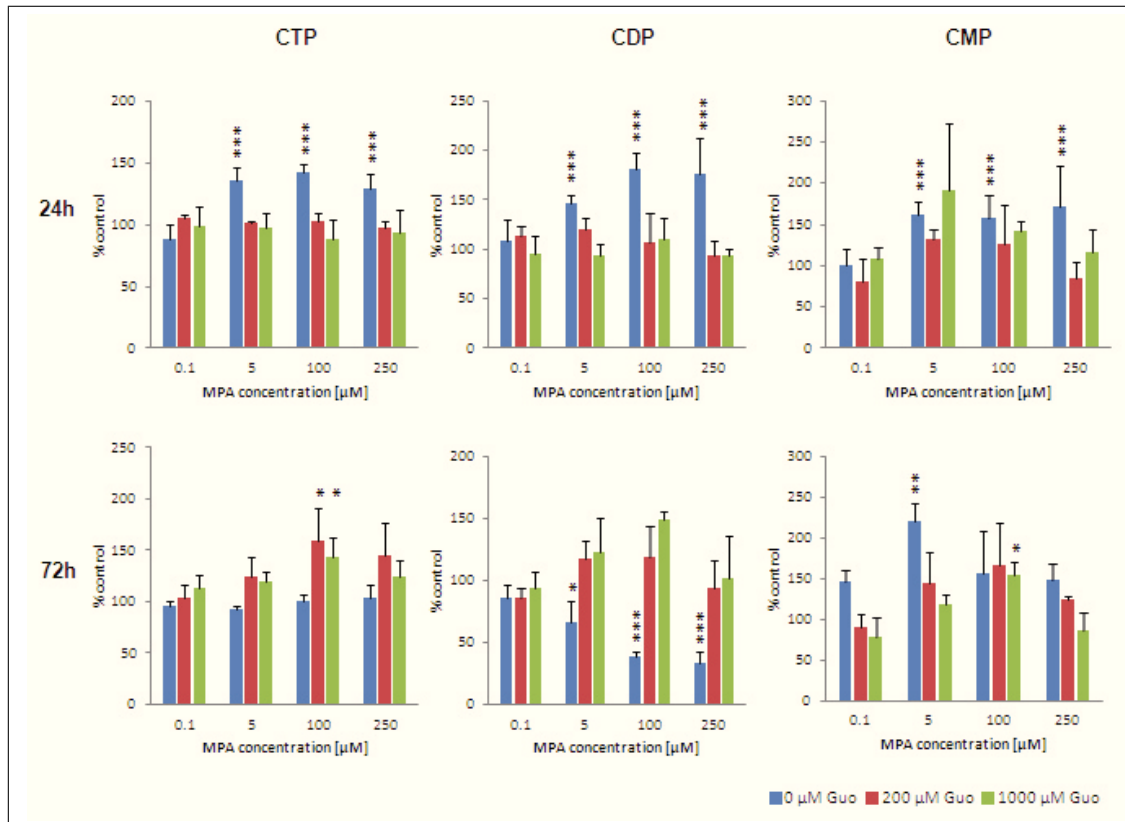


Fig. 2.25: Cytidine nucleotide levels of LS180 cells after 24h and 72h (redosed every 24h) of treatment with MPA and guanosine. Values are given as means of % of controls ($N=4$). Significance was determined using one-way ANOVA combined with Scheffe's post – hoc test with *: $p<0.05$; **: $p<0.005$; ***: $p<0.001$ versus controls.

2.5 Effects on nucleotide levels and energy charge

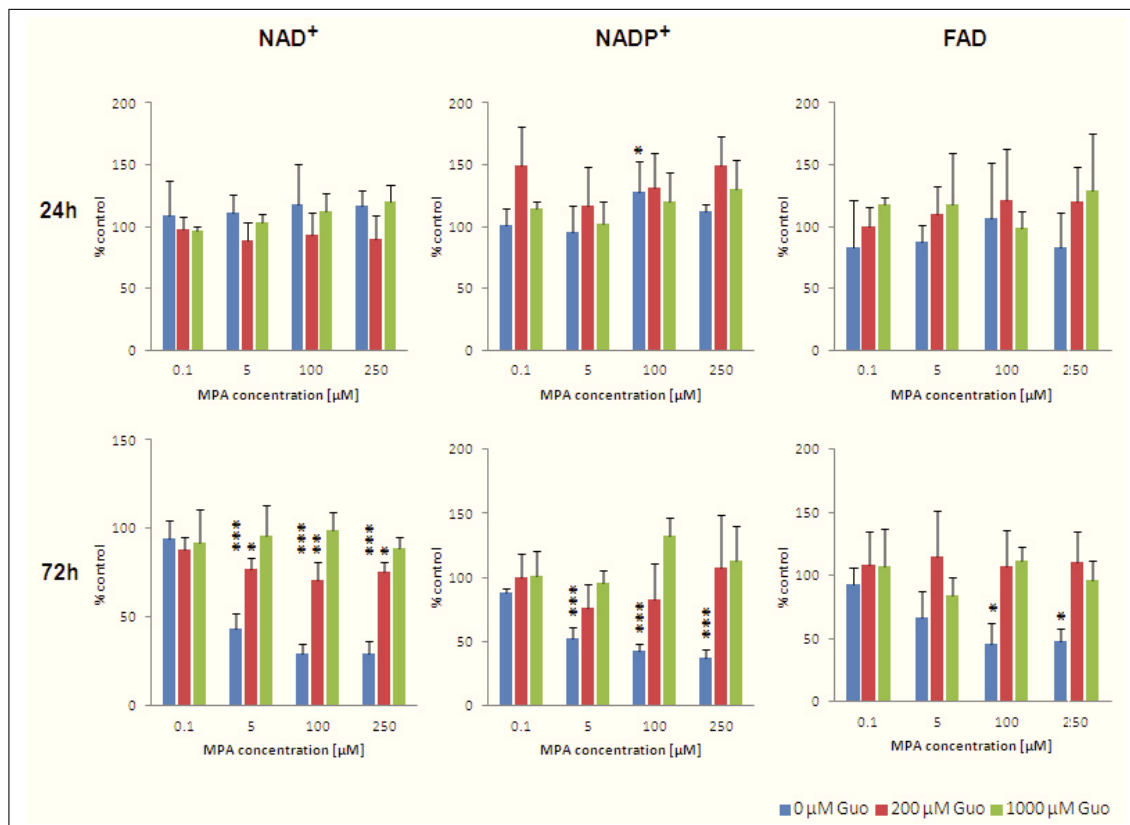


Fig. 2.26: NAD⁺, NADP⁺, and FAD levels of LS180 cells after 24h and 72h (redosed every 24h) of treatment with MPA and guanosine. Values are given as means of % of controls (N=4). Significance was determined using one-way ANOVA combined with Scheffe's post – hoc test with *: $p < 0.05$; **: $p < 0.005$; ***: $p < 0.001$ versus controls.

2 Results and Discussion

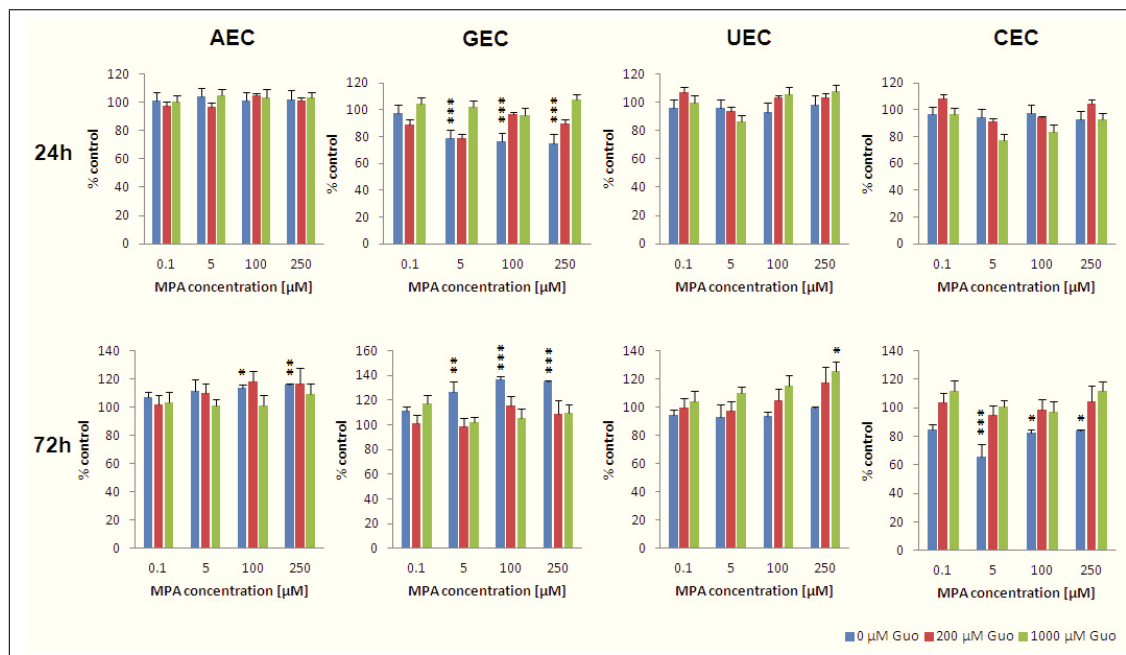


Fig. 2.27: Energy charges for adenosine (AEC), guanosine (GEC), uridine (UEC), and cytidine (CEC) nucleotides in LS180 cells after 24h and 72h (re-dosed every 24h) of treatment with MPA and guanosine. Values are given as means of % of controls (N=4). Significance was determined using one-way ANOVA combined with Scheffe's post – hoc test with *: $p < 0.05$; **: $p < 0.005$; *: $p < 0.001$ versus controls.**

Table 2.2: Influence of exogenous guanosine (Guo) on nucleotide levels and energy charge. Statistically significant changes ($\uparrow\downarrow$, number of displayed arrows reflects the most significant change within one treatment group of increasing MPA concentrations versus controls) and trends ($\uparrow\downarrow$, not statistically significant) in compound concentrations versus controls are summarized, $p < 0.05$: \uparrow/\downarrow , $p < 0.01$: $\uparrow\uparrow/\downarrow\downarrow$, $p < 0.001$: $\uparrow\uparrow\uparrow/\downarrow\downarrow\downarrow$.

	0 μM Guo		200 μM Guo		1000 μM Guo	
	24h	72h	24h	72h	24h	72h
ATP	$\downarrow\downarrow\downarrow$	$\downarrow\downarrow\downarrow$	-	-	\uparrow	-
ADP	-	$\downarrow\downarrow\downarrow$	-	\downarrow	-	-
AMP	-	$\downarrow\downarrow\downarrow$	-	$\downarrow\downarrow$	-	-
GTP	$\downarrow\downarrow\downarrow$	$\downarrow\downarrow\downarrow$	$\downarrow\downarrow\downarrow$	$\downarrow\downarrow\downarrow$	$\downarrow\downarrow\downarrow$	$\downarrow\downarrow\downarrow$
GDP	$\downarrow\downarrow\downarrow$	$\downarrow\downarrow\downarrow$	$\downarrow\downarrow\downarrow$	$\downarrow\downarrow\downarrow$	$\downarrow\downarrow\downarrow$	$\downarrow\downarrow\downarrow$
GMP	$\downarrow\downarrow\downarrow$	$\downarrow\downarrow\downarrow$	$\downarrow\downarrow\downarrow$	$\downarrow\downarrow\downarrow$	$\downarrow\downarrow\downarrow$	$\downarrow\downarrow\downarrow$
UTP	$\uparrow\uparrow\uparrow$	$\uparrow\uparrow\uparrow$	\uparrow	$\uparrow\uparrow\uparrow$	$\uparrow\uparrow\uparrow$	$\uparrow\uparrow\uparrow$
UDP	$\uparrow\uparrow\uparrow$	$\downarrow\downarrow\downarrow$	-	-	-	$\uparrow\uparrow$
UMP	$\uparrow\uparrow\uparrow$	$\uparrow\uparrow$	-	\uparrow	-	-
CTP	$\uparrow\uparrow\uparrow$	-	-	\uparrow	-	$\uparrow\uparrow$
CDP	$\uparrow\uparrow\uparrow$	$\downarrow\downarrow\downarrow$	-	-	-	\uparrow
CMP	$\uparrow\uparrow\uparrow$	$\uparrow\uparrow$	\uparrow	\uparrow	\uparrow	$\uparrow\uparrow\uparrow$
NAD ⁺	-	$\downarrow\downarrow\downarrow$	-	$\downarrow\downarrow$	-	-
NADP ⁺	$\uparrow\uparrow$	$\downarrow\downarrow\downarrow$	-	-	-	-
FAD	-	$\downarrow\downarrow$	-	-	-	-
AEC	-	\downarrow	$\downarrow\downarrow$	$\downarrow\downarrow$	-	-
GEC	$\downarrow\downarrow\downarrow$	$\uparrow\uparrow\uparrow$	-	-	-	-
UEC	-	-	-	-	-	\uparrow
CEC	-	$\downarrow\downarrow\downarrow$	-	-	-	-

2 Results and Discussion

media were not supplemented with guanosine and values returned to control levels under treatment with 200 μ M and 1000 μ M guanosine (Fig. 2.22 and Fig. 2.27), examination of Na⁺-K⁺-ATPase expression levels in MPA-treated LS180 cells seemed valuable. Additionally ATPase α and β subunits were found by Asif et al. and Shipkova et al. to be covalently modified by the AcMPAG metabolite of MPA [175, 176]. To evaluate adenosine nucleotide and AEC levels in the context of Na⁺-K⁺-ATPase expression levels, western blots for the determination of Na⁺-K⁺-ATPase expression levels of lysates of LS180 cells treated with 0, 0.1, 1, 5, 10, 100, and 250 μ M MPA and 0, 200, and 1000 μ M guanosine were run. Western blots are shown in Figure 2.28 and expression levels normalized based on β -actin and calculated as % of controls in Figure 2.29.

There were no significant changes in Na⁺-K⁺-ATPase expression levels, although a trend toward overexpression could be observed in LS180 cells treated with high MPA concentrations and no guanosine for 24h (Fig. 2.29). After 72h or when culture media were supplemented with guanosine Na⁺-K⁺-ATPase expression returned to control levels. In comparison to changes in ATP and ADP concentrations as summarized in Table 2.2, decreases in ATP levels and normal levels of ADP after 24h MPA treatment (without guanosine) may at least partially be related to overexpression of Na⁺-K⁺-ATPase, although multiple reasons, e.g. decreases in oxidative phosphorylation and/or tricarboxylic acid (TCA) cycle activity, may also contribute to the decrease of ATP levels.

2.5.4 Influence of MPA treatment on cAMP and cGMP levels

While cAMP and cGMP are well-characterized in their functions as second messengers roles of cUMP and cCMP as signaling molecules are still widely unknown [161]. cAMP and cGMP are synthesized from the cytosolic purine nucleotides ATP and GTP by adenylyl and guanylyl cyclases, respectively [161, 179, 180]. cAMP and cGMP are degraded by phosphodiesterases [180]. cAMP acts mostly but not exclusively through activation of cAMP-dependent protein kinases. It influences cell metabolism, morphology, gene transcription, and regulates functions of ion channels and other proteins [161, 181]. cGMP also regulates fundamental processes within cells such as gene expression, cell growth, and apoptosis. It is involved in contraction/relaxation of smooth muscle [179] which is of special interest in the GI tract regulating its muscle tone via the nitric oxide-cGMP signaling pathway [182].

To rule out depletion of cAMP and/or cGMP which could be expected from findings described in Section 2.5.2; levels of both cyclic nucleotide monophosphates in LS180 cells under MPA treatment with and without exogenous guanosine supplementa-

2.5 Effects on nucleotide levels and energy charge

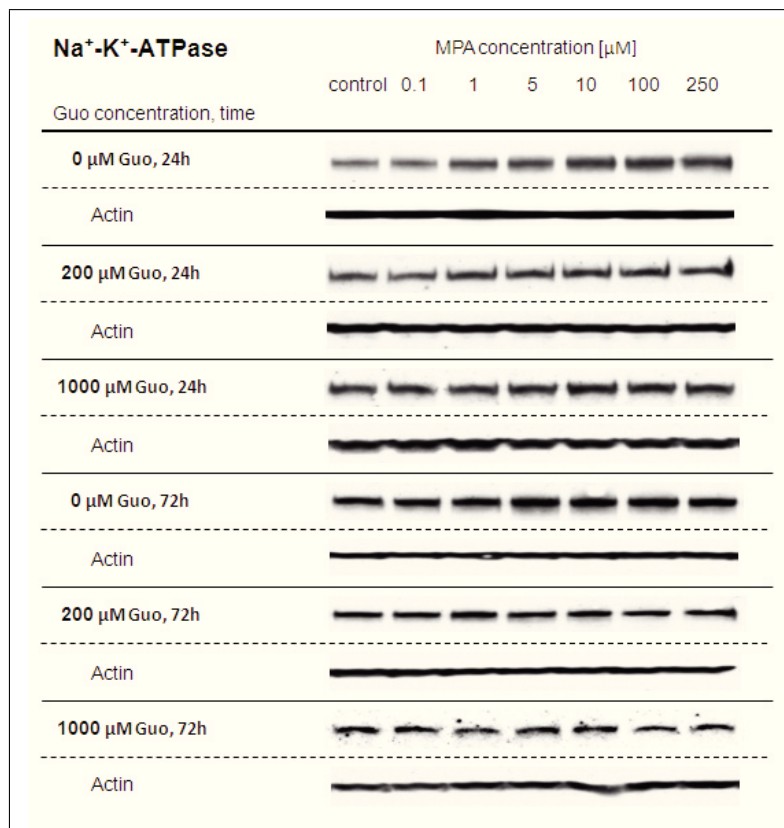


Fig. 2.28: Western blots for determination of expression levels of Na⁺-K⁺-ATPase in LS180 cells after treatment with MPA and guanosine for 24h and 72h. Bands are shown with their respective β -actin bands ($N=3$). Relative intensities normalized based on β -actin and calculated as % of controls are shown in Figure 2.29. Na⁺-K⁺-ATPase gave a band at 120kDa (predicted 95kDa), difference between actual and predicted band size probably due to post-translational modifications [125]; bands for Na⁺-K⁺-ATPase at higher molecular weights than the predicted have been reported in the literature already (most likely due to phosphorylation or glycosylation state of the protein) [177] and have been reported in product sheets for other available Na⁺-K⁺-ATPase antibodies [178].

2 Results and Discussion

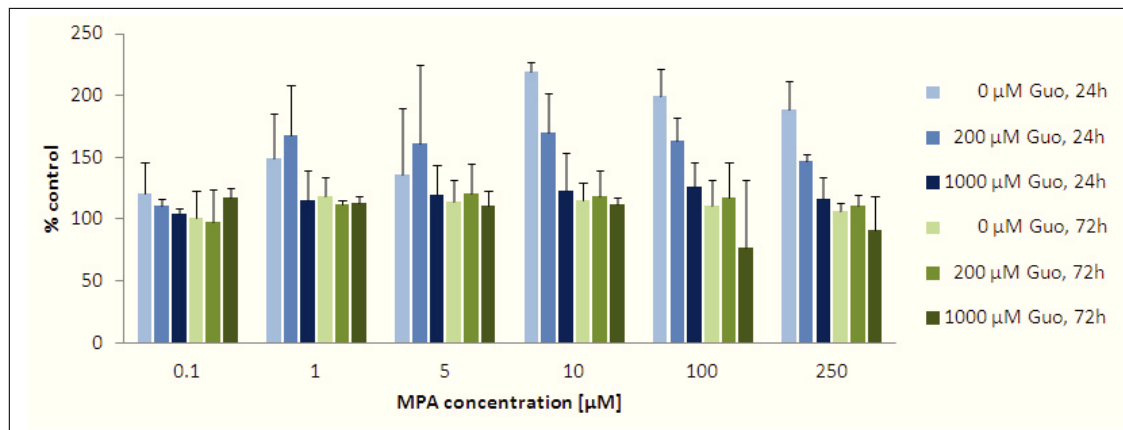


Fig. 2.29: Expression levels of $\text{Na}^+\text{-K}^+\text{-ATPase}$ in LS180 cells after treatment with MPA and guanosine for 24h and 72h. Values are given as means of % of controls of relative intensities normalized based on $\beta\text{-actin}$ ($N=3$). Western blots with their respective $\beta\text{-actin}$ bands are shown in Figure 2.28. No statistically significant differences in $\text{Na}^+\text{-K}^+\text{-ATPase}$ expression levels versus controls were found after treatment with increasing concentrations of MPA and guanosine for 24h and 72h ($p=0.59$ for $10\mu\text{M}$ MPA versus control, $0\mu\text{M}$ guanosine, 24h).

tion were measured using enzyme-linked immunosorbent assays (ELISAs, Cyclic AMP/GMP Competitive Enzyme Immunoassays Kit, Cayman Chemical). Aliquots of cell lysates that were used for caspase-3 western blots (Sec. 2.3.2) and western blots for validation of proteomics experiments (Sec. 2.7.1) were used.

Competitive enzyme immunoassays that are based on competition of free cAMP/cGMP and a cAMP/cGMP-acetylcholinesterase conjugate (cAMP/cGMP tracer) for a limited number of cAMP/cGMP-specific antibody binding sites were used. Dependent on a sample's amount of cAMP/cGMP, only a proportion of the tracer is able to bind to the antibody. The tracer-antibody complex is bound to a second antibody immobilized on the ELISA plate. Providing the substrate for acetylcholinesterase, an enzymatic reaction is initiated. The reaction's yellow-colored product strongly absorbs at 412nm. Color intensity is proportional to the amount of tracer bound which is inversely proportional to the sample's cAMP/cGMP concentration.

As can be seen in Figure 2.30 cAMP concentrations after 24h treatment are unaffected for all combinations of MPA and guanosine. After 72h a trend towards elevated cAMP levels in LS180 cells not supplemented with guanosine occurred. cAMP levels in cells supplemented with $200\mu\text{M}$ guanosine increased with MPA concentration. The increases were rather small and seemed to reach statistical significance

2.5 Effects on nucleotide levels and energy charge

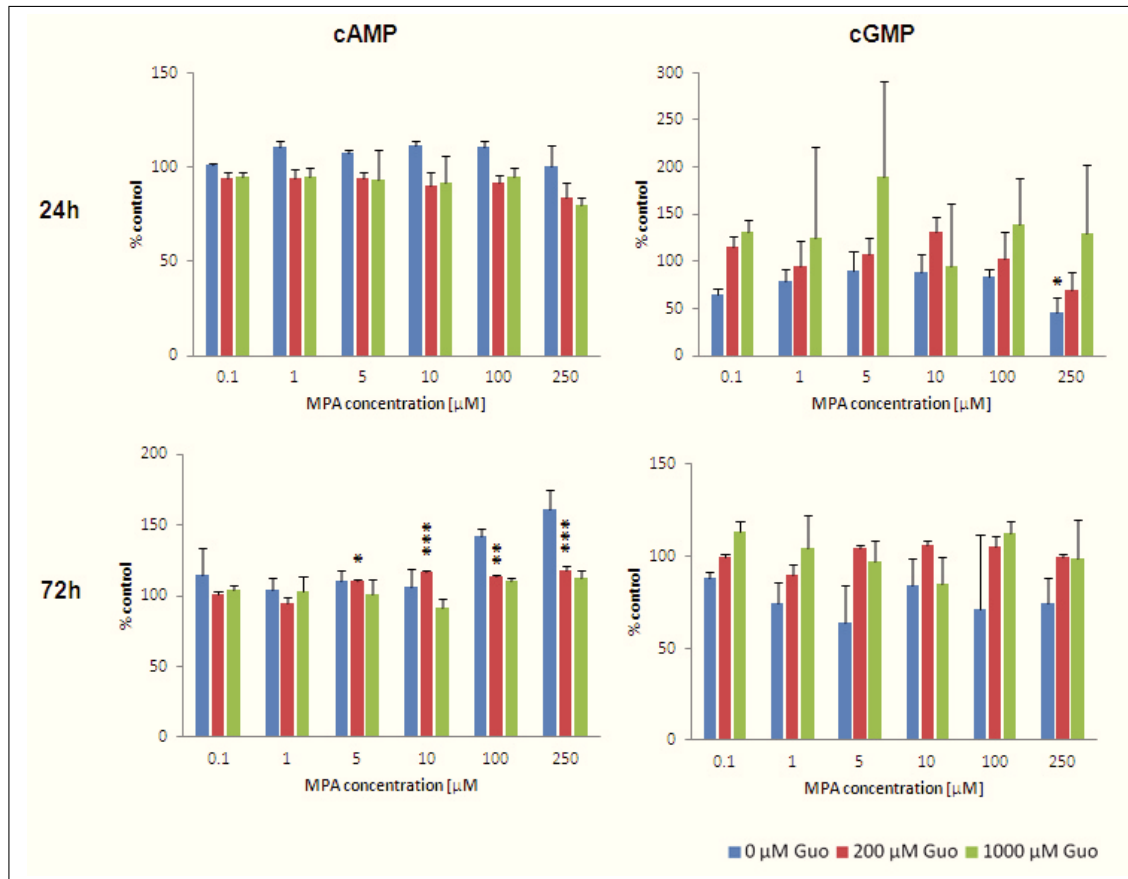


Fig. 2.30: cAMP and cGMP levels in LS180 cells after treatment with MPA and guanosine for 24h and 72h. Values are given as means of % of controls ($N=3$). Measurement of absorbance using a cAMP/cGMP standard allowed calculation of the absolute amount of cAMP/cGMP as well as calculation of the values as % of controls. Statistically significant differences in cAMP levels versus controls were only found after treatment with increasing concentrations of MPA and 200 μM guanosine after 72h for the four highest MPA concentrations used (due to relatively small standard deviations of this set of samples). A statistically significant difference in cGMP levels versus controls was only found after treatment with increasing concentrations of MPA and without guanosine supplementation after 24h for the highest MPA concentration.

2 Results and Discussion

only due to very small standard deviations of this set of samples. Most importantly cells treated with 1000 μ M guanosine did not show changes in cAMP levels incubated with MPA. cGMP levels of LS180 cells were not affected significantly by MPA treatment, except for 250 μ M MPA without guanosine supplementation. These data emphasized once more the importance of guanosine supplementation for these experiments.

Only little research on the influence of MPA on cAMP or cGMP concentrations *in vitro* and *in vivo* has been performed. The available literature is not consistent and described effects are cell type-dependent. Studying the reduction in β -adrenergic response of C6 glioma cells (rat glioma) Franklin et al. measured decreased cAMP responses to (+/-)isoprenaline, used as β -adrenergic stimulant, after MPA treatment [183]. Responses were restored by addition of guanine (intermediate of the salvage pathway of purine synthesis, conversion by HGPRT to GMP directly, or conversion to guanosine by purine nucleoside phosphorylase and consecutive conversion to GMP by guanosine kinase/5'-nucleotidase) along with MPA (after 3h, 31 μ M MPA, 166 μ M guanine). In another study the ability of prostaglandin E₁ and isoproterenol to elevate intracellular cAMP concentrations in cultured normal rat kidney cells was decreased by MPA (20-100 μ M) by 50-70% with the response being maximal after 2h [184].

While Naor et al. found basal and hormone-induced cGMP concentrations decreased to undetectable levels (method used not mentioned) in cultured pituitary cells (primary cultures of cells from the pituitary gland of adult female rats) [185], Messina et al. report intracellular cGMP levels to be increased during MPA-induced neuroblastoma differentiation in LAN5 and SHEP cells (human neuroblastoma) [180].

Overall most negative effects of MPA on nucleotide levels (Tab. 2.1) were ameliorated or fully reversed by supplementation with guanosine (Tab. 2.2). In a physiologic context and for discussion of our data presented in the next sections, experiments using 1000 μ M guanosine supplementation are the most relevant. Despite supplementation with 1000 μ M guanosine levels of all guanosine nucleotides were significantly decreased ($p < 0.001$) as well as levels of uridine and cytosine nucleotides upregulated with effects on the UEC (these findings will be discussed in later sections).

2.6 HPLC-MS method development and preliminary studies for method validation

In the context of a different study performed in our laboratory “A High-Throughput Ultra High-Performance Liquid Chromatography-Tandem Mass Spectrometry Assay for the Quantification of Mycophenolic Acid and its Major Metabolites Mycophenolic Acid Glucuronide and Mycophenolic Acid Acyl Glucuronide in Human Plasma and Urine” was developed by Klepacki et al. [186]. The assay met all predefined acceptance criteria and the quantification of MPA was successfully cross-validated with an HPLS-MS assay routinely used for clinical therapeutic drug monitoring in our laboratory.

While this newly developed assay uses human ethylenediaminetetraacetic acid (EDTA) plasma and urine as matrices an assay for the determination of intracellular and extracellular drug concentrations in cell extracts (MeOH extracts) and cell culture media of LS180 cells was developed (Sec. 2.6.1) and it was attempted to validate this assay in these media. The routinely used assay for clinical therapeutic drug monitoring served as basis, but since this assay only measures MPA concentrations with MMF as an internal standard, modification of the assay was necessary. During assay development and validation problems with the stabilities of MPA metabolites presented themselves. As these problems have not been described in the literature before, they will be presented in Section 2.6.2.

2.6.1 HPLC-MS method development

An HPLC-MS assay was developed for MPA, MMF, MPAG, AcMPAG, DM-MPA, and MPA-GS. It was not possible to capture morpholinoethanol along with the other analytes due to low sensitivity and unsatisfying peak shape at higher concentrations (most likely due to problems with chromatography). DM-MPA-6G and DM-MPA-4G were not included in the method due to a lack of commercial availability of reference material. AcMPA-GS was not included (although it was included in Sec. 2.7.2 in the search for covalent modifications of proteins) due to very low amounts present in body fluids of transplant patients (concentrations below detection limits, Sec. 1.1.5).

Measurements were performed on an API 4000 triple quadrupole (AB Sciex) or API 5000 triple quadrupole (AB Sciex). The instrument was operated in the positive multiple reaction monitoring (MRM) mode with electrospray ionization (ESI) source and was equipped with an Agilent 1100 HPLC system (Agilent 1100 HPLC pump, Agi-

2 Results and Discussion

lent 1100 inline extraction system, Agilent 1100 well plate autosampler, Agilent 1100 binary pump, and Agilent 1100 column thermostat). Analytes were extracted using a ZORBAX Eclipse XDB-C8, 5 μ m (4.6mm x 5mm) column (Agilent Technologies) and separated using a ZORBAX Eclipse XDB-C8, 3.5 μ m (4.6mm x 150mm) column (Agilent Technologies). The solvents were 0.1% aqueous formic acid (FA, mobile phase A) and methanol + 0.1% FA (mobile phase B). The gradient used for inline extraction was: 0.0-0.5min 15% methanol at a flow rate of 3000 μ L/min, 0.5-0.6min 15%-98% methanol at a flow rate of 3000 μ L/min, 0.6-3.5min 98% methanol at a flow rate of 100 μ L/min, 3.5-4.3min 98% methanol at a flow rate of 4000 μ L/min, 4.3-4.8min 98%-15% methanol at a flow rate of 4000 μ L/min, 4.8-4.9min 15% methanol at a flow rate of 3000 μ L/min for re-equilibration to starting conditions. The gradient used for separation (at a constant flow rate of 1000 μ L/min) was: 0.0-0.5min 50% methanol, 0.5-2.5min 50-82% methanol, 2.5-6.7min 82-98% methanol, 6.7-7.0min 98-50% methanol for re-equilibration to starting conditions. Nitrogen was used as drying gas and collision gas. The mass spectrometry parameters were: ion transition MPA: $m/z = 343.1 [M+Na]^+ \rightarrow 187.3$ with 50msec dwell time, 66V declustering potential (DP), 25V collision energy (CE), and 16V collision cell exit potential (CXP); ion transition MMF: $m/z = 434.3 [M+H]^+ \rightarrow 195.3$ with 50msec dwell time, 61V DP, 47eV CE, 14V CXP; ion transition MPAG/AcMPAG: $m/z = 519.0 [M+Na]^+ \rightarrow 343.0$ with 50msec dwell time, 66V DP, 25eV CE, 16V CXP; ion transition DM-MPA: $m/z = 307.2 [M+H]^+ \rightarrow 193.1$ with 50msec dwell time, 56V DP, 31eV CE, 16V CXP, ion transition MPA-GS: $m/z = 505.3 [M+Na]^+ \rightarrow 343.1$ with 50msec dwell time, 81V DP, 35eV CE, 10V CXP; ion transition MPA-d3: $m/z = 346.3 [M+Na]^+ \rightarrow 232.1$ with 50msec dwell time, 66V DP, 25eV CE, 16V CXP; ion transition MPAG-d3: $m/z = 522.0 [M+Na]^+ \rightarrow 346.0$ with 50msec dwell time, 66V DP, 25eV CE, 16V CXP. MPA-d3 and MPAG-d3 were used as internal standards. The source temperature was set to 450°C with a capillary voltage of 5000V and collisionally activated dissociation (CAD) set to 12. The column oven temperature was set to 65 \pm 5°C. The injection volume was 100 μ L. Total run time was 7.0min.

In Figure 2.31 a representative total ion chromatogram showing peaks of all analytes included in the above described method is depicted. MeOH/H₂O (1:1) was used as matrix. MPAG and AcMPAG (pink) are only distinguishable by their retention times (3.5min for MPAG and 4.3min for AcMPAG) as the glucuronide metabolites are of the same mass and share the same ion transition. Small amounts of MPA (blue) are detected at the retention times of the glucuronides due to in-source fragmentation of MPAG and AcMPAG in the electrospray interface after separation.

2.6 HPLC-MS method development and preliminary studies for method validation

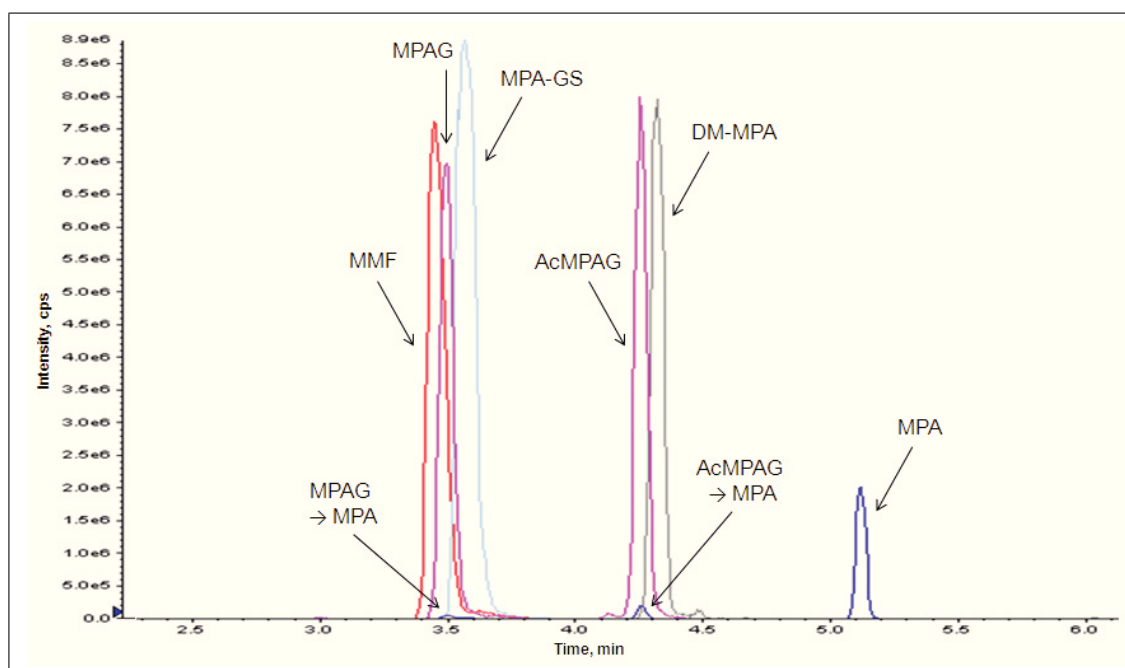


Fig. 2.31: Representative total ion chromatogram of all analytes included in the HPLC-MS method for quantification of MPA, MMF, and their metabolites. The chromatogram was recorded under the conditions described above in MeOH/H₂O (1:1) as matrix.

2.6.2 Preliminary studies prior to HPLC-MS method validation

Limits of detection

Limits of detection in MeOH/H₂O (1:1) were found to be 250pM for MPA, 25pM for MMF, MPAG, AcMPAG, as well as for DM-MPA, and 50pM for MPA-GS (API 4000 triple quadrupole mass spectrometer).

Possible pH- and matrix component-dependency of the stability of AcMPAG and MPAG

Validation was started at a time when LS180 cell culture media were still supplemented with 10% FBS. During method validation in cell culture media as matrix (media at neutral pH, extracted with 30% 0.2M ZnSO₄/70% MeOH-solution at pH=5.82 as the normal pH of this solution) remarkable effects were seen, starting with calibration curves showing rapid degradation of AcMPAG. In publications it is often recommended to acidify samples which are going to be subjected to measurement of AcMPAG levels to a pH of 2 immediately [187] as AcMPAG and acyl glucuronides in general are known to be instable at neutral pH and to be more stable in acidic environments [187, 188].

For a quick scan of pH-dependent effects, cell culture media containing all analytes at medium concentration ranges were extracted with two different MeOH/ZnSO₄-solutions acidified with FA to pH=4.47 (0.01% FA) and pH=3.75 (0.1% FA). Usage of MPA-d₃ and MPAG-d₃ as internal standards revealed pH-dependent conversion of MPAG-d₃ to AcMPAG-d₃, which only became obvious due to usage of the deuterated forms of the analytes MPA and MPAG. Figure 2.32 shows chromatograms of analytes recorded in the internal standard channel after extraction of 10.000μM calibrators with MeOH/ZnSO₄-solutions of different pH values. Degradation of MPAG-d₃ (retention time ca. 3.5min) can be seen as well as formation of AcMPAG-d₃ (retention time ca. 4.2min) and even MPA-d₃ (retention time ca. 3.5min) at lower pH values. Since all analytes (undeuterated) were spiked into samples the respective contributions to the occurring analyte formation/degradation as well as mechanisms (intra- or intermolecular conversion) remain unknown.

For a more qualitative and quantitative approach starting conditions for experiments were refined. Four buffers of different pH values were used. 10mM ammonium acetate was used as matrix to clarify the above described interconversions

2.6 HPLC-MS method development and preliminary studies for method validation

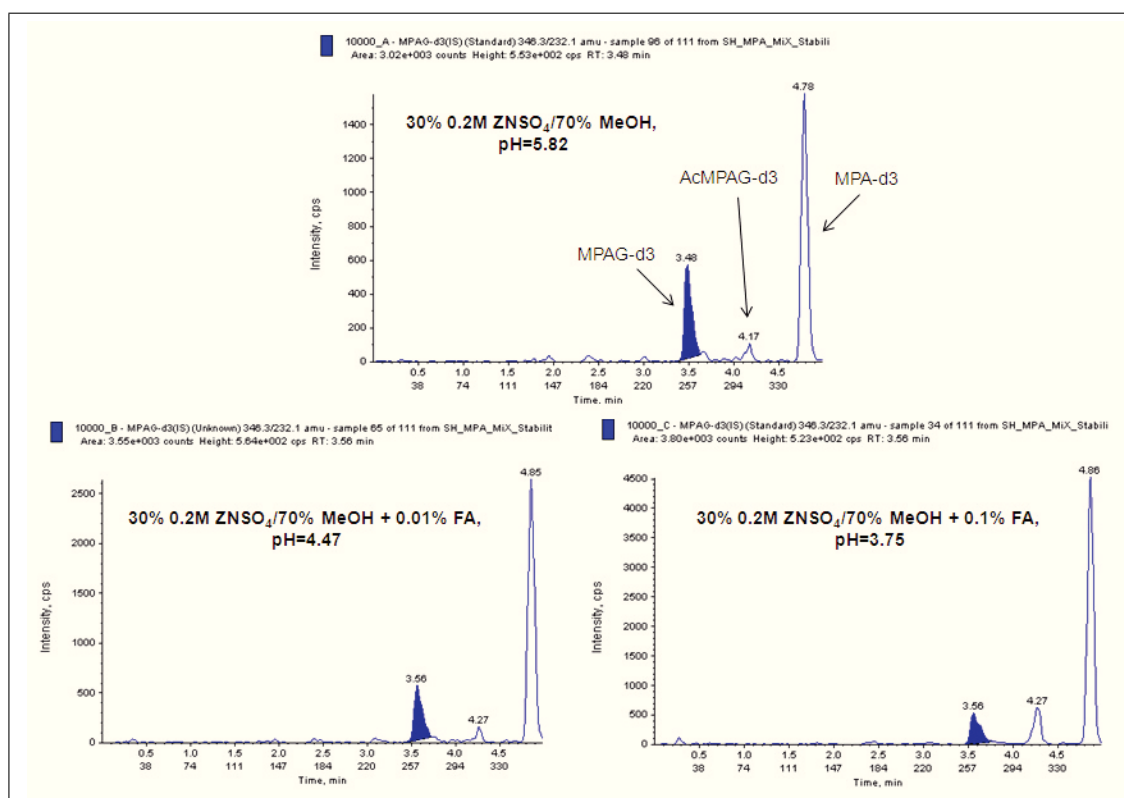


Fig. 2.32: Ion chromatograms of calibrators ($10.000\mu\text{M}$) extracted with MeOH/ZnSO₄-solutions of different pH values for stability experiments for MPA method development recorded in the internal standard channel. *The experiment was preliminary and due to the described stability problems no absolute concentrations were calculated. The experiment was performed with an N=3 showing similar results.*

2 Results and Discussion

which were initially thought to be only pH-dependent. The pH values of interest were chosen to be pH=2, 5, 7, and 9 to cover the entire pH range of the GI tract (Fig. 1.6). Knowledge of pH-dependent (and matrix component-dependent as described below) drug/metabolite stability/conversion within the GI tract (especially in terms of metabolites forming covalent adducts with proteins, Sec. 2.7.2) is not only important in terms of extraction method and HPLC-MS method validation, but is also inevitable when researching/discussing the reasons for GI toxicity of MPA.

The 10mM ammonium acetate buffers (slightly basic) were put to neutral or acidic pH with HCl (pH=2, 5, and 7), or to a basic pH (pH=9) with ammonium hydroxide. Different sets of samples (MPAG alone, MPAG + MPA, MPAG + MMF; 0, 100, 1000, 10000 μ M) were prepared in buffers of distinct pH values and measured immediately or incubated for different time periods (30min, 2h, 5h, 24h) on ice. MPAG alone was used to check on intramolecular conversion of MPAG to AcMPAG, MPAG + MPA were used in case of intermolecular conversion of MPAG to AcMPAG and the availability of free MPA as a prerequisite, MPAG + MMF as a negative control in case of intermolecular conversion (MMF turned out to be relatively stable over at least 24h even at 37°C in cell culture medium in previously conducted experiments, data not shown; MMF is also used as an internal standard in the above mentioned clinical assay). No internal standard was used due to possible interference with analytes.

Surprisingly, no excessive conversion of MPAG to AcMPAG or MPA was seen in any sample at any pH value. This led to the idea of other matrix components, present in the used cell culture media but not in the used buffers, triggering analyte degradation/conversion.

A vast amount of literature on the stability/instability and reactivity of drugs and/or their glucuronide metabolites in the presence of albumin and/or FBS is available [189–197]. While much of the literature deals with pH- and albumin-dependent acyl migration and protein binding of glucuronides, hydrolysis of glucuronides in the presence of albumins is addressed as well [194]. Examining the stability of glucuronides matrices such as buffers, human serum albumin (HSA) solutions (eventually of different HSA percentages), and human plasma are often routinely investigated [190–192]. Drug/metabolite conversion, degradation, binding to matrix components, and even stereoselectivity of reactions are not unusual [193]. Thus, Akira et al. found the extent of hydrolysis of synthetic probenecid glucuronides in plasma larger than that in buffer [194], and Mc Gurk et al. described mefenamic acid 1-O-acyl glucuronide to be relatively stable at physiological pH values (more

instable at basic pH values) [195].

Data discussed in this section gives hints for future experiments of MPA method validation and necessary experiments preceding MPA method validation including extraction methods. Thus, the stabilizing effect of low pH values which is discussed in the literature and recommended for sample handling, may be due to conversion of MPAG to AcMPAG in the presence of albumin especially since the matrix used in the above cited assays and studies is generally human plasma which provides a certain amount of HSA.

2.7 Investigation of proteome alterations in LS180 cells after MPA treatment

Two kinds of experiments were conducted to identify MPA-induced changes in the proteome of LS180 cells. Overall changes to the protein content of cells were identified successfully using Stable Isotopic Labeling by Amino Acids in Cell Culture (SILAC) technology. Additionally an anti-MPA/AcMPAG antibody was used to detect direct protein targets of MPA and certain MPA metabolites (this experiment did not yield reasonable results as discussed in Section 2.7.2).

As data analysis in this section inevitably involves database searches and usage of the available online tools, it is remarked that ambiguities regarding the nomenclature of genes and proteins are a major problem in the literature and databases [198] (e.g. EC numbers not being assigned for many proteins). In this thesis, protein/gene names used by the Uniprot database were chosen to identify proteins/genes as well as Uniprot abbreviations. In cases of mistakable, intricate or not assigned abbreviations, the gene symbol was used as abbreviation for the encoded protein.

2.7.1 SILAC

For SILAC experiments two cell culture populations (i.e. treated and untreated cells) were grown in cell culture media supplemented with light (normal) amino acids (here L-lysine was used, but L-arginine or L-lysine and L-arginine in combination are routinely used as well) for one population and heavy (isotopic) amino acids for the other [199, 200]. Cellular proteins were labeled with the chemically identical light/heavy forms of the respective amino acids as cells proliferated and lysates of treated/untreated (labeled/unlabeled) cell populations were processed and analyzed

2 Results and Discussion

together eliminating errors due to unequal sampling. Isotopically different peptides were distinguished by MS analysis and differential proteome expression was quantified.

After a successful initial screen for positive/negative correlations of protein expression levels and MPA concentrations by GelC-MS of lysates of MPA-treated LS180 cells (no SILAC labeling, N=1 only, Sec. 3.9) SILAC experiments were conducted to identify and quantify proteome alterations in LS180 cells reliably. LS180 cells were labeled with light and heavy lysine according to the manufacturer's manual of the used labeling kit (Invitrogen, SILAC Protein Identification and Quantification Kits, Carlsbad, CA). Cells were treated with 0, 0.1, 5, 100, and 250 μ M MPA for 72h (redosed every 24h, supplemented with 1000 μ M guanosine). After extraction, lysis (Sec. 3.4), protein determination (Sec. 3.3), and in-solution tryptic digestion (Sec. 3.9.2) were performed and labeling efficiency was checked to be sufficient (>99%) for cell lysates grown in media containing heavy lysine (0.1, 5, 100, and 250 μ M MPA, Sec. 3.9). For SILAC experiments MPA treated lysates (labeled with heavy lysine, 20 μ g) were combined with equal amounts of control lysates (labeled with light lysine, 20 μ g). Samples were processed and analyzed by GelC-MS as described in Section 3.9.1.

Initial data filtering

Analysis of MS data using the MaxQuant software package (version 1.2.2.5, Max Planck Institute of Biochemistry, Martinsried, Germany; Sec. 3.9.2) conveyed a total of 2095 protein IDs. After removing protein ID hits without sufficient amounts of data for statistical analysis the remaining 268 IDs were filtered for changes in H/L ratios of >20% inbetween H/L=1 (ideal control value) versus H/L of 250 μ M MPA-treated/-untreated cell lysates (threshold H/L=1.2 for upregulated proteins, threshold H/L=0.8 for downregulated proteins). 75 proteins passed the threshold criteria out of which 35 proteins showed statistically significant changes among H/L ratios of treatments (no H/L-labeled set for controls was run since no H-labeled controls were available (no additional control labeled with heavy lysine was prepared) and H/L ratio of controls ideally equals 1; only treatments of different MPA concentrations, i.e. 0.1, 5, 100, and 250 μ M, were compared among each other). The 35 proteins are listed in Table 2.3 - Table 2.6 sorted by their percentagewise increases/decreases in levels. Abbreviations of protein names and genes, Uniprot accession numbers, Ensemble gene IDs, the number of unique peptides that served to identify respective proteins, means \pm standard deviations of SILAC H/L ratios,

2.7 Investigation of proteome alterations in LS180 cells after MPA treatment

and Pearson product-moment correlation coefficients are given as well (for detailed explanation please see tables). Pearson product-moment correlation coefficients only served to illustrate linearity of H/L ratios and concentration changes, but were not used as a threshold criterion for sorting of proteins since non-linearity of H/L ratios-concentration relationship was not supposed to be a criterion for exclusion.

Table 2.3: LS180 proteins of levels increased by >30% after MPA treatment identified by SILAC. Shown are protein numbers (assigned for clarity), protein names, protein and gene (*italic*) abbreviations, Uniprot accession numbers and Ensemble gene IDs, numbers of unique peptides identified, SILAC heavy/light (H/L) ratios for four MPA concentrations, Pearson product-moment correlation coefficients *r* for the correlation/linear dependence of H/L ratios and MPA concentrations, and the increase in protein levels after 250 μ M MPA treatment compared to a H/L ratio=1 as expected for controls (= calculation as % of controls). H/L ratios are given as means \pm standard deviations (N=3). Significance was determined for effects of increasing MPA concentrations using one-way ANOVA combined with Scheffe's post – hoc test with */ #/ o: $p < 0.05$; **/ ##/ oo: $p < 0.005$; ***/ ###/ ooo: $p < 0.001$ versus treatment with 0.1, 5, and 100 μ M MPA. *: significance versus treatment with 0.1 μ M MPA, #: significance versus treatment with 5 μ M MPA, o: significance versus treatment with 100 μ M MPA. Due to lack of H/L-labeled controls only treatments of different MPA concentrations were compared among each other.

#	Protein name	Abbr. prot.	Uniprot acc. no.	Unique peptides	SILAC H/L ratio				r	H/L 250 μ M MPA vs. H/L=1 [%]
		<i>Abbr. gene</i>	Ensemble gene ID		0.1 μ M MPA	5 μ M MPA	100 μ M MPA	250 μ M MPA		
1	Long-chain acyl-CoA synthetase 5	ACSL5 <i>ACSL5</i>	Q9ULC5 ENSG00000197142	18	0.83 \pm 0.20	1.07 \pm 0.08	1.44 \pm 0.21 *	1.94 \pm 0.15 ** ##	0.977	193.6
2	UDP glucuronosyltransferase 1A1	UGT1A1 <i>UGT1A1</i>	P22309 ENSG00000167165	7	1.12 \pm 0.25	1.45 \pm n.a.	1.55 \pm 0.23	1.91 \pm 0.29 *	0.917	191.0
3	Very long-chain specific acyl-CoA dehydrogenase	VLCAD <i>ACADVL</i>	P49748 ENSG00000072778	25	0.94 \pm 0.14	1.02 \pm 0.11	1.21 \pm 0.20	1.83 \pm 0.16 ** ## o	0.990	183.0
4	Annexin A1	ANXA1 <i>ANXA1</i>	P04083 ENSG00000135046	14	1.17 \pm 0.20	1.14 \pm 0.11	1.68 \pm 0.21	1.75 \pm 0.17 * #	0.891	174.6
5	Peroxisomal acyl-CoA oxidase 1	AOX <i>ACOX1</i>	Q15067 ENSG00000161533	15	0.88 \pm 0.11	1.01 \pm 0.09	1.28 \pm 0.10 *	1.75 \pm 0.08 *** ## oo	0.992	174.5
6	Fatty acid-binding protein 1	FABP1 <i>FABP1</i>	Q6FGL7 ENSG00000163586	4	0.84 \pm 0.33	0.91 \pm 0.05	1.88 \pm 0.31 * #	1.70 \pm 0.21 *	0.771	169.9
7	Integrin β -4	ITGB4 <i>ITGB4</i>	P16144 ENSG00000132470	46	1.07 \pm 0.06	1.27 \pm 0.02	1.34 \pm 0.04 *	1.44 \pm 0.11 **	0.836	143.5
8	Guanine nucl.-binding protein G(I)/G(S)/G(O) subunit γ -12	GNG12 <i>GNG12</i>	Q9UBI6 ENSG00000172380	3	1.01 \pm 0.12	1.17 \pm 0.03	1.15 \pm 0.11	1.35 \pm 0.04 *	0.888	135.4

Table 2.4: LS180 proteins of levels increased by >20% but <30% after MPA treatment identified by SILAC. For explanation of the depicted parameters please refer to Table 2.3.

#	Protein name	Abbr. prot.	Uniprot acc. no.	Unique peptides	SILAC H/L ratio				r	H/L 250 μ M MPA vs. H/L=1 [%]
		<i>Abbr. gene</i>	Ensemble gene ID		0.1 μ M MPA	5 μ M MPA	100 μ M MPA	250 μ M MPA		
9	Single-stranded DNA-binding protein 1, mitochondrial	MtSSB <i>SSBP1</i>	Q04837 ENSG00000106028	7	0.97 \pm 0.10	1.04 \pm 0.11	1.02 \pm 0.10	1.29 \pm 0.07 *	0.926	128.8
10	Acetyl-CoA acyltransferase	ACAA2 <i>ACAA2</i>	P42765 ENSG00000167315	8	0.96 \pm 0.14	0.89 \pm 0.01	1.09 \pm 0.11	1.28 \pm 0.06 * ‡	0.979	128.4
11	Dihydrolipoamide dehydrogenase	DLD <i>DLD</i>	P09622 ENSG00000091140	11	0.96 \pm 0.04	1.04 \pm 0.07	1.09 \pm 0.10	1.27 \pm 0.07 **	0.967	127.1
12	Trifunctional enzyme subunit α (Long-chain 3-hydroxyacyl-CoA dehydrogenase)	TFP <i>HADHA</i> (LCHAD)	P40939 ENSG00000084754	21	0.87 \pm 0.13	0.94 \pm 0.10	1.04 \pm 0.07	1.26 \pm 0.04 ** *	0.988	126.4
13	Electron-transfer-flavoprotein	α -ETF <i>ETFA</i>	P13804 ENSG00000140374	12	0.90 \pm 0.02	0.99 \pm 0.08	1.09 \pm 0.09 *	1.26 \pm 0.04 ** ‡	0.974	125.5
14	NAD(P)H dehydrogenase, quinone 1	NQO1 <i>NQO1</i>	P15559 ENSG00000181019	8	1.11 \pm 0.04	1.09 \pm 0.00	1.25 \pm 0.01 * ‡	1.25 \pm 0.06 * ‡	0.847	124.6
15	Heat shock 70kDa protein 9 (mortalin)	HSPA9 <i>HSPA9</i>	P38646 ENSG00000113013	25	0.98 \pm 0.08	1.02 \pm 0.05	1.03 \pm 0.01	1.24 \pm 0.07 ** ‡ ◦	0.956	124.5
16	Delta(3,5)-Delta(2,4)-dienoyl-CoA isomerase, mitochondrial	ECH1 <i>ECH1</i>	Q13011 ENSG00000104823	14	0.91 \pm 0.05	0.88 \pm 0.07	1.03 \pm 0.06	1.22 \pm 0.10 * ‡	0.995	122.4
17	Glycerol-3-phosphate dehydrogenase 2, mitochondrial	GPD2 <i>GPD2</i>	P43304 ENSG00000115159	22	0.91 \pm 0.03	1.04 \pm 0.05	1.02 \pm 0.10	1.22 \pm 0.13 *	0.886	122.3
18	GTP:AMP phosphotransferase, mitochondrial (Adenylate kinase 3)	AK3 <i>AK3</i>	Q9UIJ7 ENSG00000147853	7	0.79 \pm 0.13	0.86 \pm 0.09	1.01 \pm 0.07	1.21 \pm 0.14 *	0.988	121.4
19	Elongation factor Tu/P43	EF-Tu <i>TUFM</i>	P49411 ENSG00000178952	18	0.98 \pm 0.02	1.00 \pm 0.02	0.99 \pm 0.01	1.20 \pm 0.09 ** ‡ ◦ ◦	0.918	120.4
20	Succinyl-CoA ligase [ADP/GDP-forming] subunit α	SCS- α <i>SUCLG1</i>	P53597 ENSG00000163541	3	0.88 \pm 0.14	1.06 \pm 0.05	1.05 \pm 0.07	1.20 \pm 0.06 *	0.842	120.1

Table 2.5: LS180 proteins of levels decreased by >30% after MPA treatment identified by SILAC. Shown are protein numbers (assigned for clarity), protein names, protein and gene (*italic*) abbreviations, Uniprot accession numbers and Ensemble gene IDs, numbers of unique peptides identified, SILAC heavy/light (H/L) ratios for four MPA concentrations, Pearson product-moment correlation coefficients *r* for the correlation/linear dependence of H/L ratios and MPA concentrations, and the increase in protein levels after 250 μ M MPA treatment compared to a H/L ratio=1 as expected for controls (= calculation as % of controls). H/L ratios are given as means \pm standard deviations (*N*=3). Significance was determined for effects of increasing MPA concentrations using one-way ANOVA combined with Scheffe's post – hoc test with */ #/ o: *p*<0.05; **/ ##/ oo: *p*<0.005; ***/ ###/ ooo: *p*<0.001 versus treatment with 0.1, 5, and 100 μ M MPA. *: significance versus treatment with 0.1 μ M MPA, #: significance versus treatment with 5 μ M MPA, o: significance versus treatment with 100 μ M MPA. Due to lack of H/L-labeled controls only treatments of different MPA concentrations were compared among each other.

#	Protein name	Abbr. prot. <i>Abbr. gene</i>	Uniprot acc. no. Ensemble gene ID	Unique peptides	SILAC H/L ratio				<i>r</i>	H/L 250 μ M MPA vs. H/L=1 [%]
					0.1 μ M MPA	5 μ M MPA	100 μ M MPA	250 μ M MPA		
21	Polymeric immunoglobulin receptor	PIgR <i>PIGR</i>	P01833 ENSG00000162896	13	0.97 \pm 0.04	0.78 \pm 0.05 *	0.45 \pm 0.05 *** ##	0.35 \pm 0.05 *** ###	-0.888	34.8
22	Regenerating islet-derived protein 4	REG-4 <i>REG4</i>	Q9BYZ8 ENSG00000134193	8	0.86 \pm 0.06	0.93 \pm 0.15	0.61 \pm 0.12	0.48 \pm 0.15 * #	-0.950	47.7
23	Solute carrier family 12 member 2	SLC12A2 <i>SLC12A2</i>	P55011 ENSG00000146828	30	0.96 \pm 0.05	0.99 \pm 0.05	0.63 \pm 0.07 ** ##	0.48 \pm 0.06 *** ###	-0.952	48.0
24	Creatine kinase B-type	B-CK <i>CKB</i>	P12277 ENSG00000166165	16	0.93 \pm 0.05	0.74 \pm 0.06 *	0.59 \pm 0.06 **	0.50 \pm 0.05 *** #	-0.969	49.8
25	Cadherin-17	CDH17 <i>CDH17</i>	Q12864 ENSG00000079112	24	0.98 \pm 0.04	0.96 \pm 0.05 oo	0.75 \pm 0.02 ** ## oo	0.63 \pm 0.04 *** ### o	-0.969	62.7
26	Dihydropyrimidinase-like 2 variant	DRP-2 <i>DPYSL2</i>	Q16555 ENSG00000092964	7	1.13 \pm 0.13	0.97 \pm 0.24	0.84 \pm 0.05	0.63 \pm 0.09 *	-0.946	63.4
27	Stromal cell-derived factor 2-like 1	SDF2L1 <i>SDF2L1</i>	Q9HCN8 ENSG00000128228	3	1.08 \pm 0.02	1.02 \pm 0.28	0.83 \pm 0.07	0.67 \pm 0.06 *	-0.978	66.5
28	Acetyl-CoA acetyltransferase	ACAT2 <i>ACAT2</i>	Q9BWD1 ENSG00000120437	8	1.04 \pm 0.08	1.00 \pm 0.05	0.95 \pm 0.08	0.70 \pm 0.03 ** ## o	-0.983	70.0

Table 2.6: LS180 proteins of levels decreased by <30% but >20% after MPA treatment identified by SILAC. Shown are protein numbers (assigned for clarity), protein names, protein and gene (*italic*) abbreviations, Uniprot accession numbers and Ensemble gene IDs, numbers of unique peptides identified, SILAC heavy/light (H/L) ratios for four MPA concentrations, Pearson product-moment correlation coefficients *r* for the correlation/linear dependence of H/L ratios and MPA concentrations, and the increase in protein levels after 250 μ M MPA treatment compared to a H/L ratio=1 as expected for controls (= calculation as % of controls). H/L ratios are given as means \pm standard deviations (N=3). Significance was determined for effects of increasing MPA concentrations using one-way ANOVA combined with Scheffe's post – hoc test with */ #/ ○: $p < 0.05$; **/ ##/ ○○: $p < 0.005$; ***/ ###/ ○○○: $p < 0.001$ versus treatment with 0.1, 5, and 100 μ M MPA. *: significance versus treatment with 0.1 μ M MPA, #: significance versus treatment with 5 μ M MPA, ○: significance versus treatment with 100 μ M MPA. Due to lack of H/L-labeled controls only treatments of different MPA concentrations were compared among each other.

#	Protein name	Abbr. prot.	Uniprot acc. no.	Unique peptides	SILAC H/L ratio				r	H/L 250 μ M MPA vs. H/L=1 [%]
		<i>Abbr. gene</i>	Ensemble gene ID		0.1 μ M MPA	5 μ M MPA	100 μ M MPA	250 μ M MPA		
29	Tubulin α -4A chain	TUBA4A <i>TUBA4A</i>	P68366 ENSG00000127824	3	1.12 \pm 0.09	0.97 \pm 0.03	0.96 \pm 0.10	0.74 \pm 0.05 **	-0.926	74.0
30	UDP-glucose:glycoprotein glucosyltransferase 1	UGT1 <i>UGGT1</i>	Q9NYU2 ENSG00000136731	33	0.93 \pm 0.03	0.93 \pm 0.03	0.89 \pm 0.07	0.74 \pm 0.08 *	-0.978	74.4
31	Tubulin α -1C chain	TUBA1C <i>TUBA1C</i>	Q9BQE3 ENSG00000167553	2	1.13 \pm 0.09	0.97 \pm 0.01	0.96 \pm 0.10	0.75 \pm 0.05 **	-0.909	75.3
32	Sodium/potassium-transporting ATPase subunit β -1	ATP1B1 <i>ATP1B1</i>	P05026 ENSG00000143153	6	0.92 \pm 0.06	1.02 \pm 0.00	0.79 \pm 0.04 ##	0.77 \pm 0.05 * ##	-0.824	77.1
33	Tubulin β chain	TUBB <i>TUBB</i>	P07437 ENSG00000196230	4	1.15 \pm 0.11	1.05 \pm 0.10	0.98 \pm 0.11	0.77 \pm 0.07 *	-0.969	77.1
34	GTP-binding nuclear protein RAN	RAN <i>RAN</i>	P62826 ENSG00000132341	8	1.08 \pm 0.09	0.93 \pm 0.01	0.92 \pm 0.02 *	0.79 \pm 0.03 **	-0.867	78.9
35	Tubulin β -4A chain	TUBB4A <i>TUBB4A</i>	P04350 ENSG00000104833	1	1.13 \pm 0.11	1.05 \pm 0.07	1.01 \pm 0.09	0.79 \pm 0.07 *	-0.966	79.2

Table 2.7: Description of proteins with changed levels as identified by SILAC. Cell compartments, regulation of expression, and short descriptions of physiological functions are given for proteins listed in Table 2.3 - Table 2.6.

#	Protein	Cell compartment	Regulation of expression	Physiological function
1	ACSL5	Mitochondrion outer membrane, ER [201]	Upregulated by glucose/carbohydrates and insulin [202], regulated by fatty acids and insulin [203]	Conversion of free long-chain fatty acids into fatty acyl-CoA esters, lipid biosynthesis, fatty acid degradation, ATP + long-chain fatty acid + CoA \leftrightarrow AMP + diphosphate + acyl-CoA [201]
2	UGT1A1	Microsome, ER membrane [204]	PXR-mediated regulation, upregulated by certain endogenous and exogenous lipophilic compounds [205]	Glucuronidation of bilirubin IX- α and other small lipophilic molecules [204]
3	VLCAD	Mitochondrion [206]	Regulated in response to changes in energy status of cells [207]	Catalysis of the initial step of β -oxidation of long-chain fatty acids with a chain length of 14 to 20 carbons [206]
4	ANXA1	Cytosol [208]	Induction by glucocorticoids [208]	Promotion of membrane fusion, involvement in exocytosis, regulation of phospholipase A2 activity [209], which is essential for biosynthesis of mediators of inflammation as prostaglandins and leukotrienes [210]
5	AOX	Peroxisome [211]	Regulated by peroxisome proliferator-activated receptor (PPAR) α [212]	Fatty acid β -oxidation (first enzyme of pathway, desaturation of acyl-CoAs to 2-trans-enoyl-CoAs) [213], highest activity against medium-chain fatty acyl-CoAs [211]
6	FABP1	Peroxisome [214]	Regulated by transcription factor pancreatic and duodenal homeobox 1 [215]	Binding of long-chain fatty acids and other hydrophobic ligands, also able to bind bile acids [214], uptake, transport and metabolism of fatty acids (assumed) [214]
7	ITGB4	Membrane [216]	Upregulated in gastric cancers [217], upregulated by certain endogenous and exogenous compounds [217, 218]	Receptor for laminin [216], critical structural role in the hemidesmosome of epithelial cells [216] (cell-matrix adhesion [219])

Continued on next page.

2.7 Investigation of proteome alterations in LS180 cells after MPA treatment

Description of proteins with changed levels as identified by SILAC, *continued from previous page.*

#	Protein	Cell compartment	Regulation of expression	Physiological function
8	GNG12	Cell membrane, cytoplasmatic side [220]	Kinin-dependent regulation [221]	Modulator/transducer in various transmembrane signaling systems [220], $\beta + \gamma$ chains required for GTPase activity, replacement of GDP by GTP, and for G protein-effector interaction [220]
9	MtSSB	Mitochondrion, Mitochondrion nucleotide [222]	Nuclear respiratory factor 2-regulated [223]	Mitochondrial biogenesis [224], evtl. associated with mitochondrial DNA replication [222], subunit of a single-stranded DNA-binding complex involved in the maintenance of genome stability [224]
10	ACAA2	Cytoplasm [225]	Induction by certain endogenous [226] and exogenous substances [227]	Involvement in lipid metabolism [225]
11	DLD	Mitochondrial matrix [228]	Regulated as part of the pyruvate dehydrogenase complex [229]	Component of the pyruvate dehydrogenase complex, α -ketoglutarate dehydrogenase complex (conversion of α -keto acids to acyl-CoA and CO ₂), and the branched-chain α -keto acid dehydrogenase complex [228], part of the mitochondrial glycine cleavage system [228]
12	TFP	Mitochondrion [230]	NAD ⁺ - and CoA-dependent [231]	Includes two domains: Long-chain enoyl-CoA hydratase (EC 4.2.1.17), Long-chain 3-hydroxyacyl-CoA dehydrogenase (EC 1.1.1.211) [230], lipid metabolism, fatty acid β -oxidation [230]
13	α -ETF	Mitochondrial matrix [232]	Dependent on developmental, nutritional (e.g. starvation), and hormonal factors [233]	Specific electron acceptor for several dehydrogenases, transfer of electrons to the main mitochondrial respiratory chain via ETF-ubiquinone oxidoreductase (ETF dehydrogenase) [232]
14	NQO1	Cytoplasm [234]	Upregulated by oxidative stress, antioxidants, heavy metals, ionizing radiation, and hypoxia [235]	Reduction of quinones to hydroquinones, involved in detoxification and biosynthetic processes [234]

Continued on next page.

2 Results and Discussion

Description of proteins with changed levels as identified by SILAC, *continued from previous page.*

#	Protein	Cell compartment	Regulation of expression	Physiological function
15	HSPA9	Mitochondrion (primarily), ER, plasma membrane, cytoplasmic vesicles [236]	Upregulated in many human tumors [237], associated with p53 inactivation [238]	Role in cell proliferation, stress response, maintenance of mitochondria [236], chaperone (assists in protein folding) [237]
16	ECH1	Peroxisomes and/or mitochondria [239]	Upregulated in gastric carcinomas, upregulation associated with tumor metastasis [240]	Isomerization of 3-trans,5-cis-dienoyl-CoA to 2-trans,4-trans-dienoyl-CoA, lipid metabolism, fatty acid β -oxidation [241]
17	GPD2	Inner mitochondrial membrane [242]	Upregulated by insulin [243], regulated by dietary effects and certain exogenous substances [243], protein kinase C might be involved in regulation [243], upregulated in cancer cells [244]	Conversion of glycerol-3-phosphate to dihydroxyacetone phosphate, constituent of the glycerol phosphate shuttle, which reoxidizes NADH formed during glycolysis [242]
18	AK3	Mitochondrion matrix [245]	Developmentally regulated [246]	$NTP + AMP \leftrightarrow NDP + ADP$ [245]
19	EF-Tu	Mitochondrion [247]	Expression altered in gastric cancers [248]	Promotion of GTP-dependent binding of aminoacyl-transfer RNA to the A-site of ribosomes during protein biosynthesis, protein biosynthesis [247]
20	SCS- α	Mitochondrion [249]	Activity allosterically regulated by GDP concentration [250], regulation of expression unclear	Catalyzes the ATP- or GTP-dependent ligation of succinate and CoA to form succinyl-CoA (nature of the β subunit determines the nucleotide specificity, i.e. $GTP + succinate + CoA \leftrightarrow GDP + phosphate + succinyl-CoA$ or $ATP + succinate + CoA \leftrightarrow ADP + phosphate + succinyl-CoA$ [249])
21	PIgR	Cell membrane, secreted [251]	Upregulated in response to viral or bacterial infection linking innate and adaptive immunity, abnormal expression in cancers [252]	Receptor binds polymeric immunoglobulin A and immunoglobulin M at the basolateral surface of epithelial cells, the complex is then transported across the cell to be secreted at the apical surface [251], immune defence of the intestinal mucosa [253]

Continued on next page.

2.7 Investigation of proteome alterations in LS180 cells after MPA treatment

Description of proteins with changed levels as identified by SILAC, *continued from previous page.*

#	Protein	Cell compartment	Regulation of expression	Physiological function
22	REG-4	Secreted, cell membrane [254]	Upregulated by mucosal injury and in tumors [254]	Lectin display, mannose-binding, evtl. involved in inflammatory and metaplastic responses of the GI epithelium [254]
23	SLC12A2	Membrane [255]	Unclear	Sodium and chloride transport and reabsorption, regulation of ionic balance and cell volume [256]
24	B-CK	Cytoplasm [257]	Tissue-specific, probably linked to cell proliferation [258]	Reversible catalysis of the transfer of phosphate between ATP and various phosphogens (e.g. creatine phosphate: ATP + creatine ↔ ADP + phosphocreatine, energy homeostasis), central role in energy transduction in tissues with large, fluctuating energy demands [257, 259]
25	CDH17	Cell membrane [260]	Upregulated in cancers [261]	Cell adhesion/connection of cells, evtl. involved in morphological organization of the intestine [260], glycoprotein [262]
26	DPYSL2	Cytoplasm [263]	Possibly altered in Alzheimer's disease [264, 265]	Remodeling of the cytoskeleton, cell migration [263], promotion of microtubule assembly [266]
27	SDF2L1	ER lumen [267, 268]	Stress-inducible [269], ubiquitously expressed in various cancer cell lines [270]	Unknown [268]
28	ACAT2	Cytoplasm [271]	Upregulated by saturated fatty acids [272] and cholesterol [273]	Involvement in lipid metabolism [274]
29	TUBA4A	Cytoplasm → cytoskeleton, microtubules [275]	Regulation of tubulin expression mostly unexplored, multiple overlapping mechanisms [275]	Tubulin is the major constituent of microtubules, binds two molecules of GTP [276]
30	UGT1	ER lumen [277]	Induction by certain drugs and chemical compounds via PXR or aryl hydrocarbon receptor [278]	Quality control for protein folding/recognition of glycoproteins with minor folding defects [277], drug and xenobiotic metabolism [278]

Continued on next page.

2 Results and Discussion

Description of proteins with changed levels as identified by SILAC, *continued from previous page.*

#	Protein	Cell compartment	Regulation of expression	Physiological function
31	TUBA1C	Cytoplasm → cytoskeleton, microtubules [276]	Regulation of tubulin expression mostly unexplored, multiple overlapping mechanisms [275]	Tubulin is the major constituent of microtubules, binds two molecules of GTP [276]
32	ATP1B1	Membrane [279]	Upregulated by prostaglandin E(1), eventually mediated through cAMP and Ca ²⁺ pathways [280]	β subunit: regulation of number of sodium pumps transported to the plasma membrane, non-catalytic component of the active enzyme (enzyme: hydrolysis of ATP coupled with the exchange of Na ⁺ and K ⁺ ions across the plasma membrane) [279]
33	TUBB	Cytoplasm → cytoskeleton, microtubules [281]	Regulation of tubulin expression mostly unexplored, multiple overlapping mechanisms [275]	Tubulin is the major constituent of microtubules, binds two molecules of GTP [281]
34	RAN	Nucleus, cytoplasm, melanosome [282]	Overexpressed in many cancers [283], feedback regulation of RAN gene expression by RAN protein [284]	GTP-binding, translocation of RNA and proteins through the nuclear pore complex, control of DNA synthesis (chromatin condensation [282]) and cell cycle progression, could be a key signaling molecule regulating microtubule polymerization during mitosis [285]
35	TUBB4A	Cytoplasm → cytoskeleton, microtubules [286]	Regulation of tubulin expression mostly unexplored, multiple overlapping mechanisms [275]	Tubulin is the major constituent of microtubules, binds two molecules of GTP [281]

Data analysis by DAVID, Pathway Palette, and Panther databases (protein networks and functional analysis)

The 35 differentially expressed and significantly affected proteins identified in MPA-treated LS180 cells were subjected to analysis through the Database for Annotation, Visualization, and Integrated Discovery (DAVID), version 6.7, available online at [287], analysis through Pathway Palette available online at [288], and Protein Analysis Through Evolutionary Relationships (PANTHER), version 7.2, available online at [289].

Databases as well as DAVID and PANTHER software require a gene or protein list to be uploaded. Although gene products, i.e. proteins, were identified in this experiment by SILAC and GelC-MS, gene lists were analyzed in certain cases. Data analysis therefore is non-redundant in the sense that proteins encoded by the same gene are presented in a single record (e.g. alternative splicing isoforms, fragments, polymorphisms, sequence conflicts). Databases which were used to identify proteins and analyze affected proteins, e.g. UniProtKB/Swiss-Prot and UniProtKB/TrEMBL, are based on this concept as well [290], therefore the terms “protein” and “gene” are used interchangeably in the following section. In all analyses, DAVID, Pathway Palette, and Panther, UniProt accession numbers (Tab. 2.3 - Tab. 2.6) served as identifiers for affected proteins.

For easier reference, differentially expressed proteins discussed in this section are always listed with the number under which they are listed in Table 2.3 - Table 2.6 and described in Table 2.7, e.g. peroxisomal acyl-coenzyme A (CoA) oxidase 1 (AOX, 5).

DAVID analysis DAVID facilitates functional annotation and systematic analysis of a given list of genes [291–293]. The gene list was analyzed using (1) DAVID’s Functional Annotation Tool (comprehending (A) Functional Annotation Clustering, (B) Functional Annotation Chart, and (C) Functional Annotation Table), as well as (2) DAVID’s Gene Functional Classification tool. Employing all DAVID tools settings were customized (for detailed description and explanation please see Section 3.9.2).

In addition, the 35 identified genes/proteins were subjected to a Pathway Enrichment Analysis using the Kyoto Encyclopedia of Genes and Genomes (KEGG) database and DAVID’s Functional Annotation Chart tool (tool 1B, settings customized as described in Section 3.9.2). KEGG pathway maps of pathways enriched in affected proteins in LS180 cells listed in Table 2.9 are shown in the appendix (Fig. 4.25 - Fig. 4.31). Differentially expressed proteins are marked with red circles.

2 Results and Discussion

Results for DAVID analyses of affected proteins in LS180 cells are described and shown in tables and figures on the following pages. The output of all DAVID tools is discussed together. To further validate the LS180 model, our data were compared to the currently available proteomics data on MPA toxicity employing rat models [175, 176, 294] and human cell culture models using cells of non-cancerous origin [295, 296]. These two data sets were individually subjected to DAVID analysis (Tool 1A and Pathway Enrichment Analysis using tool 1B). Comparison of LS180 data with these two data sets is included in the general discussion as well. To avoid confusion it should be mentioned that proteins listed in the named publications were assigned the wrong identifiers occasionally (rat instead of human, human instead of rat, *Sulfolobus solfataricus*/*Pseudomonas aeruginosa*/*Saccharomyces cerevisiae* instead of rat). Identifiers representing the correct species were reassigned prior to DAVID analysis (proteins with their correct identifiers are listed in Table 4.1 and Table 4.2 in the appendix).

The following data sets from different model types were compared:

- LS180 cell model versus rat model

For comparison of the LS180 cell model (human colon cancer) with a common rat model (Wistar rats) proteins/genes from the three available publications on this topic (kidney tissue of MMF-treated rats [175], liver and colon tissue of MMF-treated rats [176], analysis of gene expression (complementary DNA (cDNA) microarray analysis) in liver and gut of MMF-treated rats [294]) were pooled. Gene IDs were converted to protein IDs (Uniprot accession numbers) using DAVID's Gene ID Conversion tool. Protein/Gene targets were subjected to Functional Annotation Clustering (Tool 1A) and Pathway Enrichment Analysis (Tool 1B). Results are shown in Table 4.3.

- LS180 cell model versus human cells of non-cancerous origin

To compare results from LS180 cell with other human data, Pathway Enrichment Analysis was performed using protein targets listed in the available publications dealing with human models, i.e. the human embryonic kidney cell line HEK-293 [295], and the T-lymphoblast cell line CCRF-CEM [296].

Two additional publications concerning MPA-induced proteome changes are available. Ghiggeri et al. analyzed protein changes in human urine after MPA and everolimus treatment of patients [297], Petrova et al. published data from a murine

2.7 Investigation of proteome alterations in LS180 cells after MPA treatment

model of renal fibrosis [298]. These two publications were not taken into account comparing the LS180 cell model to already published data due to the everolimus-containing regimen of patients and unsuitable type of model (mouse, cystic fibrosis), respectively.

DAVID analyses results in tables and figures: Results of all DAVID analyses are shown in Table 2.8 - Table 2.11 and Figure 2.33 on the following pages, results are discussed starting on page 111.

Table 2.8: Functional Annotation Clustering of 35 significantly affected genes/proteins after MPA treatment of LS180 cells by DAVID (Tool 1A). Functional Annotation Clustering was performed using customized options as described in Section 2.7.1. 4 annotation clusters were found (# 1-4), a representative annotation term was assigned to characterize grouping terms as comprehensively as possible (for specification of all terms contributing to an annotation cluster/gene functional group see footnotes), enrichment scores are given ranking biological significance of gene groups based on overall EASE scores (for explanation see Section 3.9.2) of all enriched annotation terms, the number of genes/proteins in each cluster is given (Count) as well as the gene/protein itself including the number under which it is listed in Table 2.3 - Table 2.6 and described in Table 2.7. 51 terms were not clustered.

#	Representative annotation term	Enr. score	Count	Proteins encoded by analyzed genes
1	Guanyl nucleotide-binding ¹	4.99	8	RAN(34), EF-Tu(19), AK3(18), SCS- α (20), TUBA1C(31), TUBA4A(29), TUBB4A(35), TUBB(33)
2	Lipid catabolic process ²	3.49	4	VLCAD(3), AOX(5), ECH1(16), TFP(12)
3	Protein polymerization ³	3.15	4	TUBA1C(31), TUBA4A(29), TUBB4A(35), TUBB(30)
4	Mitochondrial membrane ⁴	2.74	6	ACSL5(1), VLCAD(3), GDP-M(17), TFP(12), ACAA2(10), SCS- α (20)

¹ GTP-binding, guanyl ribonucleotide-binding, guanyl nucleotide-binding

² Fatty acid β -oxidation, fatty acid catabolic process, fatty acid oxidation, lipid oxidation, lipid modification, cellular lipid catabolic process, organic acid catabolic process, carboxylic acid catabolic process, lipid catabolic process

³ Tubulin/FtsZ, 2-layer sandwich domain; tubulin, conserved site; tubulin/FtsZ, GTPase domain, tubulin, PIRSF002306:tubulin, protein polymerization, microtubule-based movement, pathogenic Escherichia coli infection, cellular protein complex assembly, gap junction, microtubule, cellular macromolecular complex assembly, cellular macromolecular complex subunit organization

⁴ Mitochondrial inner membrane, organelle inner membrane, mitochondrial membrane, mitochondrial envelope

Table 2.9: Pathway Enrichment Analysis of 35 significantly affected genes/proteins after MPA treatment of LS180 cells (Tool 1B and KEGG). The KEGG database and DAVID's Functional Annotation Chart tool were used and customized as described in Section 2.7.1. 7 terms were found (# 1-7). The number of genes/proteins in each cluster is given (Count), the gene/protein itself including the number under which it is listed in Table 2.3 - Table 2.6 and described in Table 2.7, as well as a p-value describing the significance of enrichment of affected proteins in the respective term. 22 genes from the list were not in the output.

#	Term	Count	Proteins encoded by analyzed genes	p-value
1	Fatty acid metabolism	7	ACAT2(28), ACSL5(1), VLCAD(3), AOX(5), TFP(12), ACAA2(10)	7.1E-7
2	Valine, leucine, and isoleucine degradation	4	ACAT2(28), DLD(11), TFP(12), ACAA2(10)	9.5E-4
3	Pathogenic Escherichia coli infection	4	TUBA1C(31), TUBA4A(29), TUBB4A(35), TUBB(33)	2.0E-3
4	Gap junction	4	TUBA1C(31), TUBA4A(29), TUBB4A(35), TUBB(33)	7.1E-3
5	Propanoate metabolism	3	ACAT2(28), TFP(12), SCS- α (20)	8.9E-3
6	Fatty acid elongation in mitochondria	2	TFP(12), ACAA2(10)	3.6E-2
7	PPAR signaling pathway	3	ACSL5(1), AOX(5), FABP1(6)	3.8E-2

Table 2.10: Functional Annotation Chart focusing main terms involved in the biochemistry of 35 significantly affected genes/proteins after MPA treatment of LS180 cells by DAVID (Tool 1B). *The Functional Annotation Chart tool's options were customized as described in Section 2.7.1. 17 terms (# 1-17) were found to accumulate in the descriptions of analyzed genes/proteins (only terms comprising 10 or more genes/proteins were allowed). The number of genes/proteins comprising the term is given (Count). The percentage of proteins out of all 35 affected genes/proteins, and p-values are listed. Due to an overlap of terms, 2 genes from the list were not in the output.*

#	Term	Count	[%]	p-value
1	Phosphoprotein	24	68.6	3.9E-4
2	Acetylation	22	62.9	1.1E-10
3	Mitochondrion ¹	16	45.7	1.1E-8
4	Nucleotide-binding ¹	16	45.7	4.0E-5
5	Purine nucleotide-binding	15	42.9	3.2E-5
6	Mitochondrion ¹	13	37.1	9.0E-9
7	Intracellular organelle lumen	13	37.1	7.7E-4
8	Organelle lumen	13	37.1	9.5E-4
9	Membrane-enclosed lumen	13	37.1	1.1E-3
10	Mitochondrial part	12	34.3	1.1E-7
11	Intracellular non-membrane-bound organelle	12	34.3	4.5E-2
12	Non-membrane-bound organelle	12	34.3	4.5E-2
13	Transit peptide	11	31.4	6.0E-9
14	Nucleotide-binding ¹	11	31.4	4.8E-4
15	Purine ribonucleotide-binding	11	31.4	6.3E-3
16	Ribonucleotide-binding	11	31.4	6.3E-3
17	Transit peptide: mitochondrion	10	28.6	8.8E-8

¹ Terms are listed repeatedly since each categories/databases defined by the settings for annotation (Sec. 2.7.1) is generally searched separately. Due to this overlap the extract of 17 terms accumulating in the descriptions of analyzed genes/proteins retrenches to 15 terms.

Table 2.11: Functional Annotation Classification of 35 significantly affected genes/proteins after MPA treatment of LS180 cells by DAVID (Tool 2). *Functional Annotation Classification was performed using customized options as described in Section 2.7.1. 4 annotation clusters were found (# 1-4). A representative annotation term was assigned to characterize grouping terms as comprehensively as possible (for a condensed specification of terms contributing to a representative annotation term please see footnotes or Figure 2.33). Enrichment scores are given ranking biological significance of gene groups based on overall EASE scores (for explanation, please see Section 3.9.2) of all enriched annotation terms. The number of genes/proteins in each cluster is given (Count) as well as the gene/protein itself including the number under which it is listed in Table 2.3 - Table 2.6 and described in Table 2.7. 20 genes from the list were not in the output.*

#	Rep. ann. term	Enr. score	Count	Proteins encoded by analyzed genes
1	Mitochondrial matrix ¹	4.76	5	MtSSB(9), HSPA9(15), α -ETF(13), VLCAD(3), EF-Tu(19)
2	Lipid catabolic process ²	3.51	4	AOX(5), ECH1(16), TFP(12), VLCAD(3)
3	Tubulin/cytoskeleton ³	2.86	4	TUBB(33), TUBA4A(29), TUBA1C(31), TUBB4A(35)
4	Transmembrane protein ⁴	0.41	3	SLC12A2(23), Cadherin-17(25), PIgR(21)

¹ Phosphoprotein, disease mutation, purine nucleoside-binding, adenylyl nucleotide-binding, acetylation, mitochondrial nucleotide, purine nucleotide-binding, mitochondrial matrix, transit peptide: mitochondrion

² α tubulin, β tubulin, acetylation, cytosol, tubulin, phosphoprotein, protein complex assembly, GTP-binding, gap junction, microtubule, cytoskeleton

³ Peroxisome, biosynthesis of unsaturated fatty acids, flavoprotein, purine nucleotide-binding, adenylyl nucleotide-binding, purine nucleoside-binding, mitochondrial nucleoid, mitochondrial matrix, phosphoprotein, generation of precursor metabolites and energy, transit peptide: mitochondrion, disease mutation, acetylation, lipid catabolic process

⁴ Transport, signal peptide, phosphoprotein, glycoprotein, cell membrane, transmembrane

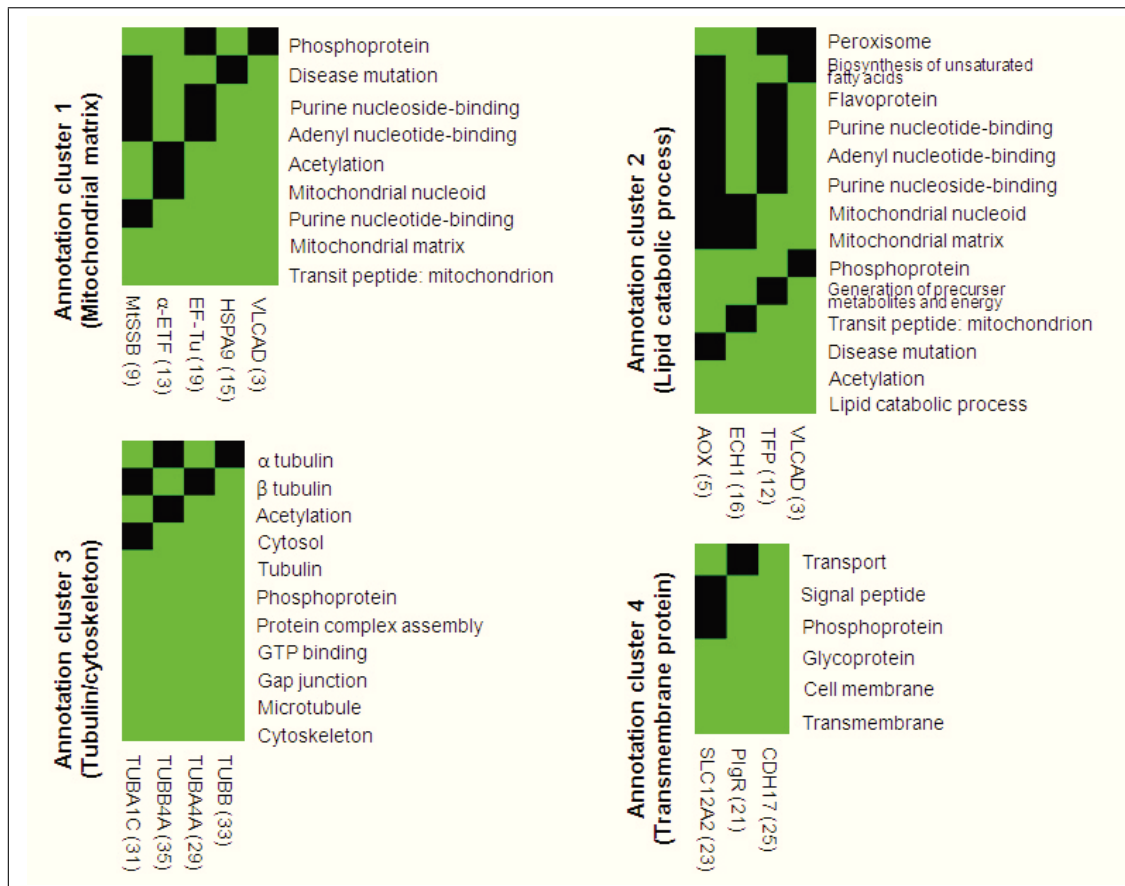


Fig. 2.33: 2D heat map (genes-to-terms 2D view) of genes and their major annotated terms in correlation to gene groups/annotation clusters 1-4. Green represents a positive correlation of gene and annotation term, black represents an unknown relationship; a group's related annotations are shown by unicolored areas (green block, right side/bottom), while scattered areas (green-black block, left side/top) depict functional differences; for further details please see [299]. Annotation terms were condensed and resorted for easier reference (by default annotation terms are ordered based on their enrichment scores associated with the groups).

Discussion of DAVID analyses results Functional Annotation Clustering (clustered or non-redundant chart report of annotation terms for all selected annotation categories [300]) of 35 significantly affected genes/proteins after MPA treatment of LS180 cells by DAVID yielded 4 annotation clusters (gene functional groups) listed in Table 2.8. Involvement of binding of guanosine nucleotides was attributed to the function of 8 proteins out of the 35 affected proteins in LS180 cells (Group #1: “Guanyl nucleotide-binding”). Data presented in Section 2.5.2 already suggested impairment of cell metabolism involving guanosine nucleotides, which is confirmed here. Commonly throughout the literature described effects of MPA are attributed to guanosine nucleotide depletion as well [148, 167, 169, 301], e.g. changes in protein glycosylation especially studied in respect of modifications of adhesion molecules [169, 301]. An effect of MPA and AcMPAG on tubulin polymerization (even in the presence of exogenous GTP) has been described before by Feichtiger et al. [302]. As tubulin subunits constitute 50% of the proteins listed in group #1 (“Guanyl nucleotide-binding”) and 100% of the proteins of group #3 (“Protein polymerization”), an effect on tubulin can be seen in LS180 cells as well. In contradiction to our findings Feichtiger et al. reported induction of tubulin polymerization while the cellular amount of all 4 tubulin subunits was decreased to 74.0-79.2% of control values in LS180 cells treated with 250 μ M MPA (Tab. 2.6). Morath et al. on the other hand found several cytoskeletal proteins (vinculin, actin, and tubulin) to be downregulated in human fibroblasts suggesting that MPA induces cytoskeletal dysfunction [303].

Expression of 4 proteins was significantly altered (increased, as described in Table 2.3 and Table 2.4) and attributed to the term “Lipid catabolic process” (Group #2 in Table 2.8). Literature on MPA’s effect on lipid and fatty acid metabolism is scarce [304]. Clinical studies show association of MMF and hyperlipidemia but without direct evidence [304]. No significant changes occurred in serum cholesterol or triglyceride levels of rabbits on high-cholesterol diets with or without MMF [304].

Comparing our data to proteomics data gained from MMF-treated rats, 4 proteins involved in fatty acid metabolism were affected in rats (#6 in Table 4.4), but Functional Annotation Clustering of rat model data only yielded clusters of proteins involved in carbohydrate or nucleotide processes (results for Functional Annotation Clustering for pooled rat model data is shown in Table 4.3, appendix). Sufficient data on MPA’s effect on glucose metabolism is lacking [304]. No effects of MMF on glucose metabolism were observed in clinical trials and effects of MMF on insulin secretion and insulin gene expression seem to differ inbetween species

2 Results and Discussion

in vitro (MMF inhibits insulin secretion in rat islets [305] versus no effect on insulin secretion or insulin gene expression in human islets [306]). Although multiple other reasons might be involved (e.g. cancerous nature of LS180 cells, differences in methods used, changes not reaching statistical significance due to a small N) this pattern is traced comparing our LS180 cell data to data from rat models. As in Table 4.3 (appendix) the term “Carbohydrate catabolic process” shows up as the most enriched term, it is not among enriched terms in Table 2.8 listing Functional Annotation Clusters from LS180 cell modifications. Comparison of Pathway Enrichment Analyses of 35 MPA-affected proteins in LS180 cells and 73 MPA-affected proteins/genes in rats using the KEGG database and DAVID’s Functional Annotation Chart tool (Tab. 2.9 versus Tab. 4.4) shows the same species-dependent pattern. For LS180 cells several of the listed terms are linked to lipid metabolism (e.g. #1: Fatty acid metabolism, #5: Propanoate metabolism, #6: Fatty acid elongation in mitochondria, #7: Peroxisome proliferator-activated receptor (PPAR) signaling pathway; KEGG pathway maps of LS180 cell model data are shown in the appendix in Figure 4.25 - Figure 4.31). Several enriched terms linked to lipid metabolism were yielded as well when analysing rat proteome data (#4: Propanoate metabolism, #6: Fatty acid metabolism, #11: Butanoate metabolism). On the other hand alterations in the expression of proteins more or less closely involved in glucose and protein metabolism/amino acid degradation are mainly affected in rats under MMF treatment (i.e. #1: Glycolysis/gluconeogenesis, #2: Pyruvate metabolism, #3: Arginine and proline metabolism, #7: Tryptophan metabolism, #8: Phenylalanine metabolism, #10: Fructose and mannose metabolism), while only two pathways concerning amino acid degradation in LS180 cells seem significantly affected (i.e. #2: Valine, leucine, and isoleucine degradation, #5: Propanoate metabolism). Metabolomics data supporting this pattern are presented in Section 2.8. Metabolomics data shows very little to no alterations in glucose metabolism in MPA-treated LS180 cells (Sec. 2.8.1 and Sec. 2.8.2), but significant effects on lipids and fatty acids occur (Sec. 2.8.3).

Results of DAVID analysis of modified proteins in human non-cancer cells were not as substantial as results gained from rat models as only 22 modified proteins found in two different cell types were included in the data set. Functional Annotation Clustering yielded four annotation terms (Tab. 4.5, appendix), Pathway Enrichment Analysis did not yield any significantly enriched pathways. Comparing the LS180 cell model to human non-cancer cell culture models there were no evident overlaps in annotation term clusters. As mentioned above the expression of

2.7 Investigation of proteome alterations in LS180 cells after MPA treatment

actin and other cytoskeletal proteins has been found to be decreased in MPA-treated human fibroblasts [303]. As discussed in Section 2.3.2 MPA's potential to induce apoptosis is strongly cell type-dependent and no significant apoptosis was seen in LS180 cells. As proteins listed under the term "Regulation of apoptosis" were found in HEK-293 and CCRF-CEM cells these two cell types might be more predisposed to impairment of mechanisms of apoptosis. No significant effects on either carbohydrate or lipid metabolism of MPA on cells of non-cancerous origin were revealed by DAVID analysis of this data set.

Use of DAVID's Functional Annotation Chart tool (linear or redundant chart report of annotation terms for all selected annotation categories [300]) revealed the 15 most affected biochemical features the differentially expressed proteins are associated with in the used databases (Tab. 2.10, default settings were used). The listed features/terms give a rough overview of protein classes, protein functions, and protein locations that are affected in LS180 cells by MPA, but classification of proteins/genes is strongly database-dependent as databases are searched separately by this tool (which leads to terms being listed repeatedly in Table 2.10). Proteins/genes listed under a specific term are not specified as this tool was just used to gain a brief overview in terms of affected protein classes and actions. To mention the most significantly affected protein groups (groups sorted according to protein counts, see p-values) proteins contributing to the term "Acetylation" (#2 in Table 2.10) were mostly proteins involved in fatty acid and lipid metabolism such as very long-chain specific acyl-CoA dehydrogenase (VLCAD, 3) and AOX(5) and protein polymerization (tubulins). The term "Mitochondrion" (#3 and 6 in Table 2.10) again includes fatty acid and lipid metabolizing proteins as well as other mitochondrial proteins (e.g. elongation factor Tu/P43 (EF-Tu, 19), mitochondrial GTP:AMP phosphotransferase (AK3, 18), see Table 2.7 for cellular location of proteins). Transport proteins also seem to be affected as the terms "Transit peptide" (#13 in Table 2.10) and "Transit peptide: mitochondrion" (#17) are enriched as well (i.e. EF-Tu and electron-transfer-flavoprotein (α -ETF, 13)). Effects on proteins involved in transport processes can also be seen in Figure 4.23 (appendix), which will be discussed later (Sec. 2.7.1). Overall Table 2.10 hints towards MPA-induced effects on acetylation, mitochondrial processes and function, and transport processes in LS180 cells. Acetylation is a post-translational modification occurring typically on the ϵ -amino group of lysine residues and influencing protein function crucially [307]. Lots of mitochondrial proteins are subject to this modification so that acetylation is closely linked to mitochondrial function [308] which may be one

2 Results and Discussion

of the reasons for the significant accumulation of proteins involving these functions.

DAVID's Functional Annotation Table tool (table report for all selected annotation categories [300]) was used to gain an overview of genes/proteins, their functions, linkage to disease, etc. Since most important characteristics (compartment, regulation, function) of each protein are listed in Table 2.7 already, the output of DAVID's Functional Annotation Table tool is not shown.

DAVID's Functional Classification tool (classification of highly related genes into functionally related groups [300], e.g. physiologic functions, cell compartment) revealed four major groups of proteins identified to be affected by MPA treatment (Tab. 2.11). The four annotation clusters are shown in Figure 2.33 as 2D heat maps to give an overview of correlations of genes/proteins and annotation terms contributing to clusters. Overall the same terms are listed as discussed before showing effects of MPA on mitochondrial, lipid catabolic, cytoskeletal, and transport processes/functions.

Pathway Palette analysis Pathway Palette is an internet-based application for peptide-, protein-, and pathway-oriented analysis of MS data [309]. It is freely accessible under [288] and enables the user to easily transition from peptides/proteins to biological pathways and networks.

Seven pathways (Pathway Enrichment Analysis) were found to contain a statistically significant number of differentially expressed proteins (Tab. 2.9). The 13 proteins of significantly enriched KEGG functional categories (EASE score < 0.05) were subjected to Pathway Palette analysis, i.e. acetyl-CoA acetyltransferase (ACAT2, 28), long-chain acyl-CoA synthetase 5 (ACSL5, 1), VLCAD(3), AOX(5), trifunctional enzyme subunit α (TFP, 12), acetyl-CoA acyltransferase (ACAA2, 10), dihydro-lipoamide dehydrogenase (DLD, 11), tubulin α -1C chain (TUBA1C, 31), tubulin α -4A chain (TUBA4A, 29), tubulin β -4A chain (TUBB4A, 35), tubulin β chain (TUBB, 33), succinyl-CoA ligase [ADP/GDP-forming] subunit α (SCS- α , 20), and fatty acid-binding protein 1 (FABP1, 6) (Sec. 2.7.1).

Pathway Palette generates a protein-protein interaction network based on the BioGRID Interaction Database and divides interaction types of the BioGrid ontology into major subtypes [310], i.e. low-throughput techniques, HTP/complex detection, HTP/pairwise (no interactions of HTP/pairwise subtype in figure), and genetic in-

2.7 Investigation of proteome alterations in LS180 cells after MPA treatment

teractions, of which the first three options are selected by default.

Selected proteins/genes were analyzed twice using the BioGrid database (Fig. 2.34, default settings used) and the Human Protein Reference Database (HPRD) which is available as an option in Pathway Palette as well (Fig. 2.35; HPRD, i.e. HPRD(+mouse):in-vivo and HPRD(+mouse):in-vitro). Proteins constituting groups #1, 2, 5, 6, and 7 assigned by Pathway Enrichment Analysis through KEGG are labeled with red stars. Proteins of groups #3 and 4, which are entirely made up by tubulin chains, are labeled with green stars for a better overview. For further explanation and clarification of data processing please see figure legends.

A summary and description of additional proteins that are potentially affected as well and numbers of their interactions with differentially expressed proteins identified by SILAC is given in Table 2.12 and Table 2.13 for proteins identified using the BioGRID and HPRD databases, respectively. Only proteins/genes with ≥ 3 interactions are listed. Eventually affected proteins identified by Pathway Palette are linked to functions/annotation terms that were found to accumulate in DAVID charts as well (i.e. regulation of cell cycle, signaling processes, transcription, tight junctions, cytoskeletal properties, and transport). As this analysis only reveals potentially affected genes, elucidation of actual differences in levels of protein expression by western blot was required. Tight junction protein ZO-1 (ZO-1) and 14-3-3 protein θ (14-3-3 θ) (#6 and #9 in Table 2.12 and Table 2.13) were chosen as representative proteins to be quantified by western blot analysis due to their simultaneous identification by both of the databases used, ubiquitin (UBC, #1 in Table 2.12) was chosen as well due to its number of interactions assigned by BioGRID. No differences in expression levels were seen after western blotting of proteins as shown and discussed later in this section.

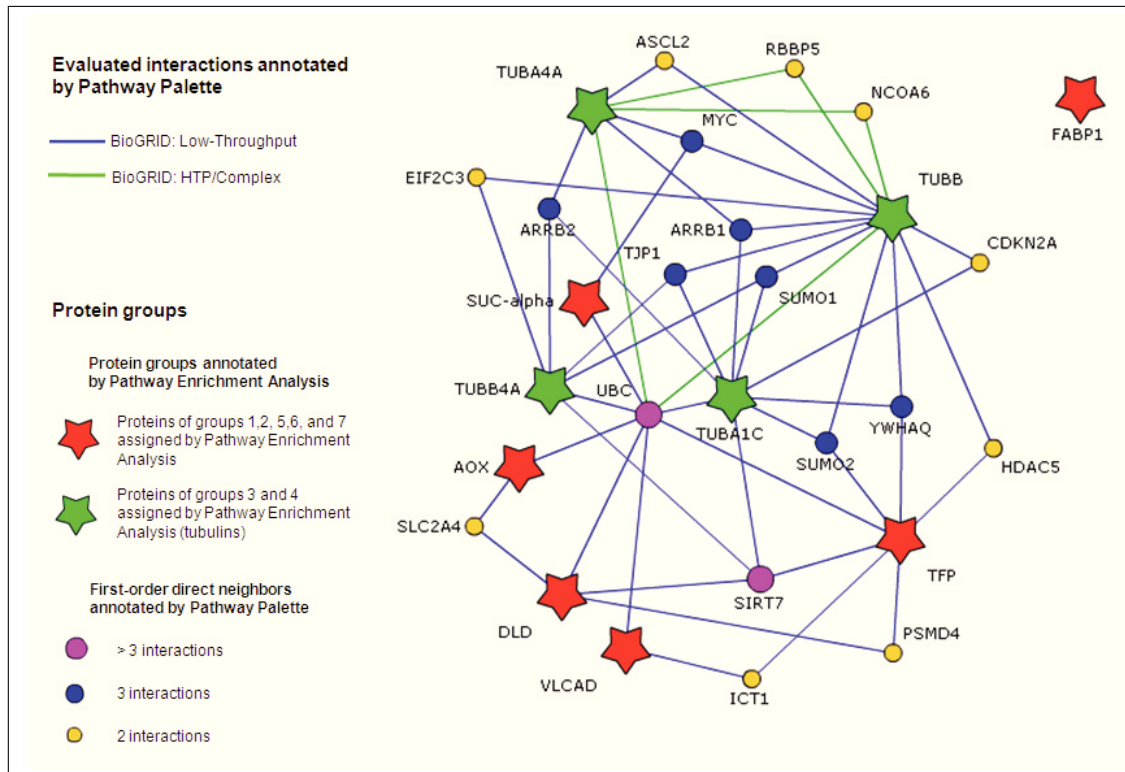


Fig. 2.34: Network of proteins of enriched pathways and first-order shared neighbors constructed using Pathway Palette and the BioGRID database. First-order shared neighbors were assigned based on interaction data in the BioGRID database using Pathway Palette. To reduce the network's complexity, interactions between the interconnecting proteins are not shown. 18 protein pairs linked through first-order shared neighbors, but no direct interactions between the proteins of affected pathways were found. Star-shaped nodes represent the proteins found in significantly affected pathways annotated by Pathway Enrichment Analysis using DAVID and KEGG with a color scheme corresponding to their pathway as classified in Table 2.9: proteins of groups #1, 2, 5, 6, and 7, red; proteins of groups #3 and 4, green. First-order interconnection proteins are depicted as circles, with their color indicating the number of interactions to proteins of groups #1-7: >3 interactions, pink; 3 interactions, blue; 2 interactions, yellow. The edge color indicates the source interaction database: BioGRID: Low-Troughput, blue; BioGRID: HTP/Complex, green; no interactions resulted from searching BioGRID: HTP/Pairwise. Proteins are indicated by their gene names. Proteins with ≥ 3 interactions are listed in Table 2.12 with their full name, abbreviation, gene name, accession number, and short description of their physiological function.

2.7 Investigation of proteome alterations in LS180 cells after MPA treatment

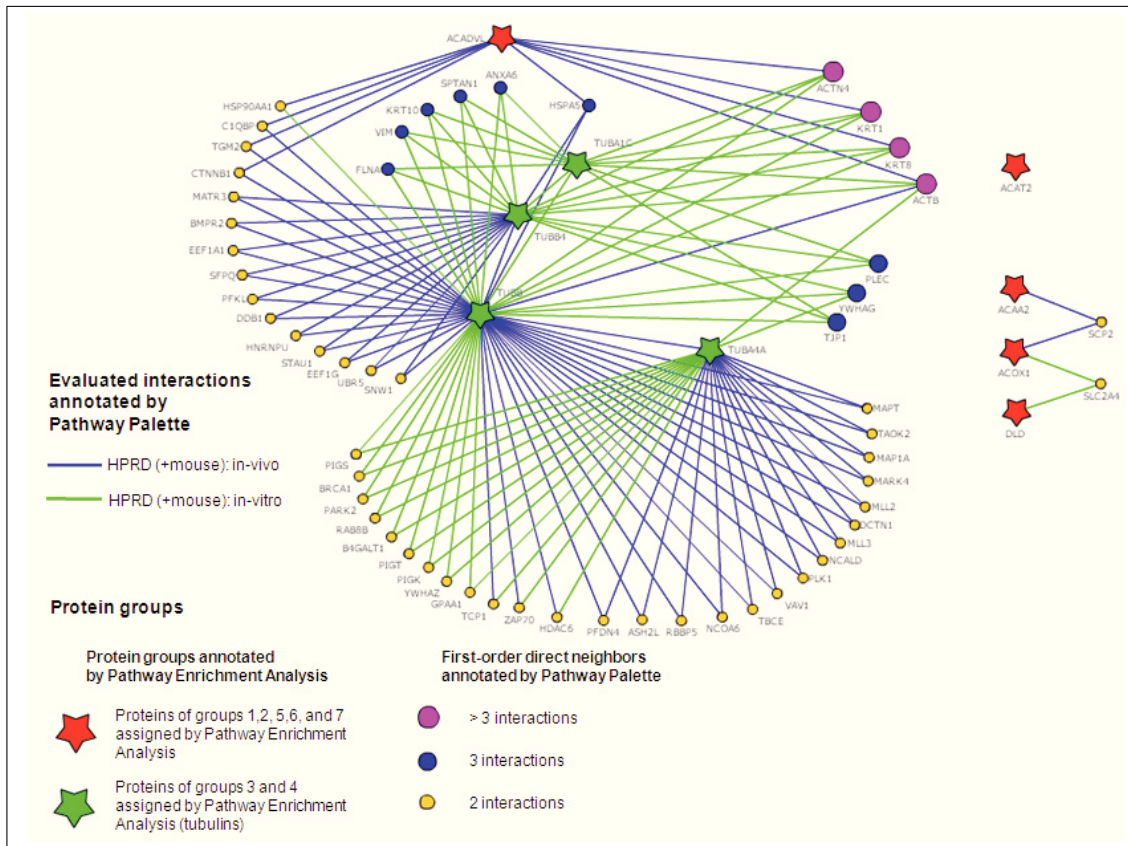


Fig. 2.35: Network of proteins of enriched pathways and first-order shared neighbors constructed using Pathway Palette and the HPRD database. *First-order shared neighbors were assigned based on interaction data in the HPRD (+mouse) database using Pathway Palette. To reduce the network's complexity, interactions between the interconnecting proteins are not shown. 58 protein pairs linked through first-order shared neighbors and 3 direct interactions between the proteins of affected pathways were found. Star-shaped nodes represent the proteins found in significantly affected pathways annotated by Pathway Enrichment Analysis using DAVID and KEGG with a color scheme corresponding to their pathway as classified in Table 2.9: proteins of groups #1, 2, 5, 6, and 7, red; proteins of groups #3 and 4, green. First-order interconnection proteins are depicted as circles, with their color indicating the number of interactions to proteins of groups #1-7: >3 interactions, pink; 3 interactions, blue; 2 interactions, yellow. The edge color indicates the source interaction database: HPRD (+mouse): in-vitro, blue; HPRD (+mouse): in-vivo, green; no interactions resulted from searching BioGRID: HTP/Pairwise. Proteins are indicated by their gene names. Proteins with ≥ 3 interactions are listed in Table 2.13 with their full name, abbreviation, gene name, accession number, and short description of their physiological function.*

Table 2.12: Description of additional proteins identified by Pathway Palette analysis using the BioGRID database. Shown are protein numbers (assigned for clarity), protein names, protein and gene (*italic*) abbreviations, Uniprot accession numbers, the number of interactions identified by Pathway Palette as shown in Figure 2.34, and a short descriptions of physiological functions.

#	Protein	Abbr. prot. <i>Abbr. gene</i>	Acc. number	No. of interactions	Physiological function
1	Polyubiquitin-C, cleaved into Ubiquitin	UBC <i>UBC</i>	P0CG48	9	Multiple functions, e.g. DNA repair, cell cycle regulation, degradation and signaling processes, activation of the transcription factor NF- κ B, and activation of kinases [311]
2	NAD ⁺ -dependent protein deacetylase sirtuin-7	SIRT7 <i>SIRT7</i>	Q9NRC8	4	Regulation of acetylation, cell survival, apoptosis, gene transcription, autophagy, DNA repair, stress response, genome stability [312]; positive regulation of transcription on exit from mitosis [313]
3	Myc-proto-oncogene protein	MYC <i>MYC</i>	P1106	3	Regulation of gene transcription, seems to activate the transcription of growth-related genes [314]
4	β -arrestin 1	ARRB1 <i>ARRB1</i>	P49407	3	Regulation of agonist-mediated G protein-coupled receptor signaling, negative regulation of NF- κ B transcription factor activity [315]
5	β -arrestin 2	ARRB2 <i>ARRB2</i>	P32121	3	Regulation of agonist-mediated G protein-coupled receptor signaling, negative regulation of NF- κ B transcription factor activity [316]
6	Tight junction protein ZO-1	ZO-1 <i>TJP1</i>	Q07157	3	Tight junction assembly, specific properties of tight junctions, stabilizing junctions, regulation of cell migration [317]
7	Small ubiquitin-related modifier 1	SUMO-1 <i>SUMO1</i>	P63165	3	Post-translational modification of proteins, which plays a crucial role in nuclear transport, DNA replication/repair, mitosis, and signal transduction [318]
8	Small ubiquitin-related modifier 2	SUMO-2 <i>SUMO2</i>	P61956	3	Post-translational modification of proteins, which plays a crucial role in nuclear transport, DNA replication/repair, mitosis, and signal transduction [319]
9	14-3-3 protein θ	14-3-3 θ <i>YWHAQ</i>	P27348	3	Regulation of signaling pathways, negatively regulates the kinase activity of 3-phosphoinositide-dependent protein kinase-1 [320]

Table 2.13: Description of additional proteins identified by Pathway Palette analysis using the HPRD database. Shown are protein numbers (assigned for clarity), protein names, protein and gene (*italic*) abbreviations, Uniprot accession numbers, the number of interactions identified by Pathway Palette as shown in Figure 2.35, and a short descriptions of physiological functions. *: previously identified and listed in Table 2.12.

#	Protein	Abbr. prot. Abbr. gene	Acc. number	No. of interactions	Physiological function
10	Actin, cytoplasmatic 1	ACTB <i>ACTB</i>	P60709	5	Involvement in various types of cell motility [321]
11	α -actinin-4	ACTN4 <i>ACTN4</i>	O43707	4	F-actin cross-linking protein, anchoring actin to various intracellular structures [322]
12	Keratin type II, cytoskeletal 1	CK-1 <i>KRT1</i>	P04264	4	May regulate the activity of kinases such as protein kinase C via binding to integrin β -1 and the receptor of activated protein kinase C [323]
13	Keratin type II, cytoskeletal 8	CK-8 <i>KRT8</i>	P05787	4	Linkage of the contractile apparatus dystrophin at the costameres of striated muscle [324]
6*	Tight junction protein ZO-1	ZO-1 <i>TJP1</i>	Q07157	3	Tight junction assembly, specific properties of tight junctions, stabilizing junctions, regulation of cell migration [317]
9*	14-3-3 protein θ	14-3-3 θ <i>YWHAQ</i>	P27348	3	Regulation of signaling pathways, negatively regulates the kinase activity of 3-phosphoinositide-dependent protein kinase-1 [320]
14	Plectin	PCN <i>PLEC</i>	Q15149	3	Interlinks intermediate filaments with microtubules and microfilaments and anchors intermediate filaments to desmosomes or hemidesmosomes [325]
15	Annexin A6	ANXA6 <i>ANXA6</i>	P08133	3	May regulate the release of Ca^{2+} from intracellular stores [326]
16	Spectrin α chain, non-erythrocytic 1	SPTAN1 <i>SPTAN1</i>	Q13813	3	Involvement in calcium-dependent movement of the cytoskeleton at the membrane [327]
17	Keratin type I, cytoskeletal 10	CK-10 <i>KRT10</i>	P13645	3	Composition of the cytoskeleton of epithelial cells [328, 329]
18	Vimentin	VIM <i>VIM</i>	P08670	3	Stabilization of cytoskeleton [330]
19	Filamin-A	FLN-A <i>FLNA</i>	P21333	3	Linkage of actin filaments, scaffold function for a wide range of cytoplasmic signaling proteins [331]

2 Results and Discussion

PANTHER analysis PANTHER is a database of gene products organized by biological functions and pathways using protein family and subfamily classification [332, 333]. It uses gene ontology (GO) terms for classification by molecular function, biological process, and cellular component. It was used to group the 35 affected genes/proteins identified by SILAC in respect of molecular functions and biological processes (Fig. 2.36). Additionally gene/protein hits were uploaded with their fold change numerical value (not possible in DAVID), sorted according to increases/decreases in affected gene/protein groups (lipid metabolism, carbohydrate metabolism, developmental processes, transport processes, protein class), and changes were depicted graphically (Fig. 4.20 - Fig. 4.24, appendix).

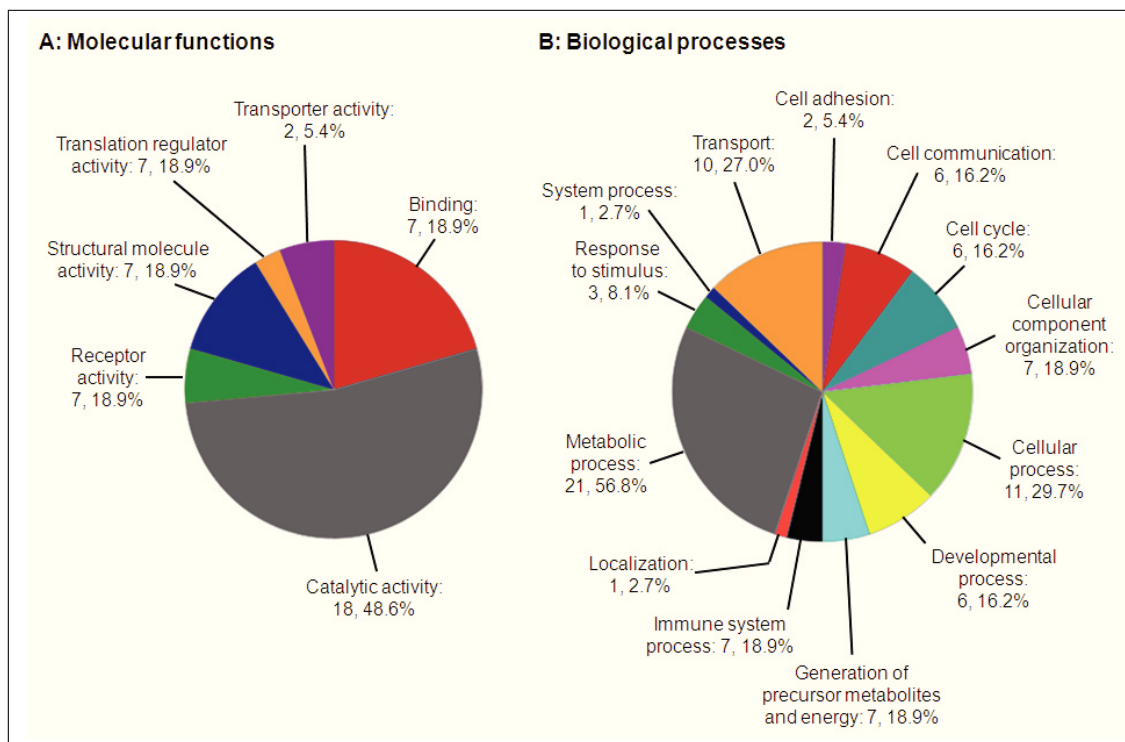


Fig. 2.36: PANTHER charts of gene ontology (GO) terms for (A) Molecular functions and (B) Biological processes of differentially expressed proteins in LS180 cells after MPA treatment. GO terms are given with number of comprised genes and percentage of gene hits versus total number of genes.

Pie charts generated using PANTHER show results closely related to results gained through DAVID as terms such as “Structural molecule activity”, “Transport”, “Cell cycle”, “Developmental process”, and “Generation of precursor metabolites and energy” constitute the most enriched groups besides groups of lesser specificity (e.g.

2.7 Investigation of proteome alterations in LS180 cells after MPA treatment

“Catalytic activity”, “Binding”, “Metabolic process”, “Cellular process”).

PANTHER charts of differentially expressed proteins linked to lipid metabolism, carbohydrate metabolism, developmental processes, and transport processes as well as proteins grouped into protein classes are shown in the appendix in Figure 4.20 - Figure 4.24, respectively. Fold changes of proteins of distinctive groups show specific patterns in increases/decreases according to their groups and GO terms. Proteins of lipid and carbohydrate metabolism seem to be constantly upregulated (Fig. 4.20 and Fig. 4.21), while most affected proteins linked to developmental and transport processes in LS180 cells after MPA treatment were downregulated (Fig. 4.22 and Fig. 4.23). Levels of tubulins are decreased, while levels of dehydrogenases and oxidoreductase are increased (Fig. 4.24).

Confirmation of MS results by immunoblot analysis

To verify SILAC GelC-MS results western blot analysis was carried out for five representative proteins. Due to the semiquantitative nature of densitometry analysis proteins with relatively high changes in expression values after 250 μ M MPA treatment compared to SILAC H/L ratio=1 (control) were chosen to be analyzed. Other factors for the selection of proteins were their biological function in relation to MPA GI toxicity and antibody availability. ACSL5 and annexin A1 (ANXA1, 4) were chosen among the proteins with increased levels after MPA treatment, SLC12A2 solute carrier family 12 member 2 (SLC12A2, 23), polymeric immunoglobulin receptor (PIgR, 21) and regenerating islet-derived protein 4 (REG-4, 22) as representatives of proteins with decreased levels.

SILAC results could only partly be confirmed by immunoblot analysis. Western blots of the five proteins are shown in Figure 2.38, the corresponding graph in Figure 2.39. To elucidate the discrepancy between MS results and western blot results, amino acid sequences of the chosen proteins are listed in the appendix. Immunogen sequences against which the respective antibodies were raised and unique peptides that served for protein identification by Mascot are marked (appendix, page 283 to 287).

Two western blots for ACSL5 were conducted with two different antibodies (antibody 1: Sigma WH0051703M1, antibody 2: Abcam ab104892), of which each one was raised against a different immunogen. Details concerning the antibodies, e.g. immunogen sequence, are listed in the appendix (page 283).

2 Results and Discussion

For the increase in ACSL5 determined by SILAC ratios, a trend was observed in expression levels determined by western blotting using antibody 1. Since western blot analysis is less sensitive than MS analysis and standard deviations are a lot higher, these results seem reasonable. The second western blot for ACSL5 using antibody 2 yielded a surprising result as drastic decreases in protein can be seen for 100 μ M and 250 μ M MPA ($66.4 \pm 8.3\%$ of controls and $8.7 \pm 1.2\%$ of controls). In this experiment only unmodified peptides were identified by MS analysis, not peptides that were covalently modified by MPA, MPA metabolites, and/or “natural” co- or post-translational modifications such as phosphorylation and glycosylation. Only unmodified peptides and standard variable modifications, i.e. methionine oxidation “Oxidation (M)”, N- α -acetylation “Acetyl (Protein N-term)”, and cyclization of N-terminal glutamine residues to pyroglutamic acid “Gln \rightarrow pyro-Glu”, were allowed for protein quantification using MaxQuant (Sec. 3.9.2). The about 2-fold increase in ACSL5 in SILAC experiments relates to these unmodified peptides. The drastic decrease seen in western blot using the second anti-ACSL5 antibody is most likely due to a modification of the antibody binding site (marked in blue in the ACSL5 amino acid sequence in the appendix, page 283). One aspect arguing strongly for this modification is the antibody binding site not being part of a unique peptide that served for protein identification. This modification would be induced by high MPA concentrations and can either be a covalently bound MPA molecule, an MPA metabolite (Sec. 2.7.2) or a “natural” modification. Since MPA is known to influence glycosylation of proteins (Sec. 1.1.4) and UTP and GTP levels were found to be affected by MPA even under 1000 μ M guanosine supplementation, glycosylation of the antibody binding site through MPA treatment is likely.

Nucleotides are intermediates in the glycosylation process of proteins and lipids [42, 334]. While glucose, galactose, and other amines are transferred to proteins via UDP intermediates, fucose and mannose are transferred via GDP (Fig. 2.37).

Although publications often only refer to MPA-induced inhibition of glycosylation of proteins (especially in context of adhesion molecules facilitating leukocyte attachment to endothelial cells) through depletion of guanosine nucleotides [42, 43, 46], augmentation of glycosylation in LS180 cells due to UTP increases could occur as well.

The results for ANXA1 western blots are consistent with the SILAC results. The immunogen sequence of the used anti-ANXA1 antibody (Cell Signaling, #3299) is unpublished. The peptide comprehends the amino acid (aa) 207 (in human, aa 206 in rabbit; tyrosine) which is marked in red in the protein sequence on page 284.

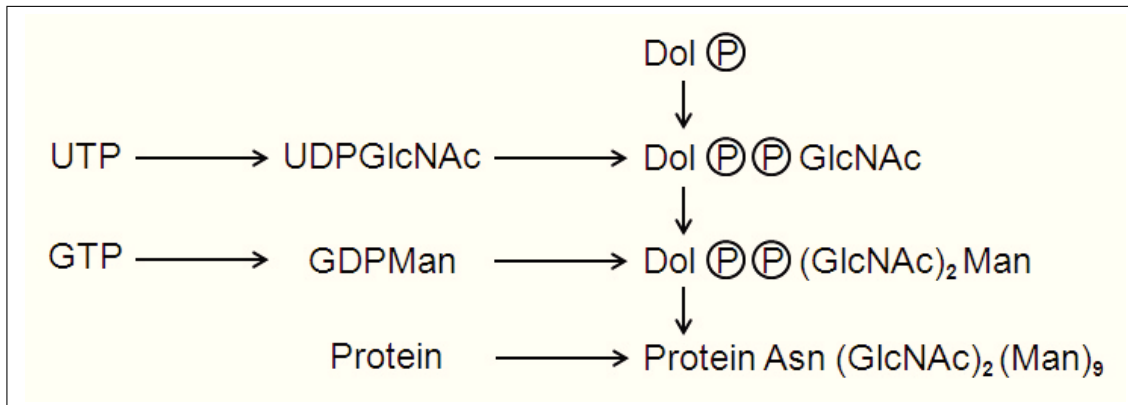


Fig. 2.37: Requirement of UTP and GTP for glycoprotein synthesis. Changes in UTP and/or GTP levels influence glycoprotein synthesis as sugar nucleotides and dolichol phosphate transfer N-acetylglucosamine and mannose to e.g. asparagine residues of proteins; Asn: asparagine, Dol: dolichol, Glc: glucose, GDP: guanosine diphosphate, GTP: guanosine triphosphate, Man: mannose, NAc: N-acetylglucosamine, P: phosphate, UDP: uridine diphosphate, UTP: uridine triphosphate. Adapted from [42].

As can be seen in the marked sequence two peptides in close proximity to aa 207 were identified as unique peptides. These two peptides are likely to be part of the immunogen as well, which would argue for a widely/fully preserved (no co- or post-translational modifications) immunogen sequence in ANXA1. This is further supported by the about 2-fold increase of protein amount in densitometry analysis of western blots.

The significant decreases in protein levels for SLC12A2, PIgR, and REG-4 seen in SILAC results were not detected in western blot analyses. Multiple bands of different molecular weights suggest post-translational modifications of SLC12A2 (Fig. 2.38) such as glycosylation, which can account for big differences in protein size [125]. SLC12A2 is also predicted to have several N-linked glycosylation sites [335, 336]. Only a trend could be seen in decreases of protein content for bands at 170kDa and 150kDa for SLC12A2. The immunogen sequence comprises two of the 28 unique peptides identifying SLC12A2 and is therefore relatively unlikely to be modified, but modification of the uncovered immunogen sequence part cannot be ruled out completely (appendix, page 285).

The immunogen sequence of the anti-PIgR antibody (Abcam, ab91269) is a peptide from the C-terminal region of the protein (page 286). Without further information available no conclusions can be drawn from distribution of unique peptides and location of the immunogen sequence. Post-translational modifications on unique

2 Results and Discussion

peptides could account for the decrease in PIgR determined by GelC-MS.

As recombinant human full length REG-4 protein served as antigen for the anti-REG-4 antibody used (Abcam, ab89917) and unique peptides are distributed relatively evenly over the full length of the protein, the reason for the discrepancy between MS and immunoblot results is unclear.

Not all SILAC results were confirmed by immunoblot analysis. SILAC results seem to be more reasonable than the immunoblot results due to reasons discussed above (especially visible in differences in western blots of ACSL5 where band intensities were dependent on the antibody/immunogen sequence of the antibody), MPA's known ability to strongly influence protein glycosylation, results from DAVID and PANTHER analyses, and results from the comparison of human cancer and rat models. Additionally SLC12A2 (#60 in Table 4, appendix) and PIgR (#70 in Table 4, appendix) were found to be covalently modified by MPA treatment in rats before [294].

It should be noted that distinctive patterns in PANTHER charts (Fig. 4.20 - Fig. 4.24, appendix). i.e. distinctive increases/decreases of all proteins attributed to a certain protein group, argue for upregulation/downregulation of specific protein groups necessary for specific cellular functions. Either protein levels themselves might be up- or downregulated or changes could be due to downregulated/upregulated post-translational modifications of the respective proteins or adduct formation of the protein/unique peptides of the protein with MPA and/or MPA metabolites (except for the above mentioned exclusions for which only unmodified unique peptides served for protein identification and quantification). Increases/decreases in post-translational modifications would have to occur for proteins of a specific protein group consistently, i.e. increase of modifications for all proteins of a certain group or decrease of modifications for all proteins of a certain group, to explain patterns in charts. Adduct formation of proteins with MPA and/or MPA metabolites could only be a reason for decreases in measured protein levels (modified unique peptides do not get picked up mass spectrometrically which results in less protein quantified). Adduct formation of proteins with MPA and/or MPA metabolites is unlikely to cause patterns as seen in PANTHER charts since adduct formation is unlikely to hit only proteins of a certain class.

Immunoblot analysis of additional potentially affected proteins identified by Pathway Palette analysis

Out of the 19 proteins listed in Table 2.12 and Table 2.13 three proteins were analyzed by western blot analysis. Ubiquitin was chosen since 9 interactions with dif-

2.7 Investigation of proteome alterations in LS180 cells after MPA treatment

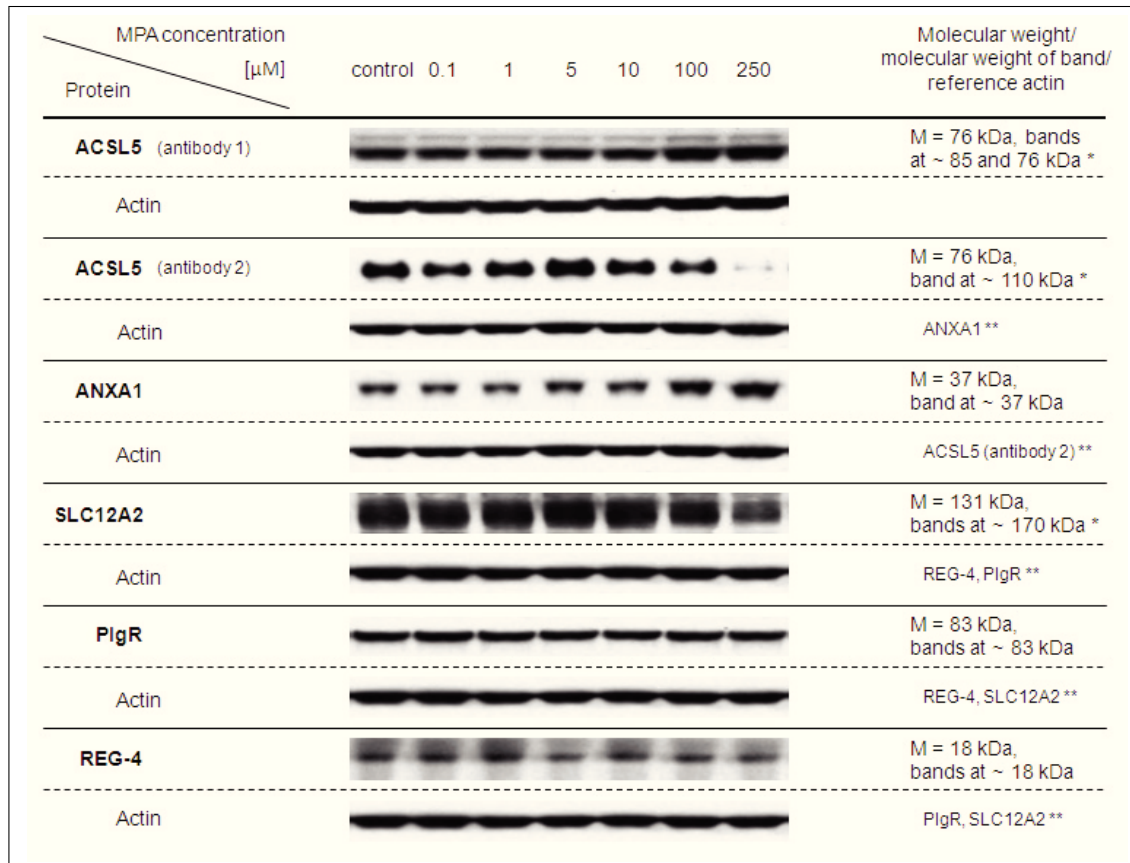


Fig. 2.38: Western blots for confirmation of results of SILAC experiments. Bands are shown with their respective β -actin bands ($N=3$). Relative intensities normalized to β -actin are shown in Figure 2.39 including their statistical analysis in the figure legend below the figure. M: molecular weight, *: difference between actual and predicted band size probably due to post-translational modifications, post-translational cleavage, splice variants, relative charge or multimerization [125], **: due to cutting/stripping of the membrane the same β -actin band served for the normalization of multiple proteins.

2 Results and Discussion

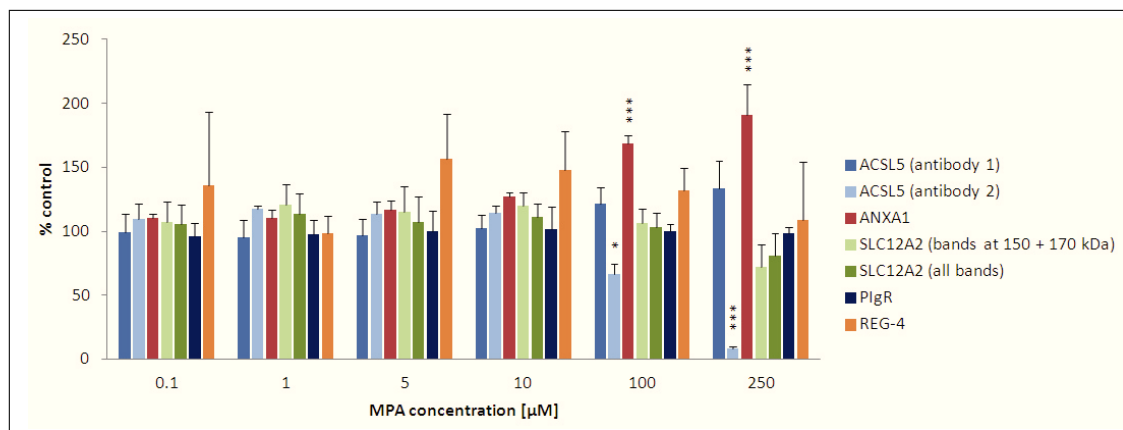


Fig. 2.39: Western blot expression levels of representative proteins identified by SILAC and GelC-MS in LS180 cells after treatment MPA and 1000 μM guanosine for 72h. Values are given as means of % of controls of relative intensities normalized to β -actin as determined by densitometry analysis ($N=3$). Western blots with their respective β -actin bands are shown in Figure 2.38. Significance was determined using one-way ANOVA combined with Scheffe's post – hoc test with *: $p<0.05$; **: $p<0.005$; ***: $p<0.001$ versus controls.

ferentially expressed proteins were found using Pathway Palette (BioGrid database only, Figure 2.34 and Table 2.12; number of interactions using the HPRD database <2 , Figure 2.35 and Table 2.13. ZO-1 and 14-3-3 θ were assigned 3 interactions each by both of the databases. Physiological functions of all three proteins may play a significant role in MPA GI toxicity as partly already demonstrated by previously discussed data, e.g. ubiquitin (cell cycle regulation) and ZO-1 (tight junction assembly, Tab. 2.12).

No statistically significant changes were found after immunoblot analysis. Considering that western blot analysis is relatively unreliable quantifying changes in levels of proteins related to MPA toxicity as already seen and discussed above, MS analysis of proteins hinted that Pathway Palette results could potentially yield different results and valuable indications of the mechanisms of MPA toxicity.

2.7 Investigation of proteome alterations in LS180 cells after MPA treatment

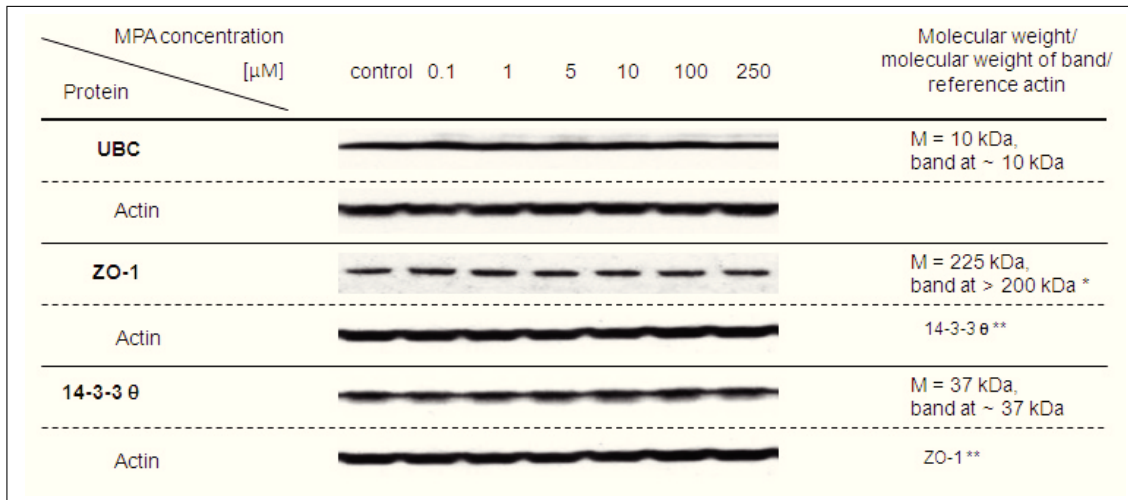


Fig. 2.40: Western blots of additional potentially affected proteins as identified by Pathway Palette analysis. Bands are shown with their respective β -actin bands ($N=3$). Relative intensities normalized to β -actin are shown in Figure 2.39 including their statistical analysis in figure legend. *M*: molecular weight, *: difference between actual and predicted band size probably due to post-translational modifications, post-translational cleavage, splice variants, relative charge or multimerization [125], **: due to cutting/stripping of the membrane the same actin band served for the normalization of multiple proteins.

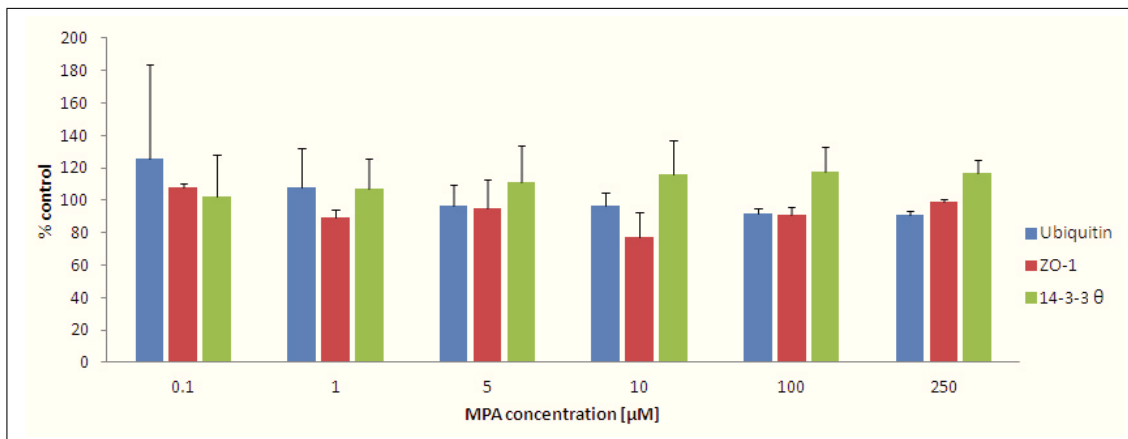


Fig. 2.41: Western blot expression levels of representative proteins identified by Pathway Palette in LS180 cells after treatment with increasing concentrations of MPA and 1000 μM guanosine for 72h. Values are given as means of % of controls of relative intensities normalized to β -actin ($N=3$). Western blots with their respective β -actin bands are shown in Figure 2.40. No statistically significant differences were found using one-way ANOVA combined with Scheffe's *post-hoc* test.

Overall this SILAC experiment shows that our LS180 cell culture model yields results relatively close to results of the often employed rat models with exemptions concerning MPA-induced changes in carbohydrate metabolism. As multiple proteins were identified to be affected by MPA that are known to be upregulated in cancers (Tab. 2.7, column “Regulation of expression”) the LS180 cell model might even make protein targets that are usually low abundance proteins more accessible. On the other hand excessive changes in these proteins might be attributable to the cancerous origin of LS180 cells and of lesser value in non-cancerous tissues. Otherwise results shown in other sections of this thesis were confirmed such as impairment of nucleotide-related processes and lipid metabolism (Sec. 2.8.3). The often investigated and discussed effects of MPA on protein glycosylation were seen to play an important role in LS180 cells and especially proteome analysis of this cell line as well.

2.7.2 Identification of protein targets using an anti-MPA/AcMPAG antibody

Following experiments performed by Asif et al. [175] and Shipkova et al. [176] an anti-MPA antibody (kind gift of Fisher Scientific) exhibiting cross-reactivity with AcMPAG as described in the literature [108, 175, 176, 337] was used to identify protein targets of MPA and certain MPA metabolites in LS180 cells directly.

Antibody binding to MPA and MPA metabolites

Nomenclature As labeling of functional groups in the MPA molecule is inconsistent in the literature, it was decided to stick to the labeling routine which is commonly cited as the IUPAC name for MPA (Fig. 2.42). The hydroxy position of the benzofuran structure which in the literature is often termed the 7-O-position (which is technically correct when starting labeling of the benzofuran at the oxo function as the highest functional group following IUPAC convention) is referred to as the 4-hydroxy position in the following. This way the labeling of functional groups of metabolites, i.e. DM-MPA, DM-MPA-6G, and DM-MPA-4G stays consistent with the published literature, except for MPAG which is often termed 7-O-glucuronide of MPA (also termed β -D-glucuronide).

Anti-MPA/AcMPAG antibody As the antibody, usually used in Enzyme Multiplied Immunoassays and Cloned Enzyme Donor Immunoassays to determine transplant patients’ MPA trough plasma concentrations, does not exhibit notable cross-

2.7 Investigation of proteome alterations in LS180 cells after MPA treatment

reactivity with MPAG, antibody binding is thought to occur at the 4-hydroxy-position of MPA and AcMPAG [108, 337] (Fig. 2.42). As of today only MPA and AcMPAG binding of the used antibody is considered in the literature [108, 187, 337, 338] although other minor MPA metabolites (DM-MPA and glucuronides, AcMPA-GS) might be captured by this antibody as well, as explained and illustrated in the next section.

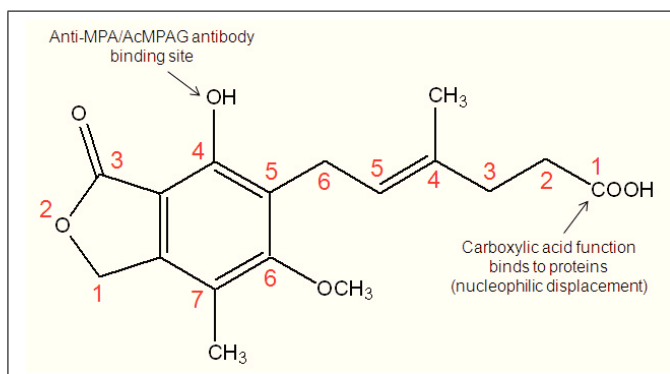


Fig. 2.42: Commonly used atom numbering scheme for MPA. The scheme is shown to avoid confusion about nomenclature of MPA metabolites. The 4-hydroxy position is considered the anti-MPA/AcMPAG antibody binding site. Nucleophilic groups of proteins can bind to MPA via the carboxylic acid function (Fig. 2.43).

Protein binding by MPA and MPA metabolites

As commonly known for carboxylic drugs [339] MPA can bind to proteins through its carboxylic acid function [340, 341] (nucleophilic displacement mechanism, explained below using the example of acyl glucuronides). Especially for HSA protein binding of MPA has been extensively studied [340, 341]. HSA is the most abundant plasma protein which commonly accounts for most of the occurring drug binding of any given drug in plasma [342], but binding to other proteins of MPA is likely as well. In addition acyl glucuronide conjugates of carboxylic acid drugs are known to be highly reactive intermediates [339]. Two hypothetical mechanisms have been postulated to explain irreversible protein binding of acyl glucuronides [107]. The first option is direct nucleophilic displacement of glucuronic acid by cysteine thiol or tyrosine residues of proteins [343] (Fig. 2.43), a second way is imine formation between the aldehyde group of an open-chain glucuronic acid and a nucleophile, i.e. lysine or the N-terminus of a protein (Schiff base mechanism) [107, 344] (Fig. 2.44).

2.7 Investigation of proteome alterations in LS180 cells after MPA treatment

Although protein adducts formed by MPA and AcMPAG are probably the most important protein modifications to focus on when elucidating the mechanisms of MPA GI toxicity due to relatively high doses of MPA in the gut lumen (Sec. 2.1.1) and known potential of toxicity of acyl glucuronides [66, 175, 176, 302], the possibility of protein binding of other MPA metabolites needs to be taken into account as well. Structural similarity of glucosides and glucuronides argue for protein adduct formation of glucosides via nucleophilic displacement and imine mechanism as well. Table 2.14 summarizes possible covalent protein modifications by MPA and MPA metabolites. Modifications by DM-MPA-4G and DM-MPA-6G were not taken into account and not incorporated in the search due to two transformation steps necessary to yield these metabolites (Fig. 1.3), their low concentrations in transplant patients (Sec. 1.1.5), and unclear clinical significance (Sec. 1.1.5). Furthermore DM-MPA-4G lacks the ability to bind the used anti-MPA/AcMPAG antibody.

Table 2.14: Covalent protein modifications by MPA and MPA metabolites. Modifications are sorted by metabolites given with their relative molecular masses (M_r) and molecular formulas. Dependent on the mechanism of adduct formation, nucleophilic displacement (ND) versus imine mechanism (IM), relative molecular masses and molecular formulas of additions to the proteins or losses differ for the respective metabolites. Each metabolite's/adduct's ability to bind the anti-MPA/AcMPAG antibody is indicated.

#	Compound	M_r met.	Molecular formula met.	Mecha- nism	M_r addi- tion ¹	Molecular formula addition ¹	M_r loss ²	Molecular formula loss ³	AB bind- ing
1	MPA	320.34	C ₁₇ H ₂₀ O ₆	ND	302.32	C ₁₇ H ₁₈ O ₅	17.10, 1.01	OH, H	✓
2	AcMPAG	496.46	C ₂₃ H ₂₈ O ₁₂	ND	302.32	C ₁₇ H ₁₈ O ₅	193.13, 1.01	C ₆ H ₉ O ₇ , H	✓
3	AcMPAG	496.46	C ₂₃ H ₂₈ O ₁₂	IM	478.44	C ₂₃ H ₂₆ O ₁₁	16.00, 2*1.01	O, 2H	✓
4	DM-MPA ⁴	306.31	C ₁₆ H ₁₈ O ₆	ND	288.29	C ₁₆ H ₁₆ O ₅	17.10, 1.01	OH, H	✓
5	AcMPA-GS	482.48	C ₂₃ H ₃₀ O ₁₁	ND	302.32	C ₁₇ H ₁₈ O ₅	179.15, 1.01	C ₆ H ₁₁ O ₆ , H	✓
6	AcMPA-GS	482.48	C ₂₃ H ₃₀ O ₁₁	IM	464.46	C ₂₃ H ₂₈ O ₁₀	16.00, 2*1.01	O, 2H	✓
7	MPAG	496.46	C ₂₃ H ₂₈ O ₁₂	ND	478.44	C ₂₃ H ₂₆ O ₁₁	17.10, 1.01	OH, H	×
8	MPAG	496.46	C ₂₃ H ₂₈ O ₁₂	IM	478.44	C ₂₃ H ₂₆ O ₁₁	16.00, 2*1.01	O, 2H	×
9	MPA-GS	482.48	C ₂₃ H ₃₀ O ₁₁	ND	464.46	C ₂₃ H ₂₈ O ₁₀	17.10, 1.01	OH, H	×
10	MPA-GS	482.48	C ₂₃ H ₃₀ O ₁₁	IM	464.46	C ₂₃ H ₂₈ O ₁₀	16.00, 2*1.01	O, 2H	×

¹ includes -H/-2H (-1.01/-2*1.01) released by the protein (Fig. 2.43/ Fig. 2.44)

² the first number gives the loss of the metabolite, the second number the loss of the protein

³ the first formula gives the loss of the metabolite, the second formula the loss of the protein

⁴ DM-MPA-4G and DM-MPA-6G were not incorporated in the search due to two transformation steps necessary to yield these metabolites (Fig. 1.3), their low concentrations in transplant patients, and unclear clinical significance (Sec. 1.1.5). Furthermore DM-MPA-4G lacks the ability to bind the used anti-MPA/AcMPAG antibody.

Table 2.15: Covalent protein adducts potentially identifiable by the IP experiment. Four different protein adducts may be identified in this experiment due to structural overlaps in modifications, i.e. molecular formulas and relative molecular masses (M_r) of additions, as specified in Table 2.14. Metabolites are sorted by mechanism of adduct formation, nucleophilic displacement (ND) versus imine mechanism (IM), relative molecular masses and molecular formulas of additions to the proteins.

Adduct #	Modification #	Metabolite	Mechanism	M_r addition ¹	Molecular formula addition ¹
1	1/2/5	MPA/AcMPAG/AcMPA-GS	ND	302.32	C ₁₇ H ₁₈ O ₅
2	3	AcMPAG	IM	478.44	C ₂₃ H ₂₆ O ₁₁
3	4	DM-MPA	ND	288.29	C ₁₆ H ₁₆ O ₅
4	6	AcMPA-GS	IM	464.46	C ₂₃ H ₂₈ O ₁₀

¹ includes -H/-2H (-1.01/-2*1.01) released by the protein (Fig. 2.43/ Fig. 2.44)

Surveying western blots for identification of protein targets using an anti-MPA/AcMPAG antibody

UGT2B7 inhibition and cell culture conditions AcMPAG toxicity being considered a major issue in MPA GI toxicity brought up the idea of inhibition of UGT2B7 to decrease AcMPAG formation. In the literature the antifungal drug fluconazole is described to inhibit UGT2B7 relatively selective at concentrations of 10-1000 μ M [345]. Inhibition of other UGT isoforms tested was only 0-15% and fluconazole concentrations as high as 2500 μ M still only provided inhibition of \leq 14% for the UGT isoforms that are involved in MPA GI metabolism but do not generate AcMPAG (i.e. UGT1A7/8/9/10).

Examining *in vitro-in vivo* extrapolation of drug interaction effects of fluconazole on the drug zidovudine glucuronidation kinetics showed strong dependency on the presence or absence of exogenous bovine serum albumin (BSA) potentially caused by drug-protein interactions of fluconazole and albumin [345]. BSA is a major constituent of FBS which is typically added to cell culture media in amounts of 10% (Sec. 3.1). Considering the above mentioned excessive binding of MPA to HSA (up to 90% of MPA is known to be bound to HSA) [340, 341] and that withdrawal of FBS (Sec. 2.3.1 and Sec. 2.3.2) had no significant effect on MPA's cytotoxic potential on LS180 cells, different conditions were tested to optimize results, e.g. sufficient amount of free MPA in LS180 cell cultures to form sufficient amounts of metabolites and ensure the use of effective fluconazole concentrations.

To further validate the model, to test the efficiency of the inhibitor fluconazole, as well as to survey the anti-MPA/AcMPAG antibody's properties, western blots

2.7 Investigation of proteome alterations in LS180 cells after MPA treatment

of lysates of LS180 cells treated with MPA for 72h (1000 μ M guanosine, with and without FBS) were conducted. Figure 2.45 shows western blot results for cells treated with ascending MPA concentrations in the presence of 10% FBS. Samples for controls and for 250 μ M MPA treatment in serum-free media were run as well. In addition, effects of 0.5mM and 5mM fluconazole in the presence and absence of 10% FBS while incubating with 250 μ M MPA were assessed.

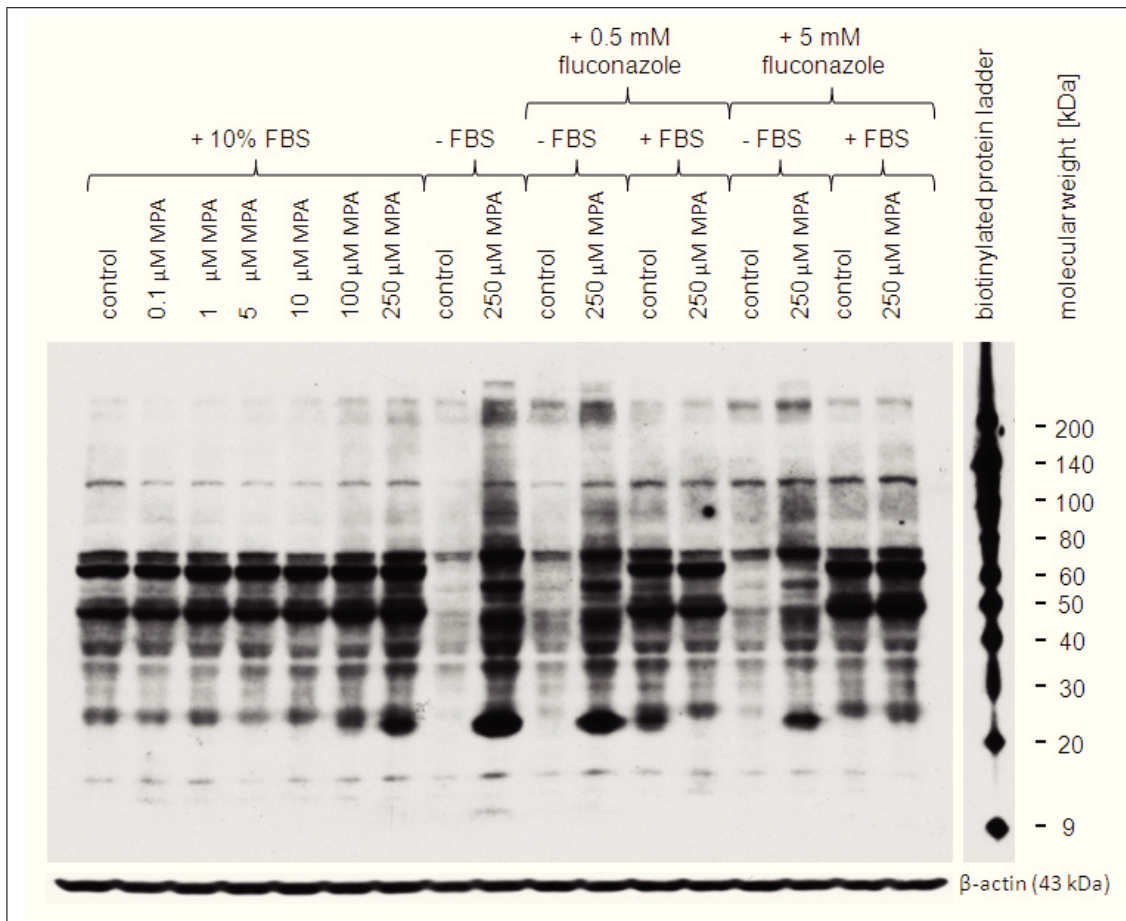


Fig. 2.45: Western blot of LS180 cell lysates after 72h of MPA and/or fluconazole treatment and incubation with an anti-MPA/AcMPAG antibody. Western blots of experiments run serum-free are shown in Figure 2.46 and Figure 4.37.

Strong bands in the control experiment conducted with 10% FBS compared to controls of experiments without FBS suggests cross-reactivity of the anti-MPA/AcMPAG antibody with FBS components. Increased band intensities of 250 μ M MPA samples generated without FBS compared to those with FBS additionally argue for capture of MPA by albumin (band at about 70kDa) and other proteins contained in FBS. Control samples incubated without FBS show light bands at certain molecular weights, suggesting cross-reactivity of the antibody with intracellular proteins

2 Results and Discussion

as well.

Treatment with 0.5mM and 5mM fluconazole in presence and absence of FBS showed decreases in band sizes for 5mM fluconazole compared to 0mM and 0.5mM fluconazole samples (250 μ M MPA) without FBS (e.g. band at about 25kDa). Reason for this decrease could be the desired competitive inhibition of UGT2B7, therefore lowered intracellular AcMPAG levels resulting in less AcMPAG protein adducts as detected by the anti-MPA/AcMPAG antibody. Another explanation could be however binding of fluconazole to proteins (serum protein binding of fluconazole is known to be 14% [346, 347]) that are also prone to MPA and/or MPA metabolite binding.

Based on the above listed findings the experiment was repeated without addition of FBS to the culture medium. Figure 2.46 (below) and Figure 4.37 (appendix) show the same western blot of LS180 cell lysates after 72h of MPA treatment and incubation with the anti-MPA/AcMPAG antibody (different film exposure times). In Figure 4.37 especially differences in bands resulting from proteins of high and low molecular weights can be identified, whereas Figure 2.46 facilitates differences in protein binding of MPA/MPA metabolites of proteins of medium molecular weight range. In this experiment 2.5mM fluconazole was applied additionally to 0.5mM and 5mM, with 5mM fluconazole still yielding the most promising results for decreasing responses to MPA treatment of LS180 cells.

The western blots showed that the most promising option for immunoprecipitation (IP) experiments described in the next paragraph was denial of FBS in LS180 cell culture media for experiments using the anti-MPA/AcMPAG antibody. For experiments described in the following sections the use of FBS was waived as done before already for better comparability of results and to avoid diminishing the free MPA/MPA metabolite fraction as described above.

As the use of 5mM fluconazole for UGT2B7 inhibition seemed most reasonable, the cytotoxic potential of fluconazole on LS180 cells was evaluated. LS180 cells were treated with concentrations of fluconazole (0, 10, 25, 50, 100, 250, 500, 1000, 2500, and 5000 μ M, no FBS, 1000 μ M guanosine) for 72h (redosed every 24h). Under the chosen conditions fluconazole exhibited significant cytotoxic potential (Fig. 4.38; as fluconazole is not described in the literature to act as an antiproliferative, cytotoxic effects are most likely to account for decreases in LS180 cell number). No significant change in LDH activities was found, but a trend towards an increase for higher fluconazole concentrations reflecting increased necrosis of LS180 cells could be seen. No proteomics experiments were conducted using fluconazole due to difficulties with

2.7 Investigation of proteome alterations in LS180 cells after MPA treatment

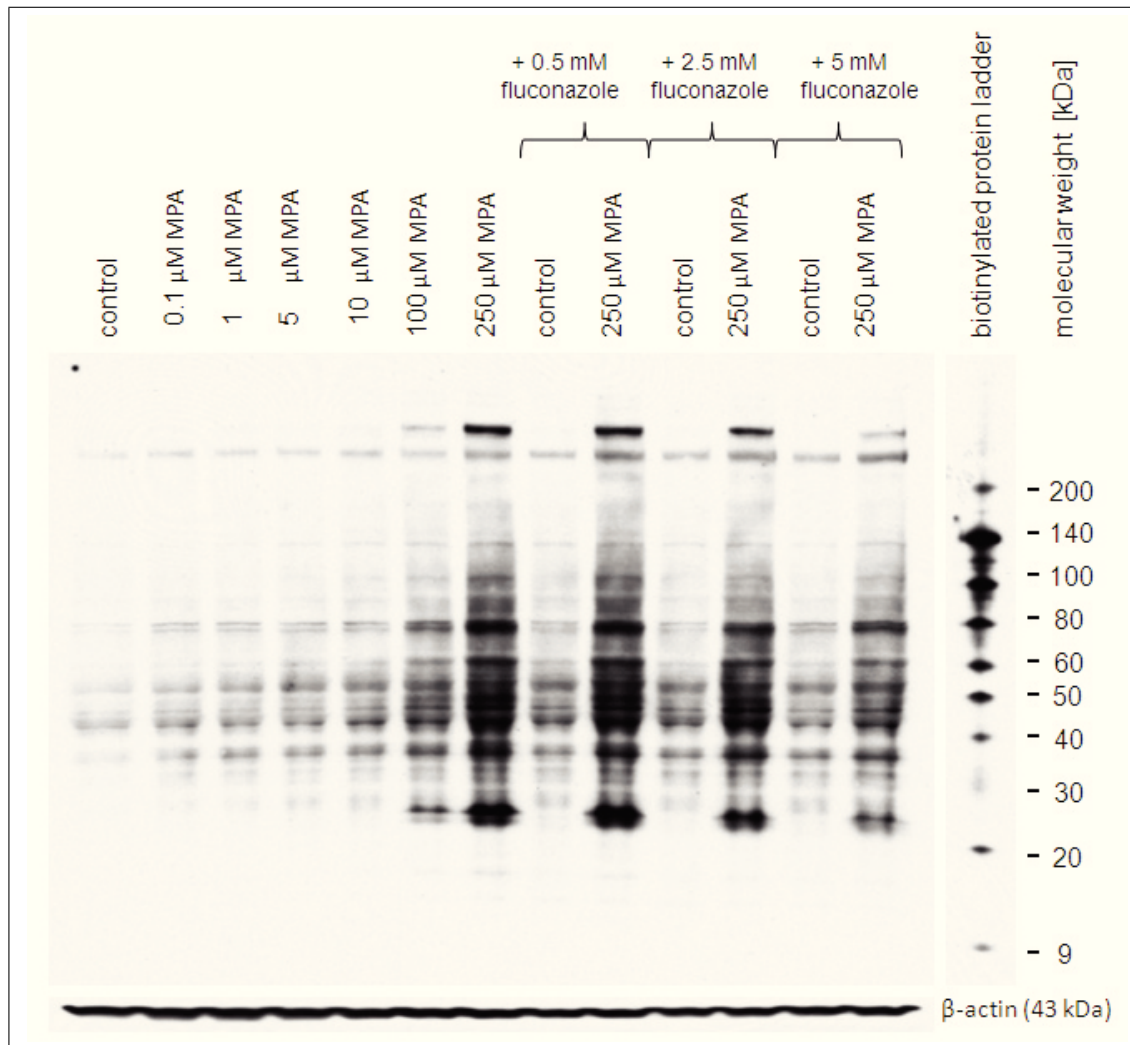


Fig. 2.46: Western blot of LS180 cell lysates after 72h of MPA and/or fluconazole treatment in FBS-free media and incubation with an anti-MPA/AcMPAG antibody. A film developed after a longer exposure time is shown in Figure 4.37 to facilitate visualization of proteins at low and high molecular weights. A western blot of the same experiment run with FBS is shown in Figure 2.45.

2 Results and Discussion

the initial experiment (MPA treatment only) and performance of the antibody/IP as described below. However as $63.8 \pm 5.6\%$ of cells still survived, drug concentrations of 5mM fluconazole should be considered as a potential UGT2B7 inhibitor in future proteomics experiments involving LS180 cells.

IP of covalently modified proteins and analysis The same LS180 cell lysates (1000 μ M guanosine, no FBS, 72h treatment, redosed every 24h) that had served before for e.g. the assessment of cAMP/cGMP levels of LS180 cells under MPA treatment and the Thermo Scientific Pierce Classic IP Kit were used for antigen IP. For an IP a sample is incubated with a specific antibody (here anti-MPA/AcMPAG) to form an immune complex which is then linked to a solid substrate (here Protein A/G Plus Agarose, kit component). This way the complex can be isolated and concentrated for further analysis.

The IP was conducted according to the protocol provided by the manufacturer of the IP kit (Sec. 3.9.2). Sample preparation by in-solution tryptic digestion and analysis by HPLC-MS is described in Section 3.9.2. Database searches for covalent modifications of proteins by MPA and MPA metabolites were performed as described in Section 3.9.2.

No covalent protein adducts as listed in Table 2.15 were found. As the IP was conducted with the maximal amount of sample possible (1mg of total protein), in-solution tryptic digestion was performed with the entire amount of sample yielded after the IP step (150 μ L), protein concentrations of samples were undetectably low (samples were assayed before the in-solution digestion step as described in Section 3.3), and protocols were strictly followed, it is likely that the IP part of this experiment did not yield satisfactory results. Western blots shown in Figure 2.45 and Figure 2.46/4.37 were produced using the antibody shortly after delivery by the manufacturer and show the antibody's potency for the detection of MPA and MPA metabolites. The actual experiment was conducted over 12 months later after storage of the antibody at 4°C. Aliquots of the antibody that were stored at -20°C were lost due to a freezer failure. Remanufacturing of the antibody was not considered due to an 8 month period for delivery of the original antibody.

Unfortunately, no covalently modified proteins were found in LS180 cells which would have elucidated results from SILAC and other experiments. Decreases and increases in protein levels measured by SILAC and GelC-MS which eventually are

partly due to covalent modifications by MPA and MPA metabolites could have been clarified by knowledge of covalent modifications of proteins by MPA and MPA metabolites or at least been further elucidated.

It should be mentioned that the possibility of MPAG forming adducts with proteins needs to be considered as well. Although MPAG is described as non-toxic throughout the literature and has never been considered to form covalent protein adducts it exhibits a carboxy function as MPA does, which is known for protein binding (nucleophilic displacement). Additionally adduct formation via the glucuronic acid moiety and the imine mechanism should be possible as well. Taking these options into account, MPAG's toxic potential in terms of covalent modifications of proteins, eventually compromising protein function or antigen formation eventually triggering immune reactions, is unlikely to be inferior to the potential of MPA or AcMPAG.

2.8 Metabolome analysis in LS180 cells after MPA treatment

NMR spectroscopy is a reliable, non-invasive technique to determine changes in concentrations of certain small organic molecules (metabolites) in biological samples. Additionally the use of labeled precursors and consecutive ^{13}C isotopomer analysis provides a quantitative approach for the assessment of metabolic pathways.

LS180 cells were incubated with 0, 0.1, 5 and $100\mu\text{M}$ MPA and $1000\mu\text{M}$ guanosine for 72h (redosed every 24h). No FBS was used to avoid MPA/MPA metabolite-serum component interactions (Sec. 2.7.2). For the last 5h of the 72h incubation time cell cultures were treated with media containing 5mM [$1\text{-}^{13}\text{C}$]glucose, instead of 25mM (4500mg/L) unlabeled glucose as in the routinely used medium. For these 5h cells were redosed with DMSO for controls or MPA in respective concentrations and $1000\mu\text{M}$ guanosine (no FBS) and subsequently extracted with PCA as described in Section 3.4.

The samples for metabolome analysis were prepared prior to proteomics experiments (where cells were also incubated with $250\mu\text{M}$ MPA) so that $100\mu\text{M}$ MPA instead of $250\mu\text{M}$ MPA was used as the highest tested drug concentration. $100\mu\text{M}$ MPA were chosen due to findings in earlier conducted experiments, i.e. proliferation assays with and without guanosine supplementation (Sec. 2.4), measurements of nucleotide levels with and without guanosine supplementation (Sec. 2.5), which had indicated that

2 Results and Discussion

100 μ M MPA was more than sufficient to induce significant changes in LS180 cells. It turned out that 250 μ M MPA treatment would have been beneficial as metabolic changes in LS180 cells just started to occur at concentrations around 100 μ M MPA.

^{31}P NMR measurements were not conducted since HPLC-MS analyses carried out prior to NMR studies had provided significant and expansive results already (Sec. 2.5). Furthermore, the magnetic field intensity used (600MHz) was incapable to resolve specific mono-, di-, and trinucleotides as it had been established already through HPLC-MS analyses.

Extracellular metabolite and glucose concentrations from cell culture media were not measured. Due to contamination of the solvent used for sample preparation the necessary magnetic field homogeneity for measurements could not be established (most likely due to paramagnetic ions in the solvent used for sample preparation).

2.8.1 Quantitative ^1H NMR spectroscopy of hydrophilic cell extracts

In Figure 2.47 simulated ^1H NMR spectra of MPA and its main metabolite MPAG are shown. Spectra were simulated, instead of recorded, using the nmrdb.org NMR simulator (<http://www.nmrdb.org/simulator>) which is operating based on an algorithm by Castillo et al. [348]. Spectra were simulated to rule out interference of drug signals with metabolite signals and compromise of signal integration and quantification. No signals attributable to MPA or MPAG were found in ^1H NMR spectra of cell extracts (Fig. 2.48).

For analysis of LS180 cell extracts, metabolically interesting and highly abundant compounds from ^1H NMR spectra (Fig. 2.48) were integrated and quantified after confirmation of signal assignment by 2D NMR (Sec. 2.8.4, Fig. 2.58, Fig. 4.34, and Fig. 4.34). In Table 2.16 absolute values of metabolites are given in $\mu\text{mol/g}$ cell wet weight and as % of controls. ^{13}C enrichments in lactate and alanine are given as well.

Integration of the glucose-1 α signal (5.24ppm; glucose-1 β at 4.655) did not seem reasonable due to low signal/noise (S/N) ratios. As the water signal at 4.72ppm potentially overlaps with the glucose-1 α resonance, suppression of the water signal, as it was used recording the ^1H NMR spectra of LS180 cell extracts, also affects the signals in close proximity, such as the glucose-1 α peak. Due to very small amounts of unmetabolized intracellular glucose, no reliable integration and calculation of glucose concentration was possible from ^1H NMR spectra of LS180 cell extracts.

2.8 Metabolome analysis in LS180 cells after MPA treatment

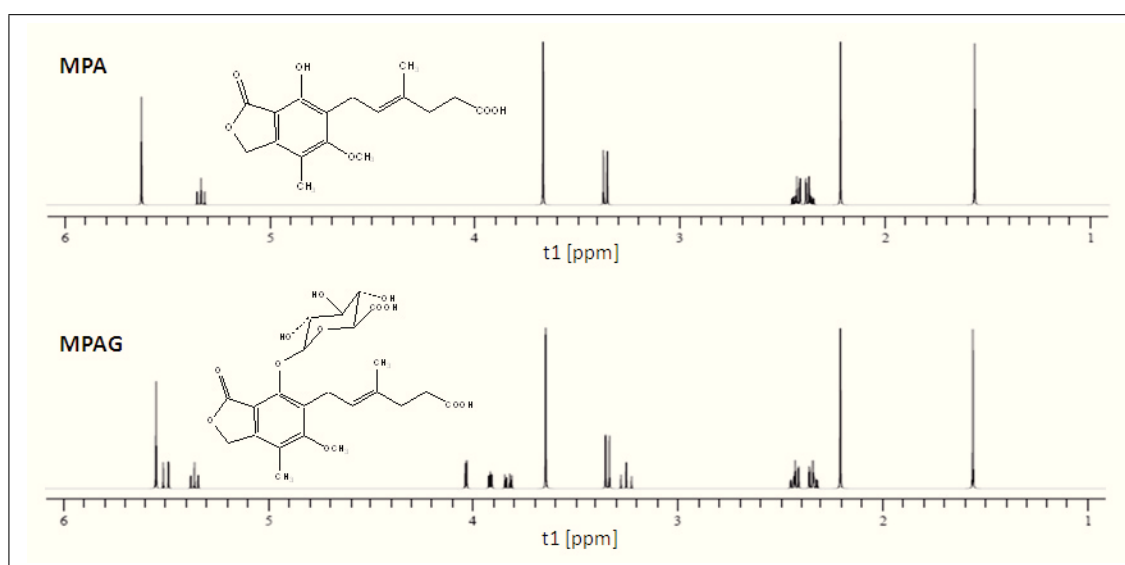


Fig. 2.47: Simulated ^1H NMR spectra of MPA and MPAG. ppm regions 1.0-6.0 are shown. ^1H NMR spectra were simulated using the [nmrdb.org](http://www.nmrdb.org/simulator) NMR simulator (<http://www.nmrdb.org/simulator>) which is operating based on an algorithm by Castillo et al. [348]

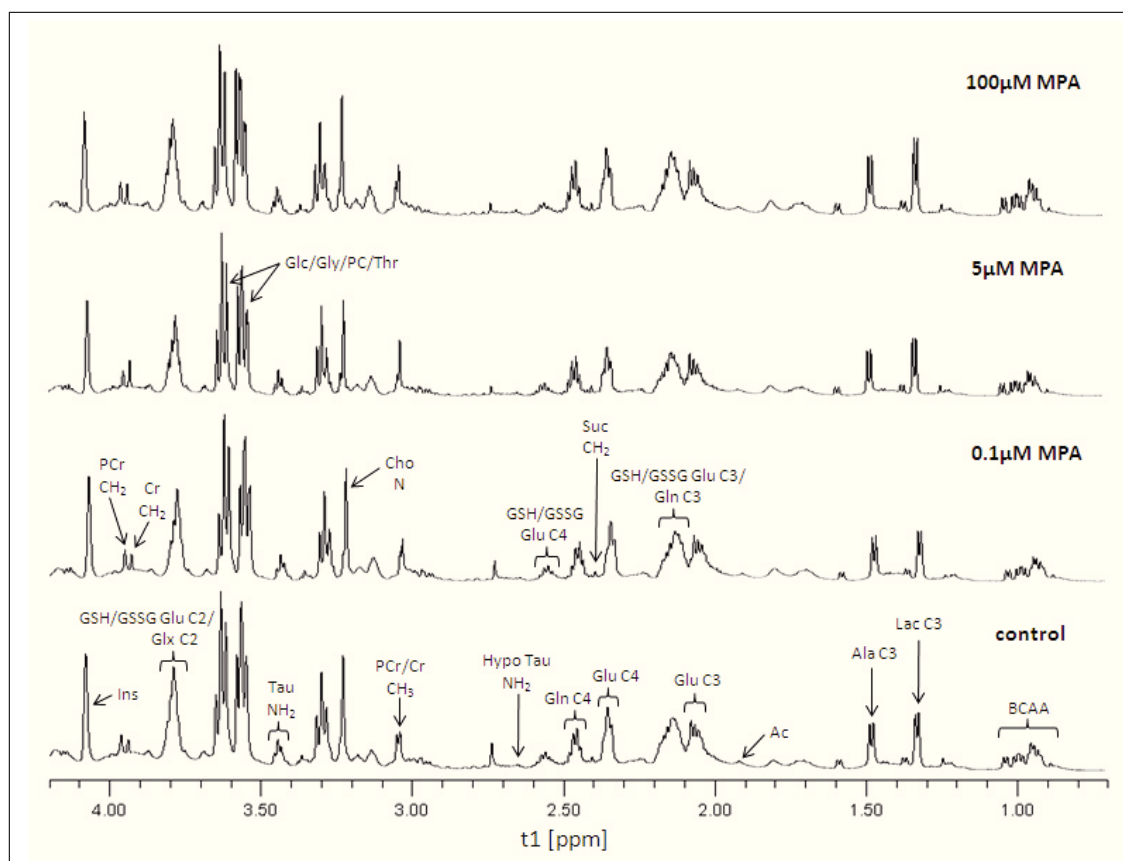


Fig. 2.48: Representative ^1H NMR spectra of LS180 cell extracts. ppm regions 1.7-4.2 are shown. Cells were incubated with 0, 0.1, 5, and $100\mu\text{M}$ MPA and $1000\mu\text{M}$ guanosine for 72h (redosed every 24h). For the last 5h cells were incubated with 5mM [$1\text{-}^{13}\text{C}$]glucose. Compounds were identified by comparison with $^1\text{H}\text{-}^{13}\text{C}$ HSQC spectra of cell extracts of same experimental conditions using published databases [349, 350]. Amino acid abbreviations are based on IUPAC nomenclature. Ac: acetate, BCAA: branched chain amino acids, Cho: choline, Cr: creatine, Glc: glucose, Glx: glutamate and glutamine, GSH: reduced glutathione, GSSG: oxidized glutathione, Hypo Tau: hypotaurine, Ins: myo-inositol, PC: phosphocholine, PCr: phosphocreatine, Suc: succinate, Tau: taurine.

2.8 Metabolome analysis in LS180 cells after MPA treatment

Table 2.16: Metabolite concentrations in LS180 cells after 72h of MPA treatment. Values were calculated from ^1H NMR spectra of cell extracts and are given in $\mu\text{mol/g}$ cell wet weight and as **% of controls** (**bold**) with standard deviations ($N=6$). Percentaged ^{13}C enrichments (*italic*) and ratios PCr/Cr (*italic*) are given. For the last 5h of incubation time LS180 cells were incubated with 5mM $[1-^{13}\text{C}]$ glucose. No statistically significant changes were found using one-way ANOVA combined with Scheffe's post – hoc test versus controls. Changes are depicted in graphs in Figure 2.49 - Figure 2.51.

	control	0.1 μM MPA	5 μM MPA	100 μM MPA
^{12}C Lac	6.71 \pm 2.25 100.0 \pm 33.5	6.20 \pm 1.27 92.4 \pm 19.0	7.05 \pm 1.75 105.1 \pm 26.1	10.78 \pm 0.92 160.8 \pm 13.8
^{13}C Lac	0.76 \pm 0.17 100.0 \pm 22.4	0.65 \pm 0.04 85.9 \pm 5.1	0.76 \pm 0.11 99.6 \pm 15.1	0.84 \pm 0.27 110.8 \pm 35.9
Lac total	7.46 \pm 2.29 100.0 \pm 30.6	6.89 \pm 1.42 92.3 \pm 19.0	7.80 \pm 1.74 104.5 \pm 23.3	11.61 \pm 1.01 155.5 \pm 13.5
% ^{13}C enrichment	<i>10.79 \pm 3.60</i> <i>100.0 \pm 33.4</i>	<i>9.75 \pm 2.29</i> <i>90.4 \pm 21.2</i>	<i>10.06 \pm 2.87</i> <i>93.3 \pm 26.6</i>	<i>7.02 \pm 1.64</i> <i>65.1 \pm 15.2</i>
^{12}C Ala	5.60 \pm 1.90 100.0 \pm 33.9	5.48 \pm 1.31 97.9 \pm 23.5	6.18 \pm 1.56 110.4 \pm 27.9	9.03 \pm 0.44 161.2 \pm 7.8
^{13}C Ala	1.08 \pm 0.31 100.0 \pm 28.8	1.02 \pm 0.41 93.9 \pm 37.5	1.08 \pm 0.23 99.8 \pm 21.6	1.30 \pm 0.48 120.0 \pm 44.4
Ala total	6.68 \pm 1.84 100.0 \pm 27.6	6.50 \pm 1.12 97.2 \pm 16.7	7.26 \pm 1.39 108.7 \pm 20.7	10.22 \pm 0.73 152.8 \pm 10.9
% ^{13}C enrichment	<i>17.05 \pm 6.79</i> <i>100.0 \pm 39.8</i>	<i>16.16 \pm 7.45</i> <i>94.8 \pm 43.7</i>	<i>15.55 \pm 5.82</i> <i>91.2 \pm 34.1</i>	<i>11.30 \pm 4.15</i> <i>66.3 \pm 24.4</i>
Glu C4	8.98 \pm 1.81 100.0 \pm 20.2	9.41 \pm 1.93 104.8 \pm 21.5	9.93 \pm 0.36 110.5 \pm 4.0	13.19 \pm 4.97 146.9 \pm 55.3
Gln C4	6.40 \pm 1.35 100.0 \pm 21.1	6.34 \pm 1.46 99.1 \pm 22.8	7.37 \pm 0.74 115.2 \pm 11.6	10.34 \pm 3.98 161.5 \pm 62.1
GSH/GSSG Glu C4	4.32 \pm 1.00 100.0 \pm 23.1	4.10 \pm 1.27 95.0 \pm 29.4	4.05 \pm 0.55 93.9 \pm 12.8	4.84 \pm 2.20 112.0 \pm 50.8
Glx C2 ¹	18.23 \pm 4.75 100.0 \pm 26.0	16.77 \pm 4.49 92.0 \pm 24.6	17.53 \pm 2.33 96.2 \pm 12.8	22.35 \pm 9.08 122.6 \pm 49.8
Cr (CH ₂)	1.80 \pm 0.38 100.0 \pm 21.2	1.64 \pm 0.46 90.9 \pm 25.6	1.74 \pm 0.41 96.4 \pm 22.6	1.38 \pm 0.23 76.4 \pm 12.8
PCr (CH ₂)	2.73 \pm 0.90 100.0 \pm 32.9	2.29 \pm 0.54 84.1 \pm 19.9	2.10 \pm 0.41 77.1 \pm 14.9	2.50 \pm 0.22 91.6 \pm 7.9
PCr/Cr (CH ₂)	<i>1.52 \pm 0.40</i> <i>100.0 \pm 26.0</i>	<i>1.44 \pm 0.27</i> <i>94.5 \pm 17.9</i>	<i>1.34 \pm 0.07</i> <i>87.7 \pm 4.5</i>	<i>1.49 \pm 0.26</i> <i>97.8 \pm 16.8</i>
BCAA	1.20 \pm 0.30 100.0 \pm 24.8	1.12 \pm 0.21 93.9 \pm 17.5	1.25 \pm 0.18 103.7 \pm 15.2	1.77 \pm 0.68 147.5 \pm 56.3
Acetate	0.70 \pm 0.24 100.0 \pm 33.8	0.68 \pm 0.15 97.9 \pm 22.0	0.67 \pm 0.11 95.8 \pm 15.7	0.99 \pm 0.35 141.2 \pm 50.6
Succinate	0.27 \pm 0.08 100.0 \pm 28.0	0.23 \pm 0.11 84.6 \pm 39.3	0.27 \pm 0.01 101.1 \pm 4.4	0.45 \pm 0.19 166.6 \pm 72.2
Choline	1.8 \pm 0.59 100.0 \pm 32.7	1.73 \pm 0.37 96.0 \pm 20.5	1.70 \pm 0.41 94.1 \pm 22.8	2.28 \pm 1.09 126.1 \pm 60.3
Taurine	3.52 \pm 0.61 100.0 \pm 17.4	3.62 \pm 0.70 102.7 \pm 20.0	4.04 \pm 0.85 114.7 \pm 24.0	4.39 \pm 1.68 124.6 \pm 47.6
Hypotaurine	1.47 \pm 0.57 100.0 \pm 38.5	1.07 \pm 0.29 72.2 \pm 19.4	1.24 \pm 0.13 84.4 \pm 8.8	1.67 \pm 0.79 113.4 \pm 53.9
myo-Inositol	18.98 \pm 4.13 100.0 \pm 21.8	18.46 \pm 3.45 97.2 \pm 18.2	18.3 \pm 2.88 95.0 \pm 15.2	19.69 \pm 7.62 103.7 \pm 40.2

¹ Glx C2 accounts for Glu C2, Gln C2, and GSH/GSSG Glu C2

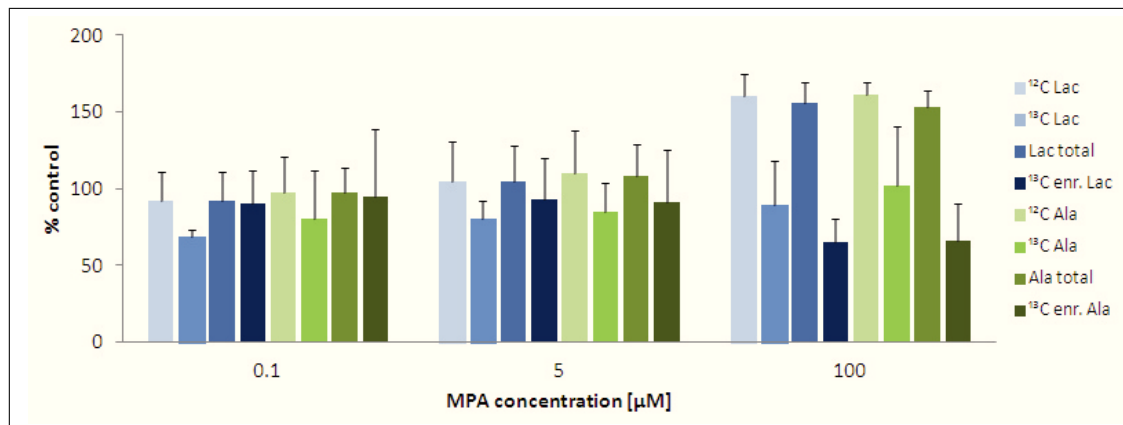


Fig. 2.49: Amounts of lactate and alanine and ¹³C enrichments calculated from ¹H NMR spectra of LS180 cell extracts. Cells were incubated with 0, 0.1, 5, and 100 μM MPA and 1000 μM guanosine for 72h (redosed every 24h). For the last 5h cells were incubated with 5mM [1-¹³C]glucose (N=6). No statistically significant changes were found using one-way ANOVA combined with Scheffe's post – hoc test. Absolute values of changes are given in Table 2.16.

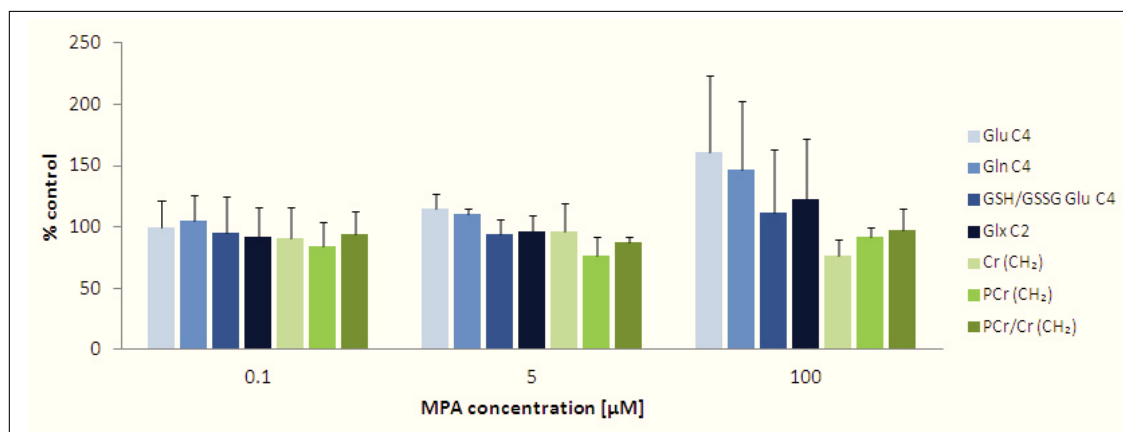


Fig. 2.50: Amounts of glutamate, glutamine, creatine, and phosphocreatine and PCr/Cr ratio calculated from ¹H NMR spectra of LS180 cell extracts. Cells were incubated with 0, 0.1, 5, and 100 μM MPA and 1000 μM guanosine for 72h (redosed every 24h). For the last 5h cells were incubated with 5mM [1-¹³C]glucose (N=6). No statistically significant changes were found using one-way ANOVA combined with Scheffe's post – hoc test. Absolute values of changes are given in Table 2.16.

None of the changes measured in metabolite concentrations from ¹H NMR spectra of LS180 cell extracts reached statistical significance, but clear trends towards elevated lactate, alanine, glutamate, glutamine, branched chain amino acid, acetate, and succinate concentrations as well as decreases in creatine and phosphocreatine

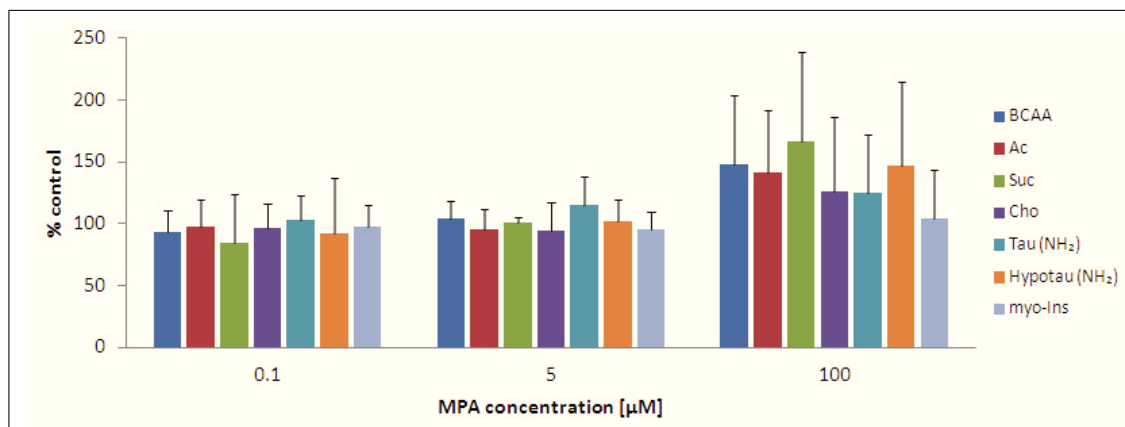


Fig. 2.51: Amounts of remaining metabolites from ^1H NMR spectra of LS180 cell extracts. Cells were incubated with 0, 0.1, 5, and $100\mu\text{M}$ MPA and $1000\mu\text{M}$ guanosine for 72h (redosed every 24h). For the last 5h cells were incubated with 5mM $[1-^{13}\text{C}]$ glucose. No statistically significant changes were found using one-way ANOVA combined with Scheffe's *post – hoc* test. Absolute values of changes are given in Table 2.16.

for $100\mu\text{M}$ MPA-treated samples was observed.

Remarkable are the elevated ^{12}C lactate and ^{12}C alanine levels while levels of ^{13}C lactate and ^{13}C alanine stay relatively constant. Percentaged ^{13}C enrichments of both metabolites therefore drops to about 65% of control values (not significant). These findings will be discussed in the context of results from ^{13}C NMR measurements in the next section.

2.8.2 Quantitative ^{13}C NMR spectroscopy of cell extracts

Incubation of cell cultures with labeled glucose results in formation of isotopomers of TCA cycle intermediates and therefore diversely ^{13}C -marked sets of the same metabolite [102, 351]. ^{13}C patterns of metabolites are dependent on a cell's utilization of the two enzymatic routes of pyruvate turnover, pyruvate dehydrogenase (PDH, EC 1.2.4.1) and pyruvate carboxylase (PC, EC 6.4.1.1), and enables identification of drug dependent alterations in PDH and PC fluxes additionally to metabolic changes. ^{13}C labeling patterns in glutamate and glutamine obtained through ^{13}C NMR spectroscopy allowed for the determination of potential changes in metabolic fluxes in LS180 cells. The metabolic distribution of the ^{13}C label of $[1-^{13}\text{C}]$ glucose via glycolysis, pyruvate metabolism, and the TCA cycle resulting in labeled metabolites of glutamate, glutamine, lactate, and alanine among others (signals were assigned to the ^{13}C NMR spectra of LS180 cell extracts as shown in Figure 2.52) is depicted

2 Results and Discussion

in the appendix (Fig. 4.32). In Table 2.17 isotopomers of α -ketoglutarate (precursor of glutamate and glutamine) and oxaloacetate (precursor of aspartate) derived from [1- ^{13}C]glucose via the initial metabolites pyruvate and oxaloacetate in the 1st and 2nd TCA cycle turn are listed.

Table 2.17: Isotopomers derived in 1st and 2nd turn of the TCA cycle from [1- ^{13}C]glucose metabolized via PDH and PC, respectively. The columns “Initial metabolite”, pyruvate (Pyr) or oxaloacetate (OAA), and “Formed isotopomers”, α -ketoglutarate (α -KG) or oxaloacetate, list positions of ^{13}C labels within metabolites or the utilization/formation of unlabeled metabolites. Isotopomer formation from [1- ^{13}C]glucose is graphically depicted in Figure 4.32 in the appendix.

Enzyme	Turn	Initial metabolite		Formed isotopomers	
		Pyr	OAA	α -KG	OAA
PDH	1	[3]	[^{12}C]	[4]	[2], [3]
		[^{12}C]	[2]	[3]	[2], [3]
	[^{12}C]	[3]	[2]	[1], [4]	
	[3]	[2]	[3,4]	[1,2], [3,4]	
	[3]	[3]	[2,4]	[1,3], [2,4]	
PC	1	[3]		[2], [3]	[2], [3]
		[^{12}C]	[1]	[^{12}C]	[1], [2], [3], [4]
	[^{12}C]	[2]	[3]		
	[^{12}C]	[3]	[2]	[2], [3]	
	[^{12}C]	[4]	[1]	[1], [4]	
	[3]	[1]	[4]	[^{12}C]	
	[3]	[2]	[3,4]	[2], [3]	
	[3]	[3]	[2,4]	[1,3], [2,4]	
	[3]	[4]	[1,4]	[2], [3]	

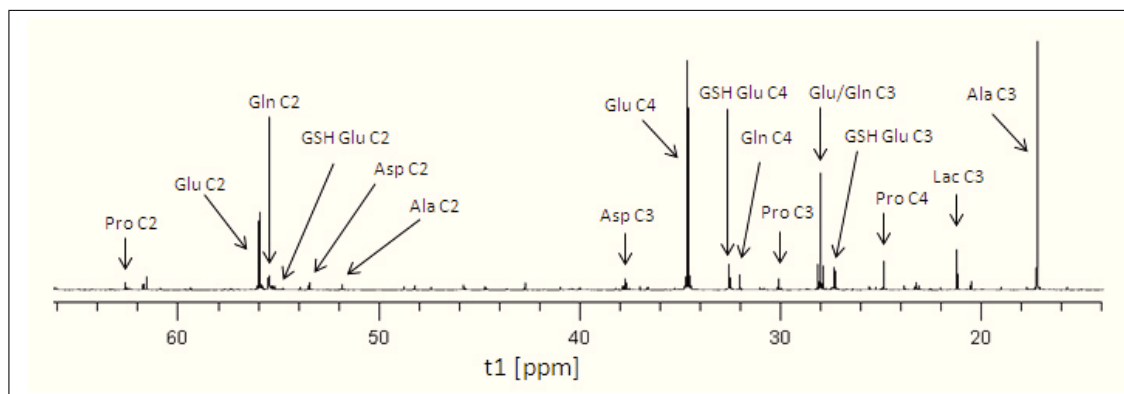


Fig. 2.52: Representative ^{13}C NMR spectrum of an LS180 cell extract. The ppm region 14–66 is shown. Cells were incubated with 0, 0.1, 5, and $100\mu\text{M}$ MPA and $1000\mu\text{M}$ guanosine for 72h (redosed every 24h). For the last 5h cells were incubated with 5mM [$1\text{-}^{13}\text{C}$]glucose. Compounds were identified by comparison with $^1\text{H}\text{-}^{13}\text{C}$ HSQC spectra of cell extracts of same experimental conditions using published databases [349, 350]. Amino acid abbreviations are based on IUPAC nomenclature; GSH: reduced glutathione.

Levels of relevant isotopomers quantified from ^{13}C NMR spectra of LS180 cell extracts are given in Table 2.18, changes are depicted graphically in Figure 2.53 and Figure 2.54. Mono and double labels of metabolites dependent on the number of TCA cycle turns were quantified separately to determine TCA cycle ratios (please see below and Section 3.6.3). To avoid confusion please note that values in Table 2.16 listing concentrations of total metabolites calculated from ^1H NMR spectra are given in $\mu\text{mol/g}$ cell wet weight while concentrations of metabolites labeled in certain carbon positions calculated from ^{13}C NMR spectra are given in nmol/g cell wet weight in Table 2.18.

None of the changes listed in Table 2.18 for labeling patterns in glutamate or glutamine reached statistical significance. Overall a strong concentration-dependent trend towards increased concentrations of glutamate and glutamine, mono- as well as doubly-labeled, can be seen. From the amounts of mono and double labels in compounds conclusions can be drawn about TCA cycle progression in general and under the respective treatment conditions. Mono labels can be seen in glutamate and glutamine (C2 and C4, emerging via PC and PDH after the 1st turn, respectively) and double labels in glutamate C4 (emerging via PC and PDH; please see Figure 4.32 and Table 2.17) but not in integratable amounts in glutamine C4 (synthesized from Glu) or glutamine C4 in GSH (synthesized from glutamate), which confirms 5h to be an appropriate incubation time for treatment of LS180 cells with

2 Results and Discussion

[1-¹³C]glucose to generate integratable spectra without allowing cells to metabolize [1-¹³C]glucose too extensively.

Table 2.18: Isotopomer concentrations in LS180 cells after 72h of MPA treatment. Values were calculated from ¹³C NMR spectra of cell extracts and are given in nmol/g cell wet weight and in % of controls (**bold**) with standard deviations. For the last 5 hours of the incubation time LS180 cells were incubated with 5 mM [1-¹³C]glucose (N=3). No statistically significant changes were found using one-way ANOVA combined with Scheffe's post – hoc test. Changes are depicted in graphs in Figure 2.53 - Figure 2.54.

	control	0.1 μM MPA	5 μM MPA	100 μM MPA
Glu C4 mono	574.1 ± 86.9	693.7 ± 322.9	714.3 ± 305.0	1186.4 ± 406.6
	100.0 ± 15.1	120.8 ± 56.3	124.4 ± 53.1	206.7 ± 70.8
Glu C4 double	38.2 ± 0.8	58.0 ± 25.8	60.5 ± 31.1	107.9 ± 40.7
	100.0 ± 2.2	152.0 ± 67.6	158.5 ± 81.4	282.6 ± 106.5
Glu C4 total	612.2 ± 87.0	751.7 ± 347.2	774.8 ± 336.1	1294.3 ± 447.2
	100.0 ± 14.2	122.8 ± 56.7	126.6 ± 54.9	211.4 ± 73.0
Gln C4 total ¹	133.3 ± 40.4	168.8 ± 92.9	184.4 ± 106.0	300.7 ± 104.3
	100.0 ± 30.3	126.6 ± 69.7	138.3 ± 79.5	225.6 ± 78.3
Glu C2 mono	1646.0 ± 320.9	2076.6 ± 1035.2	2181.7 ± 1049.4	3431.2 ± 1098.9
	100.0 ± 19.5	126.2 ± 62.9	132.5 ± 63.8	208.5 ± 66.8
Glu C2 double	158.3 ± 40.0	177.8 ± 99.9	192.9 ± 79.8	304.0 ± 122.4
	100.0 ± 25.2	112.3 ± 63.1	121.8 ± 50.4	192.0 ± 77.3
Glu C2 total	1804.4 ± 360.2	2254.4 ± 1128.0	2374.6 ± 1127.5	3735.2 ± 1221.2
	100.0 ± 20.0	124.9 ± 62.5	131.6 ± 62.5	207.0 ± 67.7
Gln C2 mono	153.7 ± 25.2	182.9 ± 107.4	193.8 ± 102.5	344.3 ± 132.6
	100.0 ± 16.4	119.0 ± 69.8	126.1 ± 66.7	224.0 ± 86.3
Gln C2 double	262.3 ± 56.6	299.4 ± 153.2	326.2 ± 168.2	491.8 ± 167.0
	100.0 ± 21.6	114.2 ± 58.4	124.4 ± 64.1	187.5 ± 63.7
Gln C2 total	416.0 ± 80.3	482.3 ± 260.0	520.0 ± 270.5	836.1 ± 299.6
	100.0 ± 19.4	115.9 ± 62.5	125.0 ± 65.0	201.0 ± 72.0
Glx C3 mono	251.1 ± 64.0	344.2 ± 175.0	353.6 ± 176.3	548.5 ± 176.7
	100.0 ± 25.5	137.1 ± 69.7	140.8 ± 70.2	218.4 ± 70.4
Glx C3 double	26.1 ± 8.1	30.8 ± 15.9	32.4 ± 15.4	62.3 ± 17.1
	100.0 ± 31.2	117.9 ± 60.7	123.9 ± 58.8	238.6 ± 65.6
Glx C3 total	277.2 ± 71.9	375.0 ± 190.9	386.0 ± 190.7	610.8 ± 193.8
	100.0 ± 25.9	135.3 ± 68.9	139.2 ± 68.8	220.4 ± 69.9
GSH Glu C4 total ¹	195.3 ± 41.0	245.1 ± 118.1	251.7 ± 117.8	409.3 ± 175.8
	100.0 ± 21.0	125.4 ± 60.5	128.8 ± 60.3	209.5 ± 90.0

¹ due to a low S/N ratio peaks arising from double labels were not integratable, total amounts of metabolites basically relate to mono-labeled metabolites

Utilization of oxidative versus anaplerotic glucose metabolism and TCA cycle ratios

To quantify relative contributions of the oxidative (via PDH) versus the anaplerotic (via PC) pathway (Fig. 4.32) the ratios of [4-C¹³]/[2-C¹³]Glx (glutamate and glutamine) as described by Zwingmann et al. were used [102]. No difference in metabolic

2.8 Metabolome analysis in LS180 cells after MPA treatment

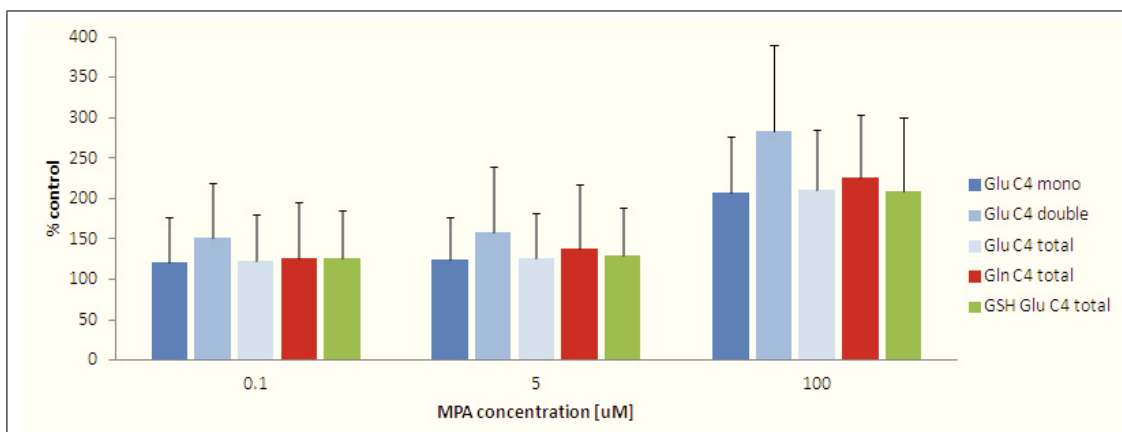


Fig. 2.53: Amounts of C4-labeled glutamate, glutamine, and glutamate in GSH calculated from ^{13}C NMR spectra of LS180 cell extracts. Cells were incubated with 0, 0.1, 5, and 100 μM MPA and 1000 μM guanosine for 72h (redosed every 24h). For the last 5h cells were incubated with 5mM $[1-^{13}\text{C}]$ glucose ($N=3$). Absolute values of changes are given in Table 2.18. No statistically significant changes were found using one-way ANOVA combined with Scheffe's *post – hoc* test.

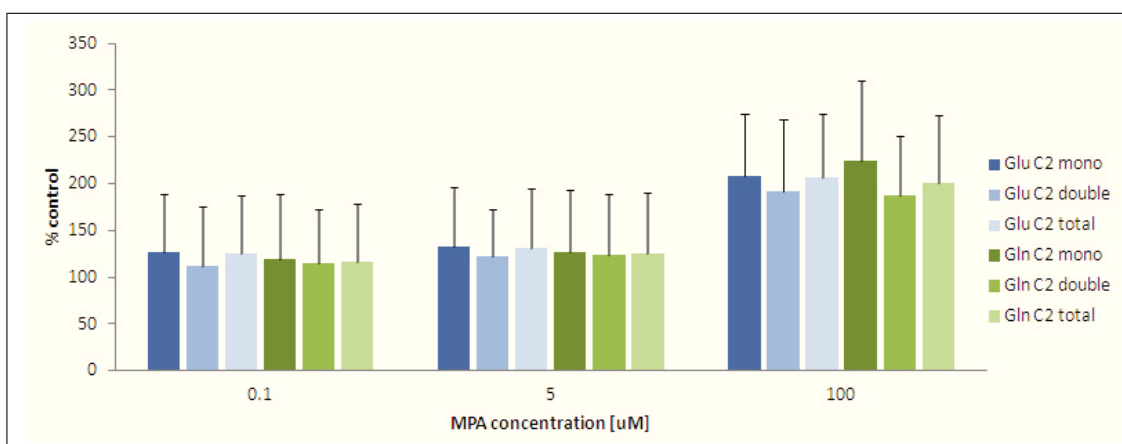


Fig. 2.54: Amounts of C2-labeled glutamate, glutamine, and glutamate in GSH calculated from ^{13}C NMR spectra of LS180 cell extracts. Cells were incubated with 0, 0.1, 5, and 100 μM MPA and 1000 μM guanosine for 72h (redosed every 24h). For the last 5h cells were incubated with 5mM $[1-^{13}\text{C}]$ glucose ($N=3$). Absolute values of changes are given in Table 2.18. No statistically significant changes were found using one-way ANOVA combined with Scheffe's *post – hoc* test.

2 Results and Discussion

fluxes through PC versus PDH (in oxidative to anaerobic glucose metabolism) was found in LS180 cells treated with increasing concentrations with MPA for 72h. In the first two rows of Table 2.19 ratios of PDH and PC fluxes calculated as % of controls are given.

After the first TCA cycle turn $[4-^{13}\text{C}]\text{Glx}$ is generated through PDH activity, the second turn leads to a doubly-labeled $[3,4-^{13}\text{C}]\text{Glx}$ (and $[2,4-^{13}\text{C}]\text{Glx}$) [102]. Ratios of double to mono labels arising from the C4 position in Glx give the number of turns that $[2-^{13}\text{C}]\text{acetyl-CoA}$ formed from $[1-^{13}\text{C}]\text{glucose}$ has passed through the TCA cycle (Fig. 4.32). Ratios of double to mono labels in the C4 position of glutamate were used to assess the increase in TCA cycle progression in MPA-treated LS180 cells. The third line of Table 2.19 shows ratios calculated as % of controls. Changes in TCA cycle progression were not statistically significant, but a trend towards an increase of TCA cycle speed was obvious. This finding is coherent with the assumed increase in mitochondrial metabolism in LS180 cells under MPA treatment as discussed in the next paragraph.

Table 2.19: Changes in metabolic fluxes and number of TCA cycle turns in MPA-treated LS180 cells. Values were calculated from metabolite concentrations from ^{13}C NMR spectra of cell extracts and are given in % of controls with standard deviations ($N=3$). For the last 5h of the incubation time LS180 cells were incubated with 5mM $[1-^{13}\text{C}]\text{glucose}$. No statistically significant changes were found after one-way ANOVA combined with Scheffe's post – hoc test.

	control	0.1 μM MPA	5 μM MPA	100 μM MPA
PDH/PC (Glu C4/C2)	100.0 \pm 7.9	99.5 \pm 7.0	96.7 \pm 5.1	101.2 \pm 3.5
PDH/PC (Gln C4/C2)	100.0 \pm 14.3	110.9 \pm 6.1	109.7 \pm 7.7	114.0 \pm 2.6
TCA cycle ratio	100.0 \pm 16.1	126.6 \pm 17.7	120.8 \pm 16.3	134.5 \pm 9.0

Overall no statistically significant changes in metabolite or isotopomer concentrations were found in LS180 cells treated with MPA concentrations up to 100 μM . Since trends can be seen up to 100 μM MPA, treatment with 250 μM MPA as used in other experiments would most likely have elucidated metabolomic changes in LS180 cells further. On the other hand our other data, especially those gained from proteomics experiments (Sec. 2.7), did not point towards significant changes in carbohydrate metabolism in MPA-treated LS180 cells either.

It needs to be kept in mind that for this experiment LS180 cells received an extra dose of MPA due to the exchange of cell culture media containing $[^{12}\text{C}]\text{glucose}$ for $[1-^{13}\text{C}]\text{glucose}$ -containing media 5h prior to the end of the 72h incubation time.

Several observations point towards abnormalities in cell metabolism that could be

2.8 Metabolome analysis in LS180 cells after MPA treatment

related to the cancerous nature of LS180 cells (as seen and discussed in previous sections) or even their colonic origin. Therefore a brief outline of the metabolism of cancer and intestinal cells is given below.

In malignant cells metabolic deviations occur, e.g. glycolytic and oxidative pathways, ATP-generating mechanisms, and growth rate are affected [119]. With cancer state progression these deviations increase, i.e. the degree of alteration correlates with the grade and progression of malignancy (LS180 are grade II tumor cells).

While cancer cells usually are known to exhibit enhanced glycolysis rates, mitochondrial metabolism, and ATP generation through oxidative phosphorylation is suppressed in comparison to normal cells (Warburg effect) [352]. For a long time glycolytic tumor cells were thought to basically transform the majority of pyruvate generated by glycolysis into lactate [353]. In this case only a small portion of the residual pyruvate would be metabolized through the TCA cycle and high glycolysis rates can cause glutamine to be the main carbon source for respiration instead of glucose in cancer cells. On the other hand cancer cells might be able to adapt their metabolism dependent on microenvironments and cellular needs and reversibly shift inbetween oxidative phosphorylation, i.e. increased TCA cycle activity, and glycolysis for ATP generation (Crabtree effect) [352].

Rapidly dividing cells as they constitute the linings of the intestine are known to preferentially utilize certain amino acids, especially glutamine and arginine, besides glucose [354]. In the intestine homeostasis of precursor utilization is regulated by food intake and protein turnover. In addition gut barrier function in inflammation and intestinal stress responses were found to be closely related to glutamine metabolism [354, 355].

The trend towards increased TCA cycle progression with higher doses of MPA in LS180 cells with trends towards increases in ^{13}C -labeled lactate and alanine but decreased ^{13}C enrichments in lactate and alanine (due to increases in ^{12}C lactate and ^{12}C alanine) might be due to the above described Crabtree effect in cancer cells. As lactate and alanine can be built from pyruvate generated from glutamine via the TCA cycle elevated lactate and alanine concentrations with relatively low ^{13}C enrichments could be a relict of the metabolic peculiarity of intestinal cells and/or the Crabtree effect.

In addition to these metabolic abnormalities is tumoral PDH known to differ from normal PDH. Tumoral PDH can give rise to the compound acetoin by non-oxidative decarboxylation of pyruvate and cancer cells can utilize an alternative metabolic pathway circumventing the TCA cycle [119]. Acetoin signals are present in ^1H - ^{13}C heteronuclear single quantum coherence (HSQC) spectra of LS180 cell extracts

(Sec. 2.8.4). This confirms that the cancerous nature of this cell culture model needs to be kept in mind.

2.8.3 Quantitative ^1H NMR spectroscopy of lipid extracts

From ^1H NMR spectra of lipid extracts of MPA-treated LS180 cells the amounts of certain lipids, fatty acids, and carbon positions were determined. Absolute quantification of lipids was not carried out due to different chain lengths of fatty acids and overlap of signals (Sec. 3.6.3). Lipids were quantified as % of controls.

Representative examples of spectra for each condition are shown in Figure 2.55. Table 2.20 summarizes amounts of compounds under the different MPA concentrations used, changes are depicted graphically with statistically significant changes in Figure 2.56 and Figure 2.57.

Table 2.20: Changes in concentrations of lipids/lipid compounds in LS180 cells after 72h of MPA treatment. Cells were incubated with 0, 0.1, 5, and 100 μM MPA and 1000 μM guanosine for 72h (redosed every 24h). For the last 5h cells were incubated with 5mM [$1\text{-}^{13}\text{C}$]glucose. Values were calculated from ^1H NMR spectra of lipid extracts and are given in % of controls with standard deviations ($N=6$). Significance was determined using one-way ANOVA combined with Scheffe's post – hoc test with *: $p < 0.05$; **: $p < 0.005$; ***: $p < 0.001$ versus controls.

	control	0.1 μM MPA	5 μM MPA	100 μM MPA
Chol C18	100.0 \pm 9.0	100.9 \pm 14.0	105.0 \pm 7.8	110.6 \pm 11.4
Chol C19	100.0 \pm 11.5	93.7 \pm 7.5	102.5 \pm 7.5	120.4 \pm 8.2 *
F α	100.0 \pm 11.7	99.4 \pm 13.1	109.0 \pm 7.6	128.5 \pm 4.7 **
F β ¹	100.0 \pm 12.5	100.1 \pm 8.9	112.3 \pm 10.7	125.1 \pm 13.0 *
F (CH ₂) _x +F ω -1 ¹	100.0 \pm 9.4	99.9 \pm 12.5	110.0 \pm 8.9	126.2 \pm 16.5 *
PtdCho α	100.0 \pm 17.1	107.9 \pm 17.8	111.4 \pm 10.3	134.0 \pm 20.1 *
PtdCho β	100.0 \pm 27.9	93.6 \pm 22.4	96.6 \pm 8.7	127.3 \pm 24.6 **
N ⁺ (CH ₃) ₃	100.0 \pm 9.3	103.8 \pm 14.5	108.1 \pm 8.9	121.3 \pm 15.7
DAG β	100.0 \pm 27.9	95.4 \pm 8.3	93.2 \pm 16.4	104.7 \pm 29.0
TAG β	100.0 \pm 19.3	109.7 \pm 19.5	109.6 \pm 31.3	158.9 \pm 19.0
F Δ -1 (MUFA) ¹	100.0 \pm 11.8	97.6 \pm 10.7	104.6 \pm 8.2	118.3 \pm 13.3
F Δ -CH ₂ - Δ (PUFA)	100.0 \pm 9.7	101.0 \pm 12.9	105.3 \pm 9.1	116.7 \pm 4.4
TDB (MUFA + PUFA) ¹	100.0 \pm 10.2	99.3 \pm 11.0	107.5 \pm 8.2	119.6 \pm 13.3

¹ values were corrected for overlap with cholesterol signals according to number of protons of respective cholesterol signals using cholesterol C18 values as correction factors, for details please see Section 3.6.3

Significant increases were measured in fatty acids (for F α , F β , F γ , and F(CH₂)_x + F ω -1 (overlap of signals)) as well as cholesterol (Chol C19), and phosphatidylcholine (PtdCho; increases in PtdCho α and PtdCho β). Results for PtdCho were relatively consistent (PtdCho α and PtdCho β significantly increased versus trends towards

2.8 Metabolome analysis in LS180 cells after MPA treatment

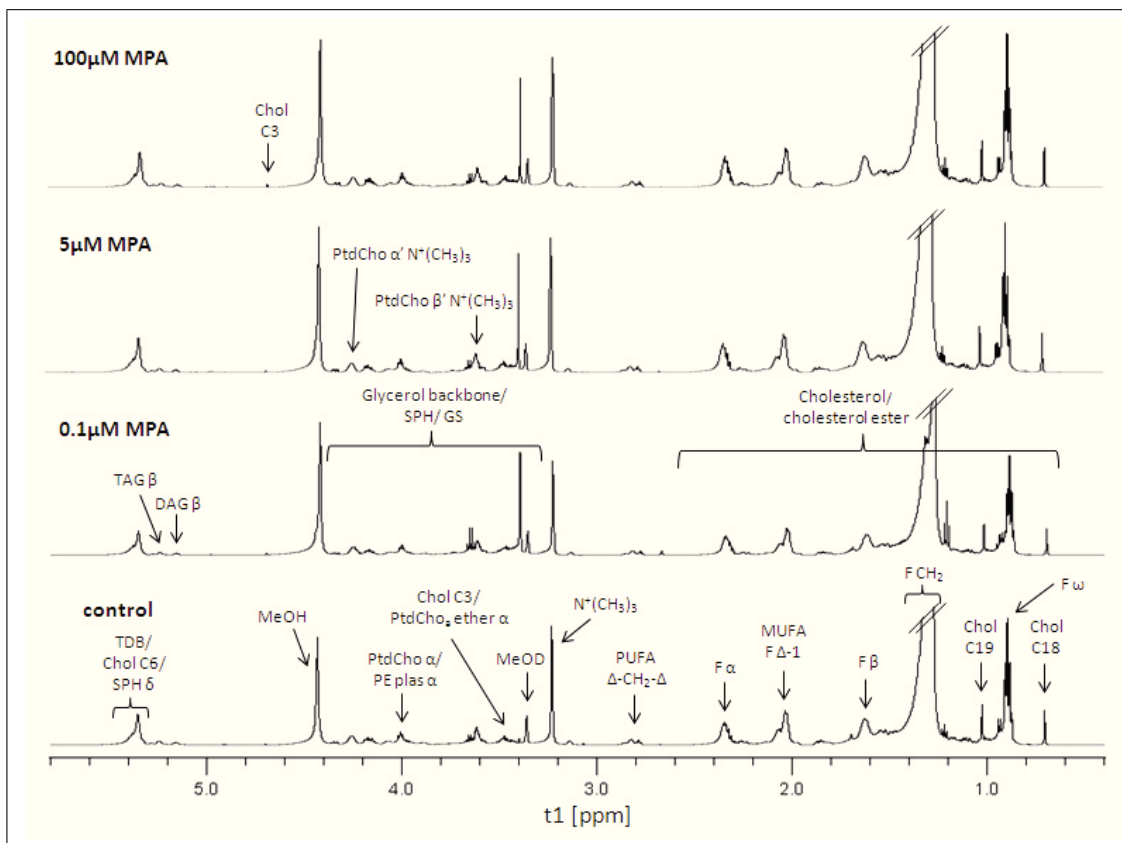


Fig. 2.55: ^1H NMR spectra of LS180 lipid extracts. ppm regions 0.4–5.8 are shown. Cells were incubated with 0, 0.1, 5, and $100\ \mu\text{M}$ MPA and $1000\ \mu\text{M}$ guanosine for 72h (redosed every 24h). For the last 5h cells were incubated with $5\ \text{mM}$ $[1\text{-}^{13}\text{C}]$ glucose. Compounds were identified by comparison with $^1\text{H}\text{-}^{13}\text{C}$ HSQC spectra of cell extracts of same experimental conditions using published databases [349, 350]. Amino acid abbreviations are based on IUPAC nomenclature, Chol: cholesterol/cholesterol ester, F: fatty acid, $F_{\alpha/\beta}$: carbon atom in α/β -position to carbonyl carbon atom, F_{Δ} : carbon atom at a double bond, F_{ω} : terminal carbon atom, MUFA: monounsaturated fatty acids, PE: phosphatidylethanolamine, plas: plasmalogen, PtdCho: phosphatidylcholine, PUFA: polyunsaturated fatty acids, SPH: sphingomyeline, TDB: total number of double bonds (MUFA and PUFA).

2 Results and Discussion

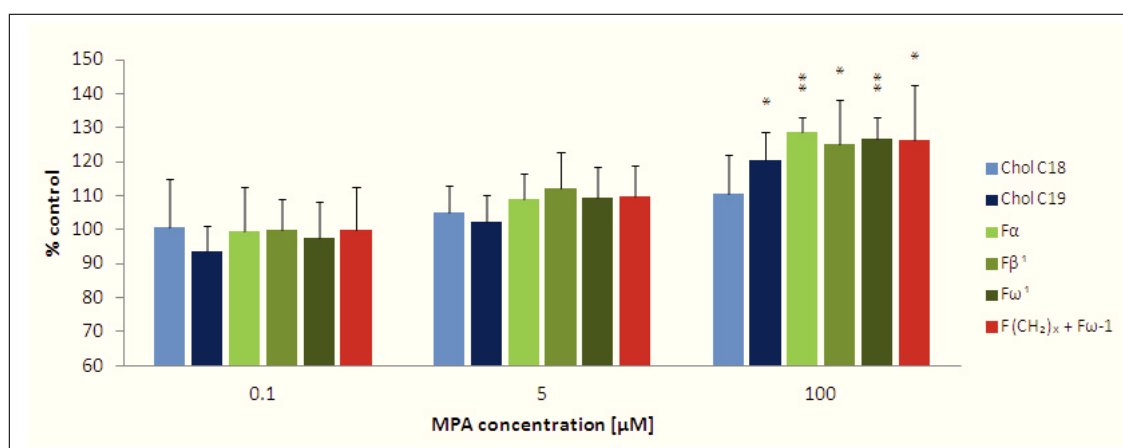


Fig. 2.56: Changes in concentrations of cholesterol and certain fatty acid signals calculated from ¹H NMR spectra of LS180 lipid extracts. Cells were incubated with 0, 0.1, 5, and 100 μM MPA and 1000 μM guanosine for 72h (redosed every 24h). For the last 5h cells were incubated with 5mM [1-¹³C]glucose (N=6). Chol: cholesterol/cholesterol ester, F: fatty acid, F_α/F_β: carbon atom in α/β-position to carbonyl carbon atom, F_Δ: carbon atom at a double bond, F_ω: terminal carbon atom. Significance was determined using one-way ANOVA combined with Scheffe's post-hoc test with *: *p*<0.05; **: *p*<0.005; ***: *p*<0.001 versus controls.

¹ values were corrected for overlap with cholesterol signals according to number of protons of respective cholesterol signals using cholesterol C18 values as correction factors, for details please see Section 3.6.3

2.8 Metabolome analysis in LS180 cells after MPA treatment

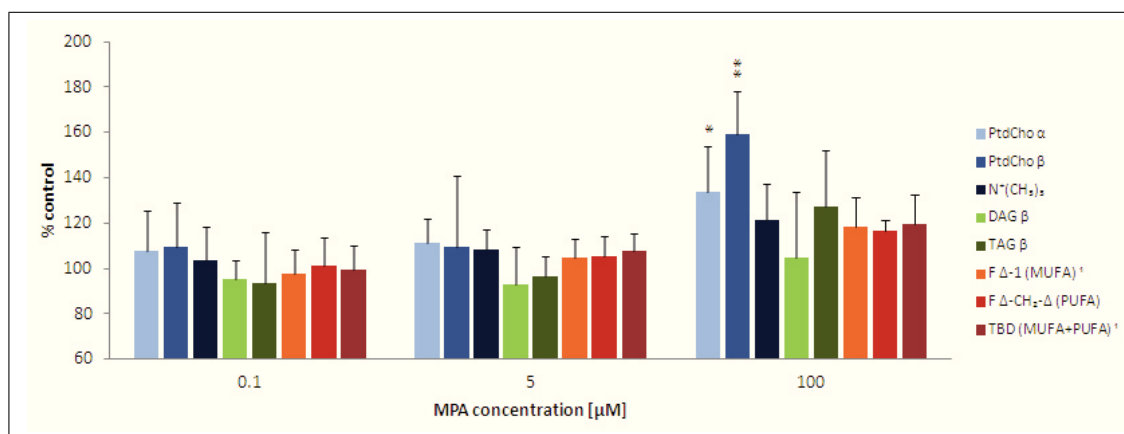


Fig. 2.57: Changes in concentrations of phosphatidylcholine, trimethyl ammonium compounds, acyl glycerols, and mono- and polyunsaturated fatty acids calculated from ¹H NMR spectra of LS180 cell extracts. Cells were incubated with 0, 0.1, 5, and 100 μM MPA and 1000 μM guanosine for 72h (redosed every 24h). For the last 5h cells were incubated with 5mM [1-¹³C]glucose (N=6). DAG: diacyl glycerols, MUFA: monounsaturated fatty acids, N⁺(CH₃)₃: trimethyl ammonium compounds/choline headgroup, PtdCho: phosphatidylcholine, PUFA: polyunsaturated fatty acids, TAG: triacyl glycerols, TBD: total number of double bonds. Significance was determined using one-way ANOVA combined with Scheffe's post – hoc test with *: $p < 0.05$; **: $p < 0.005$; ***: $p < 0.001$ versus controls.

¹ values were corrected for overlap with cholesterol signals according to number of protons of respective cholesterol signals using cholesterol C18 values as correction factors, for details please see Section 3.6.3

2 Results and Discussion

increases in levels of the choline headgroup) as results for cholesterol (Chol C19 significantly increased versus trends towards increases in Chol C18) were as well. Increases in concentrations of fatty acids on the other hand were confirmed by significant increases for all quantified positions within a fatty acid. Compositions of fatty acids (number of double bonds) do not seem to change since the increase in $F(\text{CH}_2)_x + F\omega-1$ is likely to be due to enhanced $F\omega-1$ synthesis.

After metabolism of glucose to acetyl-CoA, entry of acetyl-CoA into the TCA cycle, further metabolism, and export of citrate into the cytosol, citrate is converted into fatty acids via resynthesis of acetyl-CoA. Mono- (MUFA) and polyunsaturated fatty acids (PUFA) with double bonds in certain positions are synthesized by selective dehydration at the cytosolic membrane of the ER [356]. Via glycerin aldehyde-3-phosphate derived from glycolysis glycerol emerges as the backbone for diacyl glycerols, triacyl glycerols, and phospholipids. Phospholipids are a main constituent of biomembranes and are often esters of divers amino alcohols. PtdCho is the most prominent membrane phospholipid. PtdCho is an important constituent of the GI tract (e.g. intestinal cell membranes) and crucial for maintenance of GI barrier function [357]. Intracellular PtdCho is secreted by epithelial cells and passaged across tight junctions into the apical mucus layer [358]. PtdCho contributes in large parts to the colonic mucus layer establishing a hydrophobic surface [357]. In the plasma membrane of enterocytes it modulates the mucosal signaling state as cellular membrane and lipid composition are regulatory parameters of signaling pathways of inflammation [357]. Interestingly, decreased levels of luminal PtdCho in colonic mucus have been linked repeatedly to ulcerative colitis, an IBD similar to Crohn's disease [357, 359] (not found in Crohn's disease patients [359, 360]). The finding of upregulated intracellular PtdCho in MPA-treated LS180 cells is contradictory to the above described mechanisms of impaired barrier function, but suggests disturbances of lipid levels strongly linked to mucosal defense. The upregulation of certain membrane components/lipids could also be a secondary effect of MPA toxicity in LS180 cells. Compromised proliferation patterns (Sec. 2.4.1) could trigger upregulation of main compounds constituting membranes and mucus barriers as important lines of epithelial defense. Another interesting aspect is that PtdCho is synthesized from choline via the Kennedy-pathway involving cytidine nucleotides [361]. Phosphocholine and CTP form CDP-choline and PP_i , consecutively CDP-choline and diacyl glycerol (or alkyl-acylglycerol) are converted to PtdCho (with CMP as byproduct). Elevated levels of cytidine nucleotides observed in previous experiments under the here used experimental conditions (72h incubation time, $1000\mu\text{M}$ guanosine;

Sec. 2.5.2, Tab. 2.2) might contribute to or precondition for PtdCho biosynthesis.

Cholesterol is a fundamental part of cellular function and cell membranes [362]. Involvement in the cell signaling of growth factors and modulation of immune responses (after conversions into hormones, e.g. androgens) makes it especially interesting in terms of MPA GI toxicity. With increases in PtdCho and cholesterol levels homeostasis of two major membrane constituents is affected in LS180 cells treated with MPA. The importance of membrane integrity in epithelial defense of the GI tract is explained in terms of Crohn's disease in the introduction (Sec. 1.2.3) and further discussed in Section 2.59 in context of the development of a coculture model of LS180 cells and murine macrophages.

Results from NMR experiments confirmed results from proteomics studies as in both analyses certain lipid compounds/proteins and pathways involved in lipid metabolism were significantly affected. Most proteins listed in Section 2.7 and which were assigned functions in lipid metabolism, i.e. "Fatty acid metabolism" and "Fatty acid elongation in mitochondria" in Table 2.9 and "Lipid catabolic processes" in Table 2.8 and Table 2.11 were significantly upregulated in LS180 cells under MPA treatment (with the exemption of ACAT2, which was downregulated), which is consistent with increases but no decreases in certain lipophilic compounds. The term "Mitochondrial membrane" in Table 2.8 lists almost exclusively proteins that were found to be increased in their levels (with the exemption of SCS- α , which was downregulated). This coincidence might hint at already above discussed imbalances in membrane composition.

2.8.4 ^1H - ^{13}C HSQC NMR spectroscopy of hydrophilic and lipophilic cell extracts

Several ^1H - ^{13}C HSQC NMR spectra were recorded to assign signals from 1D NMR experiments and metabolic changes as a result of MPA treatment. As an example the ^1H - ^{13}C HSQC spectrum of ppm regions 0.0-3.0 (t1) and 10-40 (t2) of an LS180 control cell extract (hydrophilic extract) is shown in Figure 2.58. ppm regions 2.9-5.0 (t1) and 33-80 (t2) and 4.0-6.5 (t1) and 80-110 (t2) of the same sample are shown in Figure 4.33 and Figure 4.34 in the appendix.

Significant overlaps of signals could be observed (e.g. for the lactate C3 signal) as well as metabolites linked to the previously discussed metabolic abnormalities of cancer cells (acetoin). Quantification of metabolites as well as the choices of peaks

2 Results and Discussion

for quantification are described based on the recorded ^1H - ^{13}C HSQC spectra in Section 3.6.3.

As for hydrophilic cell extracts several ^1H - ^{13}C HSQC spectra of lipophilic cell extracts were recorded to revise integrated signals and metabolic changes as a result of MPA treatment. Representative spectra of a lipophilic extract are shown in Figure 4.35 and Figure 4.36 in the appendix and their use for quantification is discussed in Section 3.6.3.

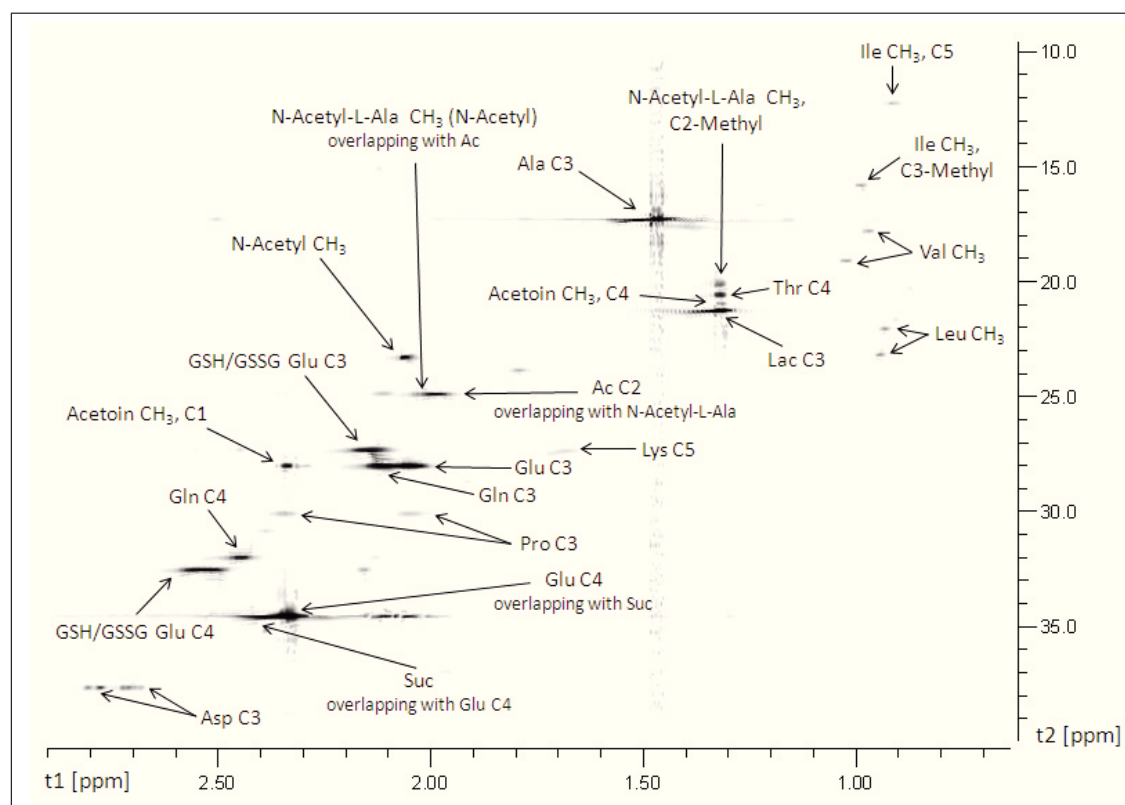


Fig. 2.58: ^1H - ^{13}C HSQC spectrum of ppm regions 0.0-3.0 (t1) and 10-40 (t2) of LS180 cell extracts. Compounds were identified using published databases [349, 350] and were compared to ^1H and ^{13}C NMR spectra of cell extracts of same experimental conditions (controls). Amino acid abbreviations are based on IUPAC nomenclature; Ac: Acetate, GSH: reduced glutathione, GSSG: oxidized glutathione, Suc: succinate. ppm regions 2.9-5.0 (t1)/33-80 (t2) and 4.0-6.5 (t1)/80-110 (t2) of the same ^1H - ^{13}C HSQC spectrum are shown in Figure 4.33 and Figure 4.34 (appendix).

2.9 In vitro gut inflammation model

To integrate the potential implications of inflammation and immunologic factors into the previously conducted research using LS180 cells an *in vitro* gut inflammation model was developed. On the basis of a previously described model, a coculture systems of the intestinal cell line Caco-2 and the murine macrophage cell line RAW 264.7 [363], a modified coculture system using LS180 instead of Caco-2 cells was designed. Coculture systems based on RAW 264.7 cells are often used in the literature to study induction of inflammation in conjunction with various cell types [363–365].

Considering that side effects of MPA show patterns similar to IBD (Sec. 1.2.3) and that in already existing coculture models of inflammation, factors such as integrity of the epithelial barrier, secretion of cytokines by macrophages, and changes in the epithelium are taken into account, it was decided to examine these factors more thoroughly using the coculture system of LS180 and RAW 264.7 cells. While validating the *in-vitro* coculture system of LS180 and RAW 264.7 cells, limitations of the model were noted. This included that LS180 cells did not form a confluent monolayer (Sec. 2.9.1). In addition, MPA and AcMPAG failed to induce cytokine release from RAW 264.7 cells as it was seen with LPS as a positive control (Sec. 2.9.2).

In the planned *in-vitro* coculture system LS180 cells were supposed to be seeded at the apical side of transwell inserts and RAW 264.7 cells at the basolateral side (Fig. 2.59). Stimulation of RAW 264.7 cells with LPS as positive control (0.1 μ g/mL and 5 μ g/mL), MPA (5 μ M and 100 μ M), and AcMPAG (5 μ M) for a duration of 4h was supposed to lead to cytokine release by RAW 264.7 cells. Cytokines were supposed to increase mRNA expression of certain proteins in LS180 cells. Monitoring of the following parameters was chosen to measure the potential to induce an inflammatory response to the test compounds because of their established use in existing models of inflammation and their role in the pathogenesis of inflammation and Crohn's disease:

- LPS as inflammatory stimulus

LPS is a cell wall component of gram-negative bacteria [366] and stimulates cells through TLR4 to release cytokines critical for the activation of immune responses [367]. LPS is often used as an inflammatory stimulus *in vitro* to induce e.g. the release of proinflammatory cytokines from macrophages [363, 366].

2 Results and Discussion

- Release of cytokines from RAW 264.7 cells

Dysregulation of TNF- α secreted by macrophages induces destruction of the epithelium [84] and is linked to IBD pathogenesis (Sec. 1.2.3, Fig. 1.8) [368]. Additionally TNF- α and IL-1 β have the potential to activate signaling pathways linked to the regulation of adhesion molecule expression for the recruitment of leukocytes [369]. Other proinflammatory cytokines such as IL-6 and INF- γ secreted by macrophages are often monitored in models of inflammation [370] and play a distinctive role in IBD development and progression [371].

- Cell monolayer integration of LS180 cells

Transepithelial electrical resistance (TEER) measurements are commonly used to determine damage of cell monolayers in cell culture systems and the possibility of uncontrolled paracellular diffusion of substances [363]. TEER values are dependent on the integrity of tight junctions inbetween epithelial cells. As findings from previous studies, such as differential expression of structural proteins (Sec. 2.7.1, effects on gap junctions, decreases in cadherin-17 after MPA treatment) and imbalances in proliferation, strongly point towards impairment of barrier function of the epithelium (Sec. 2.4.1) TEER measurements seemed to be useful in the assessment of this aspect of MPA GI toxicity.

- mRNA expression of marker proteins in LS180 cells

After epithelial injury IL-8 is secreted by epithelial cells to recruit neutrophils from the blood stream into inflamed tissues (Sec. 1.2.3, Fig. 1.8) [84, 372]. As IL-8 release is a keyfactor in the epithelial immune response and manifests in the development and progression of Crohn's disease as depicted in Figure 1.8, IL-8 mRNA expression in LS180 cells was chosen as a marker for the effect of proinflammatory cytokines released by RAW 264.7 cells. As a second marker serotonin transporter (SERT, also 5-hydroxytryptamine transporter) was chosen. SERT excretes serotonin (5-hydroxytryptamine), which is essential for many functions involved in the health of the GI tract [373, 374]. Inflammation, infection, and certain symptoms of IBD are known to be related to altered serotonergic signaling. These symptoms are evoked by imbalances in gut motor activity and altered secretion [374] causing diarrhea [375]. Cell growth e.g. of epithelial microvilli can be affected as well [376]. SERT mRNA expression therefore seemed to be a comprehensive measure of GI conditions including multiple aspects potentially causing MPA adverse events in the GI tract.

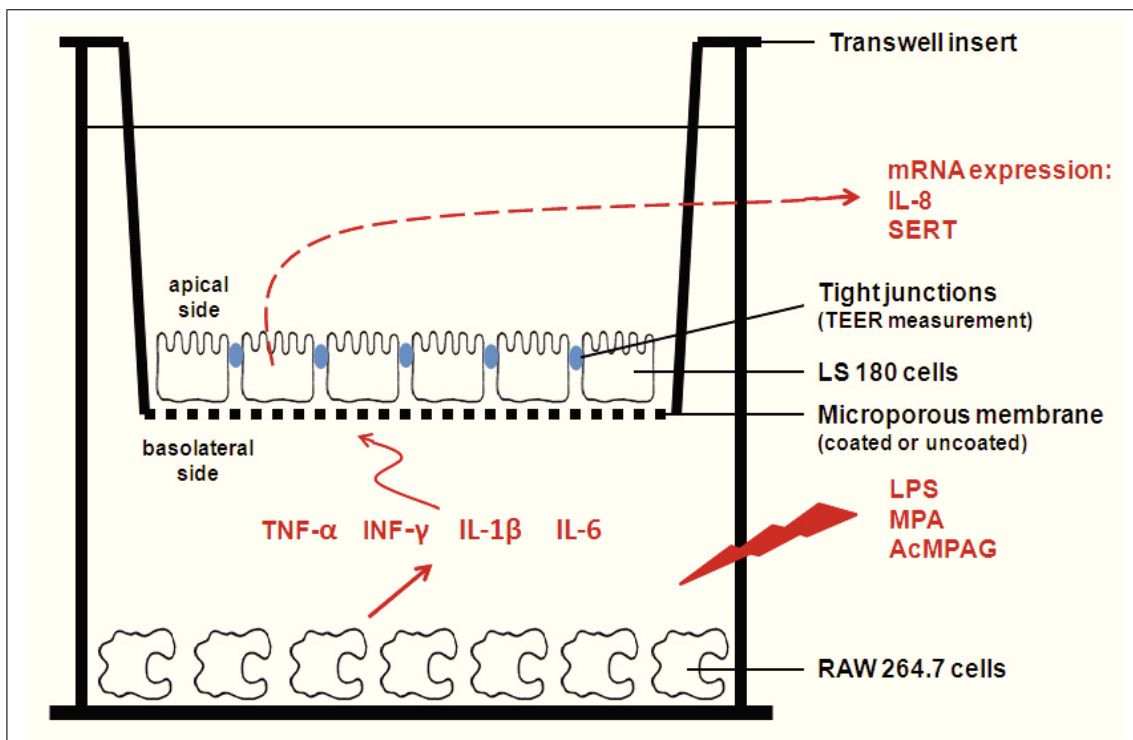


Fig. 2.59: *In vitro* gut inflammation model. *AcMPAG*: mycophenolic acid acyl glucuronide, *IL*: interleukin, *INF- γ* : interferon- γ , *LPS*: lipopolysaccharide, *mRNA*: messenger ribonucleic acid, *SERT*: serotonin transporter, *TEER*: transepithelial electrical resistance, *TNF- α* : tumor necrosis factor- α .

2.9.1 Evaluation of cell monolayer integration

As discussed initially LS180 cells are a suitable model for e.g. induction studies, but not preferable when studying drug transport due to poor monolayer integration (Sec. 2.2) [113, 377]. TEER measurements of LS180 cells seeded onto culture inserts (Millipore Hanging Cell Culture Inserts, PIHT30R48, $0.4\mu\text{M}$) was evaluated before coculturing of LS180 and RAW 264.7 cells and drug treatment.

Usually integration of cell monolayers to confluency is accompanied by a rapid rise in TEER values [377]. For Caco-2 cells which are described to have physiologically valuable properties in terms of tight junctions, transport properties and integration [113, 377] TEER values often exceed $1000\Omega\text{cm}^2$ [377, 378].

TEER values for LS180 cells were close to $1\Omega\text{cm}^2$ ($0.97\Omega\text{cm}^2$ - $1.06\Omega\text{cm}^2$). Cultures were maintained over several days until cells started to grow from patches into clumps. At this time there were still remarkable spaces inbetween islets and no rise in TEER measureable. Despite seeding of cells at different densities to allow for establishment of a monolayer from different starting points, no satisfying results were gained.

Cell growth, function, migration, and attachment is dependent on the nature of the surface on which cells are plated [379]. *In vitro* these characteristics can be improved by coating surfaces with components of the extracellular matrix, e.g. proteins such as collagen, fibronectin, or laminin. It was tried to facilitate cell adhesion and growth of LS180 cells into a monolayer by coating cell culture inserts with two different matrix proteins, i.e. rat tail collagen and human fibronectin (Sec. 3.10.1), but no improvement of monolayer formation was seen when TEER values were measured. These findings, which are also widely reported in the literature (TEER values close to $0\Omega\text{cm}^2$ for LS180 cells on uncoated inserts, no literature available for LS180 cells grown on coated inserts) [113, 377], suggested again that LS180 cells are not suitable for *in vitro* studies requiring a confluent monolayer. Measurements of TEER therefore had to be waived in our coculture experiments.

2.9.2 Cytokine release from RAW 264.7 cells

Western blot analysis of cell culture media of RAW 264.7 cells treated with LPS, MPA, and AcMPAG showed only significant changes in levels of secreted proteins for the positive control LPS (Fig. 2.60 and Fig. 2.61). While the response to LPS in a concentration as low as $0.1\mu\text{g}/\text{mL}$ was relatively excessive for $\text{TNF-}\alpha$, $\text{INF-}\gamma$, and $\text{IL-1}\beta$ and while IL-6 was secreted in measurable amounts as a response to $5\mu\text{g}/\text{mL}$

LPS, no response occurred to MPA or AcMPAG as inflammatory stimuli. The induction of cytokine release through LPS shows the validity of this part of the cell culture model, but suggests that neither MPA nor AcMPAG possess inflammatory potential in the here applied concentrations. It needs to be taken into account that the innate immune response which was mimicked by macrophages activated by LPS reacts to structural motives expressed in proteins of bacteria, viruses, and fungi which are commonly called pathogen-associated molecular patterns (PAMPs) [367]. PAMPs from LPS are known to stimulate TLR4 and other particular TLRs expressed by cells of the innate immune system [367]. Since this respective pathway is needed/was chosen as a comparison when conducting experiments with macrophages and LPS as a positive control a strong response to LPS can be expected. Although no statistically significant differences occurred for MPA and AcMPAG versus controls, a trend was found towards an increase in cytokine levels in boxplot diagrams of TNF- α (band at 48kDa) and INF- γ measured in cell culture media of RAW 264.7 cells after treatment with MPA and AcMPAG for 4h despite missing PAMPs in the tested compounds (Fig. 2.62).

2 Results and Discussion

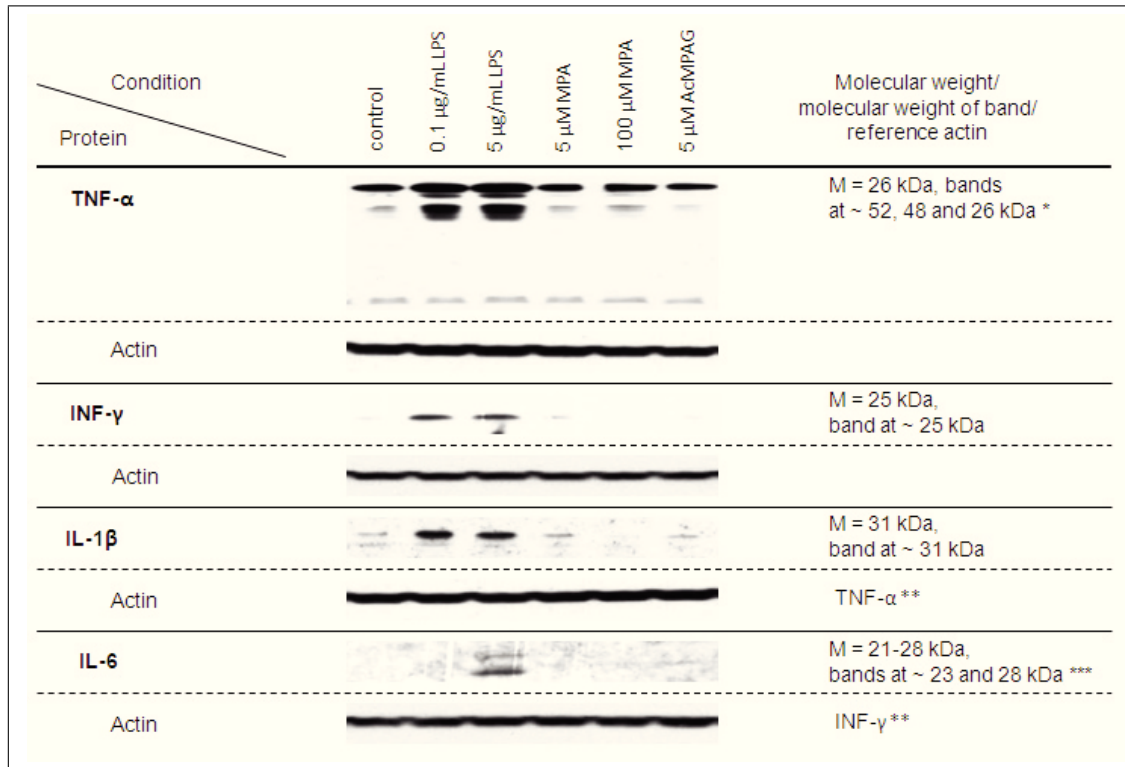


Fig. 2.60: Western blots of inflammatory markers of cell culture media of RAW 264.7 cells after treatment with LPS, MPA, and AcMAG for 4h. Bands are shown with their respective β -actin bands ($N=3$). Relative intensities as determined by densitometry analysis normalized based on β -actin are shown in Figure 2.61 including their statistical analysis in figure legend. M: molecular weight, *: based on the information provided in the vendor's product sheet, the vendor is unsure about the identity of the extra bands; difference between actual and predicted band size probably due to post-translational modifications, post-translational cleavage, splice variants, relative charge or multimerization [125], **: due to cutting/stripping of the membrane the same actin band served for the normalization of multiple proteins, ***: 23-25kDa O-glycosylated, 28-30kDa both O- and N-glycosylated.

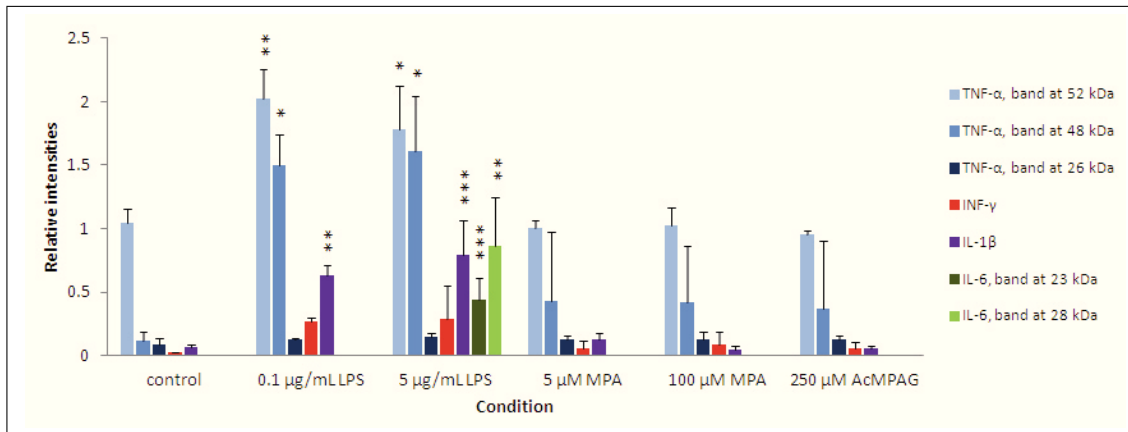


Fig. 2.61: Levels of inflammatory markers of cell culture media of RAW 264.7 cells after treatment with LPS, MPA, and AcMAG for 4h. Values are given as means of % of controls with standard deviations of relative intensities normalized based on β -actin ($N=3$). Western blots with their respective β -actin bands are shown in Figure 2.60. Significance was determined by one-way ANOVA combined with Scheffe's post – hoc test with *: $p<0.05$; **: $p<0.005$; ***: $p<0.001$ versus controls.

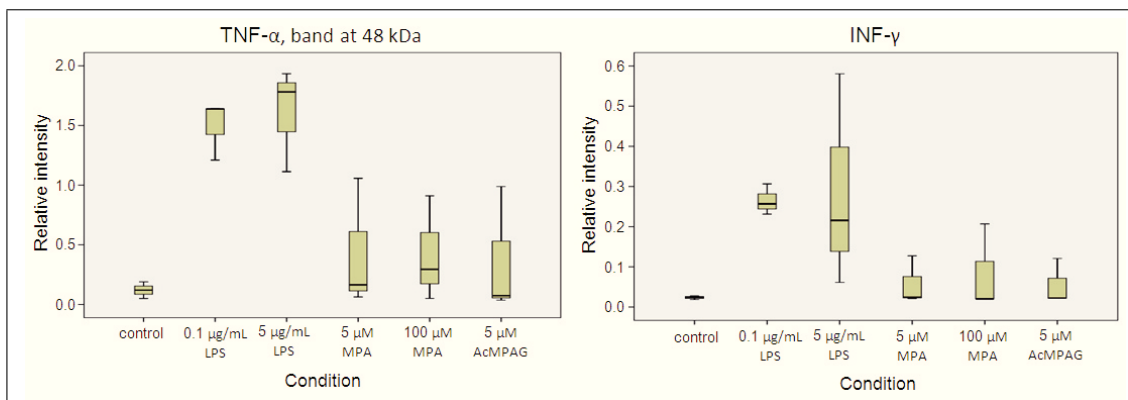


Fig. 2.62: Boxplot diagrams of levels of TNF- α (band at 48kDa) and INF- γ measured in cell culture media of RAW 264.7 cells after treatment with LPS, MPA, and AcMPAG for 4h. Values are depicted as relative intensities with standard deviations (densitometry units normalized based on β -actin ($N=3$)). Western blots with their respective β -actin bands are shown in Figure 2.60 and a bar graph including statistically significant changes is shown in Figure 2.61.

2.9.3 mRNA levels of IL-8 and SERT in LS180 cells

Aim of these experiments was the analysis of the inflammatory potential of MPA and AcMPAG in contrast to a positive control of known inflammatory potential and changes to the epithelium (LS180 cells) induced by an immune response to MPA and AcMPAG. As no significant release into the culture medium for either of the measured cytokines by MPA or AcMPAG could be observed, no further experiments in this direction were conducted.

2.9.4 Evaluation of the LS180-RAW 264.7 coculture model

As discussed above this coculture models seems potent to measure responses of the second cell type (LS180 or Caco-2 cells) to compounds of inflammatory potential. If only changes in mRNA levels or other intracellular changes of the second cell type are supposed to be evaluated, LS180 cells might be a useful choice. Lack of monolayer integrity in untreated LS180 cells is a limitation. The use of Caco-2 cells should be considered when pursuing experiments requiring a cell monolayer over LS180 cells.

In this experiment the inflammatory potential of MPA and AcMPAG in comparison to LPS was tested. Modification of the coculture system, i.e. cocultivation of LS180 and RAW 264.7 cells in the same culture dish instead of hanging inserts for LS180 cells, would be an interesting approach to assess potential inflammatory responses to the modifications of proteins caused by MPA and MPA metabolites. Although most, but not all, proteins that were affected in their expression levels as identified by SILAC and GelC-MS (Sec. 2.7.1) or that were covalently modified as described in the literature (Sec. 2.7.2) are intracellular proteins, an effect on RAW 264.7 cells can not fully be ruled out. The same modifications as found in the proteome of LS180 cells might as well occur in RAW 264.7 cells, so that a coculture or even a monoculture of RAW 264.7 cells could be used to measure inflammatory markers and inflammatory potential of intracellular protein modifications caused by MPA and MPA metabolites.

2.10 Summary discussion, conclusions, and perspectives

With the validation of the LS180 cell culture model in respect of its applicability in studies concerning MPA's GI toxicity a stable, predictable, and easy-to-handle cell culture model became available. Due to the stable expression of common drug-metabolizing enzymes over several passages, its fast proliferation rate, and its resilience (cell viability is not compromised by the withdrawal of FBS over several days), this cell culture model has the potential to be a valuable tool in the clarification of pharmacokinetic-induced mechanisms of toxicity in general and MPA-induced GI side effects in particular.

In the scope of this thesis the model was systematically validated and improved in terms of physiological aspects, that are often ignored in studies dealing with MPA side effects (reversal of certain MPA-induced effects by supplementation with exogenous guanosine). Possible toxicity of the MMF ester moiety morpholinoethanol or drug-drug interactions of this moiety with MPA are usually not taken into account either. Our initial experiments compared morpholinoethanol and morpholinoethanol in combination with MPA to MPA alone, MMF, and controls. As no effects of morpholinoethanol or drug-drug interactions in LS180 cells were seen in these initial experiments the toxicity of this compound was not further researched.

As no cytotoxic effects of MPA on LS180 cells were found LS180 cells provided a solid basis for consecutive in-depth studies. This is especially beneficial for experiments requiring higher amounts of sample material such as NMR-based studies.

MPA's antiproliferative properties are often claimed to be reversible by supplementation with guanine/guanosine. This work systematically looked at LS180 cell proliferation profiles over different periods of time while cells were supplemented with different guanosine concentrations. We found imbalances and significantly decreased cell proliferation after 3 days and especially after 5 days, a time span that generally does not get monitored although renewal of the GI epithelium takes up to 5 days. Intracellular guanosine nucleotide depletion was not reversible and only marginally improved by guanosine supplementation, although it is often claimed to be reversible, especially for the GI epithelium due to nucleotide supply through food. These results show that MPA's antiproliferative properties have most likely been underestimated. Direct impairment of the intestinal epithelium by MPA and an immune reaction to the luminal content could probably be the most obvious trigger of Crohn's disease-like patterns prominent in MPA therapy.

2 Results and Discussion

The HPLC-MS assay for MPA, MMF, and metabolites that was developed and consecutive identification of pH-dependency of matrix effects compromising metabolite stabilities, that have not been described before, provide a basis and important clues in terms of sample extraction and preparation in case of matrices containing proteins such as albumin. This observation could become relevant especially in terms of clinical samples and clinical trials analyzing blood and urine from transplant patients, make further analysis of these effect indispensable and might finally provide a reliable method for determination of metabolite concentrations in matrices that are especially clinically relevant.

Very valuable information was gained from proteomics experiments based on SILAC and GelC-MS. The observation that especially proteins involved in lipid metabolism and structural proteins are affected in LS180 cells is consistent with other human data. A comprehensive portfolio of online analysis tool was used for analysis of our data and data published within the last years by other work groups and revealed important inconsistencies comparing data from our human cancer cell line with data gained by the use of rat models. The use of these or similar analysis tools and the use of databases is inevitable dealing with results from proteomic research due to the often times immense data load and complexity of data. The present data was pooled and subjected to a comprehensive analysis to compare different types of models that are used throughout the literature to clarify mechanisms of MPA toxicity, an approach that has not been conducted before, but was useful in terms of e.g. validation of models and comparison and pooling of data in general.

Metabolome analysis revealed a changed lipid metabolism, but a widely unaffected carbohydrate metabolism. Especially membrane- and therefore barrier-constituting lipids were significantly upregulated again hinting towards defects of the epithelial barrier. These results are compatible with results from HPLC-MS and SILAC experiments. This shows that the combination of molecular biology methods, HPLC-MS, metabolomics and proteomics approaches which are frequently used in our laboratory are able to generate a unique framework of mechanisms of action/toxicity, to gain comprehensive insights into complex biochemical problems, and even to validate models and evaluate previously collected data.

It needs to be kept in mind that LS180 cells are cancer cells, which can be reflected in results. On the other hand our model based on human cancer cells might in certain respects provide more reliable results than results are gained by the use

2.10 Summary discussion, conclusions, and perspectives

of e.g. rat model as it is consistently seen in the outcome of our proteomics studies.

For the elucidation of direct inflammatory processes linked to MPA another unique cell culture model was created. As LS180 cells performed strongly in our previous studies and as they provided certain benefits over Caco-2 cells, a commonly-used model based on Caco-2 and RAW 264.7 cells was modified. Neither MPA nor AcMPAG did show direct inflammatory responses, whereas LPS triggered an extensive response. Slight modifications to our LS180-based model such as direct cocultivation of both cell lines in one cell culture dish could be used for further studies which would include assessment of the inflammatory potential of MPA-/MPA metabolite-induced changes to LS180 cells such as covalently modified proteins.

Relying on the results gained from experiments using the LS180 cell culture model MPA's GI toxicity could result, as stated in the introduction, from impairment of epithelial proliferation, consecutive loss of the GI barrier, and penetration of the mucosa by luminal bacteria and proteins.

In Figure 2.63 the proposed molecular mechanisms of MPA's toxicity are summarized in context of the used methods.

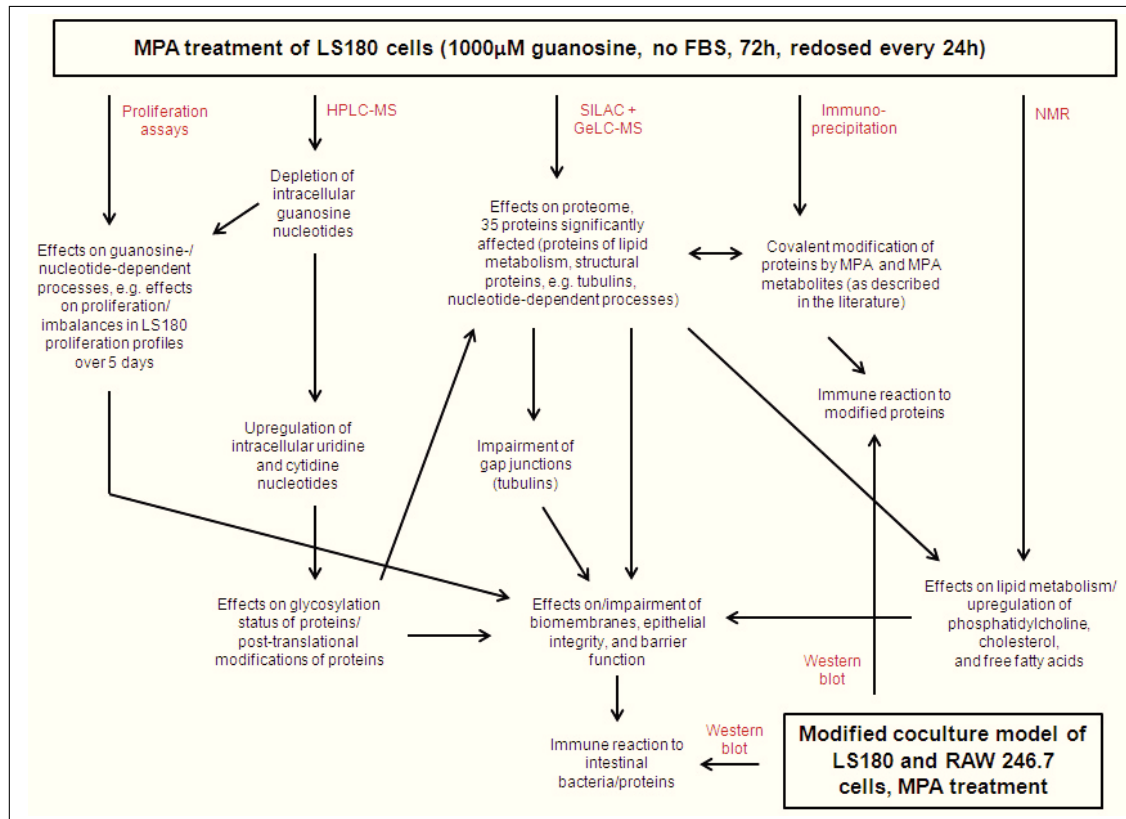


Fig. 2.63: Proposed molecular mechanisms of MPA's GI toxicity elucidated using the LS180 cell culture model and various methods. *The listed MPA-dependent effects were determined using the LS180 cell culture model except for "Covalent modification of proteins by MPA and MPA metabolites". This experiment did not yield analyzable results, but covalent modifications of proteins have been described in the literature before. The LS180-RAW 246.7 cell coculture model as it was used by us did not show immune reactions to MPA or MPA metabolites. A modified coculture model as discussed in later sections could provide information about immune reactions to modified proteins and/or intra- and extracellular parameters. FBS: fetal bovine serum, GeLC: gel-based liquid chromatography, HPLC: high performance liquid chromatography, MPA: mycophenolic acid, MS: mass spectrometry, NMR: nuclear magnetic resonance, SILAC: stable isotopic labeling by amino acids in cell culture.*

3 Materials and Methods

3.1 Cell cultures and incubation conditions

LS180 cells were purchased from the American Type Culture Collection (ATCC, Manassas, VA; no. CL-187). This cell line was derived from a human type II colon tumor. LS180 cells were cultured in Dulbecco's Modified Eagle Medium (DMEM)-high glucose (Sigma, St. Louis, MO; DMEM 2964) and supplemented with antibiotics (100U/ml penicillin and 100 μ g/mL streptomycin, Sigma). For certain experiments (as specified in text) LS180 cells were supplemented with 10% FBS (FetalPlex Animal Serum Complex; Gemini Bio-Products, West Sacramento, CA). Cells were subcultivated every 3-4 days (split ratio 1:3) using an EDTA solution (1L ESPG solution: 9g NaCl, 0.2g EDTA, 1g glucose, 20mL 1M KP_i pH 7.6 (about 2.1g H_2KPO_4 and 14.7g HK_2PO_4 for 100mL) dissolved in 1L H_2O , filtered sterile) to minimize clumping.

RAW 264.7 cells were purchased from ATCC (no. TIB-71) and cultivated in DMEM-high glucose (Sigma, DMEM 2964). The medium was supplemented with antibiotics and with 10% FBS for general culturing and proliferation assays. Conducting experiments for the inflammation model no FBS was used.

CCD-18Co cells were purchased from ATCC (no. CRL-1459) and cultivated in Eagle's Minimum Essential Medium (EMEM; Corning cellgro; no. 10-010-C1, with 2mM L-glutamine) and supplemented with antibiotics, 10% FBS, and 1% non-essential amino acids (Cellgro).

All cell types were cultured at 37°C in a humidified atmosphere with 5% CO_2 . LS180 cells were grown and subcultivated in 75cm² and 225cm² flasks (DB Falcon). For NMR experiments LS180 cells were grown on 150x15mm tissue culture dishes (Nunc), for HPLC-MS and all other experiments on standard 100x20mm tissue culture dishes (DB Falcon). RAW 264.7 and CCD-18Co cells were grown on standard 100x20mm tissue culture dishes.

3 Materials and Methods

All solutions/media that consisted of partly unsterile components/supplements (ESPG solution, media supplemented with guanosine, media containing labeled glucose or amino acids) were filtered sterile using filter units of $0.2\mu\text{m}$ pore size (Nalgene).

3.1.1 Experimental conditions and drug treatment

For experiments all cells were plated in relation to incubation times. According to each cell type's doubling time (Sec. 3.2.1) cell densities were calculated to reach almost 100% confluency for controls at harvesting time, e.g. LS180 cells were seeded to 75, 50, 35, or 25% confluency for 12, 24, 48, or 72h incubations, respectively (doubling time of $51.1\pm 2.7\text{h}$).

MPA, MMF, and all MPA metabolites were purchased from Toronto Research Chemicals (North York, Ontario, Canada). Morpholinoethanol was purchased from Sigma Aldrich (purity 99%).

Drugs were spiked into cell culture media from concentrated stocks in DMSO/MeOH. The final DMSO/MeOH concentration in culture media was 0.05% unless otherwise specified.

3.2 Cell proliferation, cell viability, and other assays

3.2.1 Doubling time

Doubling time of all cell types was assessed by cell counts using a Nexelon Bioscience Cellometer TM Auto T4 and the Cellometer Auto T4 software (N=3). Prior to counting cells were stained with Trypan blue. Vital cells exclude this dye whereas dead cells with compromised membrane integrity are penetrated and selectively take on a blue color [380]. Using the Cellometer Auto T4 software cell numbers were automatically corrected for dead cells. Doubling time of LS180 cells was determined to be $51.1\pm 2.7\text{h}$, doubling time of RAW 264.7 cells was $15.4\pm 0.2\text{h}$, and doubling time of CCD-18Co cells was $23.4\pm 2.4\text{h}$.

3.2.2 CyQUANT NF Cell Proliferation Assays

Cellular DNA content is highly regulated and closely corresponds to cell numbers and therefore can be used to quantify cell populations [381]. The CyQUANT NF Cell Proliferation Assay (Invitrogen) can be used to determine cellular DNA content by fluorescent dye binding. It is more sensitive than the conventional MTT assay

which is often used for proliferation studies.

96-well plates were prepared for incubation (Sec. 3.1.1), incubated with test compounds (single dose or redosed every 24h), and the CyQUANT NF Cell Proliferation Assay was performed following the manufacturer's instructions. It was incubated with 1X dye binding solution for 50-60min due to the large cell size of LS180 cells, and fluorescence intensities were measured using a fluorescence microplate reader (Thermo Scientific, Fluoroskan Ascent FL) at 485nm excitation and 530nm emission in combination with Ascent software (version 2.6).

3.2.3 LDH assays

During apoptosis and necrosis cell damage and lysis occur [382]. The soluble enzyme LDH is released from the cytosol into the cell culture medium. LDH activity measurement can be used to indicate cell death and therefore cytotoxicity-independent of mechanism.

Cayman's LDH Cytotoxicity Assay (Cayman Chemical Company, Ann Arbor, Michigan) was performed following the manufacturer's instructions. 96-well plates were prepared for incubation (Sec. 3.1.1) and incubated with test compounds (single dose or redosed every 24h), and the LDH assay was performed following the manufacturer's instructions. The assay depends on a coupled two-step reaction. LDH from the culture media oxidizes lactate to pyruvate and reduces NAD^+ to $\text{NADH} + \text{H}^+$. The provided $\text{NADH} + \text{H}^+$ serves to catalyze the reduction of the tetrazolium salt 2-p-iodophenyl-3-p-nitrophenyl-5-phenyl tetrazolium chloride by diaphorase. The amount of the product formazan, which absorbs at 490-520nm, is proportional to the LDH concentrations in the culture media.

3.2.4 Caspase-3 western blots

In the process of apoptosis caspase-3 is cleaved into two activated fragments [144]. To test for induction of apoptosis in LS180 cells western blots for caspase-3 and cleaved caspase-3 were conducted (Sec. 3.5.1). Samples were extracted for western blots as described in Section 3.4.

3.2.5 cAMP/cGMP assays

cAMP and cGMP are second messengers and regulate a variety of cellular processes [161]. Cyclic AMP/GMP XP Assays (Cell Signaling Technology) were performed according to the manufacturer's manual. 50 μL cell lysate containing 175 μg

3 Materials and Methods

protein were used per well. cAMP/cGMP levels in samples compete with fixed amounts of horseradish peroxidase (HRP)-linked cAMP/cGMP for binding to a anti-cAMP/cGMP XP rabbit monoclonal antibody immobilized onto a 96-well plate. After washing the finally added HRP substrate 3,3',5,5'-tetramethylbenzidine develops color and the absorbance at 450nm is inversely proportional to the quantity of cAMP/cGMP in the sample.

3.3 Protein determination

The bicinchoninic acid (BCA) protein assay uses the reduction of Cu^{2+} to Cu^+ by protein in alkaline environment with the extent of reduction being proportional to protein content [383]. The Cu^+ generated forms a purple-colored chelate complex with BCA. This complex strongly absorbs at 562nm. For determination of protein content BCA assays were used (Pierce Biotechnology). As described in the manufacturer's instructions 25 μL of BSA standard or sample were used per microplate well as well as 200 μL working solution. It was incubated at 37°C for 30min and absorbance was read at 560nm.

3.4 Extraction methods

PCA extraction for HPLC-MS and NMR measurements

Lysis with 12% PCA inactivates enzymes through irreversible denaturation of the structure of proteins and therefore stops cell metabolism.

For NMR experiments 5 150x15mm dishes were used per incubation condition and an N=6 was prepared. For HPLC-MS experiments 1 dish was used per incubation condition and an N=4 was prepared. After incubation cell culture media were removed from cells (6mL per dish/30mL per condition were collected for NMR analysis). Cells were washed 3 times with 5mL 0.9% NaCl and as much as possible of the remaining solution was removed. Cells were frozen in liquid nitrogen and extracted with 3mL 12% PCA. Extracts were sonicated for 10min on ice and centrifuged (20min, 1450g, 4°C). For NMR measurements pellets (proteins, lipids) were weighted for normalization of metabolite concentrations to cell wet weight (weight of empty tubes had been determined before) and temporarily stored at -80°C. Supernatants (cell extracts) were neutralized with KOH and centrifuged again. Supernatants and cell culture media (for NMR measurements) were frozen in liquid nitrogen and lyophilized.

For NMR measurements protein-lipid pellets were resuspended in 5mL H₂O and pH values were adjusted to pH 7 with HCl and NaOH and lyophilized.

Extraction for western blots

Prior to extraction for western blot cells were washed 3 times with ice-cold phosphate-buffered saline (PBS, Sigma). Cells were extracted with Cell Lysis Buffer (Cell Signaling, no. 9803) according to the manufacturer's instructions. 4-(2-aminoethyl) benzenesulfonyl fluoride hydrochloride (AEBSF, Sigma) was used instead of phenylmethanesulfonyl fluoride as protease inhibitor. Extracted cells were kept on ice for 10min, repeatedly vortexed, and centrifuged at 13.000g for 10min. The supernatants were subjected to protein determination (Sec. 3.3) and prepared for western blots at a concentration of 100 μ g/15 μ L in 1x Laemmli sample buffer (Bio-Rad) and stored in aliquots at -20°C.

Extraction for cAMP/cGMP assays

The same lysates that were used for western blot analyses were used for cAMP/cGMP assays. The extraction is described in Section 3.4.

Extraction for QPCR

For RNA extraction the RNeasy Mini Kit (Qiagen, Chatworth, CA, no. 74104) was used according to the manufacturer's instructions. All steps were performed on ice using nuclease-free materials. Cells (ca. 10⁶) were washed with PBS, removed from the plate, and pelleted. The pellet was resuspended in 200 μ L RLN buffer (containing 1U/ μ L RNase inhibitor and 1mM DTT) to lyse the plasma membrane (but leave the nuclear membranes intact) and the liquid preparation was placed in an Eppendorf tube. Samples were centrifuged at 1000g at 4°C to precipitate nuclei and cell debris. The supernatants were added to a second tube containing 600 μ L RLT buffer (provided) with 1% β -mercaptoethanol (ca. 800 μ L sample). 430 μ L ethanol (200 proof) were added. 700 μ L sample were added to the provided spin columns and centrifuged at 1000g, the liquid was discharged, the rest of the sample was added and the centrifugation repeated, the liquid was discharged. The column was washed twice with 700 μ L of RW1 buffer (provided). Using a new tube the column was washed twice with RPE buffer (provided). After discharge of the liquid the remaining ethanol was evaporated from the tube. To elute the sample from the column two washing steps with nuclease-free water (100 μ L + 50 μ L) were performed and the column discharged. Quantification and evaluation of purity was done spectrophoto-

3 Materials and Methods

metrically ($OD_{260} \times 1.6 = \text{RNA in } \mu\text{g}/\mu\text{L}$, for RNA purity $OD_{260}/OD_{280} > 1.8$) using $5\mu\text{L}$ of sample/nuclease-free water in $195\mu\text{L}$ milliQ water. Isolated RNA was stored at -80°C until analysis.

Extraction for SILAC

For SILAC experiments LS180 cells were extracted as described for western blots (Sec. 3.4), but cells were washed 5 times with PBS (pelleted using a centrifuge at 130g and resuspended) after removal from the cell culture dishes with ESPG solution.

3.5 Molecular biology methods

3.5.1 Western blot analysis

To validate the LS180 cell culture model (stability of metabolizing enzymes over passages, apoptotic potential of MPA by analysis of caspase-3 levels), and to validate and further investigate SILAC results, western blot analysis was carried out. Same samples were used for western blots of caspase-3 and Na^+/K^+ -ATPase, validation/further investigation of proteomics results, as well as for cAMP/cGMP ELISA assays. Protein lysis and preparation is described in Section 3.4. Samples were aliquoted prior to storage at -80°C limiting the number of freeze-thaw cycles to one.

Lysates at $100\mu\text{g}/15\mu\text{L}$ in 1x Laemmli Sample Buffer were boiled for 10min and $100\mu\text{g}$ protein ($15\mu\text{L}$) were loaded per well onto 26-well TCR-gels (Bio-Rad, Criterion Tris-HCl precast gel, no. 345-0034). $5\mu\text{L}$ Precision Plus Protein Dual Color Standard (Bio-Rad) and $2\mu\text{L}$ Biotinylated Protein Ladder (Cell Signaling) were used per gel. Proteins were separated by gel electrophoresis in an ice bucket at 170V. Proteins were transferred onto polyvinylidene fluoride membranes at 90V at 4°C for 2h. The membranes were washed in Tris-buffered saline (TBS, 1L 1X TBS: 8g NaCl, 0.2g KCl, 3g Tris-base dissolved in 1L H_2O , pH adjusted to 7.4 with HCl) with 0.1% Tween-20 (TTBS) for 15min and blocked in 5% milk in TTBS for 1h to block unspecific binding sites on the membranes to prevent antibody binding. The membranes were incubated with the respective first antibodies (Tab. 3.1) in 5% milk in TTBS for 2h (in case of the Anti-MPA/AcMPAG antibody over night) and washed 3 times for 10min in TTBS. It was incubated with the respective HRP-coupled secondary antibodies (Tab. 3.1) in 5% milk in TTBS for 1h and washed 3 times for 10min with TTBS. The membranes were incubated with chemilumi-

nescence solution (Bio-Rad, Immun-Star HRP Luminol/Enhancer and Immun-Star HRP Peroxidase Buffer mixed 1:1) for 5min. Films were exposed to the chemiluminescent membranes for varying time periods and developed using an ALLPRO 100 Film Processor. Films were scanned for densitometry using a Kodak Image Station 440CF. Band intensities were determined using 1D Image Station software (Kodak). Bands were compared within gel and reported as arbitrary units. In cases of comparison among/analysis of bands of different gels, additional samples for normalization were run.

Table 3.1: Antibodies used for experiments elucidating the mechanisms of MPA GI toxicity.

Antibody	Manufacturer	Prod. #	Host	Dilution/concentration
Anti-ANXA1	Cell Signaling	3299	Rb	1:1000
Anti-ACSL5	Sigma	WH0051703M1	Ms	1:1000
Anti-ACSL5	Abcam	ab104892	Rb	1:1000
Anti-Caspase-3	Cell Signaling	9662	Rb	1:1000
Anti-CYP3A4	Cell Signaling	12249	Rb	1:1000
Anti-CYP3A5	Sigma	C4743	Ms	1:1000
Anti-IL-1 β	Cell Signaling	2022	Rb	1:1000
Anti-IL-6	Abcam	ab6672	Rb	1:1000
Anti-INF- γ	Abcam	ab9657	Rb	0.2 μ g/mL
Anti-IMPDH1	Abcam	ab33039	Rb	1:1000
Anti-IMPDH2	Abcam	ab85702	Goat	1:1000
Anti-MDR1	Abcam	ab80594	Ms	1:1000
Anti-MPA/AcMPAG	Fisher Scientific	custom	Ms	1 μ g/mL
Anti-MRP1	Abcam	ab3368	Rat	1:500
Anti-MRP2	Cell Signaling	4446	Rb	1:1000
Anti-Na ⁺ -K ⁺ -ATPase	Cell Signaling	3010	Rb	1:1000
Anti-OAT1B1	Abcam	ab103065	Rb	1:1000
Anti-OAT1B3	Novus Biologicals	NBP1-45248	Goat	1:1000
Anti-OAT2B1	Abcam	ab83532	Rb	1:1000
Anti-PIgR	Abcam	ab91269	Rb	1:1000
Anti-PXR	Abcam	ab85451	Rb	1:1000
Anti-REG-4	Abcam	ab89917	Ms	1:1000
Anti-SLC12A2	Sigma	AV43805	Rb	1:1000
Anti-TNF α	Abcam	ab9635	Rb	1:1000
Anti-UBC	Cell Signaling	3933	Rb	1:1000
Anti-UGT1A7	Abcam	ab105685	Rb	1:1000
Anti-UGT1A9	Abcam	ab67535	Ms	1:1000
Anti-UGT1A10	Abcam	ab76677	Ms	1:1000
Anti-UGT2B7	Fisher Scientific	PA5-21507	Rb	1:500
Anti-ZO-1	Cell Signaling	5406	Rb	1:1000
Anti-14-3-3 θ	Cell Signaling	9638	Rb	1:1000
Anti-Goat	Abcam	ab86245	Chicken	1:2000
Anti-Ms	Cell Signaling	7076	Horse	1:2000
Anti-Rb	Cell Signaling	7074	Goat	1:2000
Anti-Rat	Cell Signaling	7077	Goat	1:2000

3.5.2 QPCR

Primers for QPCR were designed using Beacon Designer software (version 7.7/7.9). The iScript cDNA Synthesis Kit (Bio-Rad, no. 170-8891) was used to synthesize cDNA according to the manufacturer's instructions. Per reaction a total of 1 μ g of RNA was pipetted into a 500 μ L centrifuge tube to which nuclease-free water was added to bring the volume to 15 μ L. 5 μ L of a master mix (4 μ L 5X iScript Reaction Mix + 1 μ L of iScript Reverse Transcriptase). Tubes were incubated using an Eppendorf Mastercycler (iScript program according to the manufacturer's instructions: 5min at 25°C, 30min at 42°C, 5min at 85°C, samples held at 4°C in the end). Following cDNA synthesis samples were diluted 1:3 using nuclease-free water. Reactions were prepared using a 96-well semi-skirted plate (AB gene, no. AB-0900, suitable for use in a Bio-Rad iCycler). Each reaction consisted of 12.5 μ L 2X SYBR Green Supermix (Bio-Rad, no. 170-8890) + 0.175 μ L of each forward and reverse primer (10 μ M, final concentration 70nM) + 9.65 μ L nuclease-free water. Reaction conditions were based on the annealing temperature of the primer set (generally 60°C). The protocol was run for 55 cycles. Initial QPCR runs were followed by analysis of the expected amplicon (product) on 1.2% agarose gel.

mRNA expression was quantified using Bio-Rad iQ5 software. mRNA levels of respective genes were normalized based on mRNA levels of β -actin. All samples were amplified in triplicates. Human kidney/liver tissue (Biochain) served as positive control. Samples/diluted samples were used for calibration purposes since human kidney/liver tissue did not provide mRNA levels high enough for comparison with levels in LS180 cells.

Table 3.2: QPCR primers and conditions for sample analysis.

Target transcript	Primer set	Annealing temp. [°C]	Amplicon size	No. of cycles
UGT1A8	F: 5' ACT TAC TCA ACC TCA TAC ACT 3'	60	120	55
	R: 5' ACC ATT GGA TGA ACT CAG A 3'	60	120	55
BCRP	F: 5' GAG GAA CTG GGT AGG ATT T 3'	60	123	55
	R: 5' TAA GGA TGT AAA TGT TGG GAT 3'	60	123	55
β -actin	F: 5' GTT CAA GCG ATT CTC CTG 3'	60	106	55
	R: 5' GAT GAA ACC TTG TCT CTA CTA AA 3'	60	106	55

3.6 NMR analysis

3.6.1 Processing of cell extracts, media, and pellets

Lyophilized cell extracts were reconstituted in 600 μ L D₂O and centrifuged (20min, 1450g, 20°C). Supernatants were collected in NMR tubes and pH values were adjusted to pH 7 with deuterated hydrochloric acid (DCl) and deuterated sodium hydroxide (NaOD).

Lyophilized media were reconstituted in 800 μ L D₂O and prepared for NMR measurements as cell extracts.

Lyophilized protein-lipid samples were reconstituted in 900 μ L deuterated chloroform (CDCl₃)/deuterated methanol (CD₃OD) (2:1) and transferred into glass tubes. Tubes were plugged and centrifuged (20min, 1450g, 20°C). Supernatants (lipid extracts) were transferred into NMR tubes. The protein pellet was not continued to be used for protein determination since measured metabolite concentrations were normalized to cell wet weight as determined during sample preparation after PCA extraction.

3.6.2 Acquisition and processing parameters of NMR spectra

NMR spectra were recorded on a Bruker DRX 600 spectrometer (Bremen, Germany) equipped with a 5-mm HCN probe (¹H spectra of hydrophilic cell extracts and lipids and 2D spectra) or a 5-mm ¹H/¹³C dual probe (¹³C spectra) at frequencies of 600MHz (¹H) and 150MHz (¹³C). Spectra of hydrophilic and lipophilic extracts were recorded using established pulse sequences with water saturation independent of d1 time (d1 = 5*T₁).

Spectra were processed using MestRe-C software (version 4.9.9.9). Zero-filling to 32K was applied to all spectra. For ¹H NMR spectra a gaussian apodisation function (1-2Hz) was used, for ¹³C NMR spectra an exponential multiplication (varying parameters) was used.

¹H NMR parameters

Table 3.3 lists the parameters used for recording of ¹H NMR spectra of hydrophilic cell extracts and lipid extracts.

3 Materials and Methods

Table 3.3: Parameters for the recording of ^1H NMR spectra

Parameter	Hydrophilic extracts	Lipophilic extracts
NMR probe	5-mm HCN inverse	5-mm HCN inverse
Temperature [K]	300	300
Spectral width [Hz/ppm]	9.50/150	9.50/150
Number of scans	400	300
Flip angle	40°	40°
Repetition time [s]	17.2	17.2
Data size	16k	16k

^{13}C NMR parameters

Table 3.4 lists the parameters used for recording of ^{13}C NMR spectra of hydrophilic cell extracts.

Table 3.4: Parameters for the recording of ^{13}C NMR spectra

Parameter	Cell extracts
NMR probe	5-mm $^1\text{H}/^{13}\text{C}$ dual
Temperature [K]	300
Spectral width [Hz/ppm]	24154.59/160
Number of scans	20,000
Flip angle	27°
Repetition time [s]	3
Data size	16k

^1H - ^{13}C HSQC NMR parameters

Several ^1H - ^{13}C HSQC NMR spectra of LS180 hydrophilic cell extracts and lipid extracts were recorded for signal assignment in 1D NMR spectra as well as to check for compounds eventually arising due to MPA treatment or accumulating during MPA treatment.

Table 3.5 shows the settings for the recording of ^1H - ^{13}C HSQC NMR spectra. The resolution in F1 and the number of scans was defined by acquisition time, metabolite concentration, and desired resolution. 90° pulses were determined for each sample individually. Representative values are listed.

Table 3.5: Parameters of ^1H - ^{13}C HSQC NMR spectra

Parameter	Cell extracts	Lipid extracts
NMR probe	5-mm HCN inverse	5-mm HCN inverse
Temperature [K]	300	300
Spectral width F2 [Hz/ppm]	6009.62/10.01	6009.62/10.01
Spectral width F1 [Hz/ppm]	24154.59/160	24154.59/160
Number of scans	80	32

3.6.3 Quantitative analysis of NMR spectra

Quantification of metabolite concentrations from ^1H NMR spectra

For ^1H NMR spectra of hydrophilic extracts a capillary containing 3-(trimethylsilyl)-2,2,3,3-d₄ propionic acid (TSP) in D₂O was used as an external standard for absolute quantification of metabolites. A solution of saccharose and glutamine of known concentration served for determination of the TSP concentration inside the capillary.

For ^1H NMR spectra of lipid extracts a TSP capillary of known TSP concentration was used as standard (dissolved in CDCl₃/CD₃OD 2:1).

For calibration of the NMR spectra the TSP signal was set to 0.00ppm.

For quantification of glutamate, glutamine, and glutamate in GSH/GSSG from ^1H NMR spectra C4 signals were integrated due to a complete overlap of C2 signals and interference of C3 signals of glutamine and glutamate in GSH/GSSG (please see ^1H - ^{13}C HSQC spectra in Figure 2.58 and Figure 4.33 and ^1H NMR spectra in Figure 2.48).

Aspartate C3 signals from ^1H NMR spectra were not integrated due to an often insufficient S/N ratio and overlap with a peak of unknown origin at 2.721 ppm (^{13}C : 39.905ppm, please see Section 3.6.3).

For quantitation of Cr and PCr CH₂ signals at 3.93ppm and 3.95ppm, respectively, were integrated due to an overlap of CH₃ signals at 3.03ppm (the ^1H - ^{13}C HSQC NMR spectrum is shown in Figure 4.33 and the ^1H NMR spectrum in Figure 2.48).

Quantification of concentrations of lipophilic compounds from ^1H NMR spectra

Due to varying chain lengths of lipids and overlaps of signals an absolute quantification of lipophilic compounds was not possible and lipophilic compounds were therefore quantified as % of controls only. As cholesterol signals overlapped with

3 Materials and Methods

multiple other signals in lipid spectra (Fig 4.35) respective compounds were corrected according to the number of protons contributing to the respective cholesterol signals. Values calculated from the isolated cholesterol C18 signal served as correction factors.

Calculation of fractional ^{13}C enrichment from ^1H NMR spectra and amount of ^{13}C -labeled metabolites from ^{13}C NMR spectra

^{13}C enrichments in C3 lactate (E_{Lac}) were calculated from ^1H NMR spectra according to Zwingmann et al. [102] using peak areas of the [^1H - ^{12}C] signal ($I (^1\text{H}-^{12}\text{C})$) and the [^1H - ^{13}C] satellite signals ($I (^1\text{H}-^{13}\text{C})$) of lactate C3:

$$E_{Lac} [frac] = \frac{I (^1\text{H} -^{13}\text{C})}{I (^1\text{H} -^{12}\text{C}) + I (^1\text{H} -^{13}\text{C})}. \quad (3.1)$$

1.1% natural abundance of ^{13}C was taken into account.

From lactate concentrations [Lac] and E_{Lac} from ^1H spectra the natural abundances of metabolites ($I_{n.a.}(\text{Met})$) can be calculated from integrals of ^{13}C spectra, $I_{n.a.}(\text{Met})$ being the fraction of the integral representing the metabolite's natural abundance:

$$I_{n.a.}(\text{Met}) = \frac{I (^{13}\text{C} - \text{Lac}) * [\text{Met}]}{(E_{Lac} + 1) * [\text{Lac}]}. \quad (3.2)$$

While $I (^{13}\text{C}\text{-Lac})$ is the peak area of the [$3\text{-}^{13}\text{C}$]lactate signal from ^{13}C spectra, the concentrations of lactate and the respective metabolite [Met] are calculated from ^1H spectra. Knowing $I_{n.a.}(\text{Met})$ the metabolite's ^{13}C enrichment E_{Met} can be assessed in %:

$$E(\text{Met}) [\%] = \frac{I (^{13}\text{C} - \text{Met}) - I_{n.a.}(\text{Met}) * \text{NOE}}{(I_{n.a.}(\text{Met}))}. \quad (3.3)$$

Here $I (^{13}\text{C}\text{-Met})$ is the peak area of the metabolite of interest from ^{13}C spectra and the factor termed Nuclear Overhauser Enhancement (NOE) a correction factor to adjust intensity gain or loss of signals due to suppression of C-H coupling and saturation effects. The final concentration of metabolites from ^{13}C spectra $c (^{13}\text{C}\text{-Met})$ is given by equation 3.4, which needs to be corrected by factor 100 due to $E(\text{Met})$ given in %:

$$c (^{13}\text{C} - \text{Met}) = \frac{I (^{13}\text{C} - \text{Met}) - I_{n.a.}(\text{Met}) * \text{NOE}}{(I_{n.a.}(\text{Met}))}. \quad (3.4)$$

^{13}C enrichments in alanine (C3) were calculated accordingly.

Quantification of metabolic fluxes and TCA cycle ratios from ^{13}C NMR spectra

For determination of metabolic fluxes (PDH/PC ratios) the ratio of the C4 signal to the C2 signal (C4/C2) of glutamate and glutamine were used.

Mono and double labels of metabolites were quantified separately to determine TCA cycle ratios and an eventual increase/decrease in TCA cycle speed. The labeling pattern of C4 of glutamate served for determination of these parameters by calculating the ratio of doubly-labeled to mono-labeled signals.

^1H - ^{13}C HSQC NMR spectra

Compounds were identified using published databases [349, 350].

Noticeable signals of unknown origin occurred at 0.880ppm (t1)/15.916ppm (t2) and 2.721ppm (t1)/ 39.905ppm (t2), signals not shown/not visible due to low signal intensity in Figure 2.58). Database searches did not yield reasonable results (compounds of respective ppm values found in databases were of exogenous source and/or associated signals of respective compounds were missing). Since no significant changes in concentrations of the unknown compounds were seen after quantitative analysis of ^1H NMR spectra identification of compounds was not pursued any further.

As mentioned above (Sec. 3.6.3) calculation of fractional ^{13}C enrichment of lactate and amounts of ^{13}C -labeled metabolites relied on quantitation of peak areas of [^1H - ^{12}C] signals of lactate C3 from ^1H spectra. Using 2D NMR spectroscopy for a survey of signals/compounds and signal assignment considerable overlaps of the lactate C3 signal with other signals, i.e. N-acetyl-L-alanine, threonine, and acetoin, became apparent (Fig. 2.58). Since related signals of these compounds at other ppm regions exhibited severe overlaps with other signals, it was not possible to calculate and subtract compound concentrations from lactate concentrations derived from lactate C3 signals. This needs to be kept in mind looking at fractional ^{13}C enrichments of lactate and amounts of ^{13}C -labeled metabolites, as contribution of N-acetyl-L-alanine, threonine, and acetoin to the lactate C3 signal is likely to result in underestimation of fractional ^{13}C enrichments in lactate as well as overestimation of ^{13}C -labeled metabolite concentrations. Additionally, concentrations of N-acetyl-L-alanine, threonine, and acetoin possibly change with MPA concentrations. This possibly results in under- and/or overestimation of changes or even compensation of changes.

3.7 Measurement of high-energy phosphate levels

Samples were extracted as described in Section 3.4. Lyophilized cell extracts were reconstituted in 500 μ L H₂O. Samples were diluted 1:10 (100 μ L sample + 900 μ L HPLC H₂O) with a final internal standard concentration of 0.5 μ M (10mM stock). A nucleotide mix containing all analytes in 0.5mM concentrations served for preparation of the calibration curve (0.03125-16 μ M). N⁶-(6-aminohexyl)adenosine 3',5'-diphosphate (6-aminohexyl-ADP) was used as internal standard.

HPLC-MS measurements were performed on an API 4000 triple quadrupole (AB Sciex) with adjustments to the method which was previously published by Klawitter et al. for nucleotide measurements using a 1946D Agilent mass selective detector [160]. The instrument was operated in the negative MRM mode with ESI source and was equipped with an Agilent 1100 HPLC system. Analytes were extracted using a ZORBAX C18, 5 μ m (4.6mm x 5mm) column (Agilent Technologies) column and separated using a Phenomenex Synergy Hydro C18, 3 μ m (4.6mm x 250mm) column (Phenomenex, Torrance, CA, USA).

The solvents were 2mM/4mM dibutylammonium formate (DBAF, mobile phase A) and methanol + 0.1% FA (mobile phase B). The gradient used for inline extraction was: 0.0-0.7min 3% 4mM DBAF buffer at a flow rate of 1000 μ L/min, 0.7-0.8min 3-100% 4mM DBAF buffer at a flow rate of 1000 μ L/min, 0.8-14.0min 100% 4mM DBAF buffer at a flow rate of 100 μ L/min, 14.0-16.0min 100% 4mM DBAF buffer at a flow rate of 1000 μ L/min, 16.0-16.1min 100-3% 4mM DBAF buffer at a flow rate of 1000 μ L/min, 16.1-18.0min 3% 4mM DBAF buffer at a flow rate of 1000 μ L/min for re-equilibration to starting conditions. The gradient used for separation (at a constant flow rate of 700 μ L/min) was: 0.0-1.0min 5% 2mM DBAF buffer, 1.0-3.0min 5-20% 2mM DBAF buffer, 3.0-10.0min 20-40% 2mM DBAF buffer, 10.0-13.0min 40-52% 2mM DBAF buffer, 13.0-14.0min 52-80% 2mM DBAF buffer, 14.0-14.8min 80-5% 2mM DBAF buffer, 14.-18.0min 5% 2mM DBAF buffer for re-equilibration to starting conditions. Nitrogen was used as drying gas and collision gas.

The MS parameters were adjusted to: ion transition ATP: $m/z = 506.3 [M-H]^- \rightarrow 408.2$ with 40msec dwell time, with -83V DP, -28V CE, and -13V CXP; ion transition ADP: $m/z = 426.3 [M-H]^- \rightarrow 328.2$ with 40msec dwell time, with -90V DP, -23V CE, and -15V CXP; ion transition AMP: $m/z = 346.2 [M-H]^- \rightarrow 79.0$ with 40msec dwell time, with -80V DP, -42V CE, and -5V CXP; ion transition GTP: $m/z = 522.2 [M-H]^- \rightarrow 424.2$ with 80msec dwell time, with -85V DP, -30V CE, and -15V CXP; ion transition GDP: $m/z = 442.2 [M-H]^- \rightarrow 344.2$ with 80msec dwell time, with

-85V DP, -30V CE, and -15V CXP; ion transition GMP: $m/z = 362.2 [M-H]^- \rightarrow 79$ with 80msec dwell time, with -85V DP, -42V CE, and -7V CXP; ion transition UTP: $m/z = 483.2 [M-H]^- \rightarrow 385.3$ with 80msec dwell time, with -90V DP, -32V CE, and -14V CXP; ion transition UDP: $m/z = 403.2 [M-H]^- \rightarrow 79.0$ with 80msec dwell time, with -90V DP, -45V CE, and -15V CXP; ion transition UMP: $m/z = 323.2 [M-H]^- \rightarrow 79$ with 80msec dwell time, with -90V DP, -41V CE, and -6V CXP; ion transition CTP: $m/z = 482.3 [M-H]^- \rightarrow 384.1$ with 80msec dwell time, with -80V DP, -32V CE, and -15V CXP; ion transition CDP: $m/z = 402.2 [M-H]^- \rightarrow 304.1$ with 100msec dwell time, with -80V DP, -28V CE, and -13V CXP; ion transition CMP: $m/z = 322.1 [M-H]^- \rightarrow 79.0$ with 80msec dwell time, with -80V DP, -42V CE, and -8V CXP; ion transition NAD⁺: $m/z = 662.1 [M-H]^- \rightarrow 540.4$ with 100msec dwell time, with -75V DP, -21V CE, and -10V CXP; ion transition NADP⁺: $m/z = 742.1 [M-H]^- \rightarrow 620.5$ with 120msec dwell time, with -65V DP, -22V CE, and -17V CXP; ion transition FAD: $m/z = 784.0 [M-H]^- \rightarrow 346.1$ with 80msec dwell time, with -140V DP, -40V CE, and -13V CXP; ion transition 6-aminohexyl-ADP: $m/z = 525.0 [M-H]^- \rightarrow 233$ with 40msec dwell time, with -90V DP, -36V CE, and -19V CXP. The source temperature was set to 500°C with a capillary voltage of -4200V and CAD set to 12. The column oven temperature was set to 45±1°C. The injection volume was 100µL. Total run time was 18min.

For quantitation Analyst software (version 1.5.1) was used. Analytes were quantified without using the internal standard due to the occurrence of severe ion suppression and the achievement of more reasonable results not taking the internal standard into account.

3.8 HPLC-MS assay development

3.8.1 HPLC-MS conditions

An HPLC-MS method for quantification of MPA, MMF, and their metabolites was developed. Method development, conditions, and parameters are described in Section 2.6.1. Due to problems with the stability of certain analytes and unexpected matrix effects the method was not validated, only limits of detection (defined as a S/N ratio of 3:1) in MeOH/H₂O (1:1) were determined.

3.8.2 Stability experiments

Stability experiments performed to identify possible pH- and matrix component-dependency of the stability of AcMPAG and MPAG are described in Section 2.6.2.

3.9 Proteomics

3.9.1 Labeling of LS180 cells for SILAC experiments

Cells were labeled with heavy lysine ($[U-^{13}C_6]$ -L-lysine, MW = 152.1259; stable isotope of $[^{12}C_6]$ -L-lysine) or light lysine ($[^{12}C_6]$ -L-lysine, MW = 146.1055) according to the manufacturer's instructions (Invitrogen, SILAC Protein Identification and Quantification Kits, manual part no. 25-0841).

Labeling with heavy lysine (no double labeling, e.g. with lysine and arginine) was used to determine differences in expression levels of proteins in LS180 cells. LS180 cells of sets labeled with heavy and light lysine were treated as described for other experiments (1000 μ M guanosine, no FBS, 72h treatment, redosed every 24h). For extraction cells were washed with 5mL PBS 3 times prior to removal from plates using ESPG solution as for subcultivation. Cells were washed (pelleted and resuspended) 5 times with 3mL PBS to assure complete media removal and lysed using 300 μ L lysis buffer (Cell Signaling, containing AEBSF) as for western blot experiments (Sec. 3.4).

3.9.2 IP using an anti-MPA/AcMPAG antibody

LS180 cells were incubated with drugs for 72h without FBS and were redosed every 24h. Extraction and IP with an anti-MPA/AcMPAG antibody (kind gift of Thermo Scientific) were performed using the Pierce Classic IP Kit (Thermo Scientific) according to the protocol. A total amount of 1mg of total protein was used per IP reaction (suggested amount 0.5-1mg) and 10 μ g of affinity-purified antibody (suggested amount 2-10 μ g). Incubation time to form the immune complex was 24h with gentle end-over-end mixing at 4°C. Capture of the immune complex was performed according to protocol. The complex was eluted (3 times using 50 μ L buffer, respectively) using the low-pH elution option described in the protocol.

1D gel electrophoresis

Samples were prepared to contain 40 μ g protein per sample (20 μ g of H/L-labeled protein each) in NuPAGE LDS sample buffer (4X, diluted with water) to yield a

final volume of 20 μ L. Samples were heated for 10min under shaking at 90°C and loaded onto NuPAGE Bis-Tris 4-20% gradient gels (Invitrogen), which were run using MES SDS running buffer and an X-Cell II Mini Gel System (Invitrogen) at 200V, 120mA, 25W per gel for 30min. BenchMark Protein Ladder (Invitrogen) was used as a protein molecular mass marker. After visualizing proteins using Coomassie Blue (Invitrogen), each lane of the gel was cut into 25 bands of equal size always covering the same molecular weight ranges for all samples.

Tryptic digestion

Trypsin is widely used to break up proteins into peptides for MS analysis [384]. Tryptic cleavage occurs at the C-terminus of arginine and lysine residues and cleavage of isotopically labeled proteins yields labeled peptides. Analyzing mixtures of labeled and non-labeled peptides with C-terminal lysine, peptides show up in “peak pairs” of 6.0204Da difference.

In-gel tryptic digestion The first three cut out bands of each sample were cut into cubes and combined in one 0.6mL microcentrifuge tube. Consecutively, always two bands were cut into cubes and combined yielding 12 tubes/samples per lane. Gel bands were destained in 150 μ L 50% acetonitrile (ACN)/25mM ammonium bicarbonate (ABC) overnight. After removing the supernatant 150 μ L 50% ACN/25mM ABC were added and samples were vortexed on the shaker at medium speed for 15min. After the supernatant was removed a third washing step with 100% ACN was performed (150 μ L, 15min, vortexing). Disulfide bonds in proteins were reduced incubating with 100 μ L 10mM dithiothreitol (DTT) at 60°C for 30min and cysteine residues were alkylated with 100 μ L 20mM iodoacetamide (IAA) in the dark for 45min. Gel pieces were washed with distilled water for 15min twice, then washed once with ACN. The ACN was removed and the gel pieces were dried on a speed vac (Savant, Thermo Fischer). 100ng of trypsin were added to each sample and left at 4°C for 30min to rehydrate the gel plugs and then incubated at room temperature overnight. Tryptic digests were acidified with FA up to a final concentration of 1%. After vortexing for 15min, the digest solution was transferred to 0.65mL siliconized tubes. Peptides were extracted from the gel pieces two more times using 60 μ L 1% FA in 50% ACN and extracts were combined with the respective initial digestion supernatants. Samples were concentrated in a speed vac to the desired volume of 12 μ L, analyzed by LC-MS, and if necessary, stored at -20°C.

3 Materials and Methods

In-solution tryptic digestion 50 μ L/sample (to check for incorporation efficiency, sample volume was brought up to 50 μ L/sample with 50mM ABC) and 150 μ L/sample (for the IP experiment) were used for in-solution tryptic digestion (due to the IP the protein content was below the detection limits and the maximal amount of 150 μ L/sample was used). Digestion was performed following a modified Promega ProteaseMAX Surfactant (Trypsin Enhancer) protocol adjusted to a final volume of 50 μ L/sample and 150 μ L/sample instead of 100 μ L/sample for the assessment of incorporation efficiency and IP experiments, respectively. pH values of IP samples (eluted with low-pH elution buffer, Pierce Classic IP Kit) were adjusted to the optimal pH for trypsin digestion (pH 7.8-8.7) using 1M TRIS (pH 8.5, about 20 μ L/sample). Disulfide bonds in proteins were reduced by adding DTT to a final concentration of 20mM (stock 200mM) and heating at 56°C for 5min. Samples were cooled down on ice. Cystein residues were alkylated by adding IAA to a final concentration of 20mM (stock 200mM in 25mM ABC). Samples were vortexed, spun down, and incubated for 45min in the dark. 1% ProteaseMAX Surfactant and 1 μ g/ μ L trypsin (stock 1 μ g/ μ L in 50mM acetic acid) were added to final concentrations of 0.01% and 0.01 μ g/ μ L per sample, respectively. It was digested at 37°C overnight. FA was added to a concentration of 0.1% (stock 5% FA, about 4 μ L/sample).

For IP samples after trypsin digestion and addition of FA to a concentration of 0.1%, the pH of the samples was checked and more FA was added if necessary to adjust the pH to <4 to optimize sample binding to the resin of ZipTip Pipette Tips (Millipore). Samples were vortexed for 10min. ZipTip Pipette Tips (10 μ L) were activated by washing 3-4 times with 100% ACN and 3-4 times with 0.1% FA. Activated ZipTip Pipette Tips were used on 200 μ L pipettes on top of a 200 μ L tip and the complete sample was drawn through the Ziptip Pipette Tip multiple times. ZipTip Pipette Tips were put back onto a 10 μ L pipette, washed once with 0.1% FA and the sample was eluted from the ZipTip Pipette Tips by drawing up the elution buffer (50% ACN, 1% FA, 20 μ L/sample were pipetted into siliconized tubes) about 20 times while transferring the samples to siliconized tubes. Sample volumes were reduced using a speed vac until about 2 μ L/sample were left. About 10 μ L of 0.1% FA was added per sample to a final volume of 12 μ L. Samples were stored at -20°C until MS analysis.

HPLC-MS analysis

SILAC SILAC/Gel-C MS samples, samples of the initial screen, and a set of samples to guarantee sufficient incorporation of heavy lysine were analyzed on a LTQ-FT

Ultra hybrid mass spectrometer (Thermo Scientific). Peptide desalting and separation was achieved using a dual capillary/nano pump HPLC system (Agilent 1200, Palo Alto, CA). On this system 8 μ L of sample were loaded onto a ZORBAX 300SB-C18, 5 μ m (5x0.3mm) column (Agilent Technologies) to extract analytes and washed with 5% ACN + 0.1% FA at a flow rate of 15 μ L/min for 5min. The extraction column was switched online with the nano pump at a flow rate of 350nL/min. An 85min gradient from 8% ACN to 40% ACN was used to separate the peptides. The column was made from an in-house-pulled 360/100nm (outer/inner diameter) fused silica capillary packed with Jupiter C18 resin (Phenomenex, Torrance, CA). The column was kept at 40°C using an in-house-built column heater. Data acquisition was performed using Xcalibur software (version 2.0.6). The LC runs were monitored in positive ion mode by sequentially recording survey MS scans ($m/z = 400-2000$), in the ion cyclotron resonance cell, while three MS² were obtained in the ion trap via CID for the most intense ions. After two acquisitions of a given ion within 45s the ion was excluded for 150s.

IP experiment IP samples were analyzed on a LTQ Orbitrap XL mass spectrometer (Thermo Fisher Scientific) coupled to an Eksigent nanoLC-2D system through a nano ESI LC-MS interface. 8 μ L of sample were injected into a 10 μ L loop using the autosampler. To desalt the sample material was flushed out of the loop and loaded onto a ZORBAX 300SB-C18, 5 μ m (5x0.3mm) column (Agilent Technologies) for extraction of analytes and washed with 5% ACN + 0.1% FA at a flow rate of 1 μ L/min for 10min. The extraction column was switched online with the nano-pump at a flow rate of 350nL/min. The solvents were water + 0.1% FA (mobile phase A) and 99.9% ACN + 0.1% FA (mobile phase B). A 90min gradient from 6% ACN to 40% ACN was used to separate peptides. Peptides were separated on a house-made 100 μ m (inner diameter) x 150mm fused silica capillary packed with Jupiter C18 resin (Phenomex, Torrance, CA). Data acquisition was performed using Xcalibur software. The mass spectrometer was operated in the positive ion mode. The peptide ion masses were measured in the Orbitrap mass analyzer, whereas the peptide fragmentation was performed by CID in the linear ion trap analyzer using default settings. The ten most intense ions were selected for fragmentation in each scan cycle. Fragmented masses were excluded from further sequencing for 90s.

Database searching, protein identification, identification of covalent modifications

MS/MS spectra were extracted from raw data files and converted into mgf files using an in-house script. Mascot (Matrix Science Inc., London, UK; version 2.2) served to perform database searches against the human subset SwissProt database of the extracted MS/MS data. Peptide tolerance was set to ± 15 ppm with MS/MS tolerance set to ± 0.6 Da (spectra acquired from the LTQ-FT and LTQ Orbitrap). Full trypsin specificity was required and one missed cleavage was allowed. Carbamidomethylation on cysteine was defined as fixed modification, methionine oxidation and N-terminal acetylation were defined as variable modifications in the database search. For identification of covalent modifications of proteins by MPA/MPA metabolites Thermo Proteome Discoverer Deamon software (Thermo Scientific, version 1.1.0) was used in combination with Mascot which served to perform database searches. The modifications listed in Table 2.15 were defined as additional fixed modifications. The search was performed for potential modifications on all amino acids in groups of 5 amino acids per each run.

Scaffold Proteome software was used to validate MS/MS-based peptide and protein identifications. For each sample (12 samples a 2 bands) all Mascot DAT files were loaded together as one biological sample within Scaffold. Peptide identifications were accepted, if they could be established at greater than 95% probability as specified by the Peptide Prophet algorithm. Protein identifications were accepted, if they could be established at greater than 99% probability and contained at least one identified unique peptide.

MaxQuant software settings

Analysis of SILAC/GelC-MS data was performed using the MaxQuant software package (Max Planck Institute of Biochemistry, Martinsried, Germany, version 1.2.2.5). Parameters for “Peptide identification and quantification” were set as follows: Peptide false discovery rate (FDR): 0.01, Site FDR: 0.01, Max. peptide posterior error probability (PEP): 1, Min. peptides: 2, Min. razor + unique peptides: 1, Min. unique peptides: 1 (at greater than 99% probability). Only unmodified peptides were used and the modifications “Oxidation (M)”, “Acetyl (Protein N-term)”, and “Gln \rightarrow pyro-Glu”. Protein FDR was set to 0.01 and min. peptide length to 6 amino acids. Parameters for “MS/MS & sequences” were set to ± 15 ppm and ± 0.6 Da for MS/MS tolerance. As fixed modification “Carbamidomethyl (C)” was used. The human subset of the FASTA database (version 3.87) was used for MaxQuant analysis of

sequences.

DAVID/PANTHER software settings

(1) Employing DAVID's Functional Annotation tool (comprehending the three tools 1A-1C) default settings for annotations as of which databases to search were used, but the output was modified for further analysis using the provided tools.

(1A) LS180 cell and rat model data: For Functional Annotation Clustering Classification Stringency was customized (default medium): Kappa Similarity: Similarity Term Overlap = 4 (default 3 for medium), Similarity Threshold = 1.00 (default 0.50); Classification: Initial Group Membership = 4 (default 3), Final Group Membership = 4 (default 3), Multiple Linkage Threshold = 0.50 (default 0.50); Enrichment Thresholds: EASE score = 0.05.

(1A) Human non-cancer cell model data: For Functional Annotation Clustering, Classification Stringency was customized (default medium): Kappa Similarity: Similarity Term Overlap = 4 (default 3 for medium), Similarity Threshold = 1.00 (default 0.50); Classification: Initial Group Membership = 4 (default 3), Final Group Membership = 4 (default 3), Multiple Linkage Threshold = 0.50 (default 0.50); Enrichment Thresholds: EASE score = 0.05.

(1B) For the Functional Annotation Chart thresholds were customized: Count: 10, EASE: 0.05 (default 0.1).

(1C) Default settings were used, no customization possible.

(2) Using DAVID's Functional Classification tool Classification Stringency/search was customized: Kappa Similarity: Similarity Term Overlap = 4 (default 4), Similarity Threshold = 0.30 (default 0.35); Classification: Initial Group Membership = 4 (default 4), Final Group Membership = 3 (default 4), Multiple Linkage Threshold = 0.50 (default 0.50).

DAVID, PANTHER, and Pathway Palette analyses were performed in September 2012. As databases get continuously updated results may vary dependent on the time of analysis.

Statistics for analysis of proteomics data/EASE scores

Expression Analysis Systematic Explorer (EASE) is a customizable software application for biological data interpretation of gene lists resulting from high-throughput data sets generated by e.g. proteomics or microarray analysis [385]. The EASE method provides rapid, systematic, and robust analysis of given lists of genes and

is featured in DAVID analysis tools. A p-value of 0.05 is widely used as threshold for statistic significance of changes in data sets and is equivalent to 1.3 on a minus log scale [299] as which the EASE scores in DAVID are presented.

3.10 In vitro gut inflammation model

3.10.1 Cultivation of LS180 cells on cell culture inserts and TEER measurements

LS180 cells were cultivated on transwell inserts (Millipore, no. PIHT30R48) with a pore size of $0.4\mu\text{M}$ that were used in combination with 6-well cell culture multiwell plates (Millipore, no. PIMWS0650). LS180 cells were seeded onto inserts in different densities and grown for 1-7 days. Daily TEER measurements were performed using an EVOM2 Epithelial Voltohmmeter for TEER (World Precision Instruments) according to the manufacturer's instructions.

As TEER values indicated a not confluent monolayer at all times transwell inserts were coated with two different matrices to improve cell adhesion and growth characteristics. Human fibronectin (BD Biosciences) and rat tail collagen (BD Biosciences) served matrices. Inserts were coated according to the manufacturer's instructions.

Human fibronectin was used at different concentrations of $1\text{-}5\mu\text{g}/\text{cm}^2$. 1mg (1mg/vial) was resuspended in sterile distilled H_2O , diluted to the desired concentration using serum-free, $\text{Ca}^{2+}/\text{Mg}^{2+}$ -free culture medium (pH 7.4), added to the wells in appropriate amounts, and incubated at room temperature for 1h. The medium was aspirated and inserts rinsed with PBS.

Rat tail collagen was used at a concentration of $5\mu\text{g}/\text{cm}^2$. The stock (3.8mg/mL) was diluted to $25\mu\text{g}/\text{mL}$ using 0.02N acetic acid. The diluted material was added to inserts in appropriate amounts, inserts were incubated at room temperature for 1h, and the solution aspirated. Inserts were rinsed with PBS.

LS180 cells were seeded and grown on coated inserts as described before. Despite the coating TEER measurements indicated that LS180 cells do not grow into a confluent monolayer.

3.10.2 Treatment of RAW 264.7 cells

For western blot analysis RAW 264.7 cells were grown on standard cell culture dishes and not in 6-well plate due to the amount of material needed for the required

number of western blots. Only 8mL cell culture media per dish were used for incubations with test compounds to maintain the growth area to volume ratio that was dictated by the used 6-well plates in combination with the transwell inserts, that were planned to be used in following experiments. Cells were incubated with test compounds for 4h (media also contained 1000 μ M guanosine and no FBS) in phenol red-free media (as phenol red interferes with components of the BCA assay used for protein determination) and 7mL of cell culture media per plate were collected for western blot analysis (N=3). Cells were extracted for western blot analysis to measure β -actin. As no appropriate loading control (as which β -actin served for intracellular proteins) exists for proteins secreted into cell culture media a β -actin control was used for normalization. Cell lysates were assayed using the BCA assay for an estimate of concentration (concentrations were all within the same range) but were used unadjusted in terms of protein content (the same amount of lysate was used for all samples for the preparation for western blot analysis) so that normalization based on β -actin would at least account for deviances in cell number among samples.

3.10.3 Preparation of cell culture media for western blot analysis

Cell culture media were lyophilized and subsequently reconstituted in 500 μ L H₂O. BCA assays were run to determine the protein content of samples as described in Section 3.3. Samples were prepared for western blot analysis as described in Section 3.4 containing protein concentrations of 175 μ g/15 μ L to be able to load 175 μ g of protein per well for gel electrophoresis.

3.11 Statistics

Numerical data is presented as means \pm standard deviations. For statistical analysis SPSS software (versions 19 and 21) was used. Prior to statistical tests outliers and extreme values (analysis by boxplots) were removed. One-way analysis of variance (ANOVA) was used for comparison of more than two groups. To test for significant changes inbetween groups Scheffe's tests (unequal sample sizes due to removal of outliers and extreme values) were used as *post-hoc* tests. Significance levels were set at $p < 0.05$ (*), $p < 0.01$ (**), and $p < 0.001$ (***) .

EASE scores for data analysis of proteomics data as used by several ones of the online tools are described in Section 3.9.2.

List of Figures

0.1	Vorgeschlagene Mechanismen der GI Toxizität von MPA aufgeklärt durch das LS180-Zellkulturmodell in Kombination mit den verwendeten Methoden	5
0.2	Proposed molecular mechanisms of MPA's GI toxicity elucidated using the LS180 cell culture model and various methods	11
1.1	Chemical structures, sum formulas, and molecular weights of mycophenolic acid, enteric-coated mycophenolate sodium, mycophenolate mofetil, and 4-(2-Hydroxyethyl)morpholine	15
1.2	Pathways of purine biosynthesis and immunosuppressive mechanism of MPA	18
1.3	Metabolism of EC-MPS and MMF	23
1.4	MPA disposition	24
1.5	Correlation of GI events, MMF discontinuation, and graft survival . .	25
1.6	GI tract and supporting organs	26
1.7	Structure of the small intestine	27
1.8	Immune response of the mucosa to the gut flora	30
1.9	Relationship between transcriptomics (genomics), proteomics, and metabolomics	33
2.1	Western blots for determination of expression levels of MPA-metabolizing enzymes in LS180 cells in passages 7, 11, 15, and 19	40
2.2	Expression levels of MPA-metabolizing enzymes in LS180 cells in passages 7, 11, 15, and 19 as determined by densitometry analysis	41
2.3	Western blots for determination of expression levels of transporters of potential relevance for MPA in LS180 cells in passages 7, 11, 15, and 19	42
2.4	Expression levels of transporters of potential relevance for MPA in LS180 cells in passages 7, 11, 15, and 19 as determined by densitometry analysis	43

List of Figures

2.5	Western blots for determination of expression levels of pharmacodynamic target proteins of MPA in LS180 cells in passages 7, 11, 15, and 19	43
2.6	Expression levels of pharmacodynamic target proteins of MPA in LS180 cells in passages 7, 11, 15, and 19 as determined by densitometry analysis	44
2.7	Comparison of UGT1A8 message in LS180 cells in passages 7, 11, 15, and 19	44
2.8	Expression levels of MPA-metabolizing enzymes in LS180 cells after 24h of MPA treatment as determined by densitometry analysis	45
2.9	Expression levels of MPA efflux transporters and IMPDH isoform 1 and 2 in LS180 cells after 24h of MPA treatment as determined by densitometry analysis	46
2.10	Expression levels of MPA efflux transporters MRP1, MRP2, and MDR1 in LS180 cells after 72h of MPA treatment as determined by densitometry analysis	46
2.11	LDH activity in cell culture media of LS180 cells after treatment with a single dose and multiple doses of MPA for 24h, 48h (single dose and redosed every 24h), and 72h (single dose and redosed every 24h)	48
2.12	Western blots for determination of expression levels of caspase-3 and levels of cleaved caspase-3 in LS180 cells after treatment with increasing concentrations of MPA and 1000 μ M guanosine for 3h, 24h, and 72h	52
2.13	Expression levels of caspase-3 and levels of cleaved caspase-3 in LS180 cells after treatment with increasing concentrations of MPA and 1000 μ M guanosine for 3h, 24h, and 72h	53
2.14	Effects of drug treatment (single dose) on LS180 cell proliferation after 48h and 72h	55
2.15	Effects on LS180 cell proliferation after 24h, 48h, and 72h of MPA treatment and supplementation with 0, 100, 200, 400, and 1000 μ M guanosine (redosed every 24h, data sorted according to guanosine concentration)	58
2.16	Effects on LS180 cell proliferation after 24h, 48h, and 72h of MPA treatment and supplementation with 0, 100, 200, and 400 μ M guanosine (redosed every 24h, data sorted according to incubation time)	59

2.17	Effects on LS180 cell proliferation after 24h, 48h, 72h, and 5d of MPA treatment and supplementation with 1000 μ M guanosine (redosed every 24h, data sorted according to incubation time)	60
2.18	Effects on RAW 264.7 cell proliferation after 24h, 48h, and 72h of MPA treatment and supplementation with 0, 200, 400, and 1000 μ M guanosine (redosed every 24h, data sorted according to guanosine concentration)	61
2.19	Effects on RAW 264.7 cell proliferation after 24h, 48h, and 72h of MPA treatment and supplementation with 0, 200, 400, and 1000 μ M guanosine (redosed every 24h, data sorted according to incubation time)	62
2.20	Effects on CCD-18Co cell proliferation after 24h, 48h, 72h, and 5d of MPA treatment and supplementation with 0, 200, 400, and 1000 μ M guanosine (redosed every 24h, data sorted according to guanosine concentration)	64
2.21	Effects on CCD-18Co cell proliferation after 24h, 48h, 72h and 5d of MPA treatment and supplementation with 0, 200, 400, and 1000 μ M guanosine (redosed every 24h, data sorted according to incubation time)	65
2.22	Adenosine nucleotide levels of LS180 cells after 24h and 72h (redosed every 24h) of treatment with MPA and guanosine	73
2.23	Guanosine nucleotide levels of LS180 cells after 24h and 72h (redosed every 24h) of treatment with MPA and guanosine	74
2.24	Uridine nucleotide levels of LS180 cells after 24h and 72h (redosed every 24h) of treatment with MPA and guanosine	75
2.25	Cytidine nucleotide levels of LS180 cells after 24h and 72h (redosed every 24h) of treatment with MPA and guanosine	76
2.26	NAD ⁺ , NADP ⁺ , and FAD levels of LS180 cells after 24h and 72h (redosed every 24h) of treatment with MPA and guanosine	77
2.27	Energy charges of adenosine, guanosine, uridine, and cytidine nucleotides in LS180 cells after 24h and 72h (redosed every 24h) of treatment with MPA and guanosine	78
2.28	Western blots for determination of expression levels of Na ⁺ -K ⁺ -ATPase in LS180 cells after treatment with MPA and guanosine for 24h and 72h	81
2.29	Expression levels of Na ⁺ -K ⁺ -ATPase in LS180 cells after treatment with MPA and guanosine for 24h and 72h	82

List of Figures

2.30	cAMP and cGMP levels in LS180 cells after treatment with MPA and guanosine for 24h and 72h	83
2.31	Representative total ion chromatogram of all analytes included in the HPLC-MS method for quantification of MPA, MMF, and their metabolites	87
2.32	Ion chromatograms of calibrators (10.000 μ M) extracted with MeOH-ZnSO ₄ -solution of different pH values for stability experiments for MPA method development recorded in the internal standard channel	89
2.33	2D heat map (genes-to-terms 2D view) of genes and their major annotated terms in correlation to gene groups/annotation clusters 1-4	110
2.34	Network of proteins of enriched pathways and first-order shared neighbors constructed using Pathway Palette and the BioGRID database	116
2.35	Network of proteins of enriched pathways and first-order shared neighbors constructed using Pathway Palette and the HPRD database	117
2.36	PANTHER charts of gene ontology terms for molecular functions and biological processes of differentially expressed proteins in LS180 cells after MPA treatment	120
2.37	Requirement of UTP and GTP for glycoprotein synthesis	123
2.38	Western blots for confirmation of results of SILAC experiments	125
2.39	Western blot expression levels of representative proteins identified by SILAC and GelC-MS in LS180 cells after treatment with MPA and 1000 μ M guanosine for 72h	126
2.40	Western blots of additional potentially affected proteins as identified by Pathway Palette analysis	127
2.41	Western blot expression levels of representative proteins identified by Pathway Palette in LS180 cells after treatment with increasing concentrations of MPA and 1000 μ M guanosine for 72h	127
2.42	Commonly used atom numbering scheme for MPA	129
2.43	Irreversible binding of carboxylic acids to proteins by a nucleophilic displacement mechanism	130
2.44	Irreversible binding of acyl glucuronides to proteins by an imine mechanism	130
2.45	Western blot of LS180 cell lysates after 72h of MPA and/or fluconazole treatment and incubation with an anti-MPA/AcMPAG antibody	133
2.46	Western blot of LS180 cell lysates after 72h of MPA and/or fluconazole treatment in FBS-free media and incubation with an anti-MPA/AcMPAG antibody	135

2.47	Simulated ^1H NMR spectra of MPA and MPAG	139
2.48	Representative ^1H NMR spectra of LS180 cell extracts	140
2.49	Amounts of lactate and alanine and ^{13}C enrichments calculated from ^1H NMR spectra of LS180 cell extracts	142
2.50	Amounts of glutamate, glutamine, creatine, and phosphocreatine and PCr/Cr ratio calculated from ^1H NMR spectra of LS180 cell extracts	142
2.51	Amounts of remaining metabolites from ^1H NMR spectra of LS180 cell extracts	143
2.52	Representative ^{13}C NMR spectrum of an LS180 cell extract	145
2.53	Amounts of C4-labeled glutamate, glutamine, and glutamate in GSH calculated from ^{13}C NMR spectra of LS180 cell extracts	147
2.54	Amounts of C2-labeled glutamate and glutamine calculated from ^{13}C NMR spectra of LS180 cell extracts	147
2.55	^1H NMR spectra of LS180 lipid extracts	151
2.56	Changes in concentrations of cholesterol and certain fatty acid signals calculated from ^1H NMR spectra of LS180 lipid extracts	152
2.57	Changes in concentrations of phosphatidylcholine, trimethyl ammo- nium compounds, acyl glycerols, and mono- and polyunsaturated fatty acids calculated from ^1H NMR spectra of LS180 cell extracts . .	153
2.58	^1H - ^{13}C HSQC spectrum of ppm regions 0.0-3.0 (t1) and 10-40 (t2) of LS180 cell extracts	156
2.59	<i>In vitro</i> gut inflammation model	159
2.60	Western blots of inflammatory markers of cell culture media of RAW 264.7 cells after treatment with LPS, MPA, and AcMAG for 4h	162
2.61	Levels of inflammatory markers of cell culture media of RAW 264.7 cells after treatment with LPS, MPA, and AcMAG for 4h	163
2.62	Boxplot diagrams of levels of TNF- α and INF- γ measured in cell culture media of RAW 264.7 cells after treatment with LPS, MPA, and AcMPAG for 4h	163
2.63	Proposed molecular mechanisms of MPA's GI toxicity elucidated us- ing the LS180 cell culture model and various methods	168
4.1	Adenosine triphosphate levels of LS180 cells after 12h, 24h, and 48h of treatment with single doses of test compounds	244
4.2	Adenosine diphosphate levels of LS180 cells after 12h, 24h, and 48h of treatment with single doses of test compounds	245

List of Figures

4.3	Adenosine monophosphate levels of LS180 cells after 12h, 24h, and 48h of treatment with single doses of test compounds	246
4.4	Guanosine triphosphate levels of LS180 cells after 12h, 24h, and 48h of treatment with single doses of test compounds	247
4.5	Guanosine diphosphate levels of LS180 cells after 12h, 24h, and 48h of treatment with single doses of test compounds	248
4.6	Guanosine monophosphate levels of LS180 cells after 12h, 24h, and 48h of treatment with single doses of test compounds	249
4.7	Uridine triphosphate levels of LS180 cells after 12h, 24h, and 48h of treatment with single doses of test compounds	250
4.8	Uridine diphosphate levels of LS180 cells after 12h, 24h, and 48h of treatment with single doses of test compounds	251
4.9	Uridine monophosphate levels of LS180 cells after 12h, 24h, and 48h of treatment with single doses of test compounds	252
4.10	Cytidine triphosphate levels of LS180 cells after 12h, 24h, and 48h of treatment with single doses of test compounds	253
4.11	Cytidine diphosphate levels of LS180 cells after 12h, 24h, and 48h of treatment with single doses of test compounds	254
4.12	Cytidine monophosphate levels of LS180 cells after 12h, 24h, and 48h of treatment with single doses of test compounds	255
4.13	NAD ⁺ levels of LS180 cells after 12h, 24h, and 48h of treatment with single doses of test compounds	256
4.14	NADP ⁺ levels of LS180 cells after 12h, 24h, and 48h of treatment with single doses of test compounds	257
4.15	FAD levels of LS180 cells after 12h, 24h, and 48h of treatment with single doses of test compounds	258
4.16	Adenylate energy charge of LS180 cells after 12h, 24h, and 48h of treatment with single doses of test compounds	259
4.17	Guanylate energy charge of LS180 cells after 12h, 24h, and 48h of treatment with single doses of test compounds	260
4.18	Uridylate energy charge of LS180 cells after 12h, 24h, and 48h of treatment with single doses of test compounds	261
4.19	Cytidylate energy charge of LS180 cells after 12h, 24h, and 48h of treatment with single doses of test compounds	262
4.20	PANTHER chart of differentially expressed proteins involved in lipid metabolism in LS180 cells after MPA treatment	263

4.21	PANTHER chart of differentially expressed proteins involved in carbohydrate metabolism in LS180 cells after MPA treatment	264
4.22	PANTHER chart of differentially expressed proteins involved in developmental processes in LS180 cells after MPA treatment	265
4.23	PANTHER chart of differentially expressed proteins involved in transport processes in LS180 cells after MPA treatment	266
4.24	PANTHER chart of differentially expressed proteins according to protein class in LS180 cells after MPA treatment	267
4.25	KEGG pathway map 00071: Fatty acid metabolism	276
4.26	KEGG pathway map 00280: Valine, leucine, and isoleucine degradation	277
4.27	KEGG pathway map 05130: Pathogenic Escherichia Coli infection . .	278
4.28	KEGG pathway map 04540: Gap junction	279
4.29	KEGG pathway map 00640: Propanoate metabolism	280
4.30	KEGG pathway map 00062: Fatty acid elongation	281
4.31	KEGG pathway map 03320: PPAR signaling pathway	282
4.32	Metabolic fate of the ^{13}C label of $[1-^{13}\text{C}]$ glucose	288
4.33	^1H - ^{13}C HSQC spectrum of ppm regions 2.9-5.0 (t1) and 33-80 (t2) of an LS180 cell extract	289
4.34	^1H - ^{13}C HSQC spectrum of ppm regions 4.0-6.5 (t1) and 80-110 (t2) of an LS180 cell extract	290
4.35	^1H - ^{13}C HSQC spectrum of ppm regions 0.0-3.0 (t1)/10-60 (t2) of a lipophilic LS180 cell extract	291
4.36	^1H - ^{13}C HSQC spectrum of ppm regions 3.0-5.5 (t1)/40-75 (t2) and 5.0-5.5 (t1)/120-135 (t2) of a lipophilic LS180 cell extract	292
4.37	Western blot of LS180 cell lysates after 72h of MPA and/or fluconazole treatment in FBS-free media and incubation with an anti-MPA/AcMPAG antibody	293
4.38	Effects of fluconazole treatment on LS180 cell number and LDH activity in LS180 cell culture media after 72h (redosed every 24h) . . .	294

List of Tables

2.1	Influence of MPA, MMF, and MPA + morpholinoethanol on nucleotide levels and energy charge	68
2.2	Influence of exogenous guanosine on nucleotide levels and energy charge	79
2.3	LS180 proteins of levels increased by >30% after MPA treatment identified by SILAC	94
2.4	LS180 proteins of levels increased by >20% but <30% after MPA treatment identified by SILAC	95
2.5	LS180 proteins of levels decreased by >30% after MPA treatment identified by SILAC	96
2.6	LS180 proteins of levels decreased by <30% but >20% after MPA treatment identified by SILAC	97
2.7	Description of proteins with changed levels as identified by SILAC . .	98
2.8	Functional Annotation Clustering of 35 significantly affected genes/proteins after MPA treatment of LS180 cells by DAVID (Tool 1A) . .	106
2.9	Pathway Enrichment Analysis of 35 significantly affected genes/proteins after MPA treatment of LS180 cells (Tool 1B and KEGG)	107
2.10	Functional Annotation Chart focusing main terms involved in the biochemistry of 35 significantly affected genes/proteins after MPA treatment of LS180 cells by DAVID (Tool 1B)	108
2.11	Functional Annotation Classification of 35 significantly affected genes/proteins after MPA treatment of LS180 cells by DAVID (Tool 2) . . .	109
2.12	Description of additional proteins identified by Pathway Palette analysis using the BioGRID database	118
2.13	Description of additional proteins identified by Pathway Palette analysis using the HPRD database	119
2.14	Covalent protein modifications by MPA and MPA metabolites	131
2.15	Covalent protein adducts potentially identifiable by the IP experiment	132
2.16	Metabolite concentrations in LS180 cells after 72h of MPA treatment	141
2.17	Isotopomers derived in 1st and 2nd turn of the TCA cycle from [1- ¹³ C]glucose metabolized via PDH and PC, respectively.	144

List of Tables

2.18	Isotopomer concentrations in LS180 cells after 72h of MPA treatment	146
2.19	Changes in metabolic fluxes and number of TCA cycle turns in MPA-treated LS180 cells	148
2.20	Changes in concentrations of lipids/lipid compounds in LS180 cells after 72h of MPA treatment	150
3.1	Antibodies used for experiments elucidating the mechanisms of MPA GI toxicity	175
3.2	QPCR primers and conditions for analysis	176
3.3	Parameters for the recording of ^1H NMR spectra	178
3.4	Parameters for the recording of ^{13}C NMR spectra	178
3.5	Parameters of ^1H - ^{13}C HSQC NMR spectra	179
4.1	Proteins/genes identified in [175, 176, 294] to be affected by MPA treatment in rats	268
4.2	Proteins/genes identified in [295, 296] to be affected by MPA treatment in HEK-293 and CCRF-CEM cells, respectively	272
4.3	Functional Annotation Clustering of 74 genes/proteins affected by MPA treatment in rats	273
4.4	Pathway Enrichment Analysis of 74 proteins/genes affected by MPA treatment in rats	274
4.5	Functional Annotation Clustering of 22 proteins affected by MPA treatment in human cells of non-cancerous origin	275

Bibliography

- [1] C. R. Williams and J. L. Gooch. Calcineurin inhibitors and immunosuppression - a tale of two isoforms. *Expert Rev Mol Med*, 14:e14, Jul 2012.
- [2] Donate Life America. Statistics. <http://donatelife.net/understanding-donation/statistics/>, Oct 2012.
- [3] K. Budde, P. Glander, F. Diekmann, J. Waiser, L. Fritsche, D. Dragan, and H. H. Neumayer. Review of the immunosuppressant enteric-coated mycophenolate sodium. *Expert Opin Pharmacother*, 5(6):1333–1345, Jun 2004.
- [4] A. Bardsley-Elliot, S. Noble, and R. H. Foster. Mycophenolate mofetil: a review of its use in the management of solid organ transplantation. *BioDrugs*, 12(5):363–410, Nov 1999.
- [5] P. W. Clutterbuck and H. Raistrick. Studies in the biochemistry of microorganisms: the molecular constitution of the metabolic products of *Penicillium brevicompactum* Dierckx and related species. II. Mycophenolic acid. *Biochem J*, 27:654–667, Apr 1933.
- [6] R. Bentley and B. Goseo. Bartolomeo Gosio, 1863-1944: an appreciation. *Adv Appl Microbiol*, 48:229–250, 2001.
- [7] H. W. Florey and M. A. Jennings. Mycophenolic acid; an antibiotic from *Penicillium brevicompactum* Dierckx. *Lancet*, 1:46–49, Jan 1946.
- [8] R. H. Williams, D. H. Lively, D. C. DeLong, J. C. Cline, and M. J. Sweeny. Mycophenolic acid: antiviral and antitumor properties. *J Antibiot*, 21:463–464, Jul 1968.
- [9] S. Suzuki, T. Kimura, K. Ando, M. Sawada, and G. Tamura. Antitumor activity of mycophenolic acid. *J Antibiot*, 22:297–302, Jul 1969.
- [10] A. Mitsui and S. Suzuki. Immunosuppressive effect of mycophenolic acid. *J Antibiot*, 22:358–363, Aug 1969.

Bibliography

- [11] J. Encke, W. Uhl, W. Stremmel, and P. Sauer. Immunosuppression and modulation in liver transplantation. *Nephrol Dial Transplant*, 19 Suppl 4:v22–25, Jul 2004.
- [12] R. E. Morris, E. G. Hoyt, M. P. Murphy, E. M. Eugui, and A. C. Allison. Mycophenolic acid morpholinoethylester (RS-61443) is a new immunosuppressant that prevents and halts heart allograft rejection by selective inhibition of T- and B-cell purine synthesis. *Transplant Proc*, 22(4):1659–1662, Aug 1990.
- [13] P. Benhaim, J. P. Anthony, L. Ferreira, J. P. Borsanyi, and S. J. Mathes. Use of combination of low-dose cyclosporine and RS-61443 in a rat hindlimb model of composite tissue allotransplantation. *Transplantation*, 61(4):527–532, Feb 1996.
- [14] A. M. D'Alessandro, M. Rankin, J. McVey, G. R. Hafez, H. W. Sollinger, M. Kalayoglu, and F. O. Belzer. Prolongation of canine intestinal allograft survival with RS-61443, cyclosporine, and prednisone. *Transplantation*, 55(4):695–700, Apr 1993.
- [15] W. O. Bechstein, Y. Suzuki, T. Kawamura, B. Jaffee, A. Allison, D. A. Hullett, and H. W. Sollinger. Low-dose combination therapy of DUP-785 and RS-61443 prolongs cardiac allograft survival in rats. *Transpl Int*, 5 Suppl 1:S482–483, 1992.
- [16] P. S. Patel and I. R. Rifkin. Mycophenolate and nephrology. *Lupus*, 15:39–43, 2006.
- [17] H. W. Sollinger, M. H. Deierhoi, F. O. Belzer, A. G. Diethelm, and R. S. Kauffman. RS-61443 – a phase I clinical trial and pilot rescue study. *Transplantation*, 53(2):428–432, Feb 1992.
- [18] H. W. Sollinger, F. O. Belzer, M. H. Deierhoi, A. G. Diethelm, T. A. Gonwa, R. S. Kauffman, G. B. Klintmalm, S. V. McDiarmid, J. Roberts, and J. T. Rosenthal. RS-61443 (mycophenolate mofetil). A multicenter study for refractory kidney transplant rejection. *Ann Surg*, 216(4):513–518, Oct 1992.
- [19] H. W. Sollinger. Mycophenolate mofetil for the prevention of acute rejection in primary cadaveric renal allograft recipients. U.S. Renal Transplant Mycophenolate Mofetil Study Group. *Transplantation*, 60(3):225–232, Aug 1995.

- [20] M. Shipkova, V. W. Armstrong, M. Oellerich, and E. Wieland. Mycophenolate mofetil in organ transplantation: focus on metabolism, safety and tolerability. *Expert Opin Drug Metab Toxicol*, 1(3):505–526, Oct 2005.
- [21] G. Filler and I. Buffo. Safety considerations with mycophenolate sodium. *Expert Opin Drug Saf*, 6(4):445–449, Jul 2007.
- [22] D. Golshayan, M. Pascual, and B. Vogt. Mycophenolic acid formulations in adult renal transplantation - update on efficacy and tolerability. *Ther Clin Risk Manag*, 5(4):341–351, Aug 2009.
- [23] K. M. David, J. A. Morris, B. J. Steffen, K. S. Chi-Burris, V. P. Gotz, and R. D. Gordon. Mycophenolate mofetil vs. azathioprine is associated with decreased acute rejection, late acute rejection, and risk for cardiovascular death in renal transplant recipients with pre-transplant diabetes. *Clin Transplant*, 19(2):279–285, Apr 2005.
- [24] H. M. Kauffman, W. S. Cherikh, M. A. McBride, Y. Cheng, and D. W. Hanto. Post-transplant de novo malignancies in renal transplant recipients: the past and present. *Transpl Int*, 19(8):607–620, Aug 2006.
- [25] K. Budde, M. Durr, L. Liefeldt, H. H. Neumayer, and P. Glander. Enteric-coated mycophenolate sodium. *Expert Opin Drug Saf*, 9(6):981–994, Nov 2010.
- [26] D. C. Palmer, C. C. Tsai, S. T. Roodman, J. E. Codd, L. W. Miller, J. E. Sarafian, and G. A. Williams. Heart graft arteriosclerosis. An ominous finding on endomyocardial biopsy. *Transplantation*, 39:385–388, Apr 1985.
- [27] P. Halloran, T. Mathew, S. Tomlanovich, C. Groth, L. Hooftman, and C. Barker. Mycophenolate mofetil in renal allograft recipients: a pooled efficacy analysis of three randomized, double-blind, clinical studies in prevention of rejection. The International Mycophenolate Mofetil Renal Transplant Study Groups. *Transplantation*, 63(1):39–47, Jan 1997.
- [28] G. Ciancio, G. W. Burke, J. J. Gaynor, A. Mattiazzi, D. Roth, W. Kupin, M. Nicolas, P. Ruiz, A. Rosen, and J. Miller. A randomized long-term trial of tacrolimus and sirolimus versus tacrolimus and mycophenolate mofetil versus cyclosporine (NEORAL) and sirolimus in renal transplantation. I. Drug interactions and rejection at one year. *Transplantation*, 77(2):244–251, Jan 2004.

Bibliography

- [29] S. Vitko, R. Margreiter, W. Weimar, J. Dantal, H. G. Viljoen, Y. Li, A. Jappe, and N. Cretin. Everolimus (Certican) 12-month safety and efficacy versus mycophenolate mofetil in de novo renal transplant recipients. *Transplantation*, 78(10):1532–1540, Nov 2004.
- [30] EUROPEAN MYCOPHANOLATE MOFETIL COOPERATIVE STUDY GROUP. Mycophenolate mofetil in renal transplantation: 3-year results from the placebo-controlled trial. *Transplantation*, 68:391–396, 1999.
- [31] US RENAL TRANSPLAN MYCOPHANOLATE MOFETIL STUDY GROUP. Mycophenolate mofetil in cadaveric renal transplantation. *Am J Kidney Dis*, 34:296–303, 1999.
- [32] D. Abramowicz, D. Manas, M. Lao, Y. Vanrenterghem, D. Del Castillo, P. Wijnngaard, and S. Fung. Cyclosporine withdrawal from a mycophenolate mofetil-containing immunosuppressive regimen in stable kidney transplant recipients: a randomized, controlled study. *Transplantation*, 74:1725–1734, Dec 2002.
- [33] S. Bunnapradist, K. L. Lentine, T. E. Burroughs, B. W. Pinsky, K. L. Hardinger, D. C. Brennan, and M. A. Schnitzler. Mycophenolate mofetil dose reductions and discontinuations after gastrointestinal complications are associated with renal transplant graft failure. *Transplantation*, 82(1):102–107, Jul 2006.
- [34] M. Behrend. Adverse gastrointestinal effects of mycophenolate mofetil: aetiology, incidence and management. *Drug Saf*, 24(9):645–663, 2001.
- [35] S. Bunnapradist and P. M. Ambuhl. Impact of gastrointestinal-related side effects on mycophenolate mofetil dosing and potential therapeutic strategies. *Clin Transplant*, 22(6):815–821, 2008.
- [36] S. R. Knight, N. K. Russell, L. Barcena, and P. J. Morris. Mycophenolate mofetil decreases acute rejection and may improve graft survival in renal transplant recipients when compared with azathioprine: a systematic review. *Transplantation*, 87(6):785–794, Mar 2009.
- [37] K. Wang, H. Zhang, Y. Li, Q. Wei, H. Li, Y. Yang, and Y. Lu. Safety of mycophenolate mofetil versus azathioprine in renal transplantation: a systematic review. *Transplant Proc*, 36(7):2068–2070, Sep 2004.

- [38] L. Hedstrom, L. Gan, Y. G. Schlippe, T. Riera, and M. Seyedsayamdost. IMP dehydrogenase: the dynamics of drug selectivity. *Nucleic Acids Res Suppl*, (3):97–98, 2003.
- [39] V. Nair and Q. Shu. Inosine monophosphate dehydrogenase as a probe in antiviral drug discovery. *Antivir Chem Chemother*, 18(5):245–258, 2007.
- [40] P. Franchetti and M. Grifantini. Nucleoside and non-nucleoside IMP dehydrogenase inhibitors as antitumor and antiviral agents. *Curr Med Chem*, 6(7):599–614, Jul 1999.
- [41] A. C. Allison, T. Hovi, R. W. Watts, and A. D. Webster. The role of de novo purine synthesis in lymphocyte transformation. *Ciba Found Symp*, pages 207–224, 1977.
- [42] A. C. Allison and E. M. Eugui. Mycophenolate mofetil and its mechanisms of action. *Immunopharmacology*, 47(2-3):85–118, May 2000.
- [43] E. M. Eugui and A. C. Allison. Immunosuppressive activity of mycophenolate mofetil. *Ann N Y Acad Sci*, 685:309–329, Jun 1993.
- [44] N. A. Weimert, M. Derotte, R. R. Alloway, E. S. Woodle, and A. A. Vinks. Monitoring of inosine monophosphate dehydrogenase activity as a biomarker for mycophenolic acid effect: potential clinical implications. *Ther Drug Monit*, 29(2):141–149, Apr 2007.
- [45] KEGG PATHWAY Database. Purine Metabolism - Reference Pathway. <http://www.genome.jp/kegg/pathway/map/map00230.html>, Apr 2012.
- [46] R. A. Blaheta, K. Leckel, B. Wittig, D. Zenker, E. Oppermann, S. Harder, M. Scholz, S. Weber, H. Schuldes, A. Encke, and B. H. Markus. Inhibition of endothelial receptor expression and of T-cell ligand activity by mycophenolate mofetil. *Transpl Immunol*, 6(4):251–259, Dec 1998.
- [47] R. C. Garcia, P. Leoni, and A. C. Allison. Control of phosphoribosylpyrophosphate synthesis in human lymphocytes. *Biochem Biophys Res Commun*, 77(3):1067–1073, Aug 1977.
- [48] S. Bremer, R. Mandla, N. T. Vethe, I. Rasmussen, H. Rootwelt, P. D. Line, K. Midtvedt, and S. Bergan. Expression of IMPDH1 and IMPDH2 after transplantation and initiation of immunosuppression. *Transplantation*, 85(1):55–61, Jan 2008.

Bibliography

- [49] B. M. Goldstein and T. D. Colby. IMP dehydrogenase : structural aspects of inhibitor binding. *Curr Med Chem*, 6(7):519–536, Jul 1999.
- [50] M. Nagai, Y. Natsumeda, and G. Weber. Proliferation-linked regulation of type II IMP dehydrogenase gene in human normal lymphocytes and HL-60 leukemic cells. *Cancer Res*, 52(2):258–261, Jan 1992.
- [51] M. Shipkova, C. P. Strassburg, F. Braun, F. Streit, H. J. Grone, V. W. Armstrong, R. H. Tukey, M. Oellerich, and E. Wieland. Glucuronide and glucoside conjugation of mycophenolic acid by human liver, kidney, and intestinal microsomes. *Br J Pharmacol*, 132(5):1027–1034, Mar 2001.
- [52] Roche - MMF Medication Guide. http://www.accessdata.fda.gov/drugsatfda_docs/label/2009/050722s021,050723s019,050758s019,050759s024lbl.pdf, Apr 2012.
- [53] J. Builder, K. Landecker, D. Whitecross, and D. W. Piper. Aspirin esterase of gastric mucosal origin. *Gastroenterology*, 73(1):15–18, Jul 1977.
- [54] W. L. Doyle. Distribution of esterase in gastric mucosa. *J Gen Physiol*, 38(2):141–144, Nov 1954.
- [55] J. H. Nelson, R. G. Jensen, and R. E. Pitas. Pregastric esterase and other oral lipases – a review. *J Dairy Sci*, 60(3):327–362, Mar 1977.
- [56] L. Kass. Cytochemistry of esterases. *CRC Crit Rev Clin Lab Sci*, 10(2):205–223, 1979.
- [57] R. Bullingham, S. Monroe, A. Nicholls, and M. Hale. Pharmacokinetics and bioavailability of mycophenolate mofetil in healthy subjects after single-dose oral and intravenous administration. *J Clin Pharmacol*, 36(4):315–324, Apr 1996.
- [58] W. Arns. Noninfectious gastrointestinal (GI) complications of mycophenolic acid therapy: a consequence of local GI toxicity? *Transplant Proc*, 39(1):88–93, Jan 2007.
- [59] P. Bolin, R. Gohh, R. Kandaswamy, F. S. Shihab, A. Wiland, F. Akhlaghi, and K. Melancon. Mycophenolic acid in kidney transplant patients with diabetes mellitus: does the formulation matter? *Transplant Rev (Orlando)*, 25(3):117–123, Jul 2011.

- [60] S. E. Tett, F. Saint-Marcoux, C. E. Staatz, M. Brunet, A. A. Vinks, M. Miura, P. Marquet, D. R. Kuypers, T. van Gelder, and D. Cattaneo. Mycophenolate, clinical pharmacokinetics, formulations, and methods for assessing drug exposure. *Transplant Rev (Orlando)*, 25(2):47–57, Apr 2011.
- [61] W. A. Lee, L. Gu, A. R. Miksztal, N. Chu, K. Leung, and P. H. Nelson. Bioavailability improvement of mycophenolic acid through amino ester derivatization. *Pharm Res*, 7(2):161–166, Feb 1990.
- [62] D. Cattaneo, M. Cortinovis, S. Baldelli, A. Bitto, E. Gotti, G. Remuzzi, and N. Perico. Pharmacokinetics of mycophenolate sodium and comparison with the mofetil formulation in stable kidney transplant recipients. *Clin J Am Soc Nephrol*, 2(6):1147–1155, Nov 2007.
- [63] B. C. de Winter, T. van Gelder, P. Glander, D. Cattaneo, H. Tedesco-Silva, I. Neumann, L. Hilbrands, R. M. van Hest, M. D. Pescovitz, K. Budde, and R. A. Mathot. Population pharmacokinetics of mycophenolic acid : a comparison between enteric-coated mycophenolate sodium and mycophenolate mofetil in renal transplant recipients. *Clin Pharmacokinet*, 47(12):827–838, Dec 2008.
- [64] K. Budde, S. Bauer, P. Hambach, U. Hahn, H. Roblitz, I. Mai, F. Diekmann, H. H. Neumayer, and P. Glander. Pharmacokinetic and pharmacodynamic comparison of enteric-coated mycophenolate sodium and mycophenolate mofetil in maintenance renal transplant patients. *Am J Transplant*, 7(4):888–898, Apr 2007.
- [65] M. Miura, S. Satoh, K. Inoue, H. Kagaya, M. Saito, T. Inoue, T. Suzuki, and T. Habuchi. Influence of SLCO1B1, 1B3, 2B1 and ABCB2 genetic polymorphisms on mycophenolic acid pharmacokinetics in Japanese renal transplant recipients. *Eur J Clin Pharmacol*, 63(12):1161–1169, Dec 2007.
- [66] M. Shipkova, V. W. Armstrong, L. Weber, P. D. Niedmann, E. Wieland, J. Haley, B. Tonshoff, and M. Oellerich. Pharmacokinetics and protein adduct formation of the pharmacologically active acyl glucuronide metabolite of mycophenolic acid in pediatric renal transplant recipients. *Ther Drug Monit*, 24:390–399, Jun 2002.
- [67] R. E. Bullingham, A. J. Nicholls, and B. R. Kamm. Clinical pharmacokinetics of mycophenolate mofetil. *Clin Pharmacokinet*, 34(6):429–455, Jun 1998.

Bibliography

- [68] M. Shipkova, V. W. Armstrong, E. Wieland, P. D. Niedmann, E. Schutz, G. Brenner-Weiss, M. Voihsel, F. Braun, and M. Oellerich. Identification of glucoside and carboxyl-linked glucuronide conjugates of mycophenolic acid in plasma of transplant recipients treated with mycophenolate mofetil. *Br J Pharmacol*, 126:1075–1082, Mar 1999.
- [69] N. Picard, T. Cresteil, A. Premaud, and P. Marquet. Characterization of a phase 1 metabolite of mycophenolic acid produced by CYP3A4/5. *Ther Drug Monit*, 26:600–608, Dec 2004.
- [70] G. Redlich, U. M. Zanger, S. Riedmaier, N. Bache, A. B. Giessing, M. Eisenacher, C. Stephan, H. E. Meyer, O. N. Jensen, and K. Marcus. Distinction between human cytochrome P450 (CYP) isoforms and identification of new phosphorylation sites by mass spectrometry. *J Proteome Res*, 7(11):4678–4688, Nov 2008.
- [71] Q. Mao and J. D. Unadkat. Role of the breast cancer resistance protein (ABCG2) in drug transport. *AAPS J*, 7:E118–133, 2005.
- [72] D. A. Hesselink, R. M. van Hest, R. A. Mathot, F. Bonthuis, W. Weimar, R. W. de Bruin, and T. van Gelder. Cyclosporine interacts with mycophenolic acid by inhibiting the multidrug resistance-associated protein 2. *Am J Transplant*, 5(5):987–994, May 2005.
- [73] M. Naganuma, T. Shiga, A. Kawai, H. Kawarai, T. Hayashi, N. Matsuda, E. Fujii, H. Kurosawa, and H. Kasanuki. Influence of food on plasma concentration of mycophenolic acid in a heart transplant patient receiving concomitant tacrolimus. *J Heart Lung Transplant*, 22(9):1065–1066, Sep 2003.
- [74] R. P. Pelletier, B. Akin, M. L. Henry, G. L. Bumgardner, E. A. Elkhammas, A. Rajab, and R. M. Ferguson. The impact of mycophenolate mofetil dosing patterns on clinical outcome after renal transplantation. *Clin Transplant*, 17(3):200–205, Jun 2003.
- [75] J. C. Tierce, J. Porterfield-Baxa, A. A. Petrilla, A. Kilburg, and R. M. Ferguson. Impact of mycophenolate mofetil (MMF)-related gastrointestinal complications and MMF dose alterations on transplant outcomes and healthcare costs in renal transplant recipients. *Clin Transplant*, 19(6):779–784, Dec 2005.
- [76] A. P. Legorreta, M. Robinson, A. S. Gilmore, and S. Feng. Gastrointestinal event associate dose reduction and discontinuation of renal transplant patients receiving MMF. *Transplantation*, 82 Suppl 3, 2006.

- [77] K. L. Hardinger, D. C. Brennan, J. Lowell, and M. A. Schnitzler. Long-term outcome of gastrointestinal complications in renal transplant patients treated with mycophenolate mofetil. *Transpl Int*, 17(10):609–616, Nov 2004.
- [78] A. Vander, J. Sherman, and Duciano D. *Human physiology, The mechanisms of body function, eighth edition*, pages 553–591. M. D. Lange, 2001.
- [79] S. C. Gad. *Toxicology of the gastrointestinal tract*, pages 2–34. CRC Press, Taylor and Francis Group, 2007.
- [80] S. Silbernagl and A. Despopoulos. *Color Atlas of Physiology, sixth edition*, pages 228–267. Thieme Stuttgart, New York, 2009.
- [81] S. A. Rajasekaran. Therapeutic potential of curcumin in gastrointestinal diseases. *World J Gastrointest Pathophysiol*, 2:1–14, Feb 2011.
- [82] G. J. Mahler, M. B. Esch, R. P. Glahn, and M. L. Shuler. Characterization of a gastrointestinal tract microscale cell culture analog used to predict drug toxicity. *Biotechnol Bioeng*, 104:193–205, Sep 2009.
- [83] A. Swidsinski, V. Loening-Baucke, and A. Herber. Mucosal flora in Crohn’s disease and ulcerative colitis - an overview. *J Physiol Pharmacol*, 60 Suppl 6:61–71, Dec 2009.
- [84] A. Di Sabatino, L. Rovedatti, F. Vidali, T. T. Macdonald, and G. R. Corazza. Recent advances in understanding Crohn’s disease. *Intern Emerg Med*, May 2011.
- [85] D. K. Podolsky. Inflammatory bowel disease. *N Engl J Med*, 347(6):417–429, Aug 2002.
- [86] T. T. Macdonald and G. Monteleone. Immunity, inflammation, and allergy in the gut. *Science*, 307(5717):1920–1925, Mar 2005.
- [87] A. U. Dignass. Mechanisms and modulation of intestinal epithelial repair. *Inflamm Bowel Dis*, 7(1):68–77, Feb 2001.
- [88] R. J. Playford and S. Ghosh. Cytokines and growth factor modulators in intestinal inflammation and repair. *J Pathol*, 205(4):417–425, Mar 2005.
- [89] G. R. Martin and J. L. Wallace. Gastrointestinal inflammation: a central component of mucosal defense and repair. *Exp Biol Med (Maywood)*, 231(2):130–137, Feb 2006.

Bibliography

- [90] C. L. Cummins, L. M. Mangravite, and L. Z. Benet. Characterizing the expression of CYP3A4 and efflux transporters (P-gp, MRP1, and MRP2) in CYP3A4-transfected Caco-2 cells after induction with sodium butyrate and the phorbol ester 12-O-tetradecanoylphorbol-13-acetate. *Pharm Res*, 18:1102–1109, Aug 2001.
- [91] A. Gupta, G. M. Mugundu, P. B. Desai, K. E. Thummel, and J. D. Unadkat. Intestinal human colon adenocarcinoma cell line LS180 is an excellent model to study pregnane X receptor, but not constitutive androstane receptor, mediated CYP3A4 and multidrug resistance transporter 1 induction: studies with anti-human immunodeficiency virus protease inhibitors. *Drug Metab Dispos*, 36:1172–1180, Jun 2008.
- [92] D. P. Hartley, X. Dai, J. Yabut, X. Chu, O. Cheng, T. Zhang, Y. D. He, C. Roberts, R. Ulrich, R. Evers, and D. C. Evans. Identification of potential pharmacological and toxicological targets differentiating structural analogs by a combination of transcriptional profiling and promoter analysis in LS-180 and Caco-2 adenocarcinoma cell lines. *Pharmacogenet Genomics*, 16:579–599, Aug 2006.
- [93] S. Resta-Lenert, S. Das, S. K. Batra, and S. B. Ho. MUC17 protects intestinal epithelial cells from enteroinvasive E. coli infection by promoting epithelial barrier integrity. *Am J Physiol Gastrointest Liver Physiol*, Mar 2011.
- [94] X. D. Bu, N. Li, X. Q. Tian, and P. L. Huang. Caco-2 and LS174T cell lines provide different models for studying mucin expression in colon cancer. *Tissue Cell*, 43:201–206, Jun 2011.
- [95] M. L. Enss, M. Cornberg, S. Wagner, A. Gebert, M. Henrichs, R. Eisenblatter, W. Beil, R. Kownatzki, and H. J. Hedrich. Proinflammatory cytokines trigger MUC gene expression and mucin release in the intestinal cancer cell line LS180. *Inflamm Res*, 49:162–169, Apr 2000.
- [96] No authors listed. Biomarkers and surrogate endpoints: preferred definitions and conceptual framework. *Clin Pharmacol Ther*, 69(3):89–95, Mar 2001.
- [97] U. Christians, V. Schmitz, W. Schoning, J. Bendrick-Peart, J. Klawitter, M. Haschke, and J. Klawitter. Toxicodynamic therapeutic drug monitoring of immunosuppressants: promises, reality, and challenges. *Ther Drug Monit*, 30(2):151–158, Apr 2008.

- [98] J. K. Nicholson, J. Connelly, J. C. Lindon, and E. Holmes. Metabonomics: a platform for studying drug toxicity and gene function. *Nat Rev Drug Discov*, 1(2):153–161, Feb 2002.
- [99] J. K. Nicholson, J. C. Lindon, and E. Holmes. “Metabonomics”: understanding the metabolic responses of living systems to pathophysiological stimuli via multivariate statistical analysis of biological NMR spectroscopic data. *Xenobiotica*, 29(11):1181–1189, Nov 1999.
- [100] K. Kienzl-Wagner, J. Pratschke, and G. Brandacher. Proteomics – a blessing or a curse? Application of proteomics technology to transplant medicine. *Transplantation*, 92(5):499–509, Sep 2011.
- [101] W. B. Dunn, N. J. Bailey, and H. E. Johnson. Measuring the metabolome: current analytical technologies. *Analyst*, 130(5):606–625, May 2005.
- [102] C. Zwingmann, D. Leibfritz, and A. S. Hazell. Brain energy metabolism in a sub-acute rat model of manganese neurotoxicity: an ex vivo nuclear magnetic resonance study using [1-¹³C]glucose. *Neurotoxicology*, 25:573–587, Jun 2004.
- [103] N. Serkova, L. Litt, D. Leibfritz, B. Hausen, R. E. Morris, T. L. James, L. Z. Benet, and U. Christians. The novel immunosuppressant SDZ-RAD protects rat brain slices from cyclosporine-induced reduction of high-energy phosphates. *Br J Pharmacol*, 129(3):485–492, Feb 2000.
- [104] A. Collett, J. Tanianis-Hughes, and G. Warhurst. Rapid induction of P-glycoprotein expression by high permeability compounds in colonic cells in vitro: a possible source of transporter mediated drug interactions? *Biochem Pharmacol*, 68:783–790, Aug 2004.
- [105] J. P. Krise, J. Zygmunt, G. I. Georg, and V. J. Stella. Novel prodrug approach for tertiary amines: synthesis and preliminary evaluation of N-phosphonoxyethyl prodrugs. *J Med Chem*, 42(16):3094–3100, Aug 1999.
- [106] E. E. Englung. *Synthetic Progress Toward Parvistemonine, Spiroxins A and B, and Generation of Palmarumycin Analogues*, page 103. Englung, E. E., 2002.
- [107] H. Spahn-Langguth and L. Z. Benet. Acyl glucuronides revisited: is the glucuronidation process a toxification as well as a detoxification mechanism? *Drug Metab Rev*, 24(1):5–47, 1992.

Bibliography

- [108] M. Shipkova, E. Schutz, I. Besenthal, P. Fraunberger, and E. Wieland. Investigation of the crossreactivity of mycophenolic acid glucuronide metabolites and of mycophenolate mofetil in the CEDIA MPA assay. *Ther Drug Monit*, 32(1):79–85, Feb 2010.
- [109] C. A. Jonsson and H. Carlsten. Mycophenolic acid inhibits inosine 5'-monophosphate dehydrogenase and suppresses immunoglobulin and cytokine production of B cells. *Int Immunopharmacol*, 3(1):31–37, Jan 2003.
- [110] C. A. Jonsson and H. Carlsten. Mycophenolic acid inhibits inosine 5'-monophosphate dehydrogenase and suppresses production of pro-inflammatory cytokines, nitric oxide, and LDH in macrophages. *Cell Immunol*, 216(1-2):93–101, 2002.
- [111] E. F. Brandon, T. M. Bosch, M. J. Deenen, R. Levink, E. van der Wal, J. B. van Meerveld, M. Bijl, J. H. Beijnen, J. H. Schellens, and I. Meijerman. Validation of in vitro cell models used in drug metabolism and transport studies; genotyping of cytochrome P450, phase II enzymes and drug transporter polymorphisms in the human hepatoma (HepG2), ovarian carcinoma (IGROV-1) and colon carcinoma (CaCo-2, LS180) cell lines. *Toxicol Appl Pharmacol*, 211(1):1–10, Feb 2006.
- [112] E. G. van de Kerkhof, I. A. de Graaf, and G. M. Groothuis. In vitro methods to study intestinal drug metabolism. *Curr Drug Metab*, 8(7):658–675, Oct 2007.
- [113] A. Pfrunder, H. Gutmann, C. Beglinger, and J. Drewe. Gene expression of CYP3A4, ABC-transporters (MDR1 and MRP1-MRP5) and hPXR in three different human colon carcinoma cell lines. *J Pharm Pharmacol*, 55(1):59–66, Jan 2003.
- [114] L. Z. Benet and C. L. Cummins. The drug efflux-metabolism alliance: biochemical aspects. *Adv Drug Deliv Rev*, 50 Suppl 1:3–11, Oct 2001.
- [115] Q. Li, Y. Sai, Y. Kato, I. Tamai, and A. Tsuji. Influence of drugs and nutrients on transporter gene expression levels in Caco-2 and LS180 intestinal epithelial cell lines. *Pharm Res*, 20(8):1119–1124, Aug 2003.
- [116] R. E. Watkins, G. B. Wisely, L. B. Moore, J. L. Collins, M. H. Lambert, S. P. Williams, T. M. Willson, S. A. Kliewer, and M. R. Redinbo. The human

- nuclear xenobiotic receptor PXR: structural determinants of directed promiscuity. *Science*, 292(5525):2329–2333, Jun 2001.
- [117] H. A. Engman, H. Lennernas, J. Taipalensuu, C. Otter, B. Leidvik, and P. Artursson. CYP3A4, CYP3A5, and MDR1 in human small and large intestinal cell lines suitable for drug transport studies. *J Pharm Sci*, 90(11):1736–1751, Nov 2001.
- [118] F. M. Ingels and P. F. Augustijns. Biological, pharmaceutical, and analytical considerations with respect to the transport media used in the absorption screening system Caco-2. *J Pharm Sci*, 92(8):1545–1558, Aug 2003.
- [119] L. G. Baggetto. Deviant energetic metabolism of glycolytic cancer cells. *Biochimie*, 74:959–974, Nov 1992.
- [120] W. Lee, A. Belkhir, A. C. Lockhart, N. Merchant, H. Glaeser, E. I. Harris, M. K. Washington, E. M. Brunt, A. Zaika, R. B. Kim, and W. El-Rifai. Overexpression of OATP1B3 confers apoptotic resistance in colon cancer. *Cancer Res*, 68(24):10315–10323, Dec 2008.
- [121] A. Lampen, A. Bader, T. Bestmann, M. Winkler, L. Witte, and J. T. Borlak. Catalytic activities, protein- and mRNA-expression of cytochrome P450 isoenzymes in intestinal cell lines. *Xenobiotica*, 28(5):429–441, May 1998.
- [122] A. Nakamura, M. Nakajima, H. Yamanaka, R. Fujiwara, and T. Yokoi. Expression of UGT1A and UGT2B mRNA in human normal tissues and various cell lines. *Drug Metab Dispos*, 36(8):1461–1464, Aug 2008.
- [123] J. Fan, H. J. Maeng, Y. Du, D. Kwan, and K. S. Pang. Transport of 5,5-diphenylbarbituric acid and its precursors and their effect on P-gp, MRP2 and CYP3A4 in Caco-2 and LS180 cells. *Eur J Pharm Sci*, 42(1-2):19–29, Jan 2011.
- [124] S. Fukumori, M. Masago, K. Ishida, Y. Kayano, M. Taguchi, and Y. Hashimoto. Temperature-dependent specific transport of levofloxacin in human intestinal epithelial LS180 cells. *Biopharm Drug Dispos*, 30(8):448–456, Nov 2009.
- [125] Abcam: Why is the actual band size different from the predicted? http://www.abcam.com/assets/popups/popup_bandhelp.htm, Sept 2011.

Bibliography

- [126] C. Peiser, M. Riebe-Imre, M. Emura, and U. Mohr. Influence of culture passages on growth kinetics, xenobiotic metabolism, chromosomal stability and transformation in a clonal fetal hamster lung epithelial cell line. *Mutat Res*, 289(2):281–290, Oct 1993.
- [127] E. M. Earley. Growth characteristics, cytogenetic stability and virus susceptibility of cell lines from New Zealand rabbits. *Dev Biol Stand*, 37:35–39, Dec 1976.
- [128] H. Yu, T. J. Cook, and P. J. Sinko. Evidence for diminished functional expression of intestinal transporters in Caco-2 cell monolayers at high passages. *Pharm Res*, 14(6):757–762, Jun 1997.
- [129] C. Q. Xia, M. N. Milton, and L. S. Gan. Evaluation of drug-transporter interactions using in vitro and in vivo models. *Curr Drug Metab*, 8(4):341–363, May 2007.
- [130] E. G. Schuetz, W. T. Beck, and J. D. Schuetz. Modulators and substrates of P-glycoprotein and cytochrome P4503A coordinately up-regulate these proteins in human colon carcinoma cells. *Mol Pharmacol*, 49(2):311–318, Feb 1996.
- [131] D. A. Glesne, F. R. Collart, and E. Huberman. Regulation of IMP dehydrogenase gene expression by its end products, guanine nucleotides. *Mol Cell Biol*, 11(11):5417–5425, Nov 1991.
- [132] A. Dzidic, C. Prgomet, A. Mohr, K. Meyer, J. Bauer, H. H. Meyer, and M. W. Pfaffl. Effects of mycophenolic acid on inosine monophosphate dehydrogenase I and II mRNA expression in white blood cells and various tissues in sheep. *J Vet Med A Physiol Pathol Clin Med*, 53(4):163–169, May 2006.
- [133] S. Harmsen, I. Meijerman, C. L. Febus, R. F. Maas-Bakker, J. H. Beijnen, and J. H. Schellens. PXR-mediated induction of P-glycoprotein by anticancer drugs in a human colon adenocarcinoma-derived cell line. *Cancer Chemother Pharmacol*, 66(4):765–771, Sep 2010.
- [134] U. I. Schwarz, H. Hanso, R. Oertel, S. Miehle, E. Kuhlisch, H. Glaeser, M. Hitzl, G. K. Dresser, R. B. Kim, and W. Kirch. Induction of intestinal P-glycoprotein by St John’s wort reduces the oral bioavailability of talinolol. *Clin Pharmacol Ther*, 81(5):669–678, May 2007.

- [135] D. R. Mudra, K. E. Desino, and P. V. Desai. In silico, in vitro and in situ models to assess interplay between CYP3A and P-gp. *Curr Drug Metab*, 12(8):750–773, Oct 2011.
- [136] I. A. Hauser, L. Renders, H. H. Radeke, R. B. Sterzel, and M. Goppelt-Struebe. Mycophenolate mofetil inhibits rat and human mesangial cell proliferation by guanosine depletion. *Nephrol Dial Transplant*, 14(1):58–63, Jan 1999.
- [137] Roche Applied Science. Apoptosis Manual 4th Edition, Chapter 6. https://www.roche-applied-science.com/sis/apoptosis/docs/Apoptosis_Manual_4th_edition_Chapter_06.pdf, Nov 2011.
- [138] Roche Applied Science. Apoptosis Manual 4th Edition, Chapter 1. https://www.roche-applied-science.com/sis/apoptosis/docs/Apoptosis_Manual_4th_edition_Chapter_01.pdf, Nov 2011.
- [139] D. Sabuda-Widemann, B. Grabensee, C. Schwandt, and C. Blume. Mycophenolic acid inhibits the autocrine PDGF-B synthesis and PDGF-BB-induced mRNA expression of Egr-1 in rat mesangial cells. *Nephrol Dial Transplant*, 24(1):52–61, Jan 2009.
- [140] R. G. Cohn, A. Mirkovich, B. Dunlap, P. Burton, S. H. Chiu, E. Eugui, and J. P. Caulfield. Mycophenolic acid increases apoptosis, lysosomes and lipid droplets in human lymphoid and monocytic cell lines. *Transplantation*, 68(3):411–418, Aug 1999.
- [141] I. Dubus, B. Vendrely, I. Christophe, J. P. Labouyrie, Y. Delmas, J. Bonnet, and C. Combe. Mycophenolic acid antagonizes the activation of cultured human mesangial cells. *Kidney Int*, 62(3):857–867, Sep 2002.
- [142] R. Kaczmarek, E. Zaczynska, and M. Misiuk-Hojlo. Antiproliferative properties of mycophenolic acid on human retinal pigment epithelial cells in vitro. *Klin Oczna*, 112(7-9):201–204, 2010.
- [143] J. V. Thottassery, G. P. Zambetti, K. Arimori, E. G. Schuetz, and J. D. Schuetz. p53-dependent regulation of MDR1 gene expression causes selective resistance to chemotherapeutic agents. *Proc Natl Acad Sci USA*, 94(20):11037–11042, Sep 1997.
- [144] A. G. Porter and R. U. Janicke. Emerging roles of caspase-3 in apoptosis. *Cell Death Differ*, 6(2):99–104, Feb 1999.

Bibliography

- [145] J. Lee, M.S. Kim, E.Y. Kim, K.S. Park, C.Y. Chang, K.S. Park, D.Y. Jung, C.H. Kwon, J.W. Joh, and S.J. Kim. Mycophenolate mofetil promotes down-regulation of expanded B cells and production of TNF-alpha in an experimental murine model of colitis. *Cytokine*, 44(1):49–56, Jul 2008.
- [146] E. Andrikos, A. Yavuz, V. Bordoni, R. Ratanarat, M. De Cal, M. Bonello, G. Salvatori, N. Levin, G. Yakupoglu, M. Pappas, and C. Ronco. Effect of cyclosporine, mycophenolate mofetil, and their combination with steroids on apoptosis in a human cultured monocytic U937 cell line. *Transplant Proc*, 37(7):3226–3229, Sep 2005.
- [147] E. Messina, F. Savini, R. Lisio, C. P. Quaratino, and A. Giacomello. Neuroblastoma cell apoptosis induced by mycophenolic acid. *Adv Exp Med Biol*, 431:461–464, 1998.
- [148] E. Messina, P. Gazzaniga, V. Micheli, M. R. Guaglianone, S. Barbato, S. Morrone, L. Frati, A. M. Agliano, and A. Giacomello. Guanine nucleotide depletion triggers cell cycle arrest and apoptosis in human neuroblastoma cell lines. *Int J Cancer*, 108(6):812–817, Mar 2004.
- [149] A. Meshkini, R. Yazdanparast, and K. Nouri. Intracellular GTP level determines cell's fate toward differentiation and apoptosis. *Toxicol Appl Pharmacol*, 253(3):188–196, Jun 2011.
- [150] X. L. Zhu, L. Li, J. M. Shi, W. Y. Zheng, J. Yu, and H. Huang. Mycophenolic acid induced apoptosis in T lymphocytic cells Molt-4 and its mechanism. *Zhejiang Da Xue Xue Bao Yi Xue Ban*, 34(4):339–343, Jul 2005.
- [151] J. Zhou, M. Liu, Y. Zhai, and W. Xie. The antiapoptotic role of pregnane X receptor in human colon cancer cells. *Mol Endocrinol*, 22(4):868–880, Apr 2008.
- [152] T. J. Franklin, V. Jacobs, G. Jones, P. Ple, and P. Bruneau. Glucuronidation associated with intrinsic resistance to mycophenolic acid in human colorectal carcinoma cells. *Cancer Res*, 56(5):984–987, Mar 1996.
- [153] T. Lin, L. Meng, and R. Y. Tsai. GTP depletion synergizes the anti-proliferative activity of chemotherapeutic agents in a cell type-dependent manner. *Biochem Biophys Res Commun*, 414(2):403–408, Oct 2011.
- [154] J. A. Yalowitz, K. Pankiewicz, S. E. Patterson, and H. N. Jayaram. Cytotoxicity and cellular differentiation activity of methylenebis(phosphonate) analogs

- of tiazofurin and mycophenolic acid adenine dinucleotide in human cancer cell lines. *Cancer Lett*, 181(1):31–38, Jul 2002.
- [155] M. E. Forgue-Lafitte, A. M. Coudray, B. Breant, and J. Mester. Proliferation of the human colon carcinoma cell line HT29: autocrine growth and deregulated expression of the *c-myc* oncogene. *Cancer Res*, 49(23):6566–6571, Dec 1989.
- [156] A. B. Das, P. Loying, and B. Bose. Human recombinant Cripto-1 increases doubling time and reduces proliferation of HeLa cells independent of pro-proliferation pathways. *Cancer Lett*, 318(2):189–198, May 2012.
- [157] Y. Huang, Z. Liu, H. Huang, H. Liu, and L. Li. Effects of mycophenolic acid on endothelial cells. *Int Immunopharmacol*, 5(6):1029–1039, Jun 2005.
- [158] C. Crosnier, D. Stamataki, and J. Lewis. Organizing cell renewal in the intestine: stem cells, signals and combinatorial control. *Nat Rev Genet*, 7(5):349–359, May 2006.
- [159] L. P. Pageot, N. Perreault, N. Basora, C. Francoeur, P. Magny, and J. F. Beaulieu. Human cell models to study small intestinal functions: recapitulation of the crypt-villus axis. *Microsc Res Tech*, 49(4):394–406, May 2000.
- [160] J. Klawitter, V. Schmitz, J. Klawitter, D. Leibfritz, and U. Christians. Development and validation of an assay for the quantification of 11 nucleotides using LC/LC-electrospray ionization-MS. *Anal Biochem*, 365(2):230–239, Jun 2007.
- [161] S. Wolter, M. Golombek, and R. Seifert. Differential activation of cAMP- and cGMP-dependent protein kinases by cyclic purine and pyrimidine nucleotides. *Biochem Biophys Res Commun*, 415(4):563–566, Dec 2011.
- [162] D. E. Atkinson. The energy charge of the adenylate pool as a regulatory parameter. Interaction with feedback modifiers. *Biochemistry*, 7(11):4030–4034, Nov 1968.
- [163] W. Dudzinska, A. Lubkowska, B. Dolegowska, K. Safranow, and K. Jakubowska. Adenine, guanine and pyridine nucleotides in blood during physical exercise and restitution in healthy subjects. *Eur J Appl Physiol*, 110(6):1155–1162, Dec 2010.
- [164] T. W. Traut. Physiological concentrations of purines and pyrimidines. *Mol Cell Biochem*, 140(1):1–22, Nov 1994.

Bibliography

- [165] H. Daxecker, M. Raab, M. Cichna, P. Markl, and M. M. Mueller. Determination of the effects of mycophenolic acid on the nucleotide pool of human peripheral blood mononuclear cells in vitro by high-performance liquid chromatography. *Clin Chim Acta*, 310(1):81–87, Aug 2001.
- [166] M. Cansev. Uridine and cytidine in the brain: their transport and utilization. *Brain Res Rev*, 52(2):389–397, Sep 2006.
- [167] C. E. Cass, J. K. Lowe, J. M. Manchak, and J. F. Henderson. Biological effects of inhibition of guanine nucleotide synthesis by mycophenolic acid in cultured neuroblastoma cells. *Cancer Res*, 37(9):3314–3320, Sep 1977.
- [168] J. A. Nelson, L. M. Rose, and L. L. Bennett. Effects of 2-amino-1,3,4-thiadiazole on ribonucleotide pools of leukemia L1210 cells. *Cancer Res*, 36(4):1375–1378, Apr 1976.
- [169] M. Raab, H. Daxecker, A. Karimi, S. Markovic, M. Cichna, P. Markl, and M. M. Mueller. In vitro effects of mycophenolic acid on the nucleotide pool and on the expression of adhesion molecules of human umbilical vein endothelial cells. *Clin Chim Acta*, 310(1):89–98, Aug 2001.
- [170] J. A. Sokoloski and A. C. Sartorelli. Effects of the inhibitors of IMP dehydrogenase, tiazofurin and mycophenolic acid, on glycoprotein metabolism. *Mol Pharmacol*, 28(6):567–573, Dec 1985.
- [171] S. U. Sankatsing, P. G. Hoggard, A. D. Huitema, R. W. Sparidans, S. Kewn, K. M. Crommentuyn, J. M. Lange, J. H. Beijnen, D. J. Back, and J. M. Prins. Effect of mycophenolate mofetil on the pharmacokinetics of antiretroviral drugs and on intracellular nucleoside triphosphate pools. *Clin Pharmacokinet*, 43(12):823–832, 2004.
- [172] Y. Qiu, L. D. Fairbanks, K. Ruckermann, C. M. Hawrlowicz, D. F. Richards, B. Kirschbaum, and H. A. Simmonds. Mycophenolic acid-induced GTP depletion also affects ATP and pyrimidine synthesis in mitogen-stimulated primary human T-lymphocytes. *Transplantation*, 69(5):890–897, Mar 2000.
- [173] A. G. Therien and R. Blostein. Mechanisms of sodium pump regulation. *Am J Physiol, Cell Physiol*, 279(3):C541–566, Sep 2000.
- [174] J. D. Fondacaro. Intestinal ion transport and diarrheal disease. *Am J Physiol*, 250(1 Pt 1):1–8, Jan 1986.

- [175] A. R. Asif, V. W. Armstrong, A. Volland, E. Wieland, M. Oellerich, and M. Shipkova. Proteins identified as targets of the acyl glucuronide metabolite of mycophenolic acid in kidney tissue from mycophenolate mofetil treated rats. *Biochimie*, 89:393–402, Mar 2007.
- [176] M. Shipkova, H. Beck, A. Volland, V. W. Armstrong, H. J. Grone, M. Oellerich, and E. Wieland. Identification of protein targets for mycophenolic acid acyl glucuronide in rat liver and colon tissue. *Proteomics*, 4:2728–2738, Sep 2004.
- [177] M. Johansson, T. Jansson, N. B. Pestov, and T. L. Powell. Non-gastric H^+/K^+ ATPase is present in the microvillous membrane of the human placental syncytiotrophoblast. *Placenta*, 25(6):505–511, Jul 2004.
- [178] Pierce Antibodies Thermo Scientific. Sodium/Potassium ATPase alpha-1 Antibody (464.6). <http://www.pierce-antibodies.com/Sodium-Potassium-ATPase-alpha-1-antibody-clone-464-6-Monoclonal-MA116731.html>, Feb 2013.
- [179] R. C. Kukreja, F. N. Salloum, and A. Das. Cyclic guanosine monophosphate signaling and phosphodiesterase-5 inhibitors in cardioprotection. *J Am Coll Cardiol*, 59(22):1921–1927, May 2012.
- [180] E. Messina, F. Lupi, L. Barile, and A. Giacomello. Cyclic nucleotides and neuroblastoma differentiation. *Nucleosides Nucleotides Nucleic Acids*, 23(8-9):1551–1554, Oct 2004.
- [181] E. W. Sutherland. Studies on the mechanism of hormone action. *Science*, 177(4047):401–408, Aug 1972.
- [182] D. Groneberg, P. Konig, D. Koesling, and A. Friebe. Nitric oxide-sensitive guanylyl cyclase is dispensable for nitrergic signaling and gut motility in mouse intestinal smooth muscle. *Gastroenterology*, 140(5):1608–1617, May 2011.
- [183] T. J. Franklin and P. A. Twose. Reduction in beta-adrenergic response of cultured glioma cells following depletion of intracellular GTP. *Eur J Biochem*, 77(1):113–117, Jul 1977.
- [184] G. S. Johnson and V. R. Mukku. Evidence in intact cells for an involvement of GTP in the activation of adenylate cyclase. *J Biol Chem*, 254(1):95–100, Jan 1979.

Bibliography

- [185] Z. Naor and K. J. Catt. Independent actions of gonadotropin releasing hormone upon cyclic GMP production and luteinizing hormone release. *J Biol Chem*, 255(2):342–344, Jan 1980.
- [186] J. Klepacki, J. Klawitter, J. Bendrick-Peart, B. Schniedewind, S. Heischmann, T. Shokati, U. Christians, and J. Klawitter. A high-throughput U-HPLC-MS/MS assay for the quantification of mycophenolic acid and its major metabolites mycophenolic acid glucuronide and mycophenolic acid acylglucuronide in human plasma and urine. *J Chromatogr B Analyt Technol Biomed Life Sci*, 883-884:113–119, Feb 2012.
- [187] M. Shipkova, E. Schutz, V. W. Armstrong, P. D. Niedmann, M. Oellerich, and E. Wieland. Determination of the acyl glucuronide metabolite of mycophenolic acid in human plasma by HPLC and EMIT. *Clin Chem*, 46(3):365–372, Mar 2000.
- [188] H. Georges, N. Presle, T. Buronfosse, S. Fournel-Gigleux, P. Netter, J. Magdalou, and F. Lapicque. In vitro stereoselective degradation of carprofen glucuronide by human serum albumin. Characterization of sites and reactive amino acids. *Chirality*, 12(2):53–62, Feb 2000.
- [189] C. Li, L. Z. Benet, and M. P. Grillo. Studies on the chemical reactivity of 2-phenylpropionic acid 1-O-acyl glucuronide and S-acyl-CoA thioester metabolites. *Chem Res Toxicol*, 15(10):1309–1317, Oct 2002.
- [190] A. Bischer, P. Zia-Amirhosseini, M. Iwaki, A. F. McDonagh, and L. Z. Benet. Stereoselective binding properties of naproxen glucuronide diastereomers to proteins. *J Pharmacokinet Biopharm*, 23(4):379–395, Aug 1995.
- [191] M. Castillo and P. C. Smith. Disposition and reactivity of ibuprofen and ibufenac acyl glucuronides in vivo in the rhesus monkey and in vitro with human serum albumin. *Drug Metab Dispos*, 23(5):566–572, May 1995.
- [192] R. Sawamura, N. Okudaira, K. Watanabe, T. Murai, Y. Kobayashi, M. Tachibana, T. Ohnuki, K. Masuda, H. Honma, A. Kurihara, and O. Okazaki. Predictability of idiosyncratic drug toxicity risk for carboxylic acid-containing drugs based on the chemical stability of acyl glucuronide. *Drug Metab Dispos*, 38(10):1857–1864, Oct 2010.
- [193] I. Lammers, V. Lhiaubet-Vallet, M. Consuelo Jimenez, F. Ariese, M. A. Miranda, and C. Gooijer. Stereoselective binding of flurbiprofen enantiomers

- and their methyl esters to human serum albumin studied by time-resolved phosphorescence. *Chirality*, 24(10):840–846, Oct 2012.
- [194] K. Akira, T. Uchijima, and T. Hashimoto. Rapid internal acyl migration and protein binding of synthetic probenecid glucuronides. *Chem Res Toxicol*, 15(6):765–772, Jun 2002.
- [195] K. A. McGurk, R. P. Remmel, V. P. Hosagrahara, D. Tosh, and B. Burchell. Reactivity of mefenamic acid 1-O-acyl glucuronide with proteins in vitro and ex vivo. *Drug Metab Dispos*, 24(8):842–849, Aug 1996.
- [196] G. Skopp, L. Potsch, M. Mauden, and B. Richter. Partition coefficient, blood to plasma ratio, protein binding and short-term stability of 11-nor-delta(9)-carboxy tetrahydrocannabinol glucuronide. *Forensic Sci Int*, 126(1):17–23, Mar 2002.
- [197] P. C. Smith and J. H. Liu. Covalent binding of suprofen acyl glucuronide to albumin in vitro. *Xenobiotica*, 23(4):337–348, Apr 1993.
- [198] No authors listed. The name game. *Nature Cell Biology*, editorial(5):1–2, 2003.
- [199] R. Amanchy, D. E. Kalume, A. Iwahori, J. Zhong, and A. Pandey. Phosphoproteome analysis of HeLa cells using stable isotope labeling with amino acids in cell culture (SILAC). *J Proteome Res*, 4(5):1661–1671, 2005.
- [200] R. Amanchy, D. E. Kalume, and A. Pandey. Stable isotope labeling with amino acids in cell culture (SILAC) for studying dynamics of protein abundance and posttranslational modifications. *Sci STKE*, 2005(267):pl2, Jan 2005.
- [201] Uniprot. Q9ULC5, ACSL5_HUMAN. <http://www.uniprot.org/uniprot/Q9ULC5>, Aug 2012.
- [202] Y. Achouri, B. D. Hegarty, D. Allanic, D. Becard, I. Hainault, P. Ferre, and F. Foufelle. Long chain fatty acyl-CoA synthetase 5 expression is induced by insulin and glucose: involvement of sterol regulatory element-binding protein-1c. *Biochimie*, 87(12):1149–1155, Dec 2005.
- [203] D. J. Durgan, J. K. Smith, M. A. Hotze, O. Egbejimi, K. D. Cuthbert, V. G. Zaha, J. R. Dyck, E. D. Abel, and M. E. Young. Distinct transcriptional regulation of long-chain acyl-CoA synthetase isoforms and cytosolic thioesterase 1

Bibliography

- in the rodent heart by fatty acids and insulin. *Am J Physiol Heart Circ Physiol*, 290(6):H2480–2497, Jun 2006.
- [204] Uniprot. P22309, UD11_HUMAN. <http://www.uniprot.org/uniprot/P22309>, Aug 2012.
- [205] J. Sugatani, T. Uchida, M. Kurosawa, M. Yamaguchi, Y. Yamazaki, A. Ikari, and M. Miwa. Regulation of pregnane X receptor (PXR) function and UGT1A1 gene expression by posttranslational modification of PXR protein. *Drug Metab Dispos*, 40(10):2031–2040, Oct 2012.
- [206] N. D. Leslie, Tinkle B. T., Strauss A. W., K. Shooner, and K. Zhang. Very Long-Chain Acyl-Coenzyme A Dehydrogenase Deficiency. <http://www.ncbi.nlm.nih.gov/books/NBK6816/>, Aug 2012.
- [207] J. C. Newman, W. He, and E. Verdin. Mitochondrial protein acylation and intermediary metabolism: regulation by sirtuins and implications for metabolic disease. *J Biol Chem*, Oct 2012.
- [208] L. H. Lim and S. Pervaiz. Annexin 1: the new face of an old molecule. *FASEB J*, 21(4):968–975, Apr 2007.
- [209] Uniprot. P04083, ANXA1_HUMAN. <http://www.uniprot.org/uniprot/P04083>, Aug 2012.
- [210] NCBI. ANXA1 annexin A1 [Homo sapiens] . <http://www.ncbi.nlm.nih.gov/gene/301>, Aug 2012.
- [211] Uniprot. Q15067, ACOX1_HUMAN. <http://www.uniprot.org/uniprot/Q15067>, Aug 2012.
- [212] C. D. Kane, O. L. Francone, and K. A. Stevens. Differential regulation of the cynomolgus, human, and rat acyl-CoA oxidase promoters by PPARalpha. *Gene*, 380(2):84–94, Oct 2006.
- [213] NCBI. ACOX1 acyl-CoA oxidase 1, palmitoyl [Homo sapiens] . <http://www.ncbi.nlm.nih.gov/gene/51>, Aug 2012.
- [214] NCBI. FABP1 fatty acid binding protein 1, liver [Homo sapiens] . <http://www.ncbi.nlm.nih.gov/gene/2168>, Aug 2012.
- [215] C. Chen, R. Fang, L. C. Chou, A. W. Lowe, and E. Sibley. PDX1 regulation of FABP1 and novel target genes in human intestinal epithelial Caco-2 cells. *Biochem Biophys Res Commun*, 423(1):183–187, Jun 2012.

- [216] Uniprot. P16144, ITB4_HUMAN. <http://www.uniprot.org/uniprot/P16144>, Aug 2012.
- [217] T. Guo, L. Fan, W. H. Ng, Y. Zhu, M. Ho, W. K. Wan, K. H. Lim, W. S. Ong, S. S. Lee, S. Huang, O. L. Kon, and S. K. Sze. Multidimensional identification of tissue biomarkers of gastric cancer. *J Proteome Res*, May 2012.
- [218] W. Chen, S. Sammani, S. Mitra, S. F. Ma, J. G. Garcia, and J. R. Jacobson. Critical role for integrin-I²⁴ in the attenuation of murine acute lung injury by simvastatin. *Am J Physiol Lung Cell Mol Physiol*, 303(4):L279–285, Aug 2012.
- [219] NCBI. ITGB4 integrin, beta 4 [Homo sapiens] . <http://www.ncbi.nlm.nih.gov/gene/3691>, Aug 2012.
- [220] Uniprot. Q9UBI6, GBG12_HUMAN. <http://www.uniprot.org/uniprot/Q9UBI6>, Aug 2012.
- [221] J. Orchel, L. Witek, M. Kimsa, B. Strzalka-Mrozik, M. Kimsa, A. Olejek, and U. Mazurek. Expression patterns of kinin-dependent genes in endometrial cancer. *Int J Gynecol Cancer*, 22(6):937–944, Jul 2012.
- [222] Uniprot. Q04837, SSBP_HUMAN. <http://www.uniprot.org/uniprot/Q04837>, Aug 2012.
- [223] F. Bruni, P. L. Polosa, M. N. Gadaleta, P. Cantatore, and M. Roberti. Nuclear respiratory factor 2 induces the expression of many but not all human proteins acting in mitochondrial DNA transcription and replication. *J Biol Chem*, 285(6):3939–3948, Feb 2010.
- [224] NCBI. SSBP1 single-stranded DNA binding protein 1, mitochondrial [Homo sapiens] . <http://www.ncbi.nlm.nih.gov/gene/6742>, Aug 2012.
- [225] Uniprot. P42765, THIM_HUMAN. <http://www.uniprot.org/uniprot/p42765>, Aug 2012.
- [226] V. Severino, J. Locker, G. M. Ledda-Columbano, A. Columbano, A. Parente, and A. Chambery. Proteomic characterization of early changes induced by triiodothyronine in rat liver. *J Proteome Res*, 10(7):3212–3224, Jul 2011.
- [227] V. C. de Boer, E. M. van Schothorst, A. A. Dihal, H. van der Woude, I. C. Arts, I. M. Rietjens, P. C. Hollman, and J. Keijer. Chronic quercetin exposure

Bibliography

- affects fatty acid catabolism in rat lung. *Cell Mol Life Sci*, 63(23):2847–2858, Dec 2006.
- [228] Uniprot. P09622, DLDH_HUMAN. <http://www.uniprot.org/uniprot/P09622>, Aug 2012.
- [229] R. A. Harris, M. M. Bowker-Kinley, P. Wu, J. Jeng, and K. M. Popov. Dihydrolipoamide dehydrogenase-binding protein of the human pyruvate dehydrogenase complex. DNA-derived amino acid sequence, expression, and reconstitution of the pyruvate dehydrogenase complex. *J Biol Chem*, 272(32):19746–19751, Aug 1997.
- [230] Uniprot. P40939, ECHA_HUMAN. <http://www.uniprot.org/uniprot/P40939>, Aug 2012.
- [231] S. Eaton, T. Bursby, B. Middleton, M. Pourfarzam, K. Mills, A. W. Johnson, and K. Bartlett. The mitochondrial trifunctional protein: centre of a beta-oxidation metabolon? *Biochem Soc Trans*, 28(2):177–182, Feb 2000.
- [232] Uniprot. P13804, ETFA_HUMAN. <http://www.uniprot.org/uniprot/P13804>, Aug 2012.
- [233] M. Nagao, B. Parimoo, and K. Tanaka. Developmental, nutritional, and hormonal regulation of tissue-specific expression of the genes encoding various acyl-CoA dehydrogenases and alpha-subunit of electron transfer flavoprotein in rat. *J Biol Chem*, 268(32):24114–24124, Nov 1993.
- [234] Uniprot. P15559, NQO1_HUMAN. <http://www.uniprot.org/uniprot/P15559>, Aug 2012.
- [235] G. Z. Dong, H. Youn, M. T. Park, E. T. Oh, K. H. Park, C. W. Song, E. K. Choi, and H. J. Park. Heat shock increases expression of NAD(P)H:quinone oxidoreductase (NQO1), mediator of beta-lapachone cytotoxicity, by increasing NQO1 gene activity and via Hsp70-mediated stabilisation of NQO1 protein. *Int J Hyperthermia*, 25(6):477–487, 2009.
- [236] NCBI. HSPA9 heat shock 70kDa protein 9 (mortalin) [Homo sapiens] . <http://www.ncbi.nlm.nih.gov/gene/3313>, Aug 2012.
- [237] V. S. Mashanov, O. R. Zueva, C. Rojas-Catagena, and J. E. Garcia-Ararras. Visceral regeneration in a sea cucumber involves extensive expression of survivin and mortalin homologs in the mesothelium. *BMC Dev Biol*, 10:117, 2010.

- [238] E. E. Gestl and S. Anne Bottger. Cytoplasmic sequestration of the tumor suppressor p53 by a heat shock protein 70 family member, mortalin, in human colorectal adenocarcinoma cell lines. *Biochem Biophys Res Commun*, 423(2):411–416, Jun 2012.
- [239] NCBI. Delta(3,5)-delta(2,4)-dienoyl-CoA isomerase (ECH1). <http://www.mitosciences.com/delta-3-5-delta-2-4-dienoyl-coa-isomerase-ech1.html>, Aug 2012.
- [240] J. Zhang, M. Song, J. Wang, M. Sun, B. Wang, R. Li, Y. Huang, L. Hou, Y. Jin, M. Wang, and J. Tang. Enoyl coenzyme A hydratase 1 is an important factor in the lymphatic metastasis of tumors. *Biomed Pharmacother*, 65(3):157–162, Jun 2011.
- [241] Uniprot. Q8N1C8 (ECH1_HUMAN). <http://www.uniprot.org/uniprot/Q13011>, Aug 2012.
- [242] NCBI. GPD2 glycerol-3-phosphate dehydrogenase 2 (mitochondrial) [Homo sapiens] . <http://www.ncbi.nlm.nih.gov/gene/2820>, Aug 2012.
- [243] K. Y. Tu, H. S. Ju, F. Pettit, W. Shive, N. H. Topek, R. Matthews, and K. Matthews. Glycerol-3-phosphate dehydrogenase activity in human lymphocytes: effects of insulin, obesity and weight loss. *Biochem Biophys Res Commun*, 207(1):183–190, Feb 1995.
- [244] S. K. Chowdhury, S. Raha, M. A. Tarnopolsky, and G. Singh. Increased expression of mitochondrial glycerophosphate dehydrogenase and antioxidant enzymes in prostate cancer cell lines/cancer. *Free Radic Res*, 41(10):1116–1124, Oct 2007.
- [245] Uniprot. Q9UIJ7, KAD3_HUMAN. <http://www.uniprot.org/uniprot/Q9UIJ7>, Aug 2012.
- [246] T. Tanabe, M. Yamada, T. Noma, T. Kajii, and A. Nakazawa. Tissue-specific and developmentally regulated expression of the genes encoding adenylate kinase isozymes. *J Biochem*, 113(2):200–207, Feb 1993.
- [247] Uniprot. P49411, EFTU_HUMAN. <http://www.uniprot.org/uniprot/P49411>, Aug 2012.
- [248] C. Xu, J. Wang, J. Li, and R. Fang. Expression of elongation factor (EF)-Tu is correlated with prognosis of gastric adenocarcinomas. *Int J Mol Sci*, 12(10):6645–6655, 2011.

Bibliography

- [249] Uniprot. P53597, SUCA_HUMAN. <http://www.uniprot.org/uniprot/P53597>, Aug 2012.
- [250] H. D. Um and C. Klein. Evidence for allosteric regulation of succinyl-CoA synthetase. *Biochem J*, 295(Pt 3):821–826, Nov 1993.
- [251] Uniprot. P01833, PIGR_HUMAN. <http://www.uniprot.org/uniprot/P01833>, Aug 2012.
- [252] J. Ai, Q. Tang, Y. Wu, Y. Xu, T. Feng, R. Zhou, Y. Chen, X. Gao, Q. Zhu, X. Yue, Q. Pan, S. Xu, J. Li, M. Huang, J. Daugherty-Holtrop, Y. He, H. E. Xu, J. Fan, J. Ding, and M. Geng. The role of polymeric immunoglobulin receptor in inflammation-induced tumor metastasis of human hepatocellular carcinoma. *J Natl Cancer Inst*, 103(22):1696–1712, Nov 2011.
- [253] D. H. Reikvam, M. Derrien, R. Islam, A. Erofeev, V. Grcic, A. Sandvik, P. Gaustad, L. A. Meza-Zepeda, F. L. Jahnsen, H. Smidt, and F. E. Johansen. Epithelial-microbial crosstalk in polymeric Ig receptor deficient mice. *Eur J Immunol*, 42(11):2959–2970, Nov 2012.
- [254] Uniprot. Q9BYZ8, REG4_HUMAN. <http://www.uniprot.org/uniprot/Q9BYZ8>, Aug 2012.
- [255] Uniprot. P55011, S12A2_HUMAN. <http://www.uniprot.org/uniprot/P55011>, Aug 2012.
- [256] NCBI. SLC12A2 solute carrier family 12 (sodium/potassium/chloride transporters), member 2 [Homo sapiens] . <http://www.ncbi.nlm.nih.gov/gene/6558>, Aug 2012.
- [257] Uniprot. P12277, KCRB_HUMAN. <http://www.uniprot.org/uniprot/P12277>, Aug 2012.
- [258] E. C. Mariman, C. A. Broers, C. A. Claesen, G. I. Tesser, and B. Wieringa. Structure and expression of the human creatine kinase B gene. *Genomics*, 1(2):126–137, Oct 1987.
- [259] NCBI. CKB creatine kinase (brain) [Homo sapiens] . <http://www.ncbi.nlm.nih.gov/gene/1152>, Aug 2012.
- [260] Uniprot. Q12864, CAD17_HUMAN. <http://www.uniprot.org/uniprot/Q12864>, Aug 2012.

- [261] L. P. Huang, Y. H. Yu, C. Sheng, and S. H. Wang. Up-regulation of cadherin 17 and down-regulation of homeodomain protein CDX2 correlate with tumor progression and unfavorable prognosis in epithelial ovarian cancer. *Int J Gynecol Cancer*, 22(7):1170–1176, Sep 2012.
- [262] NCBI. CDH17 cadherin 17, LI cadherin (liver-intestine) [Homo sapiens] . <http://www.ncbi.nlm.nih.gov/gene/1015>, Aug 2012.
- [263] Uniprot. Q16555, DPYL2_HUMAN. <http://www.uniprot.org/uniprot/Q16555>, Aug 2012.
- [264] P. Natalia Silva, T. K. Furuya, I. Sampaio Braga, L. T. Rasmussen, R. W. de Labio, P. H. Bertolucci, E. S. Chen, G. Turecki, N. Mechawar, S. L. Payao, J. Mill, and M. Cardoso Smith. CNP and DPYSL2 mRNA expression and promoter methylation levels in brain of Alzheimer’s disease patients. *J Alzheimers Dis*, Sep 2012.
- [265] M. Takano, K. Maekura, M. Otani, K. Sano, T. Nakamura-Hirota, S. Tokuyama, K. S. Min, T. Tomiyama, H. Mori, and S. Matsuyama. Proteomic analysis of the brain tissues from a transgenic mouse model of amyloid I² oligomers. *Neurochem Int*, 61(3):347–355, Aug 2012.
- [266] NCBI. DPYSL2 dihydropyrimidinase-like 2 (liver-intestine) [Homo sapiens] . <http://www.ncbi.nlm.nih.gov/sites/entrez?Db=gene&Cmd=DetailsSearch&Term=1808>, Aug 2012.
- [267] Uniprot. Q9HCN8 (SDF2L_HUMAN. <http://www.uniprot.org/uniprot/Q9HCN8>, Aug 2012.
- [268] P. Tongaonkar and M. E. Selsted. SDF2L1, a component of the endoplasmic reticulum chaperone complex, differentially interacts with alpha-, beta-, and theta-defensin propeptides. *J Biol Chem*, 284(9):5602–5609, Feb 2009.
- [269] S. Fukuda, M. Sumii, Y. Masuda, M. Takahashi, N. Koike, J. Teishima, H. Yasumoto, T. Itamoto, T. Asahara, K. Dohi, and K. Kamiya. Murine and human SDF2L1 is an endoplasmic reticulum stress-inducible gene and encodes a new member of the Pmt/rt protein family. *Biochem Biophys Res Commun*, 280(1):407–414, Jan 2001.
- [270] H. Kang, A. Escudero-Esparza, A. Douglas-Jones, R. E. Mansel, and W. G. Jiang. Transcript analyses of stromal cell derived factors (SDFs): SDF-2, SDF-

Bibliography

- 4 and SDF-5 reveal a different pattern of expression and prognostic association in human breast cancer. *Int J Oncol*, 35(1):205–211, Jul 2009.
- [271] Uniprot. Q9BWD1, THIC_HUMAN. <http://www.uniprot.org/uniprot/Q9BWD1>, Aug 2012.
- [272] Z. Zhu-qin, C. Hou-zao, Y. Rui-feng, Z. Ran, J. Yu-yan, X. Yang, L. De-pei, and L. Chih-chuan. Regulation of acyl-coenzyme A: cholesterol acyltransferase 2 expression by saturated fatty acids. *Chin Med Sci J*, 25(4):222–227, Dec 2010.
- [273] R. Jiao, L. Guan, N. Yang, C. Peng, Y. Liang, K. Y. Ma, Y. Huang, and Z. Y. Chen. Frequent cholesterol intake up-regulates intestinal NPC1L1, ACAT2, and MTP. *J Agric Food Chem*, 58(9):5851–5857, May 2010.
- [274] NCBI. ACAT2 acetyl-CoA acetyltransferase 2 [Homo sapiens]. <http://www.ncbi.nlm.nih.gov/gene/39>, Aug 2012.
- [275] J. Saussede-Aim and C. Dumontet. Regulation of tubulin expression: Multiple overlapping mechanisms. *IJMMS*, 1(8):290–296, Aug 2009.
- [276] Uniprot. Q9BQE3, TBA1C_HUMAN. <http://www.uniprot.org/uniprot/Q9BQE3>, Aug 2012.
- [277] Uniprot. Q9NYU2, UGT1_HUMAN. <http://www.uniprot.org/uniprot/Q9NYU2>, Aug 2012.
- [278] S. Chen, D. Beaton, N. Nguyen, K. Senekeo-Effenberger, E. Brace-Sinnokrak, U. Argikar, R. P. Remmel, J. Trottier, O. Barbier, J. K. Ritter, and R. H. Tukey. Tissue-specific, inducible, and hormonal control of the human UDP-glucuronosyltransferase-1 (UGT1) locus. *J Biol Chem*, 280(45):37547–37557, Nov 2005.
- [279] Uniprot. P05026, AT1B1_HUMAN. <http://www.uniprot.org/uniprot/P05026>, Aug 2012.
- [280] K. Matlhagela, M. Borsick, T. Rajkhowa, and M. Taub. Identification of a prostaglandin-responsive element in the Na⁺,K⁺-ATPase beta 1 promoter that is regulated by cAMP and Ca²⁺. Evidence for an interactive role of cAMP regulatory element-binding protein and Sp1. *J Biol Chem*, 280(1):334–346, Jan 2005.

- [281] Uniprot. P07437, TBB5_HUMAN. <http://www.uniprot.org/uniprot/P07437>, Aug 2012.
- [282] Uniprot. P62826, RAN_HUMAN. <http://www.uniprot.org/uniprot/P62826>, Aug 2012.
- [283] H. F. Yuen, K. K. Chan, C. Grills, J. T. Murray, A. Platt-Higgins, O. S. Eldin, K. O’Byrne, P. Janne, D. A. Fennell, P. G. Johnston, P. S. Rudland, and M. El-Tanani. Ran is a potential therapeutic target for cancer cells with molecular changes associated with activation of the PI3K/Akt/mTORC1 and Ras/MEK/ERK pathways. *Clin Cancer Res*, 18(2):380–391, Jan 2012.
- [284] Z. Zhao, J. Wang, and X. Zhang. Feedback regulation of Ran gene expression by Ran protein. *Gene*, 485(2):85–90, Oct 2011.
- [285] NCBI. RAN RAN, member RAS oncogene family [Homo sapiens] . <http://www.ncbi.nlm.nih.gov/gene/5901>, Aug 2012.
- [286] Uniprot. B4DJ43, B4DJ43_HUMAN. <http://www.uniprot.org/uniprot/B4DJ43>, Aug 2012.
- [287] DAVID Bioinformatics Resources 6.7. National Institute of Allergy and Infectious Diseases (NIAID), NIH. <http://david.abcc.ncifcrf.gov/>, Sep 2012.
- [288] Harvard Medical School BLAIS Proteomic Center, DANA-FARBER Cancer Institute. Pathway Palette. <http://blaispathways.dfci.harvard.edu/Palette.html>, Sep 2012.
- [289] PANTHER 7.2. Panther classification system. <http://www.pantherdb.org/>, Sept 2012.
- [290] UniProt. UniProtKBDocumentation/Help. <http://www.uniprot.org/help/uniprotkb>, Sep 2012.
- [291] D. W. Huang, B. T. Sherman, and R. A. Lempicki. Systematic and integrative analysis of large gene lists using DAVID bioinformatics resources. *Nat Protoc*, 4(1):44–57, 2009.
- [292] D. W. Huang, B. T. Sherman, and R. A. Lempicki. Bioinformatics enrichment tools: paths toward the comprehensive functional analysis of large gene lists. *Nucleic Acids Res*, 37(1):1–13, Jan 2009.

Bibliography

- [293] G. Dennis, B. T. Sherman, D. A. Hosack, J. Yang, W. Gao, H. C. Lane, and R. A. Lempicki. DAVID: Database for Annotation, Visualization, and Integrated Discovery. *Genome Biol*, 4(5):P3, 2003.
- [294] M. Shipkova, B. Spielbauer, A. Volland, H. J. Grone, V. W. Armstrong, M. Oellerich, and E. Wieland. cDNA microarray analysis reveals new candidate genes possibly linked to side effects under mycophenolate mofetil therapy. *Transplantation*, 78(8):1145–1152, Oct 2004.
- [295] M. Qasim, H. Rahman, M. Oellerich, and A. R. Asif. Differential proteome analysis of human embryonic kidney cell line (HEK-293) following mycophenolic acid treatment. *Proteome Sci*, 9:57, 2011.
- [296] T. Heller, A. R. Asif, D. T. Petrova, Y. Doncheva, E. Wieland, M. Oellerich, M. Shipkova, and V. W. Armstrong. Differential proteomic analysis of lymphocytes treated with mycophenolic acid reveals caspase 3-induced cleavage of rho GDP dissociation inhibitor 2. *Ther Drug Monit*, 31(2):211–217, Apr 2009.
- [297] G. M. Ghiggeri, M. Bruschi, L. Musante, G. Candiano, C. Boccardi, L. Citti, M. P. Rastaldi, S. Mangraviti, G. Rosso, A. Larti, A. Rosati, A. Urbani, R. Gusmano, E. Bertoni, and M. Salvadori. Post-transplant proteinuria associated with everolimus: definition of main features with proteomics. *Proteomics Clin Appl*, 2(9):1327–1337, Sep 2008.
- [298] D. T. Petrova, F. Brehmer, F. C. Schultze, A. R. Asif, O. Gross, M. Oellerich, and G. Brandhorst. Differential kidney proteome profiling in a murine model of renal fibrosis under treatment with mycophenolate mofetil. *Pathobiology*, 78(3):162–170, 2011.
- [299] d. a. W. Huang, B. T. Sherman, Q. Tan, J. R. Collins, W. G. Alvord, J. Roayaei, R. Stephens, M. W. Baseler, H. C. Lane, and R. A. Lempicki. The DAVID Gene Functional Classification Tool: a novel biological module-centric algorithm to functionally analyze large gene lists. *Genome Biol*, 8(9):R183, 2007.
- [300] DAVID Bioinformatics Resources 6.7: Functional Annotation Tool. National Institute of Allergy and Infectious Diseases (NIAID), NIH. http://david.abcc.ncifcrf.gov/helps/functional_annotation.html#summary, Sep 2012.

- [301] S. Jepson, I. J. Brogan, R. W. Stoddart, and I. V. Hutchinson. Mycophenolic acid does not inhibit protein glycosylation in T lymphocytes. *Transpl Immunol*, 8(3):169–175, Nov 2000.
- [302] H. Feichtiger, E. Wieland, V. W. Armstrong, and M. Shipkova. The acyl glucuronide metabolite of mycophenolic acid induces tubulin polymerization in vitro. *Clin Biochem*, 43(1-2):208–213, Jan 2010.
- [303] C. Morath, H. Reuter, V. Simon, E. Krautkramer, W. Muranyi, V. Schwenger, P. Goulimari, R. Grosse, M. Hahn, P. Lichter, and M. Zeier. Effects of mycophenolic acid on human fibroblast proliferation, migration and adhesion in vitro and in vivo. *Am J Transplant*, 8(9):1786–1797, Sep 2008.
- [304] S. Subramanian and D. L. Trence. Immunosuppressive agents: effects on glucose and lipid metabolism. *Endocrinol Metab Clin North Am*, 36(4):891–905, Dec 2007.
- [305] G. Li, V. B. Segu, M. E. Rabaglia, R. H. Luo, A. Kowluru, and S. A. Metz. Prolonged depletion of guanosine triphosphate induces death of insulin-secreting cells by apoptosis. *Endocrinology*, 139(9):3752–3762, Sep 1998.
- [306] L. Polastri, F. Galbiati, F. Bertuzzi, P. Fiorina, R. Nano, S. Gregori, L. Aldrighetti, G. Pozza, A. Secchi, L. Adorini, and A. M. Davalli. Secretory defects induced by immunosuppressive agents on human pancreatic beta-cells. *Acta Diabetol*, 39(4):229–233, Dec 2002.
- [307] M. A. Glozak, N. Sengupta, X. Zhang, and E. Seto. Acetylation and deacetylation of non-histone proteins. *Gene*, 363:15–23, Dec 2005.
- [308] S. C. Kim, R. Sprung, Y. Chen, Y. Xu, H. Ball, J. Pei, T. Cheng, Y. Kho, H. Xiao, L. Xiao, N. V. Grishin, M. White, X. J. Yang, and Y. Zhao. Substrate and functional diversity of lysine acetylation revealed by a proteomics survey. *Mol Cell*, 23(4):607–618, Aug 2006.
- [309] M. Askenazi, S. Li, S. Singh, and J. A. Marto. Pathway Palette: a rich internet application for peptide-, protein- and network-oriented analysis of MS data. *Proteomics*, 10(9):1880–1885, May 2010.
- [310] C. Stark, B. J. Breitkreutz, T. Reguly, L. Boucher, A. Breitkreutz, and M. Tyers. BioGRID: a general repository for interaction datasets. *Nucleic Acids Res*, 34, 2006.

Bibliography

- [311] Uniprot. P0CG48 , UBC_HUMAN. <http://www.uniprot.org/uniprot/P0CG48>, Sep 2012.
- [312] F. Flick and B. Luscher. Regulation of sirtuin function by posttranslational modifications. *Front Pharmacol*, 3:29, 2012.
- [313] Uniprot. Q9NRC8, SIR7_HUMAN. <http://www.uniprot.org/uniprot/Q9NRC8>, Sep 2012.
- [314] Uniprot. P01106, MYC_HUMAN. <http://www.uniprot.org/uniprot/P01106>, Sep 2012.
- [315] Uniprot. P49407, ARRB1_HUMAN. <http://www.uniprot.org/uniprot/P49407>, Sep 2012.
- [316] Uniprot. P32121, ARRB2_HUMAN. <http://www.uniprot.org/uniprot/P32121>, Sep 2012.
- [317] Uniprot. Q07157, ZO1_HUMAN. <http://www.uniprot.org/uniprot/Q07157>, Sep 2012.
- [318] Uniprot. P63165, SUMO1_HUMAN. <http://www.uniprot.org/uniprot/P63165>, Sep 2012.
- [319] Uniprot. P61956, SUMO2_HUMAN. <http://www.uniprot.org/uniprot/P61956>, Sep 2012.
- [320] Uniprot. P27348, YWHAQ_HUMAN. <http://www.uniprot.org/uniprot/P27348>, Aug 2012.
- [321] Uniprot. P60709, ACTB_HUMAN. <http://www.uniprot.org/uniprot/P60709>, Sep 2012.
- [322] Uniprot. O43707, ACTN4_HUMAN. <http://www.uniprot.org/uniprot/O43707>, Sep 2012.
- [323] Uniprot. P04264, K2C1_HUMAN. <http://www.uniprot.org/uniprot/P04264>, Sep 2012.
- [324] Uniprot. P05787, K2C8_HUMAN. <http://www.uniprot.org/uniprot/P05787>, Sep 2012.
- [325] Uniprot. Q15149, PLEC_HUMAN. <http://www.uniprot.org/uniprot/Q15149>, Sep 2012.

- [326] Uniprot. P08133, ANXA6_HUMAN. <http://www.uniprot.org/uniprot/P08133>, Sep 2012.
- [327] Uniprot. Q13813, SPTN1_HUMAN. <http://www.uniprot.org/uniprot/Q13813>, Sep 2012.
- [328] Uniprot. P13645, K1C10_HUMAN. <http://www.uniprot.org/uniprot/P13645>, Sep 2012.
- [329] NCBI. KRT10 keratin 10 [Homo sapiens] .
<http://www.ncbi.nlm.nih.gov/gene/3858>, Sep 2012.
- [330] Uniprot. P08670, VIME_HUMAN. <http://www.uniprot.org/uniprot/P08670>, Sep 2012.
- [331] Uniprot. P21333, FLNA_HUMAN. <http://www.uniprot.org/uniprot/P21333>, Sep 2012.
- [332] P. D. Thomas, A. Kejariwal, M. J. Campbell, H. Mi, K. Diemer, N. Guo, I. Ladunga, B. Ulitsky-Lazareva, A. Muruganujan, S. Rabkin, J. A. Vandergriff, and O. Doremieux. PANTHER: a browsable database of gene products organized by biological function, using curated protein family and subfamily classification. *Nucleic Acids Res*, 31(1):334–341, Jan 2003.
- [333] H. Mi, B. Lazareva-Ulitsky, R. Loo, A. Kejariwal, J. Vandergriff, S. Rabkin, N. Guo, A. Muruganujan, O. Doremieux, M. J. Campbell, H. Kitano, and P. D. Thomas. The PANTHER database of protein families, subfamilies, functions and pathways. *Nucleic Acids Res*, 33, 2005.
- [334] K. E. Wellen and C. B. Thompson. A two-way street: reciprocal regulation of metabolism and signalling. *Nat Rev Mol Cell Biol*, 13(4):270–276, Apr 2012.
- [335] C. M. Gillen, S. Brill, J. A. Payne, and B. Forbush. Molecular cloning and functional expression of the K^+ - Cl^- cotransporter from rabbit, rat, and human. A new member of the cation-chloride cotransporter family. *J Biol Chem*, 271(27):16237–16244, Jul 1996.
- [336] Z. S. Walters, K. E. Haworth, and B. V. Latinkic. NKCC1 (SLC12A2) induces a secondary axis in *Xenopus laevis* embryos independently of its co-transporter function. *J Physiol (Lond)*, 587(Pt 3):521–529, Feb 2009.

Bibliography

- [337] L. T. Weber, M. Shipkova, V. W. Armstrong, N. Wagner, E. Schutz, O. Mehls, L. B. Zimmerhackl, M. Oellerich, and B. Tonshoff. Comparison of the EMIT immunoassay with HPLC for therapeutic drug monitoring of mycophenolic acid in pediatric renal-transplant recipients on mycophenolate mofetil therapy. *Clin Chem*, 48(3):517–525, Mar 2002.
- [338] M. Shipkova, E. Schutz, V. W. Armstrong, P. D. Niedmann, E. Wieland, and M. Oellerich. Overestimation of mycophenolic acid by EMIT correlates with MPA metabolite. *Transplant Proc*, 31(1-2):1135–1137, 1999.
- [339] L. Z. Benet, H. Spahn-Langguth, S. Iwakawa, C. Volland, T. Mizuma, S. Mayer, E. Mutschler, and E. T. Lin. Predictability of the covalent binding of acidic drugs in man. *Life Sci*, 53(8):L141–146, 1993.
- [340] L. T. Weber, M. Shipkova, T. Lamersdorf, P. D. Niedmann, M. Wiesel, A. Mandelbaum, L. B. Zimmerhackl, E. Schutz, O. Mehls, M. Oellerich, V. W. Armstrong, and B. Tonshoff. Pharmacokinetics of mycophenolic acid (MPA) and determinants of MPA free fraction in pediatric and adult renal transplant recipients. German Study group on Mycophenolate Mofetil Therapy in Pediatric Renal Transplant Recipients. *J Am Soc Nephrol*, 9(8):1511–1520, Aug 1998.
- [341] L. T. Weber, T. Lamersdorf, M. Shipkova, P. D. Niedmann, M. Wiesel, L. B. Zimmerhackl, A. Staskewitz, E. Schutz, O. Mehls, M. Oellerich, V. W. Armstrong, and B. Tonshoff. Area under the plasma concentration-time curve for total, but not for free, mycophenolic acid increases in the stable phase after renal transplantation: a longitudinal study in pediatric patients. German Study Group on Mycophenolate Mofetil Therapy in Pediatric Renal Transplant Recipients. *Ther Drug Monit*, 21(5):498–506, Oct 1999.
- [342] T. Hanai, A. Koseki, R. Yoshikawa, M. Ueno, T. Kinoshita, and H. Homma. Prediction of human serum albumin-drug binding affinity without albumin. *Anal Chim Acta*, 454:101–108, Jan 2002.
- [343] R. B. Van Breemen, C. Fenselau, W. Mogilevsky, and G. B. Odell. Reaction of bilirubin glucuronides with serum albumin. *J Chromatogr*, 383(2):387–392, Dec 1986.
- [344] P. C. Smith, L. Z. Benet, and A. F. McDonagh. Covalent binding of zomepirac glucuronide to proteins: evidence for a Schiff base mechanism. *Drug Metab Dispos*, 18(5):639–644, 1990.

- [345] V. Uchaipichat, L. K. Winner, P. I. Mackenzie, D. J. Elliot, J. A. Williams, and J. O. Miners. Quantitative prediction of in vivo inhibitory interactions involving glucuronidated drugs from in vitro data: the effect of fluconazole on zidovudine glucuronidation. *Br J Clin Pharmacol*, 61:427–439, Apr 2006.
- [346] G. Arredondo, R. Martinez-Jorda, R. Calvo, C. Aguirre, and E. Suarez. Protein binding of itraconazole and fluconazole in patients with chronic renal failure. *Int J Clin Pharmacol Ther*, 32:361–364, Jul 1994.
- [347] G. Arredondo, E. Suarez, R. Calvo, J. A. Vazquez, J. Garcia-Sanchez, and R. Martinez-Jorda. Serum protein binding of itraconazole and fluconazole in patients with diabetes mellitus. *J Antimicrob Chemother*, 43:305–307, Feb 1999.
- [348] A. M. Castillo, L. Patiny, and J. Wist. Fast and accurate algorithm for the simulation of NMR spectra of large spin systems. *J Magn Reson*, 209(2):123–130, Apr 2011.
- [349] A. Brand D. Leibfritz W. Willker, J. Engelmann. Metabolite Assignment. http://www-user.uni-bremen.de/~wie/ww_metab.html, Apr 2012.
- [350] Human Metabolome Project. Human Metabolome Database - Version 3.0. <http://www.hmdb.ca/>, Apr 2012.
- [351] A. Lapidot and A. Gopher. Cerebral metabolic compartmentation. Estimation of glucose flux via pyruvate carboxylase/pyruvate dehydrogenase by ^{13}C NMR isotopomer analysis of D-[U- ^{13}C]glucose metabolites. *J Biol Chem*, 269:27198–27208, Nov 1994.
- [352] R. Diaz-Ruiz, M. Rigoulet, and A. Devin. The Warburg and Crabtree effects: On the origin of cancer cell energy metabolism and of yeast glucose repression. *Biochim Biophys Acta*, 1807(6):568–576, Jun 2011.
- [353] S. Y. Perera, D. M. Voith, and N. P. Curthoys. Biosynthesis and processing of mitochondrial glutaminase in HTC hepatoma cells. *Biochem J*, 273(Pt 2):265–270, Jan 1991.
- [354] J. Bertrand, A. Goichon, P. Dechelotte, and M. Coeffier. Regulation of intestinal protein metabolism by amino acids. *Amino Acids*, May 2012.
- [355] N. Li, P. Lewis, D. Samuelson, K. Liboni, and J. Neu. Glutamine regulates Caco-2 cell tight junction proteins. *Am J Physiol Gastrointest Liver Physiol*, 287(3):G726–733, Sep 2004.

Bibliography

- [356] W. Müller-Esterl. *Biochemie, Eine Einführung für Mediziner und Naturwissenschaftler*. Elsevier GmbH, 2004.
- [357] R. Ehehalt, A. Braun, M. Karner, J. Fuellekrug, and W. Stremmel. Phosphatidylcholine as a constituent in the colonic mucosal barrier – physiological and clinical relevance. *Biochim Biophys Acta*, 1801(9):983–993, Sep 2010.
- [358] D. Gotthardt, A. Braun, A. Tietje, K. H. Weiss, R. Ehehalt, and W. R. Stremmel. Separate basolateral and apical phosphatidylcholine secretion routes in intestinally differentiated tumor cells. *World J Gastroenterol*, 15(46):5821–5826, Dec 2009.
- [359] W. Stremmel, A. Hanemann, R. Ehehalt, M. Karner, and A. Braun. Phosphatidylcholine (lecithin) and the mucus layer: Evidence of therapeutic efficacy in ulcerative colitis? *Dig Dis*, 28(3):490–496, 2010.
- [360] A. Braun, I. Treede, D. Gotthardt, A. Tietje, A. Zahn, R. Ruhwald, U. Schoenfeld, T. Welsch, P. Kienle, G. Erben, W. D. Lehmann, J. Fuellekrug, W. Stremmel, and R. Ehehalt. Alterations of phospholipid concentration and species composition of the intestinal mucus barrier in ulcerative colitis: a clue to pathogenesis. *Inflamm Bowel Dis*, 15(11):1705–1720, Nov 2009.
- [361] F. Gibellini and T. K. Smith. The Kennedy pathway – De novo synthesis of phosphatidylethanolamine and phosphatidylcholine. *IUBMB Life*, 62(6):414–428, Jun 2010.
- [362] H. de Boussac, A. J. Pommier, J. Dufour, A. Trousson, F. Caira, D. H. Volle, S. Baron, and J. M. Lobaccaro. LXR, prostate cancer and cholesterol: the good, the bad and the ugly. *Am J Cancer Res*, 3(1):58–69, 2013.
- [363] T. Tanoue, Y. Nishitani, K. Kanazawa, T. Hashimoto, and M. Mizuno. In vitro model to estimate gut inflammation using co-cultured Caco-2 and RAW264.7 cells. *Biochem Biophys Res Commun*, 374:565–569, Sep 2008.
- [364] T. Sakamoto, N. Takahashi, Y. Sawaragi, S. Naknukool, R. Yu, T. Goto, and T. Kawada. Inflammation induced by RAW macrophages suppresses the UCP1 mRNA induction via ERK activation in 10T1/2 adipocytes. *Am J Physiol, Cell Physiol*, Jan 2013.
- [365] M. J. Lee, M. Y. Kim, S. C. Heo, Y. W. Kwon, Y. M. Kim, E. K. Do, J. H. Park, J. S. Lee, J. Han, and J. H. Kim. Macrophages regulate smooth muscle

- differentiation of mesenchymal stem cells via a prostaglandin F₂ α -mediated paracrine mechanism. *Arterioscler Thromb Vasc Biol*, 32(11):2733–2740, Nov 2012.
- [366] H. S. Warren, C. Fitting, E. Hoff, M. Adib-Conquy, L. Beasley-Topliffe, B. Tesini, X. Liang, C. Valentine, J. Hellman, D. Hayden, and J. M. Cavaillon. Resilience to bacterial infection: difference between species could be due to proteins in serum. *J Infect Dis*, 201(2):223–232, Jan 2010.
- [367] Y. C. Lu, W. C. Yeh, and P. S. Ohashi. LPS/TLR4 signal transduction pathway. *Cytokine*, 42(2):145–151, May 2008.
- [368] C. Gerard and B. J. Rollins. Chemokines and disease. *Nat Immunol*, 2(2):108–115, Feb 2001.
- [369] T. Lawrence, D. A. Willoughby, and D. W. Gilroy. Anti-inflammatory lipid mediators and insights into the resolution of inflammation. *Nat Rev Immunol*, 2(10):787–795, Oct 2002.
- [370] G. A. Bonaterra, S. Zugel, J. Thogersen, S. A. Walter, U. Haberkorn, J. Strelau, and R. Kinscherf. Growth differentiation factor-15 deficiency inhibits atherosclerosis progression by regulating interleukin-6-dependent inflammatory response to vascular injury. *J Am Heart Assoc*, 1(6):e002550, Dec 2012.
- [371] T. Sasaki, N. Hiwatashi, H. Yamazaki, M. Noguchi, and T. Toyota. The role of interferon gamma in the pathogenesis of Crohn’s disease. *Gastroenterol Jpn*, 27(1):29–36, Feb 1992.
- [372] A. C. Chin and C. A. Parkos. Neutrophil transepithelial migration and epithelial barrier function in IBD: potential targets for inhibiting neutrophil trafficking. *Ann N Y Acad Sci*, 1072:276–287, Aug 2006.
- [373] N. van Lelyveld, J. Ter Linde, M. E. Schipper, and M. Samsom. Regional differences in expression of TPH-1, SERT, 5-HT(3) and 5-HT(4) receptors in the human stomach and duodenum. *Neurogastroenterol Motil*, 19:342–348, May 2007.
- [374] W. L. Hasler. Serotonin and the GI tract. *Curr Gastroenterol Rep*, 11:383–391, Oct 2009.
- [375] J. J. Chen, Z. Li, H. Pan, D. L. Murphy, H. Tamir, H. Koepsell, and M. D. Gershon. Maintenance of serotonin in the intestinal mucosa and ganglia of

Bibliography

- mice that lack the high-affinity serotonin transporter: abnormal intestinal motility and the expression of cation transporters. *J Neurosci*, 21:6348–6361, Aug 2001.
- [376] K. Nakamura, T. Sato, A. Ohashi, H. Tsurui, and H. Hasegawa. Role of a serotonin precursor in development of gut microvilli. *Am J Pathol*, 172:333–344, Feb 2008.
- [377] T. Aiba, M. Susa, S. Fukumori, and Y. Hashimoto. The effects of culture conditions on CYP3A4 and MDR1 mRNA induction by 1 α ,25-dihydroxyvitamin D(3) in human intestinal cell lines, Caco-2 and LS180. *Drug Metab Pharmacokinet*, 20(4):268–274, Aug 2005.
- [378] M. V. Chirayath, L. Gajdzik, W. Hulla, J. Graf, H. S. Cross, and M. Peterlik. Vitamin D increases tight-junction conductance and paracellular Ca²⁺ transport in Caco-2 cell cultures. *Am J Physiol*, 274(2 Pt 1):G389–396, Feb 1998.
- [379] M. J. Cooke, S. R. Phillips, D. S. Shah, D. Athey, J. H. Lakey, and S. A. Przyborski. Enhanced cell attachment using a novel cell culture surface presenting functional domains from extracellular matrix proteins. *Cytotechnology*, 56(2):71–79, Feb 2008.
- [380] Invitrogen. Viable cell counts using Trypan blue.
http://tools.invitrogen.com/content/sfs/appendix/Cell_Culture/Viable%20Cell%20Counts%20Using%20Trypan%20Blue.pdf, Mar 2013.
- [381] Invitrogen. CyQuant NF Cell Proliferation Assay Kit.
<http://www.probes.invitrogen.com/media/pis/mp35006.pdf>, Mar 2013.
- [382] Cayman Chemical. LDH Cytotoxicity Assay Kit.
<http://www.funakoshi.co.jp/data/datasheet/CAY/10008882.pdf>, Mar 2013.
- [383] Pierce Protein Thermo Scientific. Pierce BCA Protein Assay Kit.
<http://www.piercenet.com/instructions/2161296.pdf>, Mar 2013.
- [384] Invitrogen. *SILAC Protein Identification and Quantification Kits, For identifying and quantifying phosphoproteins and membrane proteins in human physiology, The mechanisms of body function, eighth edition*, pages 20–28. Manual part no. 25-0841, 2010.

- [385] D. A. Hosack, G. Dennis, B. T. Sherman, H. C. Lane, and R. A. Lempicki. Identifying biological themes within lists of genes with EASE. *Genome Biol*, 4(10):R70, 2003.

4 Appendix

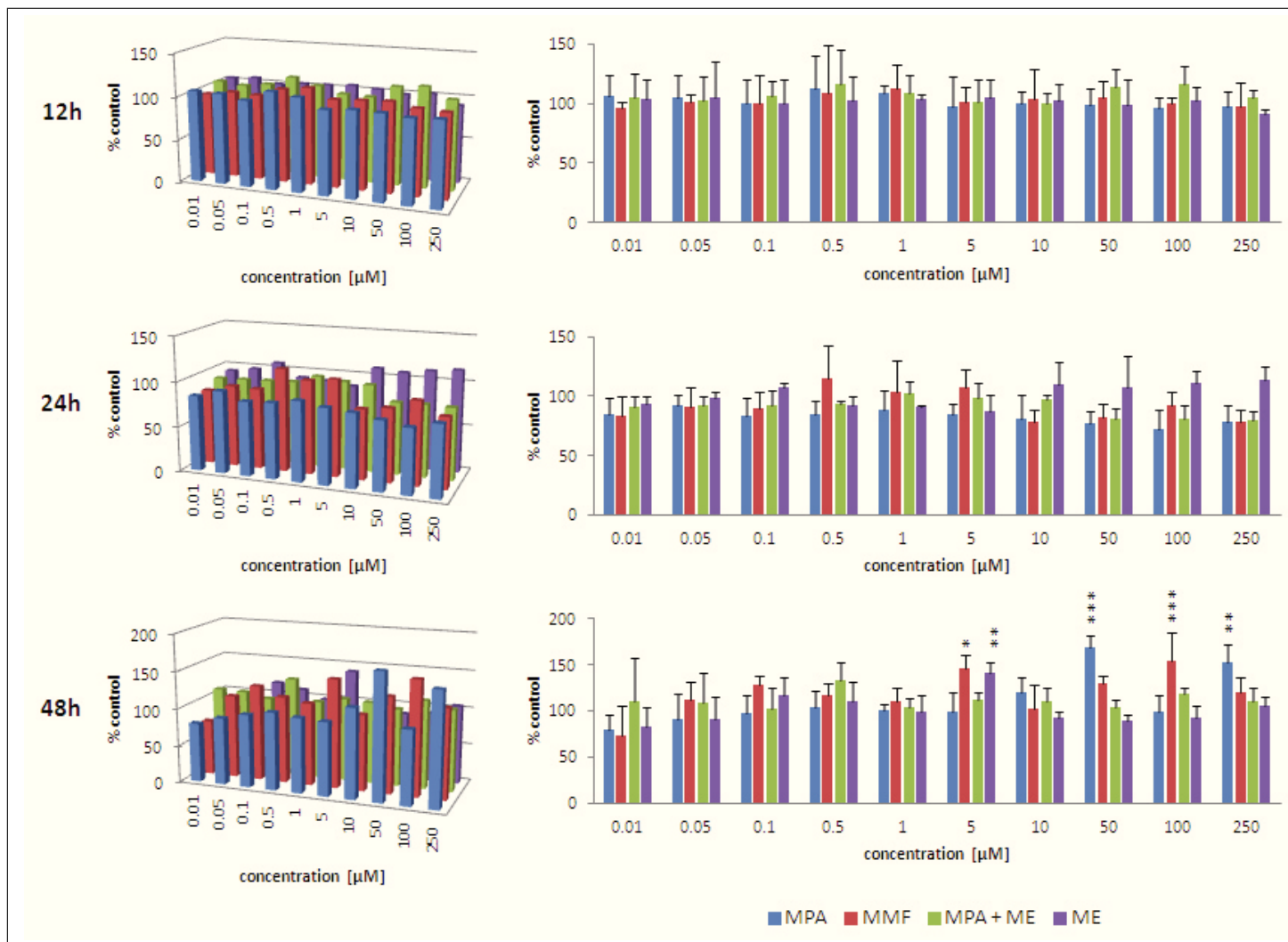


Fig. 4.1: Adenosine triphosphate levels of LS180 cells after 12h, 24h, and 48h of treatment with single doses of test compounds. Values are given as means of % of controls ($N=4$). Significance was determined using one-way ANOVA combined with Scheffe's *post-hoc* test with *: $p < 0.05$; **: $p < 0.005$; ***: $p < 0.001$ versus controls.

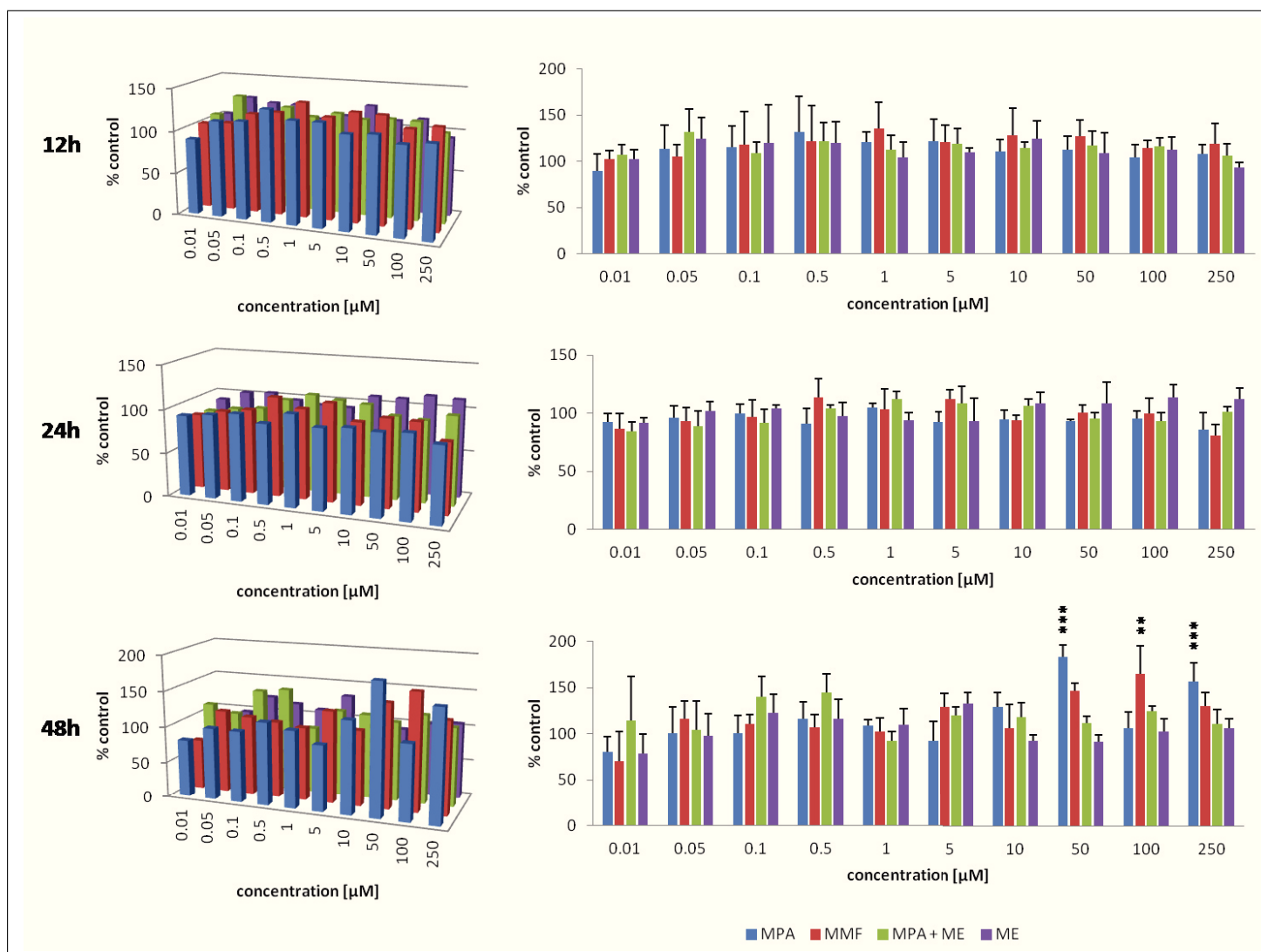


Fig. 4.2: Adenosine diphosphate levels of LS180 cells after 12h, 24h, and 48h of treatment with single doses of test compounds. Values are given as means of % of controls ($N=4$). Significance was determined using one-way ANOVA combined with Scheffe's post – hoc test with *: $p<0.05$; **: $p<0.005$; ***: $p<0.001$ versus controls.

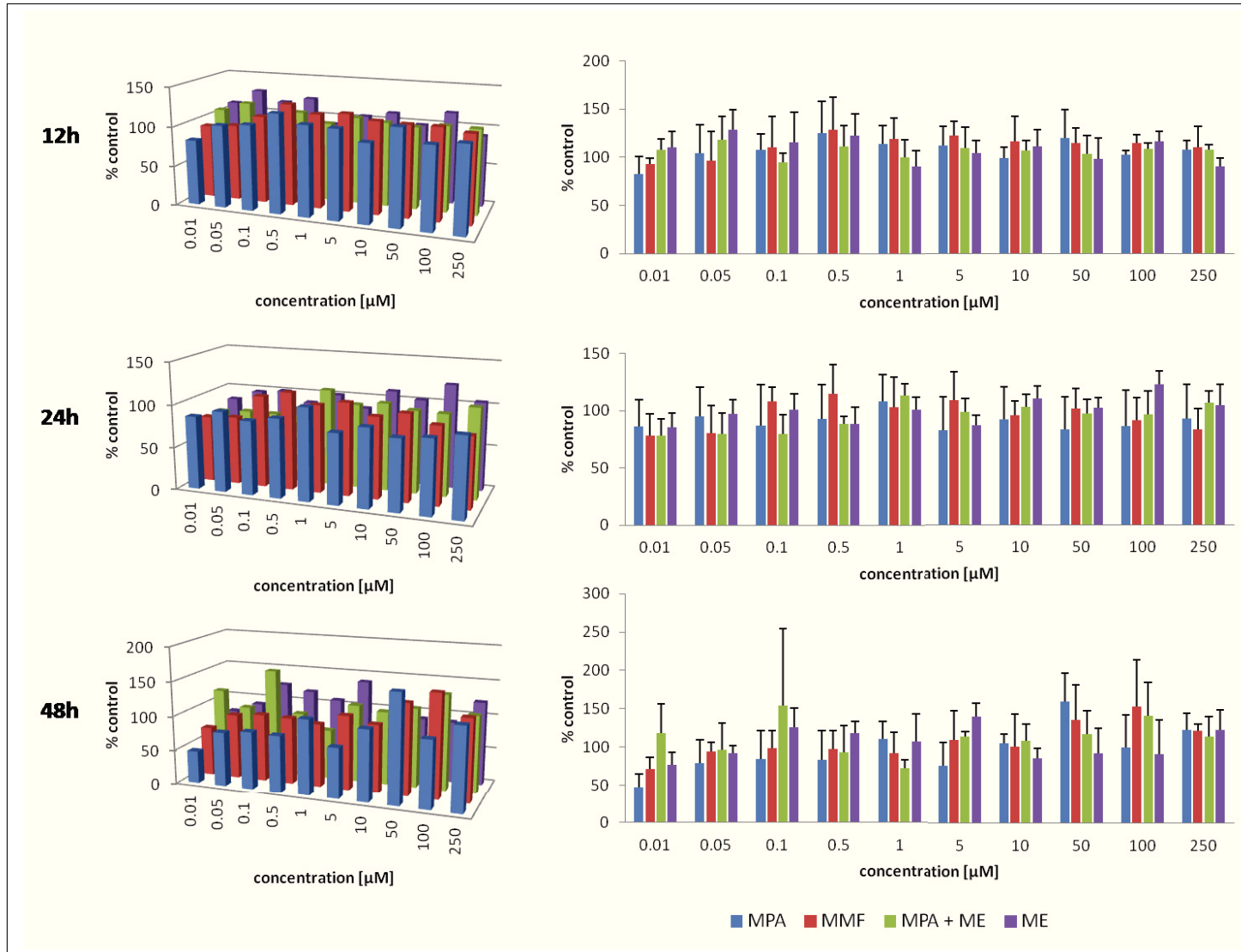


Fig. 4.3: Adenosine monophosphate levels of LS180 cells after 12h, 24h, and 48h of treatment with single doses of test compounds. Values are given as means of % of controls ($N=4$). Significance was determined using one-way ANOVA combined with Scheffe's *post-hoc* test with *: $p < 0.05$; **: $p < 0.005$; ***: $p < 0.001$ versus controls.

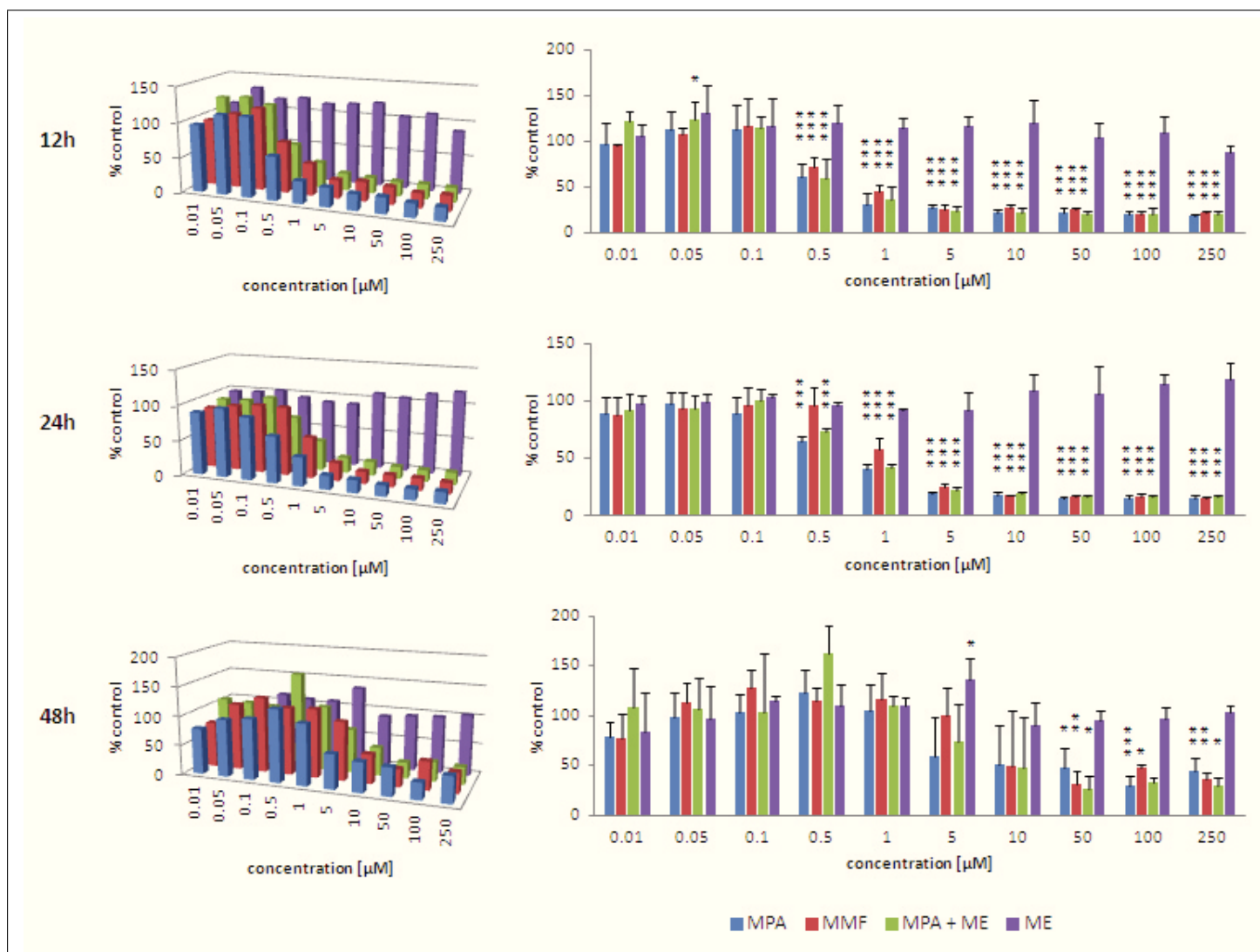


Fig. 4.4: Guanosine triphosphate levels of LS180 cells after 12h, 24h, and 48h of treatment with single doses of test compounds. Values are given as means of % of controls (N=4). Significance was determined using one-way ANOVA combined with Scheffe's post – hoc test with * : $p < 0.05$; ** : $p < 0.005$; *** : $p < 0.001$ versus controls.

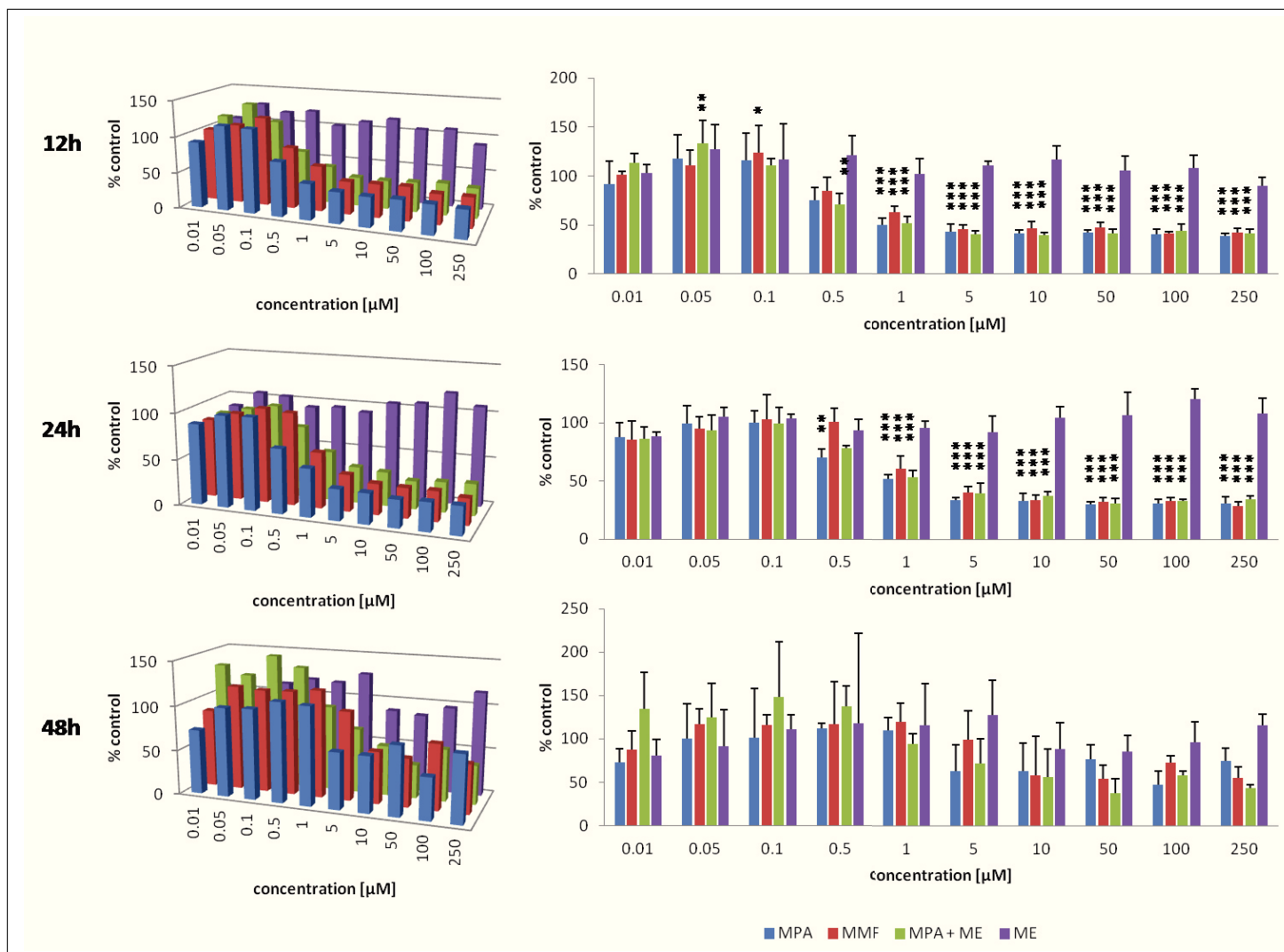


Fig. 4.5: Guanosine diphosphate levels of LS180 cells after 12h, 24h, and 48h of treatment with single doses of test compounds. Values are given as means of % of controls (N=4). Significance was determined using one-way ANOVA combined with Scheffe's post-hoc test with *: $p < 0.05$; **: $p < 0.005$; ***: $p < 0.001$ versus controls.

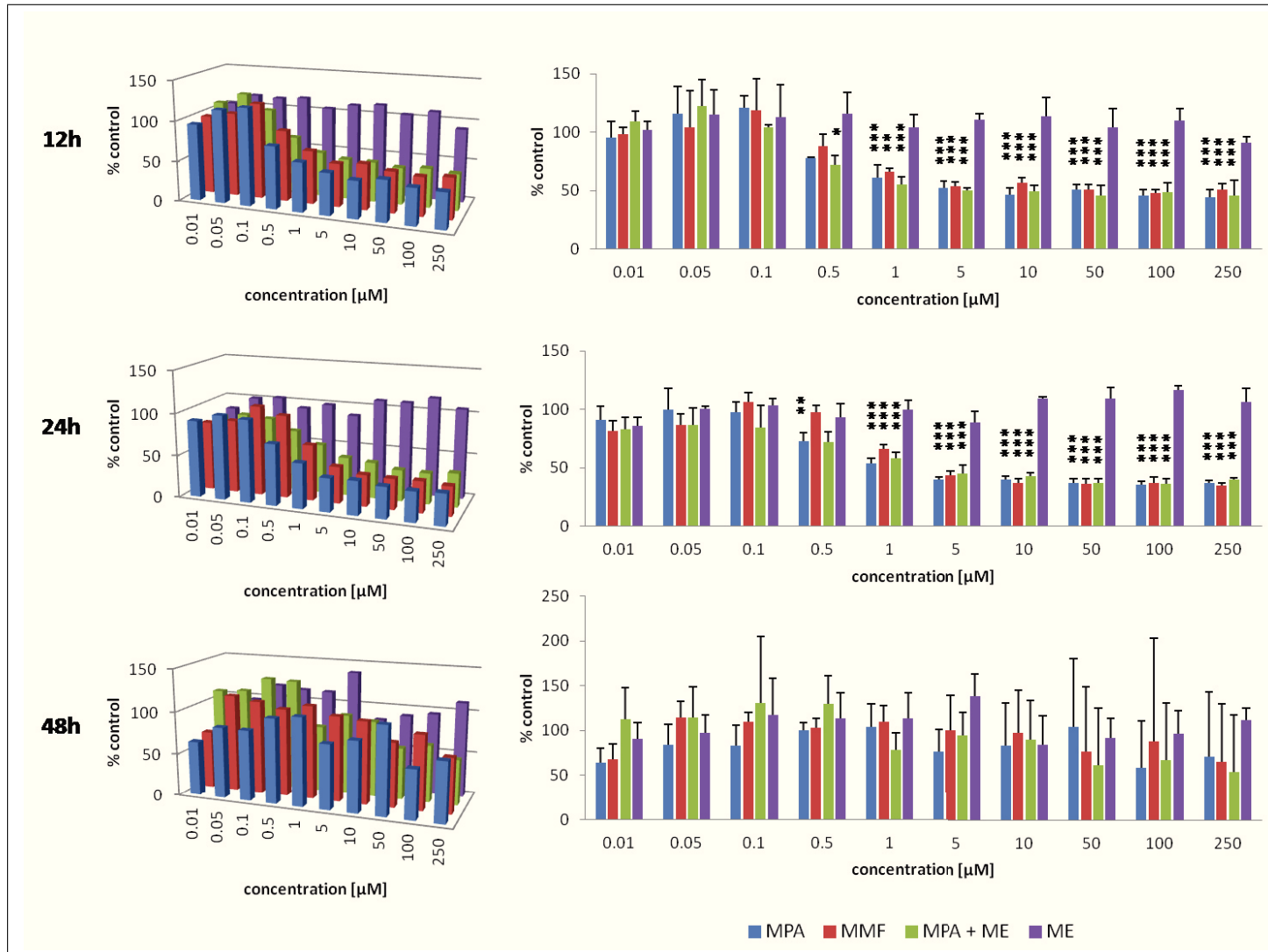


Fig. 4.6: Guanosine monophosphate levels of LS180 cells after 12h, 24h, and 48h of treatment with single doses of test compounds. Values are given as means of % of controls (N=4). Significance was determined using one-way ANOVA combined with Scheffe's post – hoc test with *: $p < 0.05$; **: $p < 0.005$; *: $p < 0.001$ versus controls.**

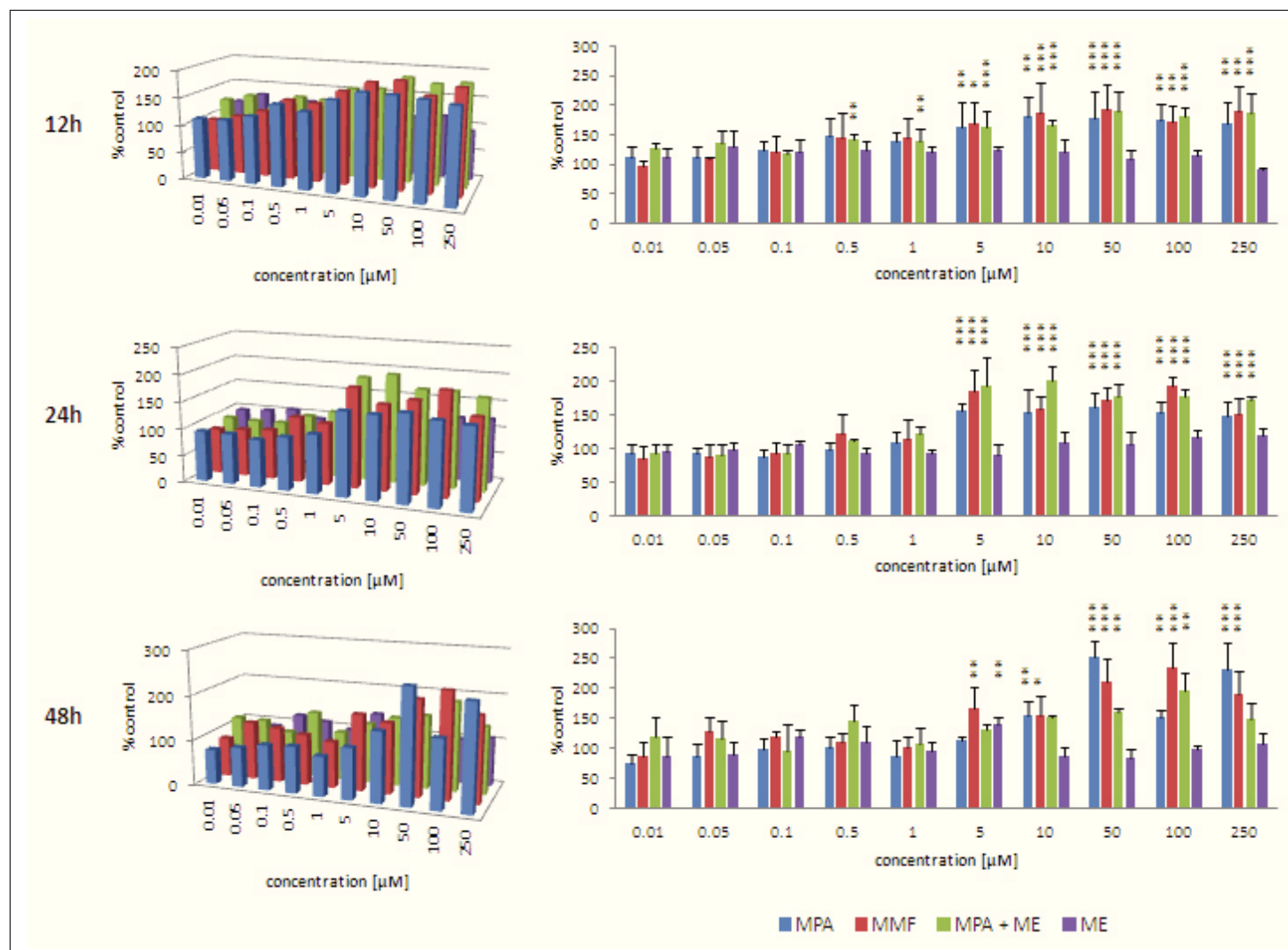


Fig. 4.7: Uridine triphosphate levels of LS180 cells after 12h, 24h, and 48h of treatment with single doses of test compounds. Values are given as means of % of controls ($N=4$). Significance was determined using one-way ANOVA combined with Scheffe's *post-hoc* test with *: $p < 0.05$; **: $p < 0.005$; ***: $p < 0.001$ versus controls.

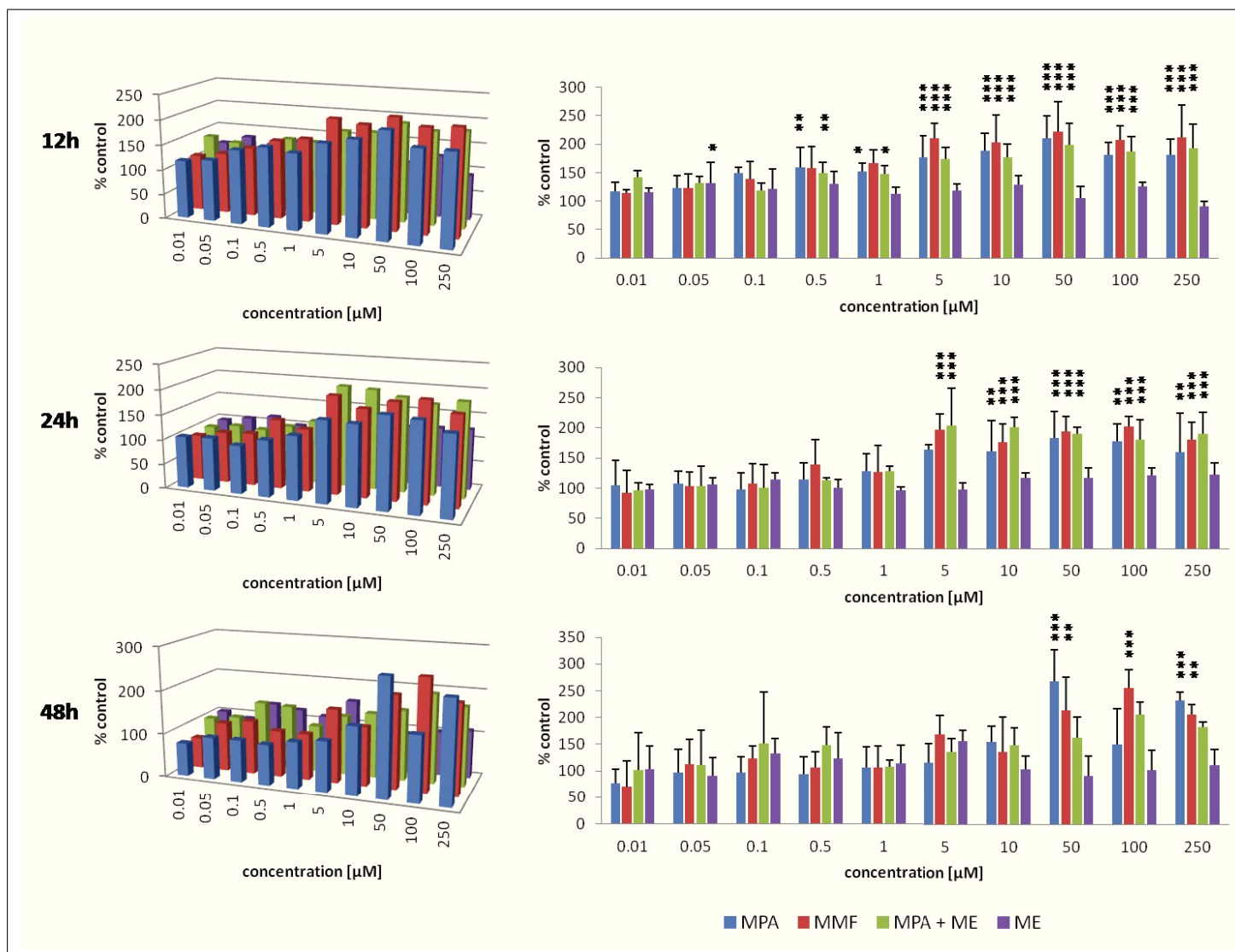


Fig. 4.8: Uridine diphosphate levels of LS180 cells after 12h, 24h, and 48h of treatment with single doses of test compounds. Values are given as means of % of controls ($N=4$). Significance was determined using one-way ANOVA combined with Scheffe's *post-hoc* test with *: $p < 0.05$; **: $p < 0.005$; ***: $p < 0.001$ versus controls.

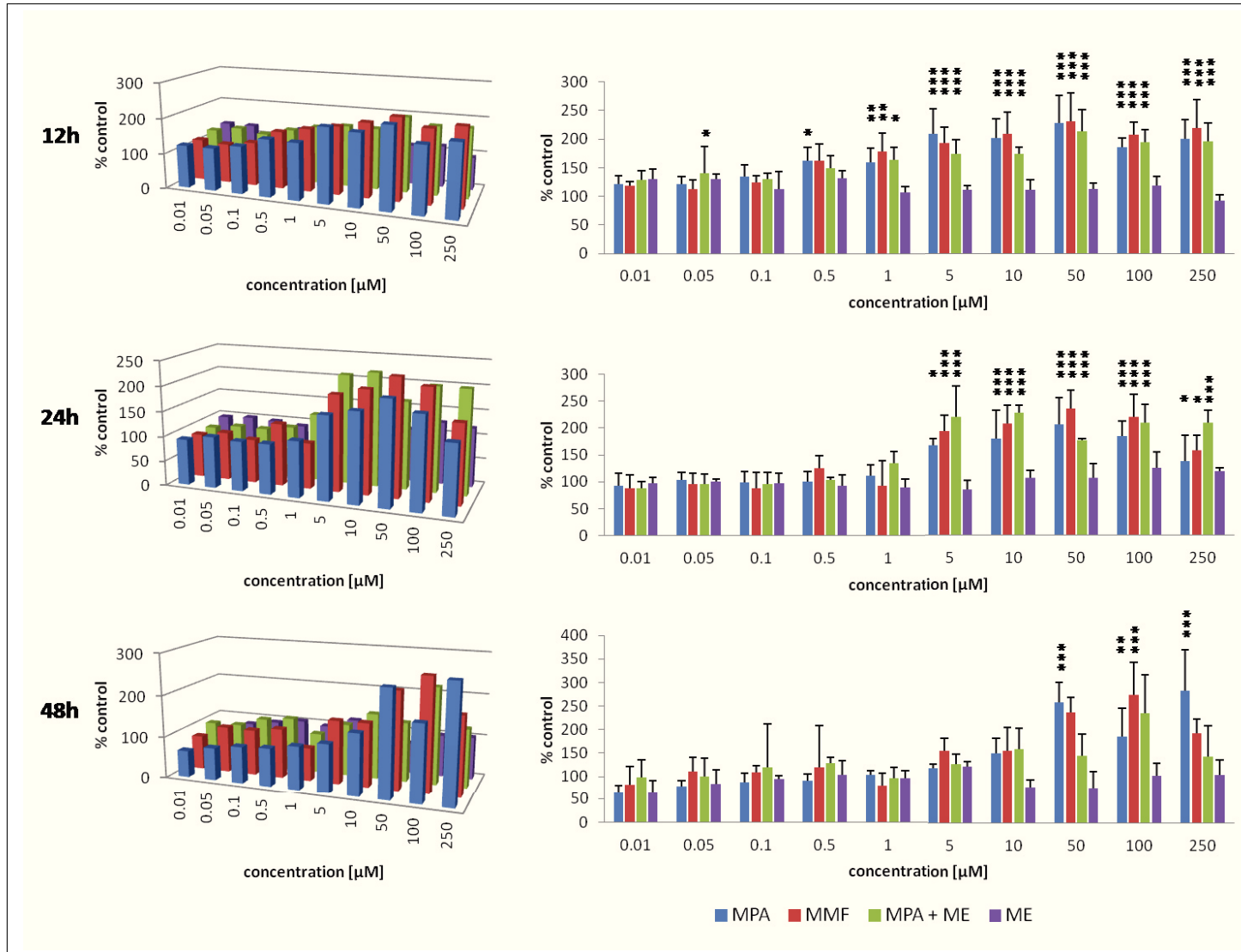


Fig. 4.9: Uridine monophosphate levels of LS180 cells after 12h, 24h, and 48h of treatment with single doses of test compounds. Values are given as means of % of controls ($N=4$). Significance was determined using one-way ANOVA combined with Scheffe's *post-hoc* test with *: $p < 0.05$; **: $p < 0.005$; ***: $p < 0.001$ versus controls.

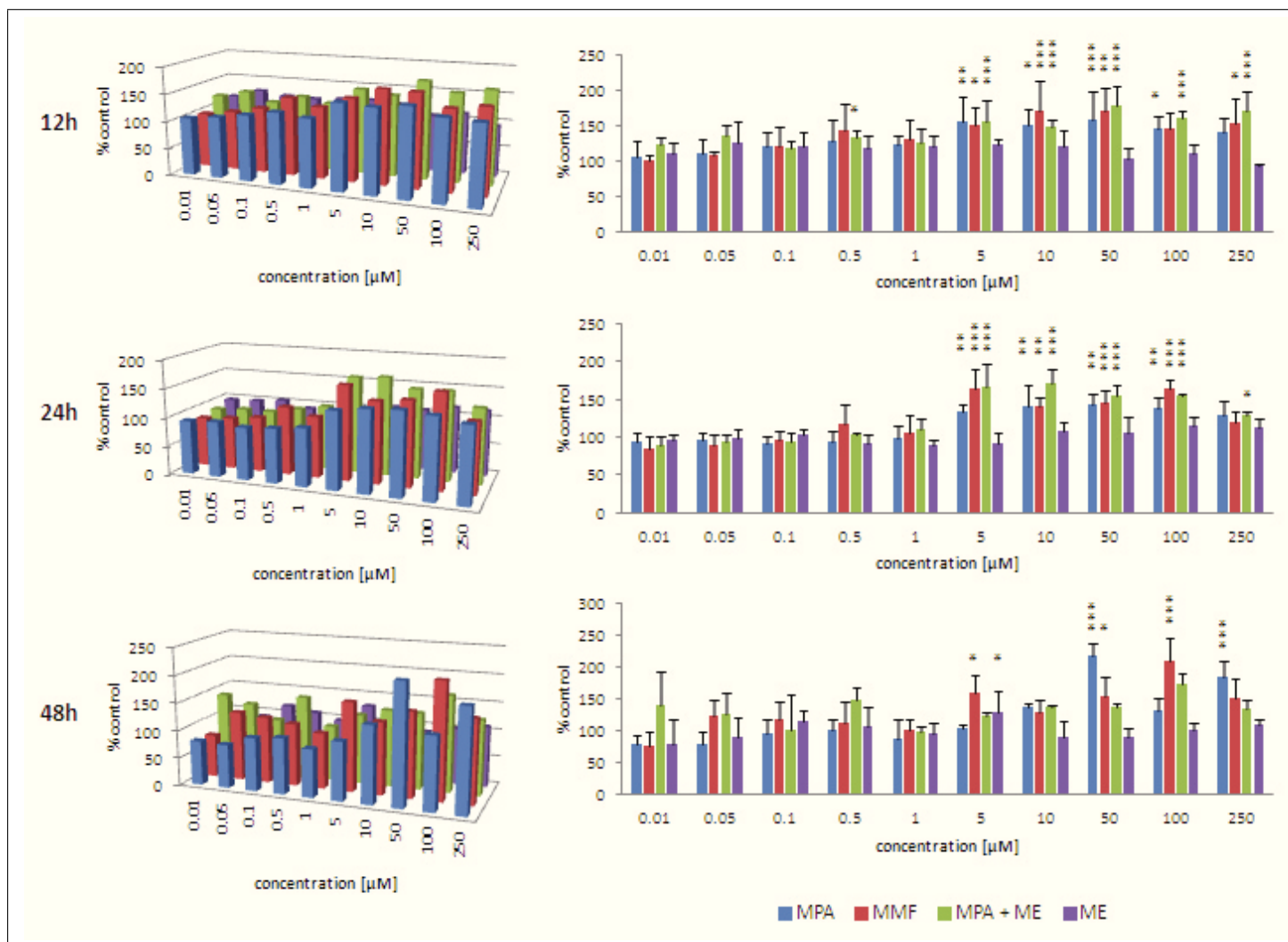


Fig. 4.10: Cytidine triphosphate levels of LS180 cells after 12h, 24h, and 48h of treatment with single doses of test compounds. Values are given as means of % of controls ($N=4$). Significance was determined using one-way ANOVA combined with Scheffe's *post-hoc* test with *: $p < 0.05$; **: $p < 0.005$; ***: $p < 0.001$ versus controls.

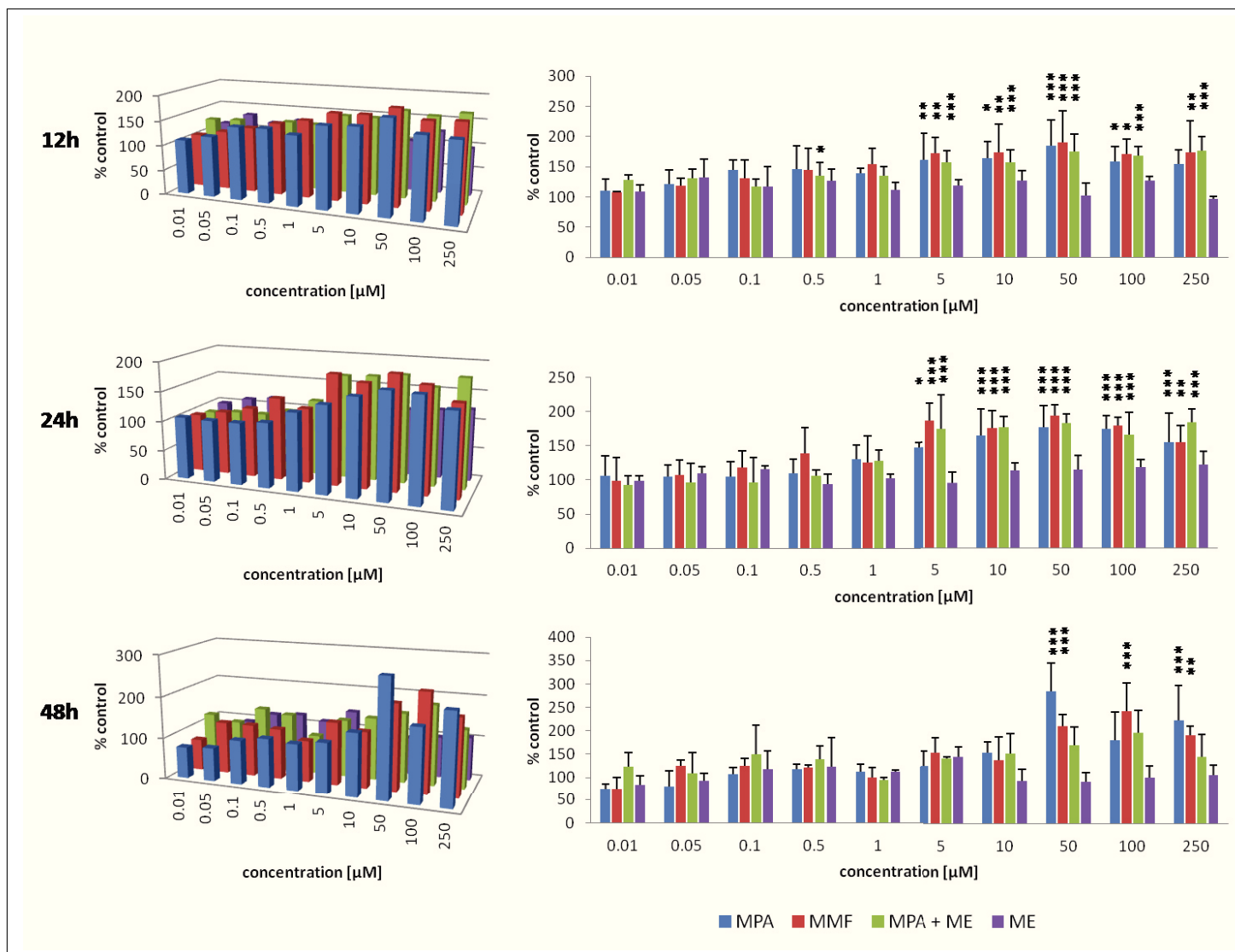


Fig. 4.11: Cytidine diphosphate levels of LS180 cells after 12h, 24h, and 48h of treatment with single doses of test compounds. Values are given as means of % of controls ($N=4$). Significance was determined using one-way ANOVA combined with Scheffe's *post-hoc* test with *: $p < 0.05$; **: $p < 0.005$; ***: $p < 0.001$ versus controls.

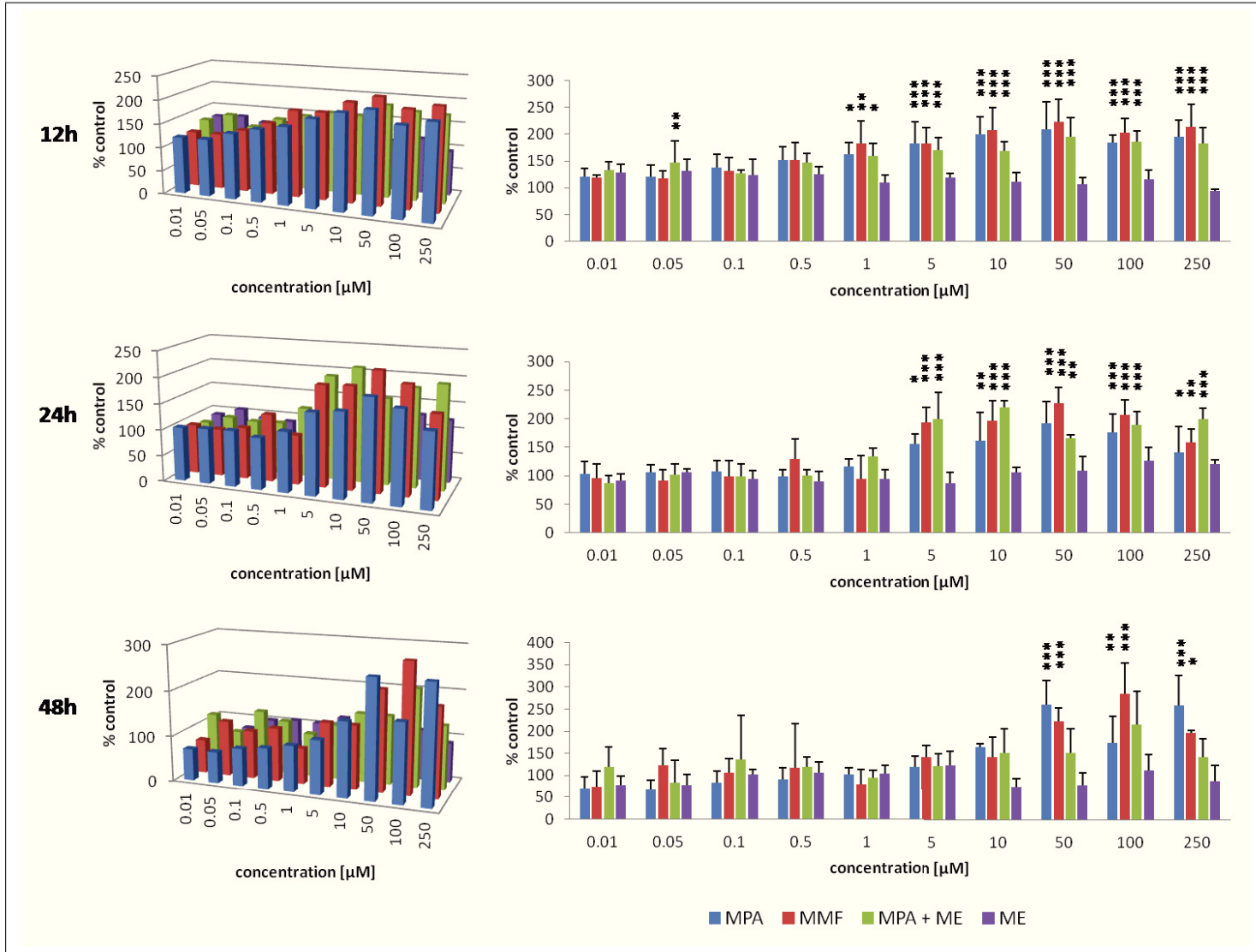


Fig. 4.12: Cytidine monophosphate levels of LS180 cells after 12h, 24h, and 48h of treatment with single doses of test compounds. Values are given as means of % of controls (N=4). Significance was determined using one-way ANOVA combined with Scheffe's post – hoc test with *: $p < 0.05$; **: $p < 0.005$; ***: $p < 0.001$ versus controls.

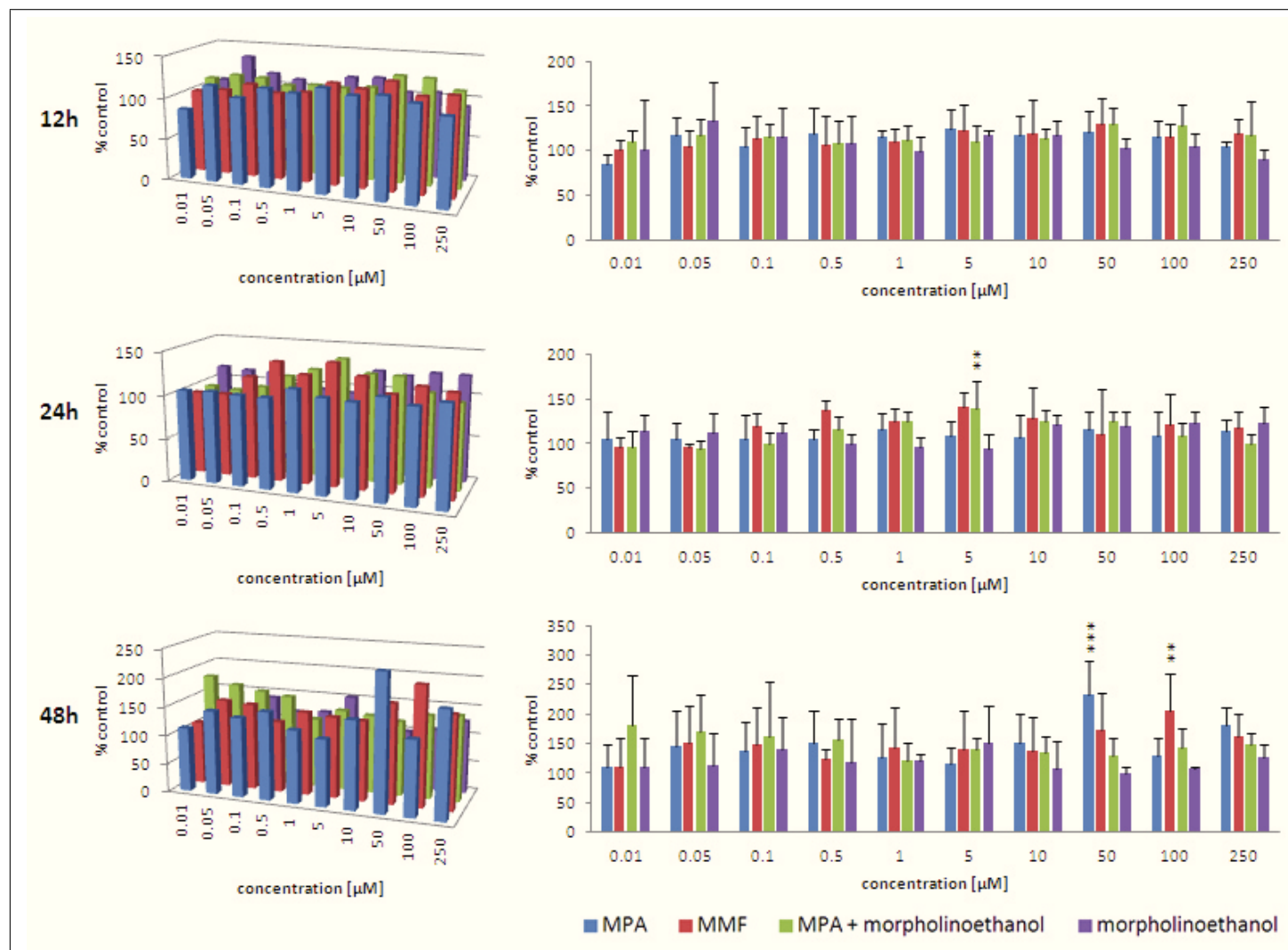


Fig. 4.13: NAD⁺ levels of LS180 cells after 12h, 24h, and 48h of treatment with single doses of test compounds. Values are given as means of % of controls (N=4). Significance was determined using one-way ANOVA combined with Scheffe's post – hoc test with *: $p < 0.05$; **: $p < 0.005$; ***: $p < 0.001$ versus controls.

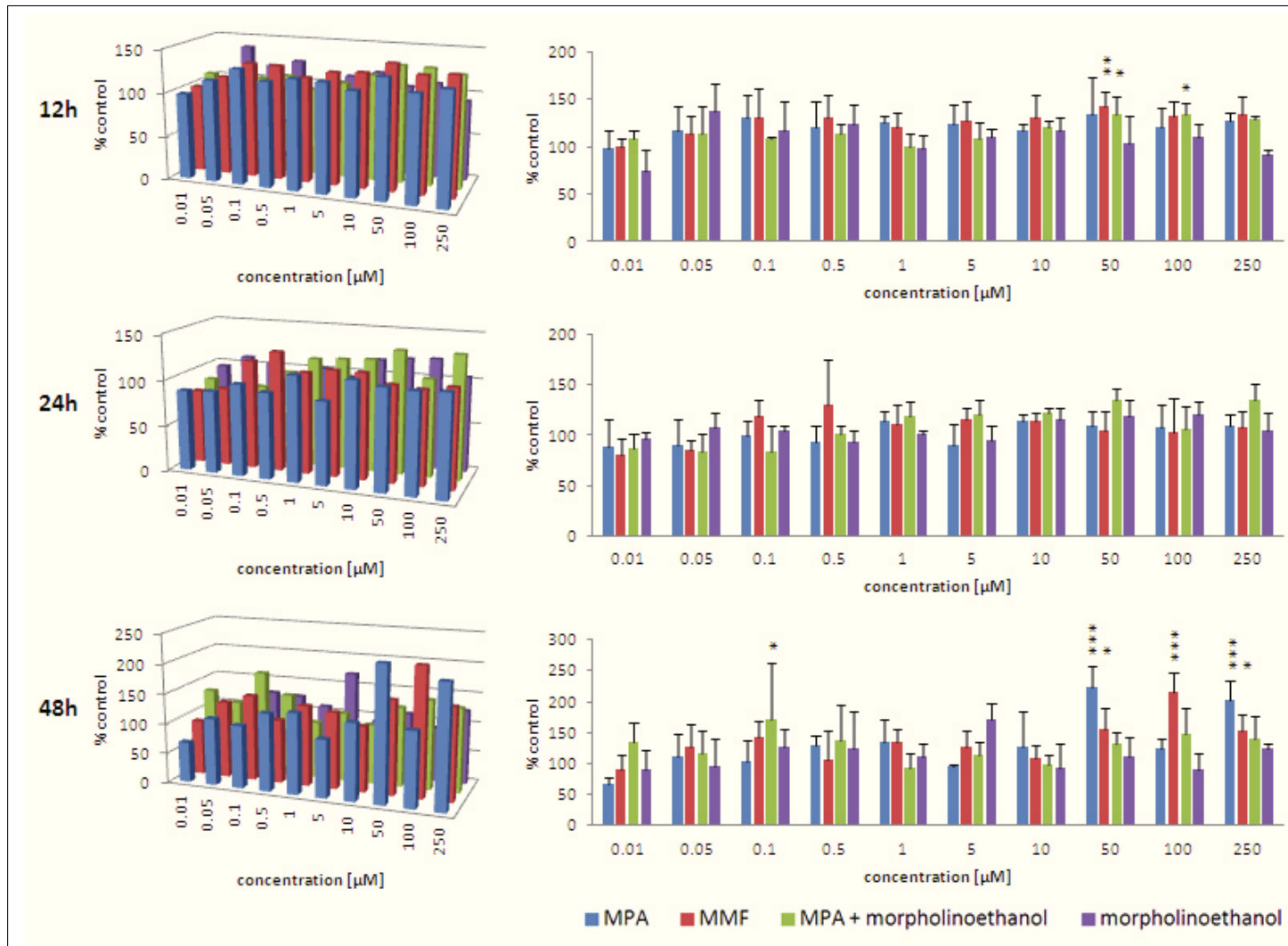


Fig. 4.14: NADP⁺ levels of LS180 cells after 12h, 24h, and 48h of treatment with single doses of test compounds. Values are given as means of % of controls (N=4). Significance was determined using one-way ANOVA combined with Scheffe's post – hoc test with *: $p < 0.05$; **: $p < 0.005$; ***: $p < 0.001$ versus controls.

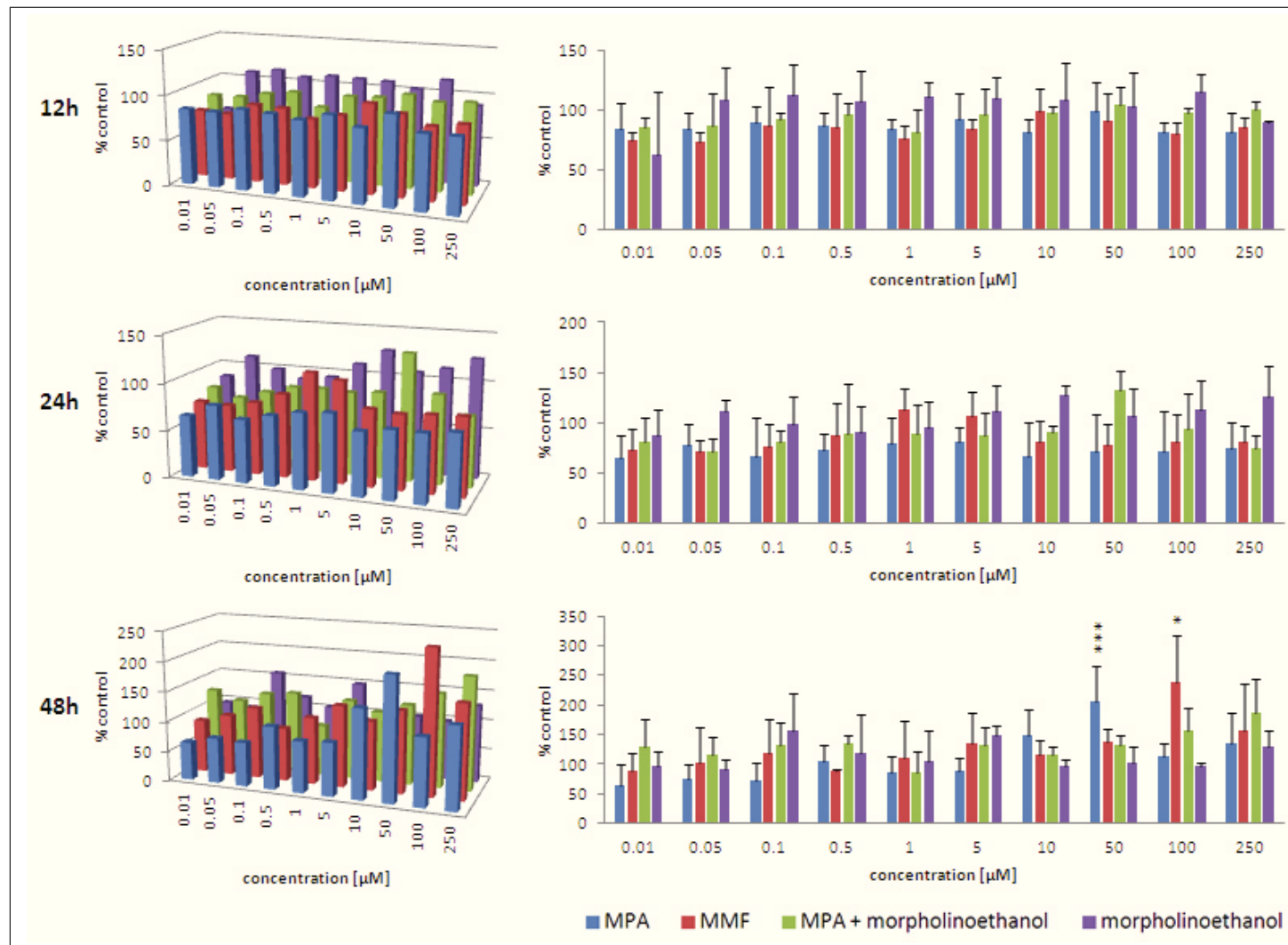


Fig. 4.15: FAD levels of LS180 cells after 12h, 24h, and 48h of treatment with single doses of test compounds. Values are given as means of % of controls ($N=4$). Significance was determined using one-way ANOVA combined with Scheffe's post – hoc test with *: $p<0.05$; **: $p<0.005$; ***: $p<0.001$ versus controls.

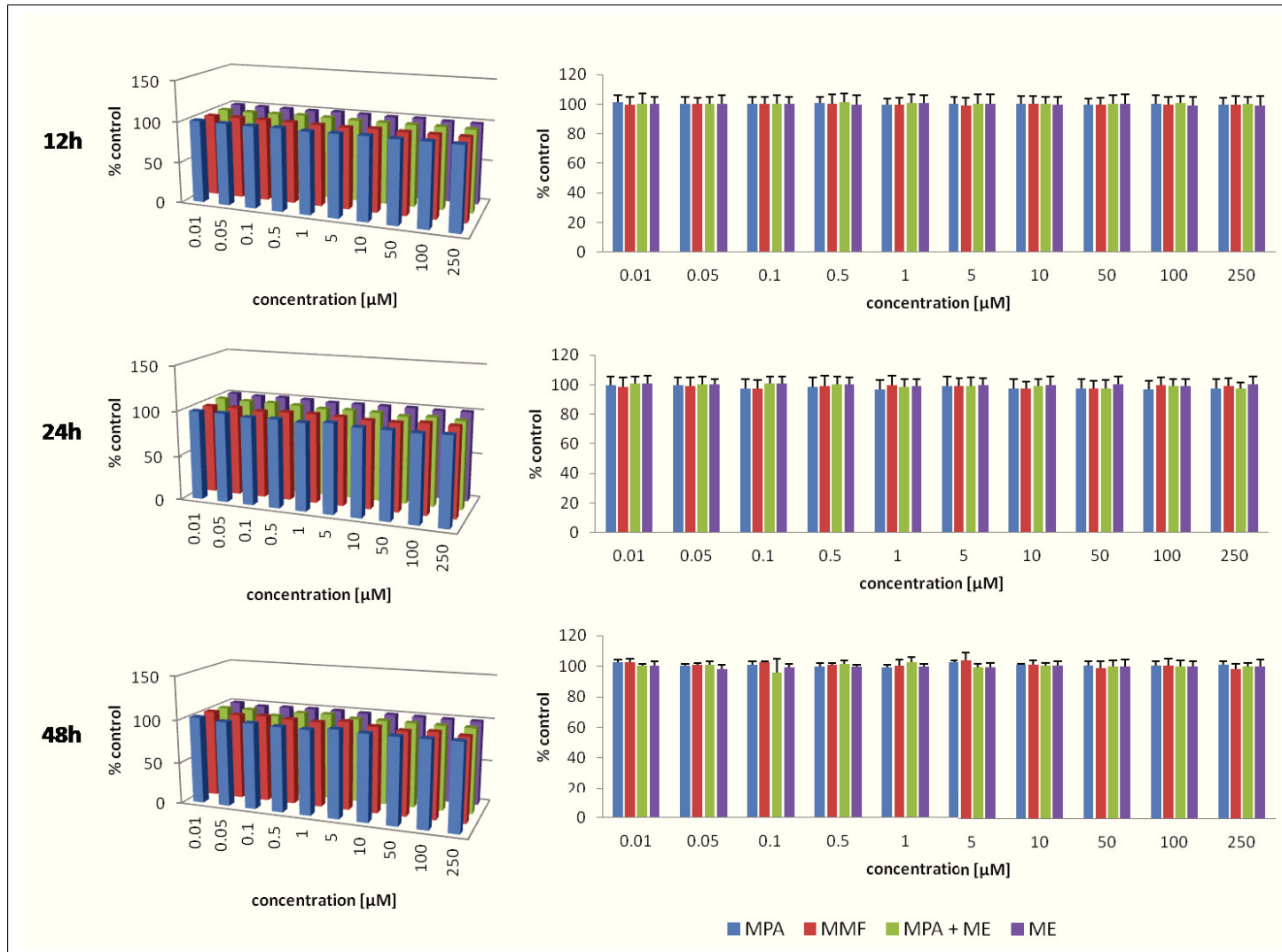


Fig. 4.16: Adenylate energy charge of LS180 cells after 12h, 24h, and 48h of treatment with single doses of test compounds. Values are given as means of % of controls ($N=4$). Significance was determined using one-way ANOVA combined with Scheffe's post – hoc test with *: $p<0.05$; **: $p<0.005$; *: $p<0.001$ versus controls.**

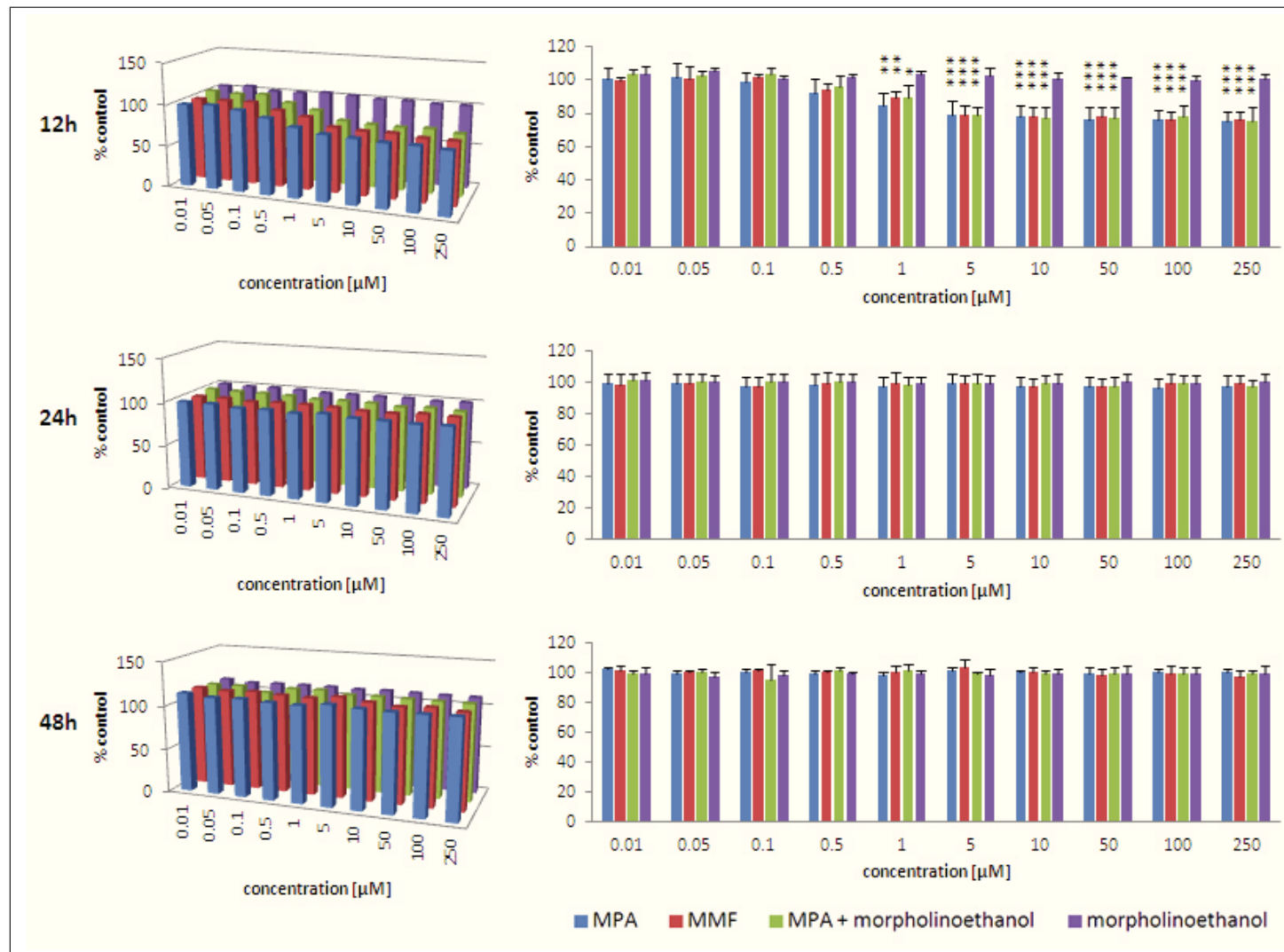


Fig. 4.17: Guanylate energy charge of LS180 cells after 12h, 24h, and 48h of treatment with single doses of test compounds. Values are given as means of % of controls ($N=4$). Significance was determined using one-way ANOVA combined with Scheffe's post – hoc test with *: $p < 0.05$; **: $p < 0.005$; ***: $p < 0.001$ versus controls.

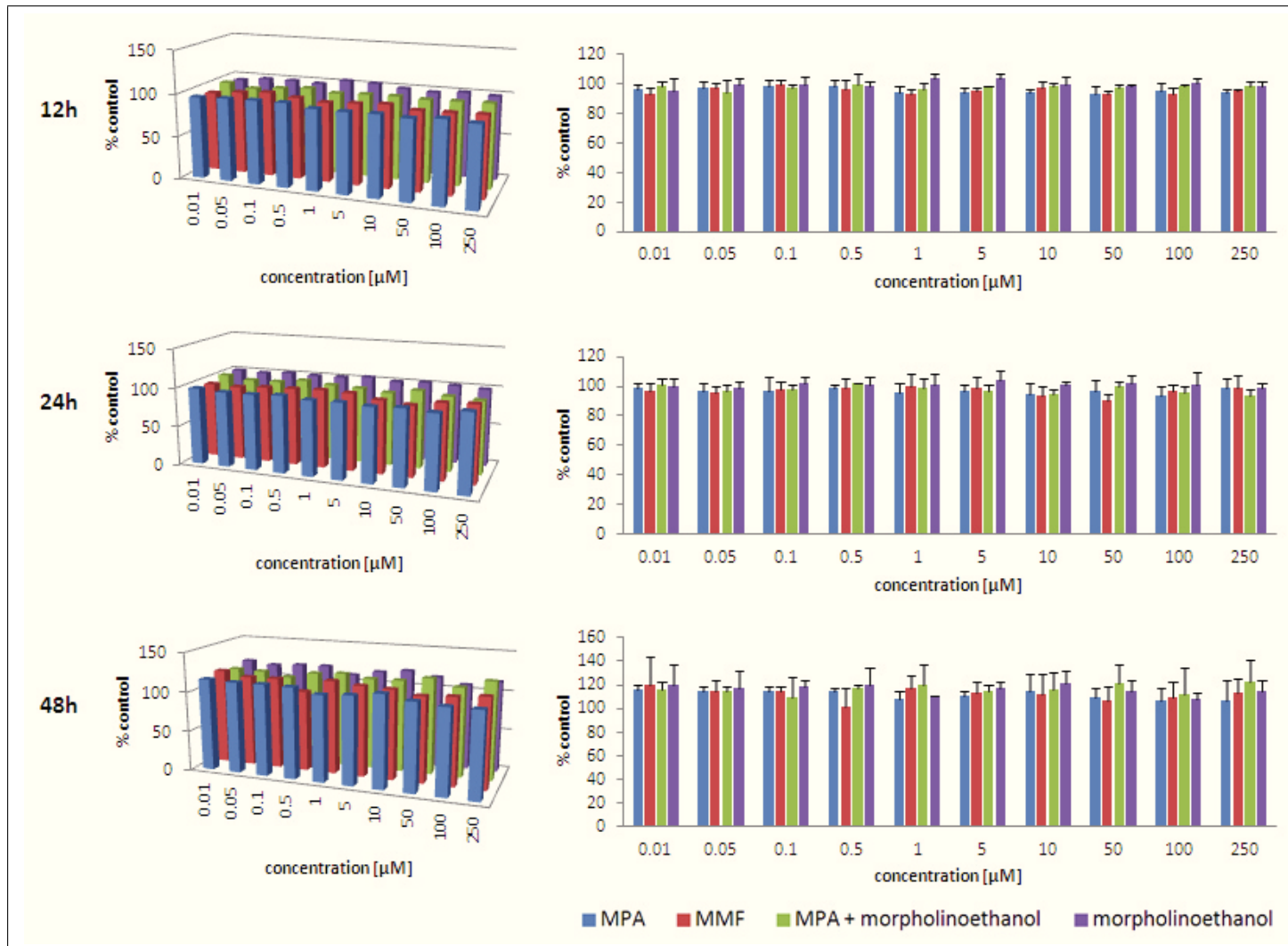


Fig. 4.18: Uridylate energy charge of LS180 cells after 12h, 24h, and 48h of treatment with single doses of test compounds. Values are given as means of % of controls ($N=4$). Significance was determined using one-way ANOVA combined with Scheffe's post – hoc test with *: $p<0.05$; **: $p<0.005$; ***: $p<0.001$ versus controls.

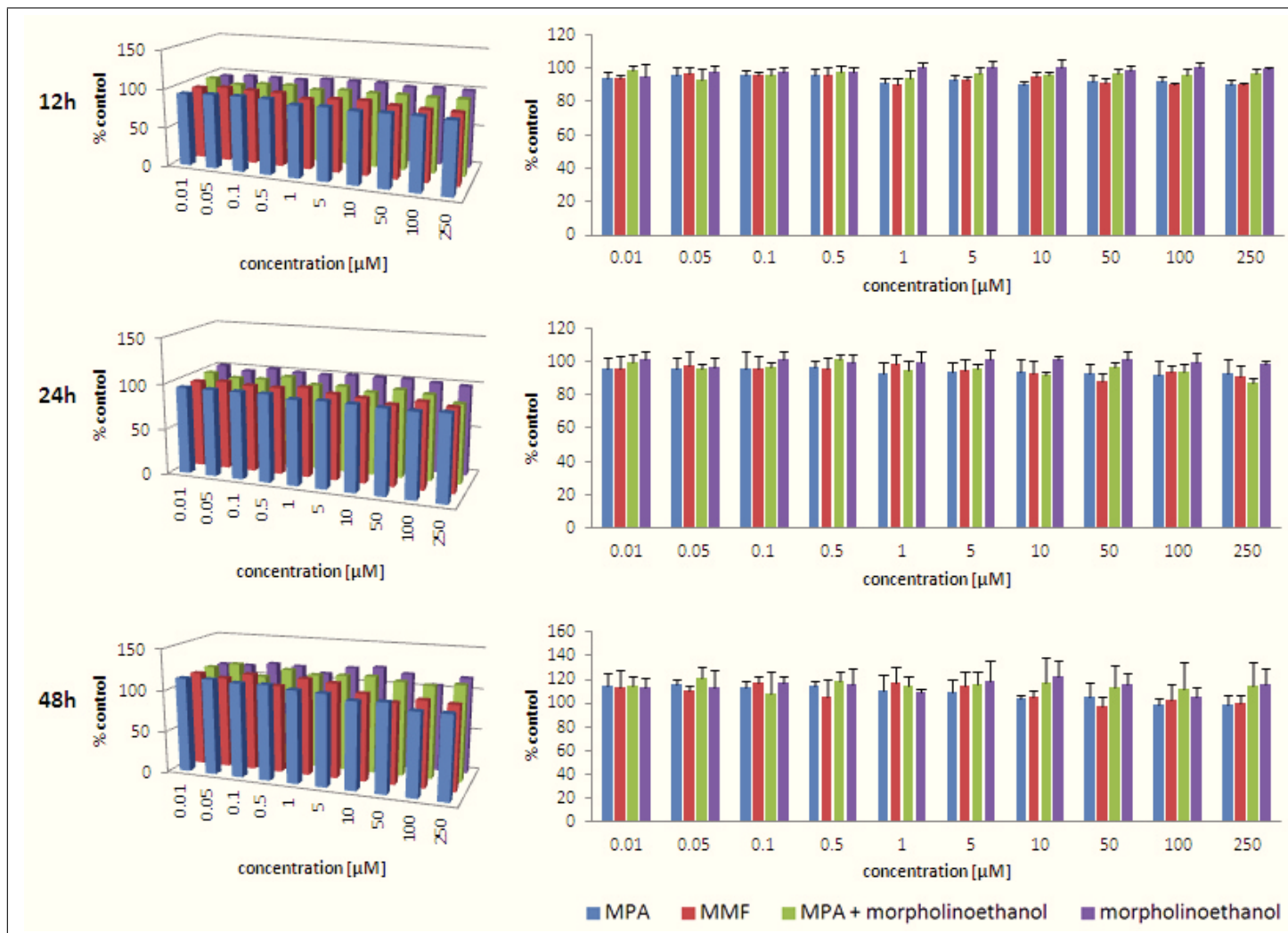


Fig. 4.19: Cytidylate energy charge of LS180 cells after 12h, 24h, and 48h of treatment with single doses of test compounds. Values are given as means of % of controls ($N=4$). Significance was determined using one-way ANOVA combined with Scheffe's *post-hoc* test with *: $p < 0.05$; **: $p < 0.005$; ***: $p < 0.001$ versus controls.

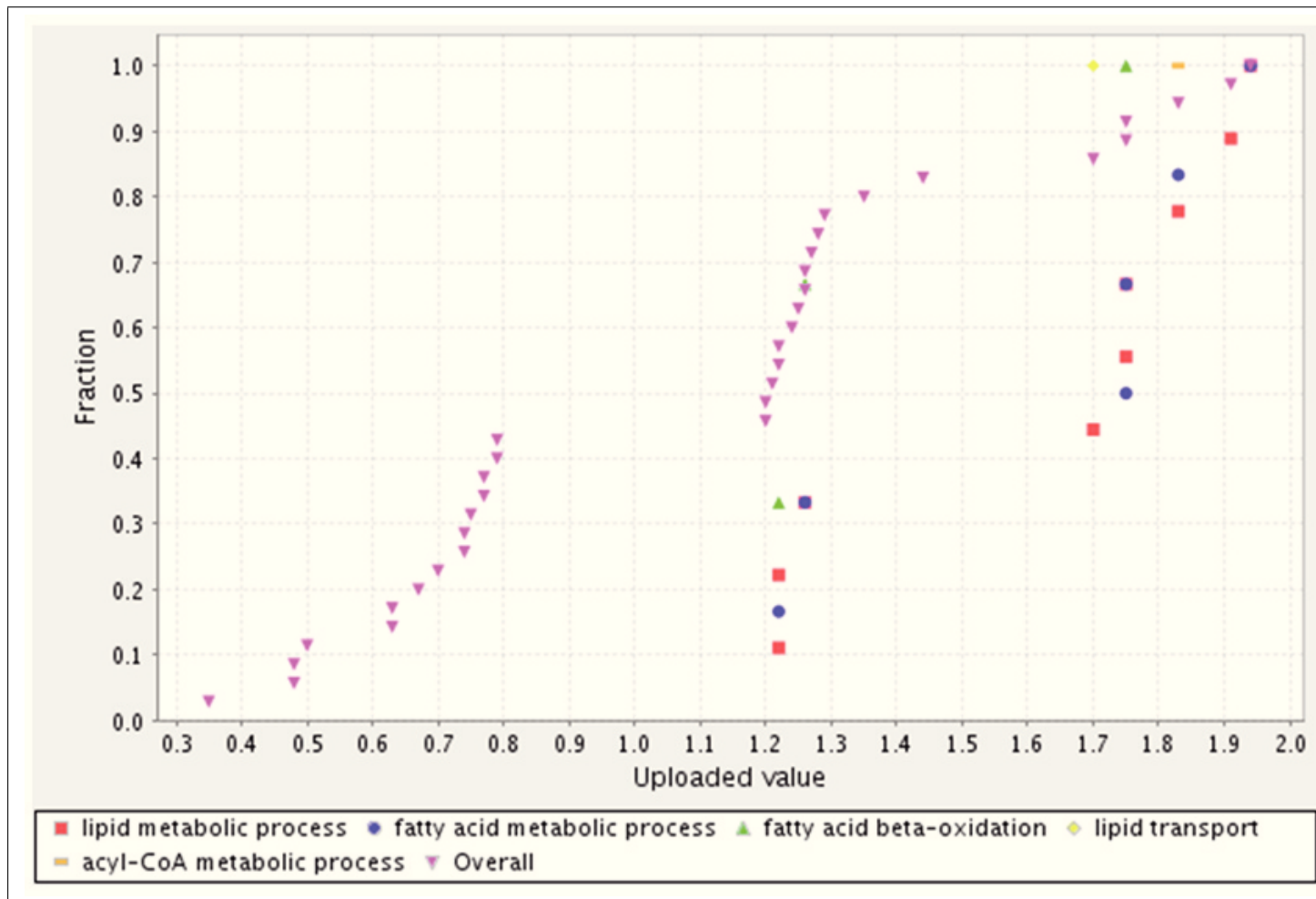


Fig. 4.20: PANTHER chart of differentially expressed proteins involved in lipid metabolism in LS180 cells after MPA treatment. The x-axis shows the fold increase (uploaded value) of a respective protein as determined by SILAC and GelC-MS, the y-axis shows the cumulative fraction (e.g. data point $x=1.4$, $y=0.75$: 75% of uploaded values have a value of 1.4 or smaller).

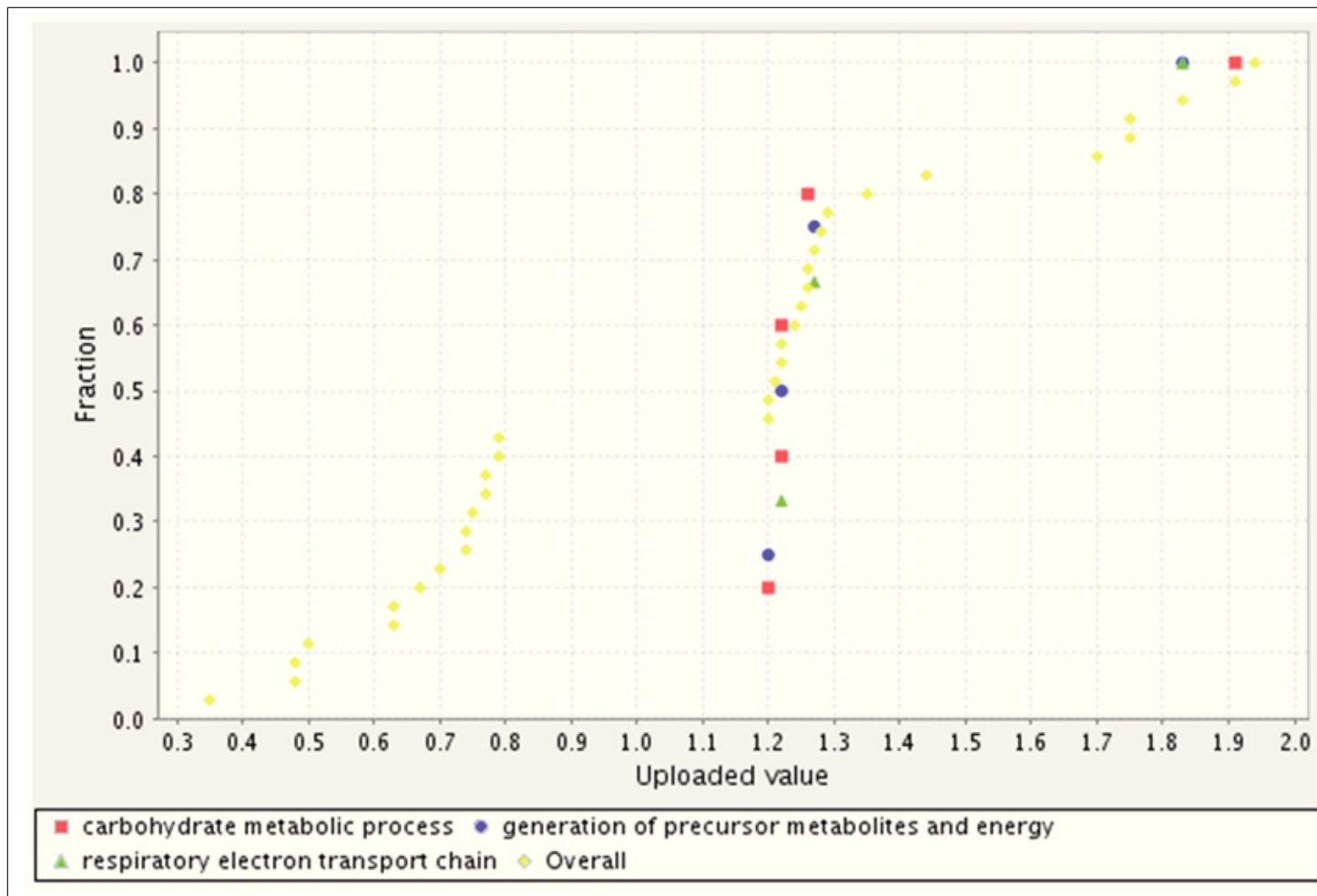


Fig. 4.21: PANTHER chart of differentially expressed proteins involved in carbohydrate metabolism in LS180 cells after MPA treatment. The x-axis shows the fold increase (uploaded value) of a respective protein as determined by SILAC and GelC-MS, the y-axis shows the cumulative fraction (e.g. data point $x=1.4$, $y=0.75$: 75% of uploaded values have a value of 1.4 or smaller).

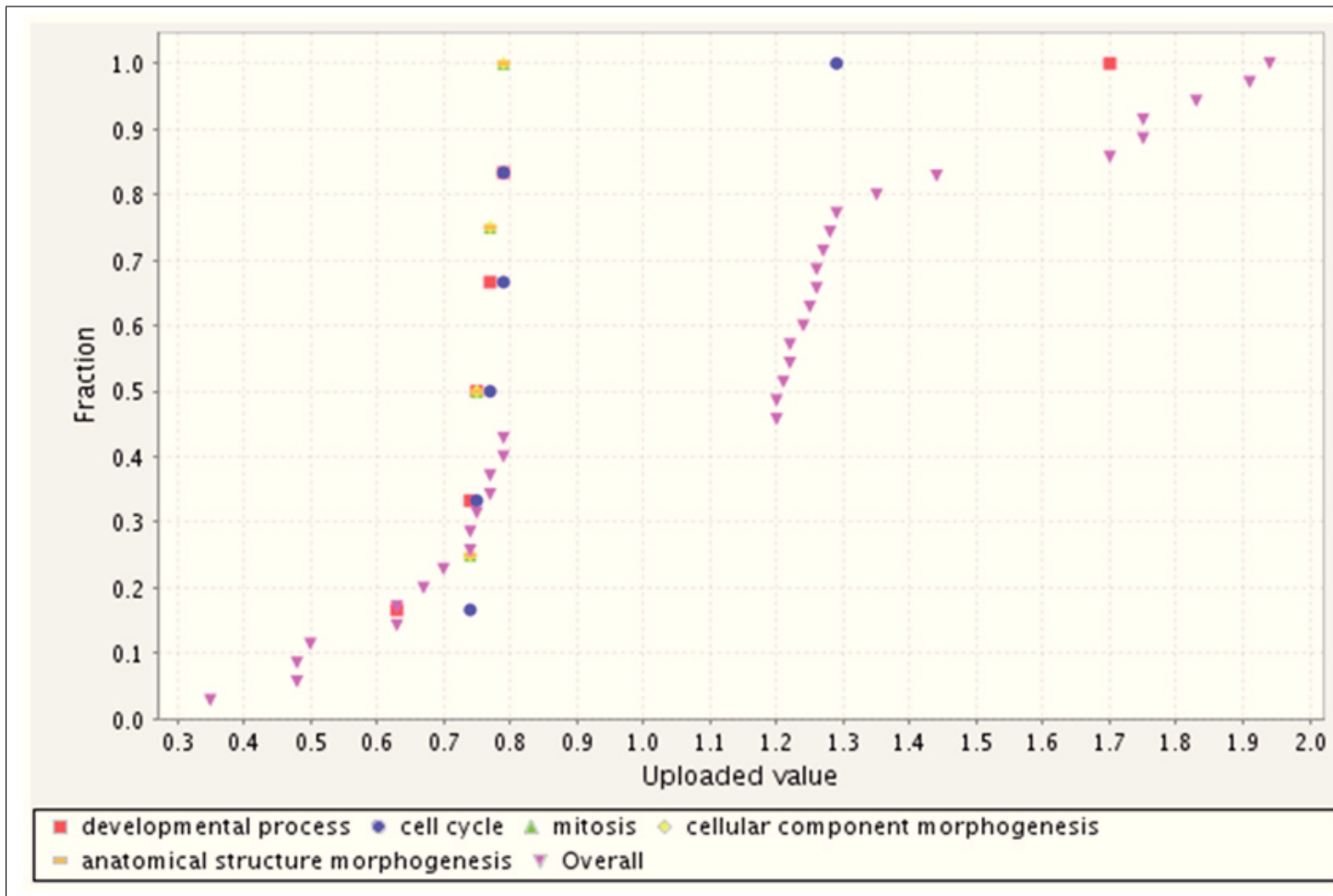


Fig. 4.22: PANTHER chart of differentially expressed proteins involved in developmental processes in LS180 cells after MPA treatment. The x-axis shows the fold increase (uploaded value) of a respective protein as determined by SILAC and GelC-MS, the y-axis shows the cumulative fraction (e.g. data point $x=1.4$, $y=0.75$: 75% of uploaded values have a value of 1.4 or smaller).

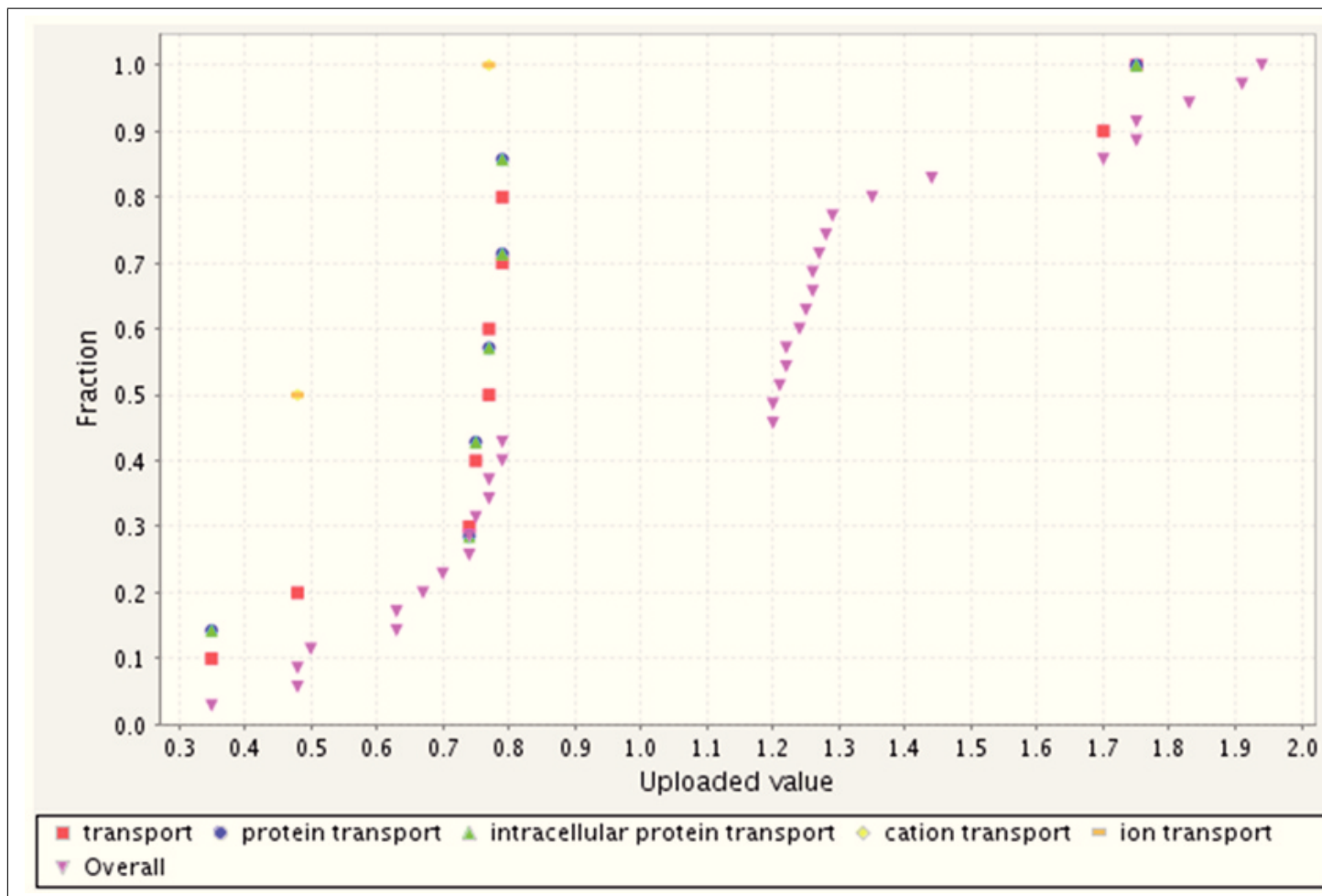


Fig. 4.23: PANTHER chart of differentially expressed proteins involved in transport processes in LS180 cells after MPA treatment. The x-axis shows the fold increase (uploaded value) of a respective protein as determined by SILAC and GelC-MS, the y-axis shows the cumulative fraction (e.g. data point $x=1.4$, $y=0.75$: 75% of uploaded values have a value of 1.4 or smaller).

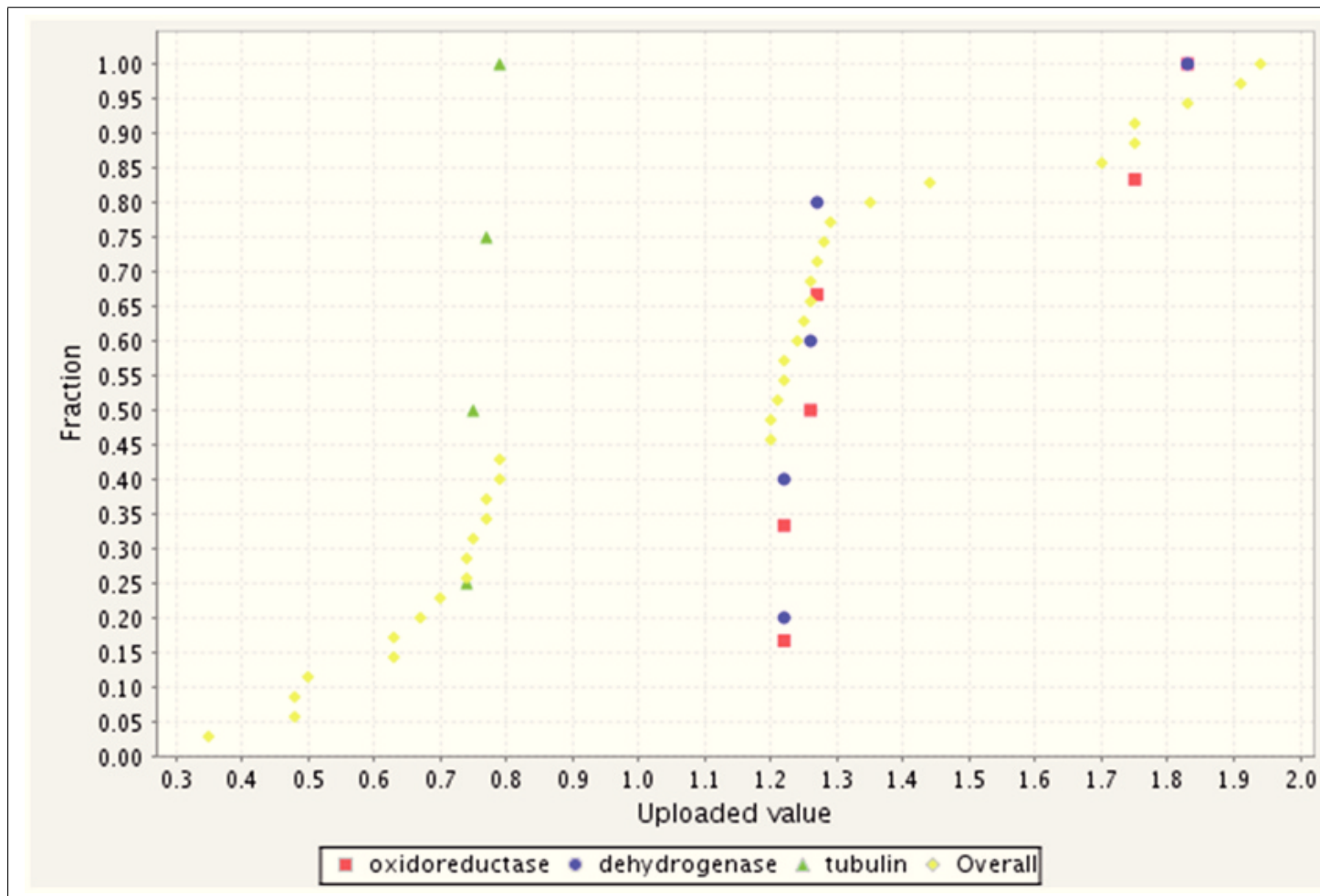


Fig. 4.24: PANTHER chart of differentially expressed proteins according to protein class in LS180 cells after MPA treatment. Shown protein classes were selected from a larger pool of protein classes. The x-axis shows the fold increase (uploaded value) of a respective protein as determined by SILAC and GelC-MS, the y-axis shows the cumulative fraction (e.g. data point $x=1.4, y=0.75$: 75% of uploaded values have a value of 1.4 or smaller).

Table 4.1: Proteins/genes identified in [175, 176, 294] to be affected by MPA treatment in rats. Proteins/genes are listed with their abbreviations, Uniprot identifiers and reference. For their physiological functions, please see the references.

#	Protein	Abbr.	Uniprot Acc.	Ref.
1	Actin, cytoplasmic 1 (β -actin)	ACTB <i>Actb</i>	P60711	[175]
2	L-lactate dehydrogenase B chain	LDH-B <i>Ldhb</i>	P42123	[175]
3	Aldose reductase	AR <i>Akr1b1</i>	P07943	[175]
4	Glyceraldehyde-3-phosphate dehydrogenase	GAPDH <i>Gapdh</i>	P04797	[175]
5	Heat shock cognate 71 kDa protein (Heat shock 70 kDa protein 8)	HSPA8 <i>Hspa8/Hsc70</i>	P63018	[175]
6	Glutathione synthetase	GSH-S <i>Gss</i>	P46413	[175]
7	Glycine amidinotransferase, mitochondrial	AGAT <i>Gatm/Agat</i>	P50442	[175]
8	Alpha-enolase	ENO1 <i>Eno1</i>	P04764	[175]
9	Hydroxyacid oxidase 2	HAOX2 <i>Hao2</i>	Q07523	[175]
10	Selenium-binding protein 1	SBP56 <i>Selenbp1</i>	Q8VIF7	[175]
11	Protein-disulfide-isomerase A3	PDIA3 <i>Pdia3</i>	P11598	[175]
12	ATP synthase subunit β , mitochondrial	ATP5B <i>Atp5b</i>	P10719	[175]
13	Phosphotriesterase-related protein	PTER <i>Pter</i>	Q63530	[175]
14	Aminoacylase-1A	ACY-1A <i>Acy1a</i>	Q6PTT1	[175]
15	Pyridoxal kinase	ALDH1 <i>Pdxk</i>	O35331	[175]
16	Aldehyde dehydrogenase, mitochondrial	ALDH1 <i>Aldh2</i>	P11884	[175]
17	Peroxiredoxin-3	PRDX3 <i>Prdx3</i>	G3V7I0	[175]
18	Triosephosphate isomerase	TIM <i>Tpi1</i>	P48500	[175]
19	Peroxiredoxin-6	PRDX6 <i>Prdx6</i>	O35244	[175]
20	Tropomyosin α -1 chain	TM-1 <i>Tpm1</i>	P04692	[175]
21	Tropomyosin α -4 chain	TM-4 <i>Tpm4</i>	P09495	[175]
22	Sodium/potassium-transporting ATPase subunit α -1	ATP1A1 <i>Atp1a1</i>	P06685	[175]
23	Elongation factor 1- α 1	EF-1- α -1 <i>Eef1a1</i>	P62630	[175]

Continued on next page.

Proteins/genes identified in [175, 176, 294] to be affected by MPA treatment in rats, continued from previous page.

#	Protein	Abbr.	Uniprot Acc.	Ref.
24	Heat shock protein HSP 90- β (Heat shock 84 kDa, HSP84)	HSP84 <i>Hsp90ab1</i>	P34058	[175]
25	Kynurenine/alpha-aminoadipate aminotransferase, mitochondrial	KAT/AadAT <i>Kat2/Aadat</i>	Q64602	[175]
26	Long-chain specific acyl-CoA dehydrogenase, mitochondrial	LCAD <i>Acadl</i>	P15650	[175]
27	Aspartate aminotransferase, cytoplasmic	GOT1 <i>Got1</i>	P13221	[175]
28	Pyruvate dehydrogenase E1 component subunit β , mitochondrial	PDHE1-B <i>Pdhb</i>	P49432	[175]
29	Ester hydrolase C11orf54 homolog	-	Q5U2Q3	[175]
30	Sulfotransferase 1C2A	ST1C2A <i>Sult1c2a</i>	Q9WUW9	[175]
31	Thiomorpholine-carboxylate dehydrogenase	CRYM <i>Crym</i>	Q9QYU4	[175]
32	Methylmalonate-semialdehyde dehydrogenase [acylating], mitochondrial	MMSDH <i>Aldh6a1</i>	Q02253	[175]
33	4-hydroxyphenylpyruvate dioxygenase	4HPPD <i>Hpd</i>	P32755	[175]
34	Malate dehydrogenase, mitochondrial	MDH2 <i>Mdh2</i>	P04636	[175]
35	Gamma-glutamyltranspeptidase 1	GGT1 <i>Ggt1</i>	P07314	[175]
36	Carbonic anhydrase 2	CA-II <i>Ca2</i>	P27139	[175]
37	Enoyl-CoA delta isomerase 1, mitochondrial	Eci1 <i>Eci1</i>	P23965	[175]
38	14-3-3 protein θ	YWHAZ <i>Ywhaz</i>	P63102	[175]
39	Pro-cathepsin H	CTSH <i>Ctsh</i>	P00786	[175]
40	4-trimethylaminobutyraldehyde dehydrogenase	TMABADH <i>Aldh9a1</i>	Q9JLJ3	[175]
41	Glutathione S-transferase α -1	GST1-1 <i>Gsta1</i>	P00502	[175]
42	Aquaporin-1	AQP-1 <i>Aqp1</i>	P29975	[175]
43	Cytochrome c oxidase subunit 2	MTCO2 <i>Mtco2</i>	P00406	[175]
44	Fructose-bisphosphate aldolase B	ALDOB <i>Aldob</i>	P00884	[175]
45	Glutathione S-transferase α -4	GST 8-8 <i>Gsta4</i>	P14942	[175]
46	Hemoglobin subunit β -1	HBB <i>Hbb</i>	P02091	[175]
47	Hemoglobin subunit α -1/2	HBA1 <i>Hba1</i>	P01946	[175]
48	Cytochrome c oxidase subunit 4 isoform 1, mitochondrial	COX IV-1 <i>Cox4i1</i>	P10888	[175]

Continued on next page.

4 Appendix

Proteins/genes identified in [175, 176, 294] to be affected by MPA treatment in rats, *continued from previous page.*

#	Protein	Abbr.	Uniprot Acc.	Ref.
49	Ribonuclease UK114	HRSP12 <i>Hrsp12</i>	P52759	[175]
50	Voltage-dependent anion-selective channel protein 1	VDAC-1 <i>Vdac1</i>	Q9Z2L0	[175]
51	Sodium/potassium-transporting ATPase subunit β -1	ATP1B1 <i>Atp1b1</i>	P07340	[175]
52	Protein disulfide-isomerase A3	PDIA3 <i>Pdia3</i>	P11598	[176]
53	Selenium-binding protein 1	SELENBP1 <i>Selenbp1</i>	Q8VIF7	[176]
54	ATP synthase subunit β , mitochondrial	ATP5B <i>Atp5b</i>	P10719	[176]
55	ATP synthase subunit α , mitochondrial	ATP5A1 <i>Atp5a1</i>	P15999	[176]
56	Catalase	CAT <i>Cat</i>	P04762	[294]
57	Dynein light chain 1, cytoplasmic	DYNLL1 <i>Dynll1</i>	P63170	[294]
58	Cytochrome c oxidase subunit 1	MTCO1 <i>Mtco1</i>	P05503	[294]
59	Lipopolysaccharide-binding protein	LBP <i>Lbp</i>	Q63313	[294]
60	Polymeric immunoglobulin receptor	PIgR <i>Pigr</i>	P15083	[294]
61	Sphingosine 1-phosphate receptor 1	S1P1 <i>S1pr1</i>	P48303	[294]
62	Hepatocyte nuclear factor 4- α	HNF-4- α <i>Hnf4a</i>	P22449	[294]
63	Lipolysis-stimulated lipoprotein receptor	LSR <i>Lsr</i>	Q9WU74	[294]
64	Retinoic acid receptor α 1	RARA <i>Rara</i>	Q9QWT4	[294]
65	CCAAT/enhancer-binding protein α	C/EBP α <i>Cebpa</i>	P05554	[294]
66	Serine/threonine-protein phosphatase PP1- α catalytic subunit	PP-1A <i>Ppp1ca</i>	P62138	[294]
67	Galectin-9	Gal-9 <i>Lgals9</i>	P97840	[294]
68	Vascular endothelial growth factor A	VEGF-A <i>Vegfa</i>	P16612	[294]
69	Solute carrier family 22 member 2	SLC22A2 <i>Slc22a2</i>	Q9R0W2	[294]
70	Sodium-coupled neutral amino acid transporter 3	SLC38A3 <i>Slc38a3</i>	Q9JHZ9	[294]
71	Sulfated glycoprotein 1	SGP-1 <i>Psap</i>	P10960	[294]
72	Hemoglobin subunit α -1/2	HBA1 <i>Hba1</i>	P01946	[294]
73	Syndecan-1	SYND1 <i>Sdc1</i>	P26260	[294]

Continued on next page.

Proteins/genes identified in [175, 176, 294] to be affected by MPA treatment in rats, continued from previous page.

#	Protein	Abbr.	Uniprot Acc.	Ref.
74	Actin, cytoplasmic 2	ACTG1 <i>Actg1</i>	P63259	[294]
75	Endoplasmic/Heat shock protein 90 kDa β member 1	HSP90B1 <i>Hsp90b1</i>	Q66HD0	[294]
76	Acyl-CoA desaturase 1	SCD1 <i>Scd1</i>	P07308	[294]
77	Stress-associated endoplasmic reticulum protein 1	SERP1 <i>Serp1</i>	Q9R2C1	[294]
78	Epoxide hydrolase 1	EPHX1 <i>Ephx1</i>	P07687	[294]
79	Fatty acid synthase	FASN <i>Fasn</i>	P12785	[294]
80	3-oxo-5-alpha-steroid 4-dehydrogenase 1	SRD5A1 <i>Srd5a1</i>	P24008	[294]

Three Uniprot accessions, i.e. G3V7I0 (#17), P00406 (#43), P05503 (#58), were unknown by DAVID and were therefore removed from the gene list for analysis. Four genes/proteins were found repeatedly (in several publications) so that 73 genes/proteins constituted the gene list for analysis.

Table 4.2: Proteins/genes identified in [295, 296] to be affected by MPA treatment in HEK-293 and CCRF-CEM cells, respectively. Proteins/genes are listed with their abbreviations, Uniprot identifiers and reference. For their physiological functions, please see the references.

#	Protein	Abbr.	Uniprot Acc.	Ref.
1	Protein SET	SET <i>SET</i>	Q01105	[295]
2	Complement component 1 Q subcomponent-binding protein, mitochondrial	C1qBP <i>C1QBP</i>	Q07021	[295]
3	Electron transfer flavoprotein subunit β	β -ETF <i>ETFB</i>	P38117	[295]
4	Cytochrome b-c1 complex subunit Rieske, mitochondrial	RISP <i>UQCRFS1</i>	P47985	[295]
5	Peroxiredoxin-1	PRDX1 <i>PRDX1</i>	Q06830	[295]
6	Stathmin	STMN1 <i>STMN1</i>	P16949	[295]
7	Thioredoxin domain-containing protein 12	ERp18 <i>TXNDC12</i>	O95881	[295]
8	Myosin regulatory light chain 12B	MLC-2 <i>MYL12B</i>	O14950	[295]
9	Histone H2B type 1-A	HIST1H2BA <i>HIST1H2BA</i>	Q96A08	[295]
10	Histone H2B type 1-C/E/F/G/I	H2B.1 A <i>HIST1H2BC</i>	P62807	[295]
11	40S ribosomal protein S12	RPS12 <i>RPS12</i>	P25398	[295]
12	Profilin-1	PFN1 <i>PFN1</i>	P07737	[295]
13	Endoplasmic/Heat shock protein 90 kDa β member 1 (Human)	HSP90B1 <i>HSP90B1</i>	P14625	[296]
14	Cofilin-1	CFL1 <i>Cfl1</i>	P45592	[296]
15	Rho GDP-dissociation inhibitor 2	Rho GDI 2 <i>ARHGDI2</i>	P52566	[296]
16	Proliferating cell nuclear antigen	PCNA <i>Pcna</i>	P04961	[296]
17	Acidic leucine-rich nuclear phosphoprotein 32 family member B	ANP32B <i>Anp32b</i>	Q9EST6	[296]
18	Deoxyuridine 5'-triphosphate nucleotidohydrolase	dUTPase <i>Dut</i>	P70583	[296]
19	Serine/arginine-rich splicing factor 2	SRSF2 <i>Srsf2</i>	Q6PDU1	[296]
20	ATP synthase subunit β , mitochondrial	ATP5B <i>Atp5b</i>	Q5M860	[296]
21	Prostaglandin E synthase 3	PTGES3 <i>Ptges3</i>	P83868	[296]
22	Peptidyl-prolyl cis-trans isomerase A	PPIase A <i>Ppia</i>	P10111	[296]
23	Rho GDP-dissociation inhibitor 2	Rho GDI 2 <i>ARHGDI2</i>	P52566	[296]

One protein was found repeatedly in both publications so that 22 proteins constituted the gene list for analysis.

Table 4.3: Functional Annotation Clustering of 74 genes/proteins affected by MPA treatment in rats. *Genes/proteins taken from [175, 176, 294]. Functional Annotation Clustering was performed using customized options as described in Section 2.7.1, 3 annotation clusters were found (# 1-3). A representative annotation term was assigned to characterize grouping terms as comprehensively as possible (for specification of most important other terms contributing to an annotation cluster/gene functional group please see footnotes). Enrichment scores are given ranking biological significance of gene groups based on overall EASE scores of all enriched annotation terms (for explanation please see Section 3.9.2). The number of genes/proteins in each cluster is given (Count) as well as the Uniprot accessions of genes/proteins from each cluster. 104 terms were not clustered.*

#	Rep. ann. term	Enr. score	Count	Proteins encoded by analyzed genes
1	Carbohydrate catabolic process ¹	5.83	7	P00884, P04764, P42123, P04636, P49432, P04797, P48500
2	Nicotinamide nucleotide metabolic process ²	2.57	4	P00884, P42123, P04636, P48500
3	Purine nucleoside triphosphate/ATP metabolic process ³	1.6	4	P15999, P10719, P06685, P07340

¹ Glycolysis, glucose catabolic process, hexose catabolic process, monosaccharide catabolic process, cellular carbohydrate catabolic process, alcohol catabolic process

² Nicotinamide metabolic process, alkaloid metabolic process, pyridine nucleotide metabolic process, oxidoreduction coenzyme metabolic process, secondary metabolic process

³ ATPase activity, coupled to (transmembrane) movement of ions/substances; ATPase biosynthetic/metabolic process; hydrolase activity, acting on acid anhydrides, catalyzing transmembrane movement of substances, (purine) ribonucleoside/ribonucleotide triphosphate biosynthetic process; P-P-bond-hydrolysis driven/primary active transmembrane transporter activity

Table 4.4: Pathway Enrichment Analysis of 74 proteins/genes affected by MPA treatment in rats. *Proteins/genes taken from [175, 176, 294]. The KEGG database and DAVID's Functional Annotation Chart tool were used and customized as described in Section 2.7.1. 11 records were found. The number of proteins/genes in each cluster is given (Count) as well as the Uniprot accessions of genes/proteins from each cluster. 55 genes from the list were not in the output.*

#	Term	Count	Uniprot acc.	P-value
1	Glycolysis/ gluconeogenesis	8	P11884, Q9JLJ3, P00884, P04764, P42123, P49432, P04797, P48500	1.7E-5
2	Pyruvate metabolism	6	P11884, Q9JLJ3, P07943, P42123, P04636, P49432	3.7E-5
3	Arginine and proline metabolism	5	P11884, Q9JLJ3, Q6PTT1, P13221, P50442	1.8E-3
4	Propanoate metabolism	4	P11884, Q02253, Q9JLJ3, P42123	4.2E-3
5	Cardiac muscle contraction	5	P06685, P07340, p10888, P04692, P09495	7.4E-3
6	Fatty acid metabolism	4	P15650, P11884, Q9JLJ3, P23965	3.8E-3
7	Tryptophan metabolism	4	P11884, Q9JLJ3, Q64602, P04762	8.9E-3
8	Phenylalanine metabolism	3	P32755, P13221, O35244	1.1E-2
9	Glutathione metabolism	4	P07314, P00502, P14942, P46413	1.2E-1
10	Fructose and mannose metabolism	3	P07943, P00884, P48500	4.0E-2
11	Butanoate metabolism	3	P11884, Q9JLJ3, P49432	4.3E-2

Table 4.5: Functional Annotation Clustering of 22 proteins affected by MPA treatment in human cells of non-cancerous origin. *Proteins taken from [295, 296]. Functional Annotation Clustering was performed using customized options as described in Section 2.7.1. Customization differed from customization for LS180 cell and rat model analyses due to the insufficient amount of data which did not allow to restrict parameters as done previously. 4 annotation clusters were found (# 1-4). A representative annotation term was assigned to characterize grouping terms as comprehensively as possible (for specification of all terms contributing to an annotation cluster/gene functional group see footnotes). Enrichment scores are given ranking biological significance of gene groups based on overall EASE scores of all enriched annotation terms (for explanation, please see Section 3.9.2). The number of proteins/genes in each cluster is given (Count) as well as the Uniprot accessions of proteins/genes from each cluster. 18 terms were not clustered.*

#	Rep. ann. term	Enr. score	Count	Proteins encoded by analyzed genes
1	Organelle lumen ¹	2.22	9	Q01105, O95881, P23528, Q07021, P38117, P14625, P12004, Q01130, O95881
2	Cellular macromolecular complex subunit organization ²	2.19	3/4	Q01105, O95881, Q96A08, P62807
3	Regulation of apoptosis ³	1.54	4/5	O95881, P23528, P14625, Q06830, O95881
4	Actin cytoskeleton organization ⁴	1.42	3/4	P52566, P23528, P07737, P16949

¹ Intracellular organelle lumen, organelle lumen, membrane-enclosed lumen

² DNA packaging, nucleosome assembly, chromatin assembly, protein-DNA complex assembly, nucleosome organization, chromatin assembly or disassembly, cellular macromolecular complex subunit organization

³ Regulation of apoptosis, regulation of programmed cell death, regulation of cell death, cellular homeostasis

⁴ cytoskeleton organization, actin cytoskeleton organization, actin filament-based process

Pathway enrichment analysis of 22 proteins affected by MPA treatment in human cells of non-cancerous origin (Proteins taken from [295, 296]) using the KEGG database and DAVID's Functional Annotation Chart tool customized as described in section 2.7.1 did not yield any enriched pathways.

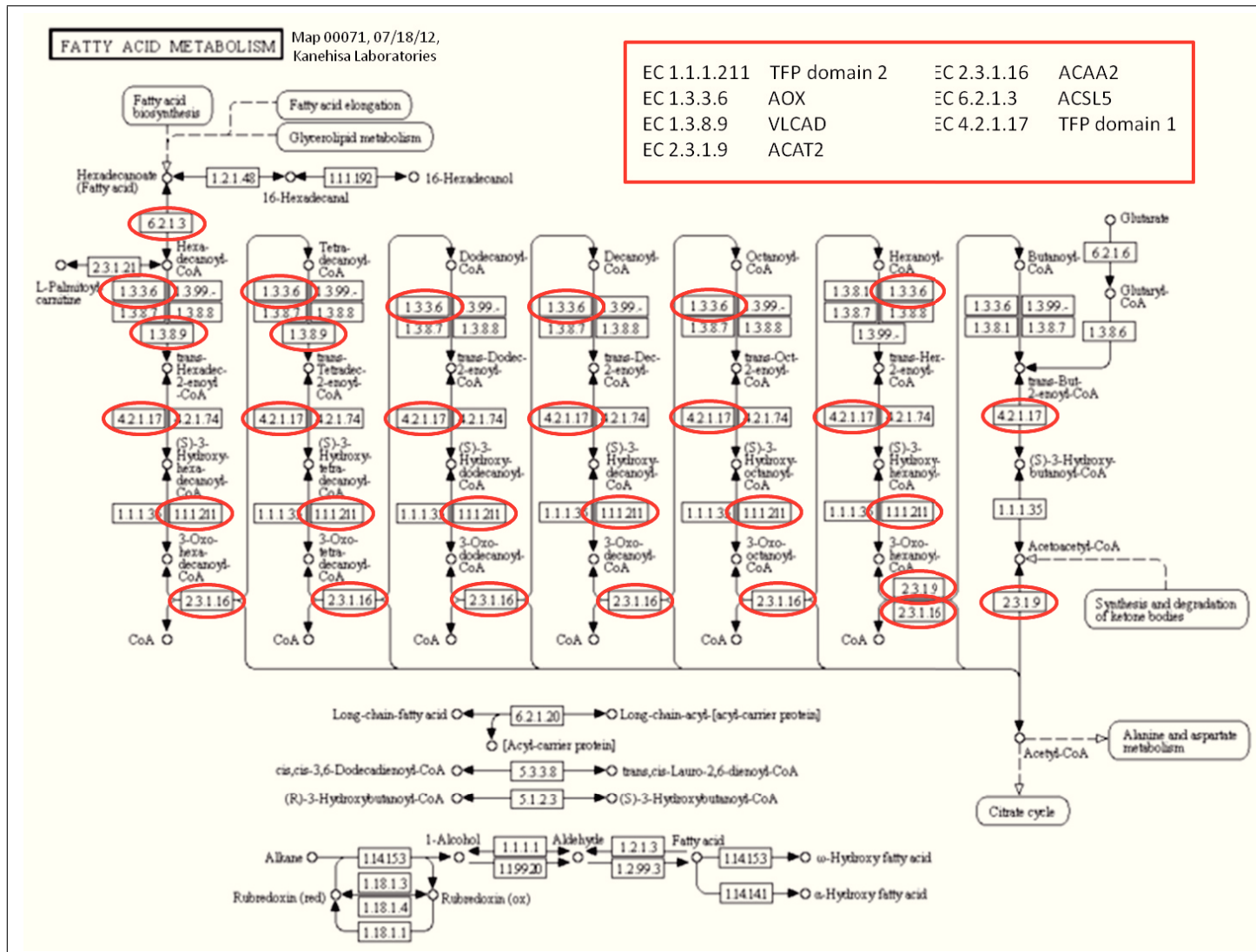


Fig. 4.25: KEGG pathway map 00071: Fatty acid metabolism. EC numbers of proteins significantly affected by MPA treatment in LS180 cells are circled in red and specified in the red box.

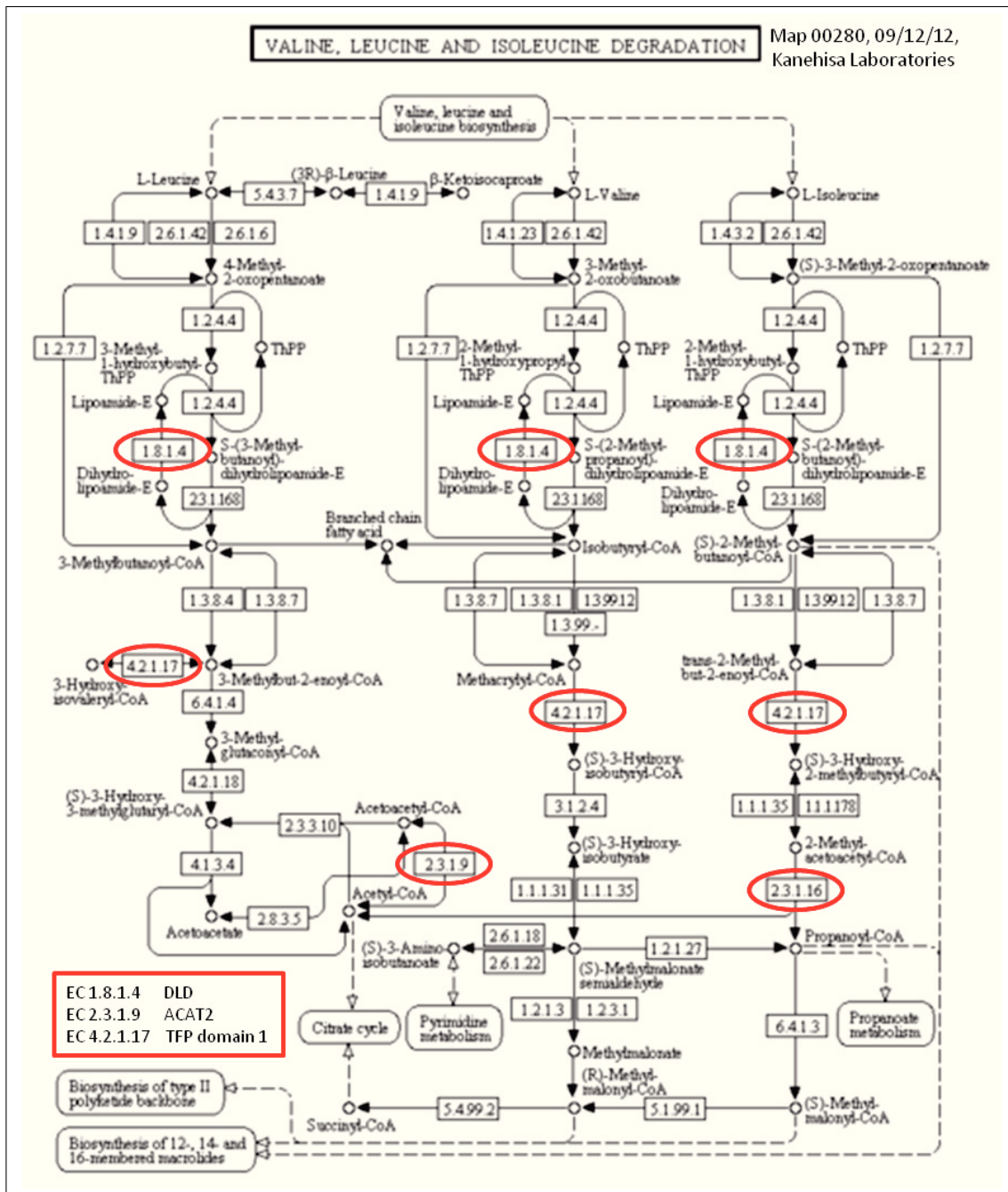


Fig. 4.26: KEGG pathway map 00280: Valine, leucine, and isoleucine degradation. EC numbers of proteins significantly affected by MPA treatment in LS180 cells are circled in red and specified in the red box.

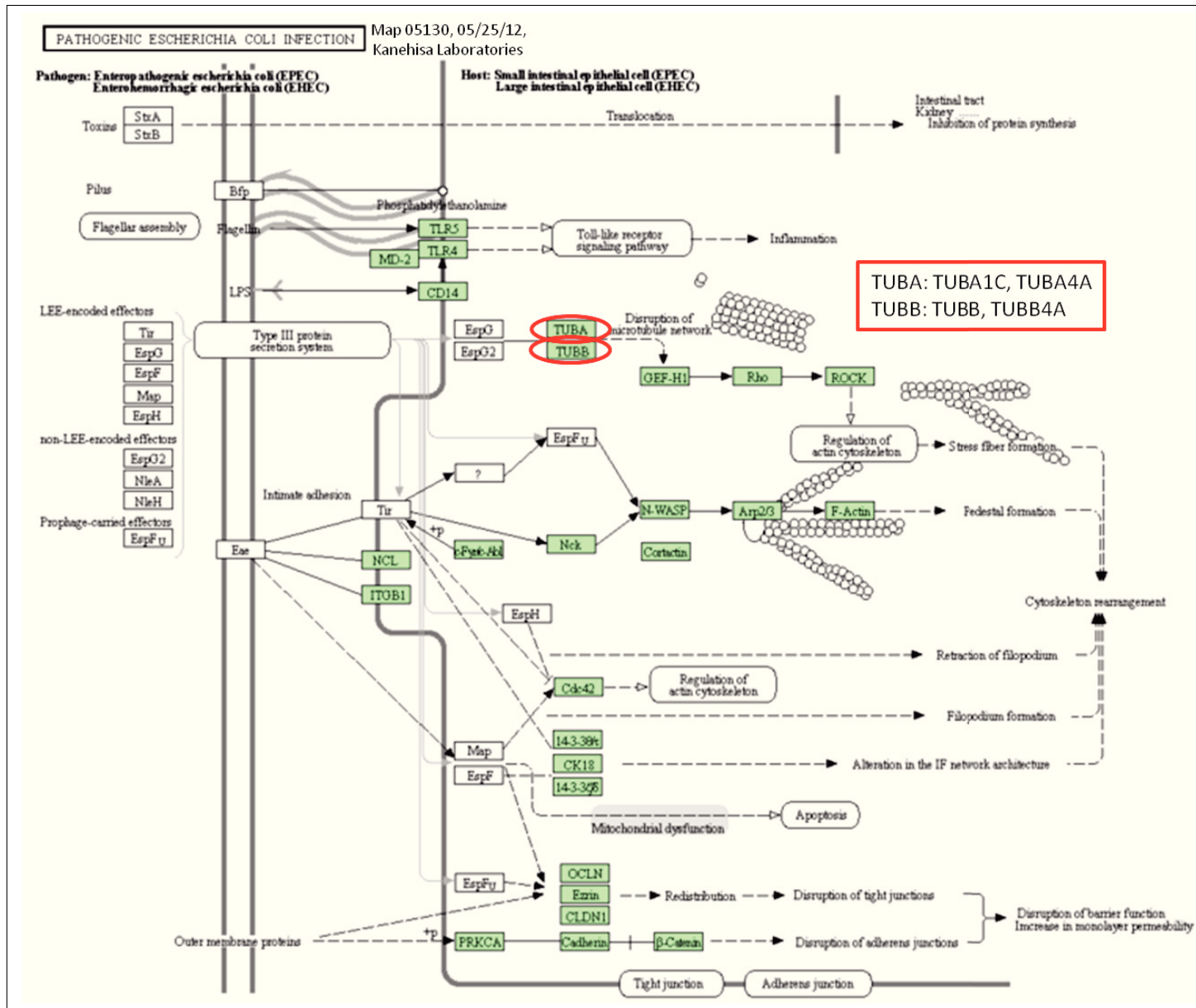


Fig. 4.27: KEGG pathway map 05130: Pathogenic Escherichia Coli infection. *Proteins significantly affected by MPA treatment in LS180 cells are circled in red and specified in the red box.*

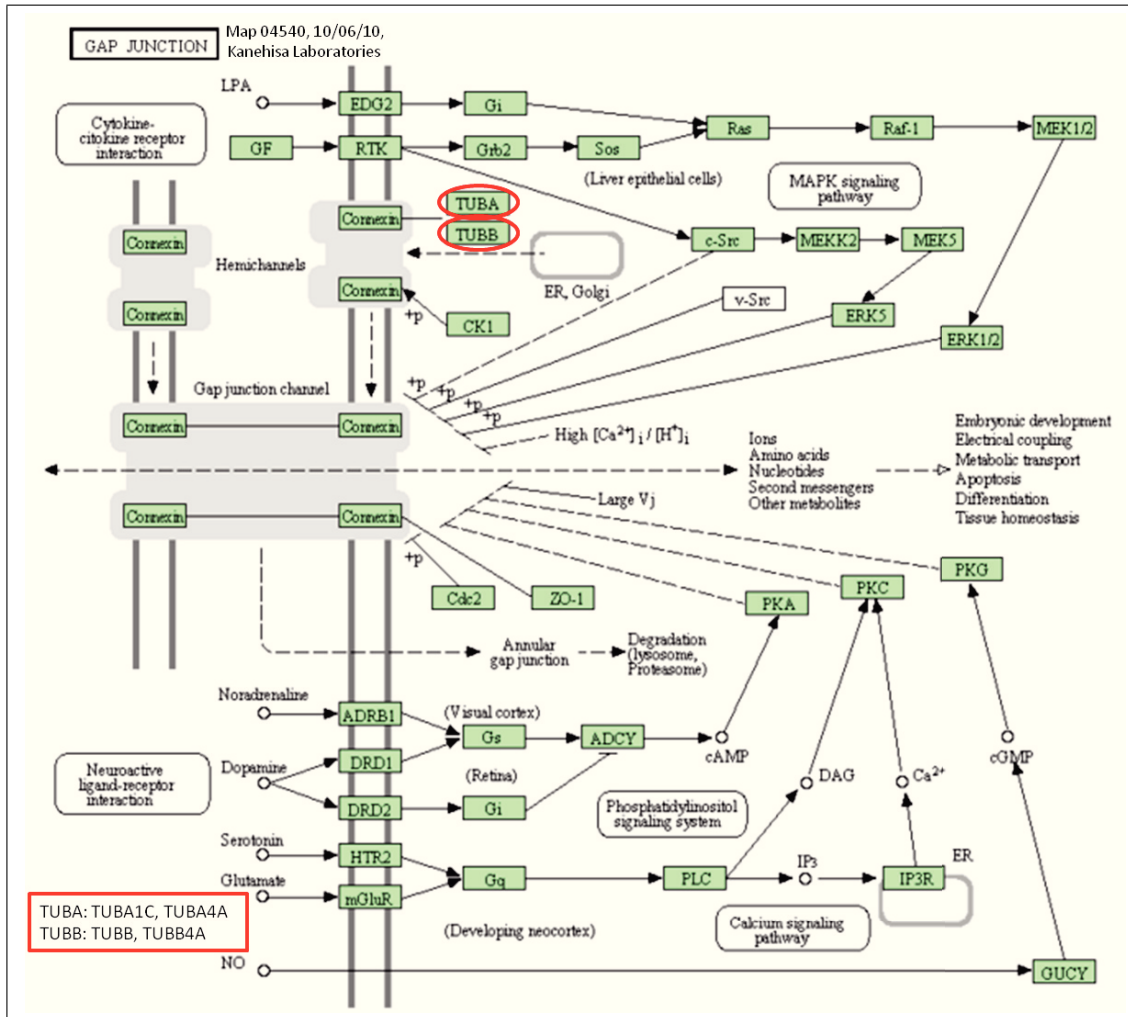


Fig. 4.28: KEGG pathway map 04540: Gap junction. *Proteins significantly affected by MPA treatment in LS180 cells are circled in red and specified in the red box.*

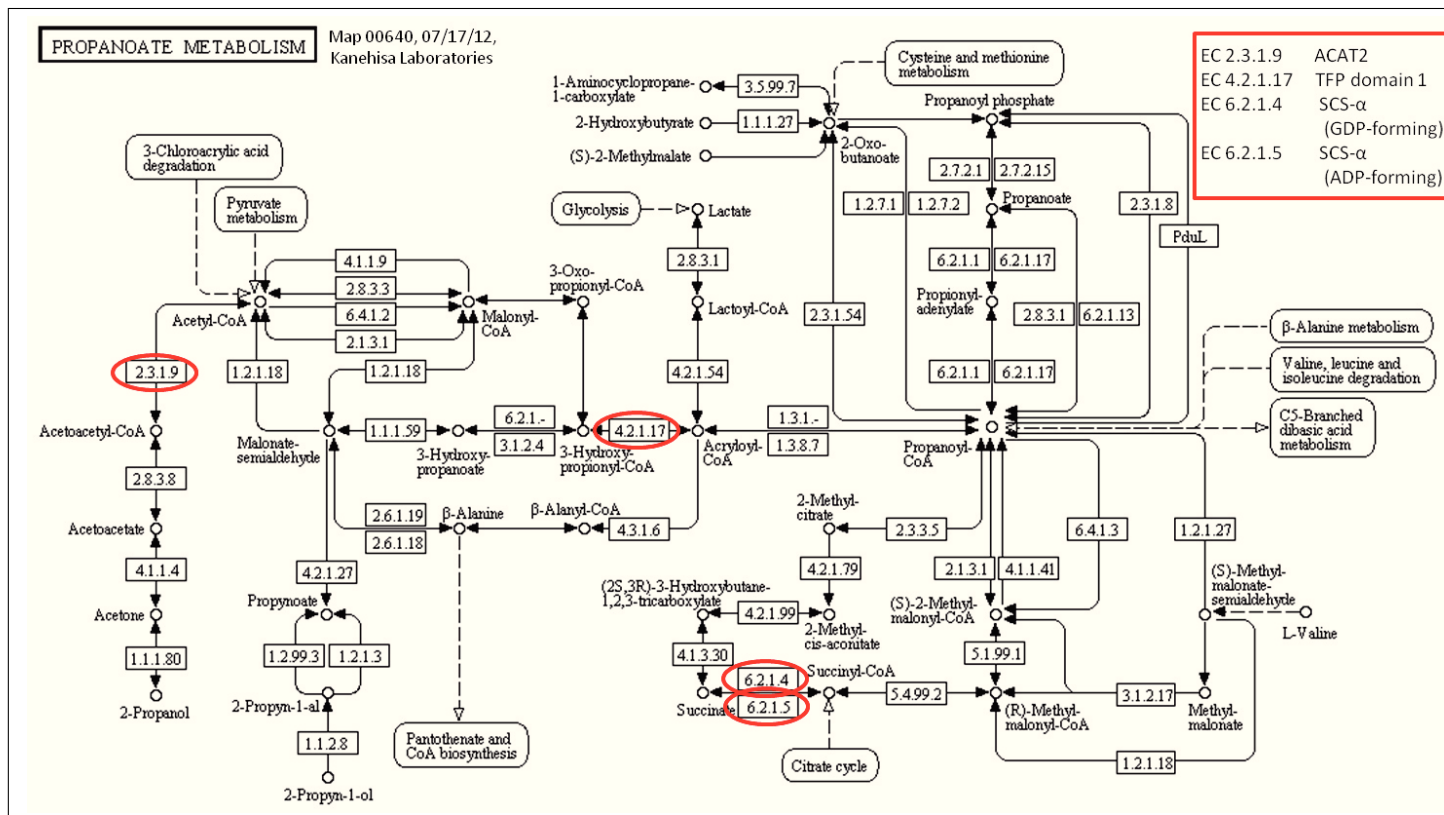


Fig. 4.29: KEGG pathway map 00640: Propanoate metabolism. EC numbers of proteins significantly affected by MPA treatment in LS180 cells are circled in red and specified in the red box.

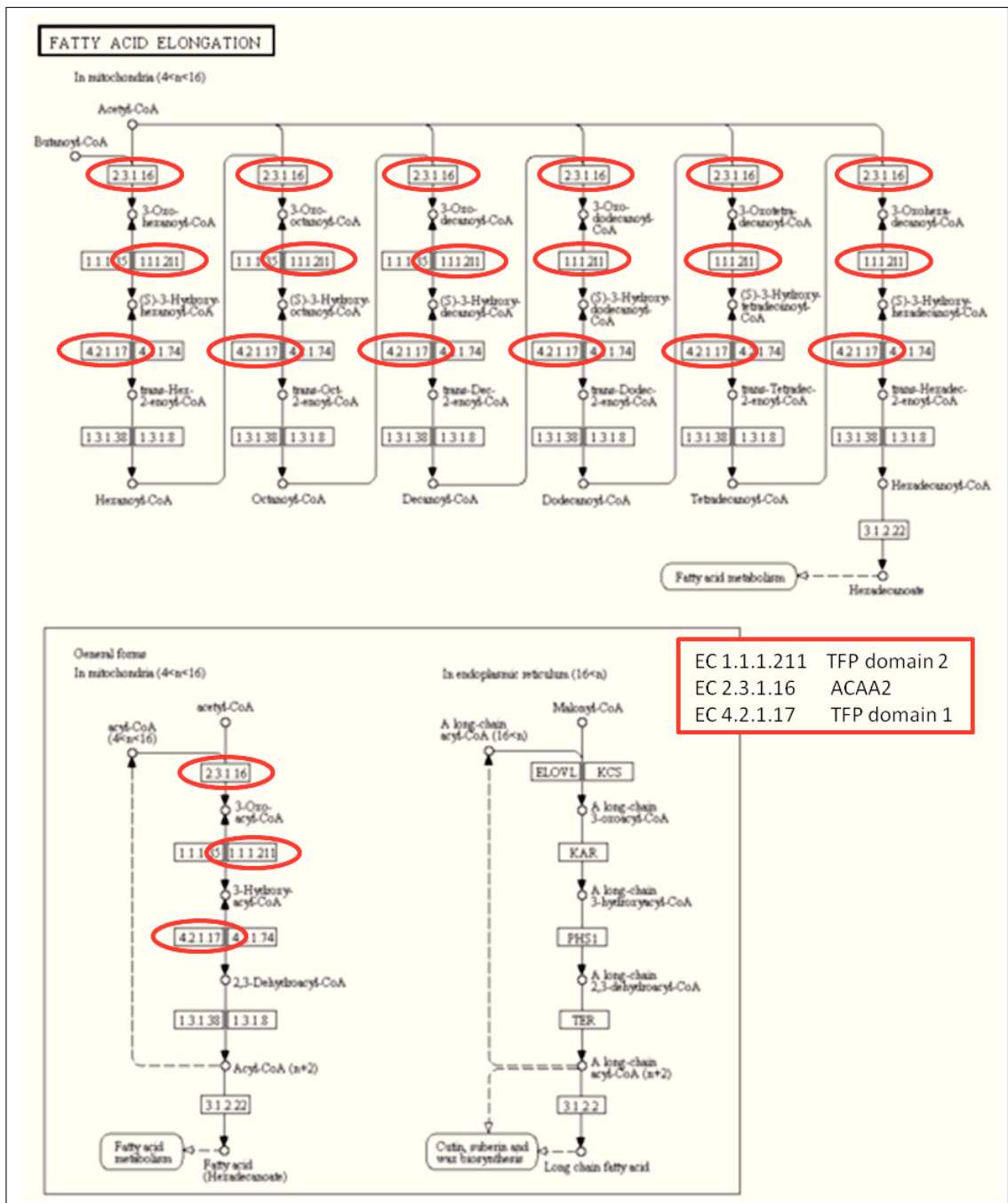


Fig. 4.30: KEGG pathway map 00062: Fatty acid elongation. *EC* numbers of proteins significantly affected by MPA treatment in LS180 cells are circled in red and specified in the red box.

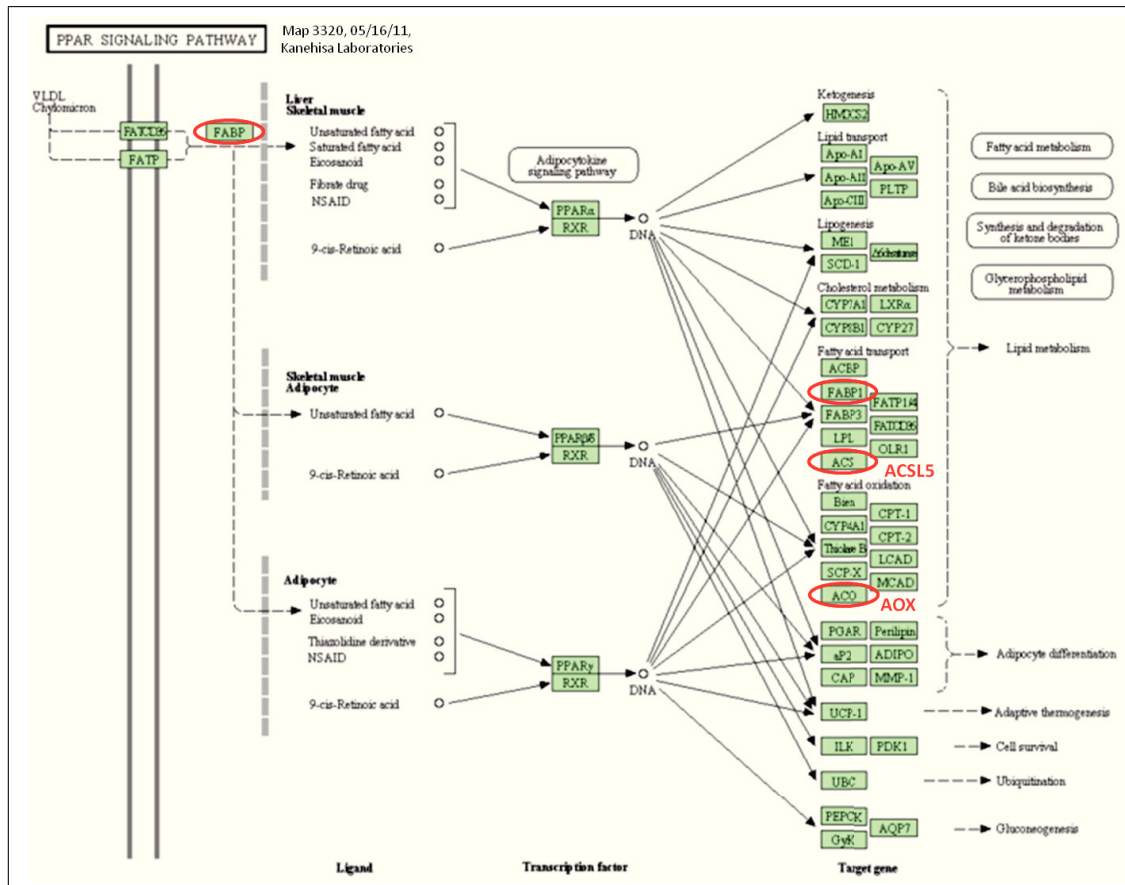


Fig. 4.31: KEGG pathway map 03320: PPAR signaling pathway. Proteins significantly affected by MPA treatment in LS180 cells are circled in red. Protein abbreviations in this figure were assigned by KEGG, proteins abbreviated differently in prior chapters were renamed in red.

Unique peptides identifying ACSL5 and immunogen sequences of the used anti-ACSL5 antibodies

As a representative example the sequence of the NP 976313.1 variant of isoform b (683 aa protein) for ACSL5 is shown below (taken from PubMed, numbers indicate numbers of first amino acids of each block). ACSL5 was identified by 18 unique peptides (Tab. 2.3), which are marked by bold letters in brackets in the amino acid sequence. Immunogen sequences of antibody 1 (Sigma, WH0051703M1, marked in red) and antibody 2 (Abcam, ab104892, marked in blue) are marked.

1 mlfifnffsplptpaliciltfgaaifwlitrpqpvlp~~l~~ldlnnqsvgieggarkgvs
61 qknndltscf~~s~~dak{**tmyevfqr**}glavsdngp~~c~~lgyrkpnqpyr~~w~~lsykqvsdraeylgs
121 **ellh**kyksspdqfvgifaqr~~p~~ewiiselacytysmvavplydtlgpeaivhivnk{**adi**
181 **am**vicdtpqk}{**alv**lignvek}gftpslk{**viil**mdpfd~~d~~dkqr}gek{**sg**ieilslydaenlg
241 **k**ehfr{**kp**vppsped~~l~~svicfts~~g~~ttgdpk}gamithq~~n~~ivsn~~a~~aafk{**c**vehayeptpddv
301 **ais**ylplahmfer}{**iv**qavvyscgar}{**vg**ffqgdir}lladdmk{**tl**kptlfpavpr}llnriyd
361 kvqneaktplkkfllklavssk~~f~~kelqk~~g~~iirhdsfwdklifakiq~~d~~slggrvr{**viv**tga
421 **ap**mstsvmtffr}aamgcqvy~~e~~aygqtectggctftlpgdwtsg~~h~~vgvplacnyvkledva
481 **dm**nyftvnnegevcikgt~~n~~vfkgylkdpek{**tq**eal~~d~~sdgwlhtgdigr}wlpngt~~l~~kiidr
541 kknifk{**la**qgeyiapek}ieniyr{**sq**pvlqifvhgeslr}{**ssl**vgvvvp~~d~~tdvlpsfaak}l
601 gvk{**gs**feelcqnqvvr}eailedlqkigkesglktfeqv~~k~~{**aif**hpepfsienglltptlk}
661 akrgelskyfr{**tq**idslyehiqd}

Unique peptides identifying ANXA1 and immunogen sequence of the used anti-ANXA1 antibody

As a representative example the sequence of the NP 000691.1 variant (646 aa protein) of ANXA1 is shown below (taken from PubMed, numbers indicate numbers of first amino acids of each block). ANXA1 was identified by 14 unique peptides (Tab. 2.3), which are marked by bold letters in brackets in the amino acid sequence (the unique peptide mygislqcqaildetkgdyek comprises the unique peptide mygislqcqaildetk of which both sequences served for identification of ANXA1 and only 13 peptides are marked in the amino acid sequence below). The immunogen sequence against which the used anti-ANXA1 (Cell signaling, #3299) antibody was raised is undisclosed by the manufacturer. Amino acid (aa) 207 (in human; aa 206 in rabbit/host; tyrosine, y) is included in the immunogen and marked in red in the sequence below.

1 m{**amvseflk**}{qawfieneeqeyvqtvk}ssk{ggpgsavspyptfnpssdvaalhk}aimvk{gv
 61 **deatiidiltk**}rnaqrqqikaaylqetgkpldetlkk{**altghleevlallk**}{tpaqfda
 121 **delr**}aamk{**glgtdedtleilasr**}tnkeirdinrvyreelkrdlak{**ditsdtsgdfr**}nal
 181 lslakgdr{**sedfgvnedladsdar**}alyeagerrk{**gtdvvnvftilttr**}sypqlrrvfqky
 241 tkyskhdmnk{**vldlelkgdiek**}cltaivkcatkspaffaeklhqamkgvgrhkalirim
 301 vsrseidmndikafyqk{**mygislqcqaildetkgdyek**}{ilvalcggn}

Unique peptides identifying SLC12A2 and immunogen sequence of the used anti-SLC12A2 antibody

As a representative example the sequence of the AAI 46840.1 variant (1196 aa protein) of SLC12A2 is shown below (taken from PubMed, numbers indicate numbers of first amino acids of each block). SLC12A2 was identified by 30 unique peptides (Tab. 2.5), which are marked by bold letters in brackets in the amino acid sequence (the unique peptides lkegldishlqgqeellssqek and keniafeeiepyr comprise the unique peptides egldishlqgqeellssqek and eniafeeiepyr respectively of which both sequences served for identification of ANXA11. Only 28 peptides are marked in the amino acid sequence below). The immunogen sequence of the used anti-SLC12A2 antibody (Sigma, AV43805) is marked in red.

1 mepr{ptapssgaplagvgetpsaaalaaar}{velpgtavssvpedaapasr}{dgggvrdeg
61 paaagdglgrplgptpsqr}{fqvdlvsenagr}{aaaaaaaaaaaaagagagak}qtpadg
121 easgesepakgseeakgrfrvnfvdpaasssaedsldaagvgdgpnvsvfqnggdtvls
181 egsslhsggggsgghqhyyydthtntyylr{tfghntmdavpr}idhvrhtaaplgekllr
241 psaelhdelekepfedgfangeestptr{davvtytaesk}gvvkfgwikgvlvrclniw
301 gvmlfirlswivgqagigslvimmatvttitglstsaiaatngfvr{gggayylisr}sl
361 gpefggaiglifafanavavamyvvgfaetvvelkehsilmideindiriigaitvvil
421 lgisvagemeweakaqivllvilllaigdfvigtfipleskkpkkgffgyksei{fnenfgpd
481 fr}eeetffsvfaiffpaatgilaganisgdladpqsaipkgllailittlvyvgiavsv
541 gscvvrdatgnydvtivteltnctsaacklnfdsscesspcsyglmnnfqvmsmvsgft
601 plisagifsatlssalaslvsapkifalck{dniypafqmfak}gygkneplrlyiltfl
661 ialgfiliaelnviapiisnfflasyalinfsvhaslakspgwrpafkyynmwisllga
721 ilccivmfvinwwaalltyvivlglyiyvtyk{kpdvvnwgsstqaltylnalqhsir}lsgv
781 edhvk{nfrpqclvmtgapnsr}{pallhlvhdfk}{nvglmicghvhmgpr}rqamkemsidqa
841 kyqrwliknkmk{afyapvhaddlr}{egaqylmqaaaglgr}mkpntlvlgfkk{dlqadmr}dv
901 dmyinlfhdafdiqygvvvir{lkegldishlqgqeellssqek}spgk{dvvsveysk}ks
961 dldtskplsekpithkesk{gpivplnvadqk}{lleastqfkk}kqgkntidvwwlfddgglt
1021 llipyllttkkkwkdekirvfiggkinridhrramatllskfr{idfsdimvlgdintkp
1081 k}{keniafeeiepyr}lheddkeqdiadkmedepwr{itdnelelyk}tktyrqirlnell
1141 k{ehsstaniivmslpvar}{kgavssalymawlealsk}{dlppillvr}{gnhqsvltfys}

Unique peptides identifying PIgR and immunogen sequence of the used anti-PIgR antibody

As a representative example the sequence of the AAI 10495.1 variant (764 aa protein) of PIgR is shown below (taken from PubMed, numbers indicate numbers of first amino acids of each block). PIgR was identified by 13 unique peptides (Tab. 2.5), which are marked by bold letters in brackets in the amino acid sequence. The immunogen sequence against which the used anti-PIgR antibody (Abcam, ab91269) was raised is undisclosed by the manufacturer. The anti-PIgR antibody was raised against a synthetic peptide selected from the C-terminal region (red) of human PIgR (the amino acid sequence is displayed from N- to C-terminus as conventional).

(N-terminus)

1 mllfvltcllavfpaistkspifgpeevnsvegnsvsitcyppptsvnrhtrkywcrqga
 61 r{**ggcitolissegyvssk**}yagranltnfpengtffvvniasqddsgrykcglginsrgls
 121 fdvslevsqpgllndtkvytvdlgrtvtincpfktenaqkrkslykqiglypvlvidss
 181 gyvnpnytgrirldiqgtgqllfsvvinqlrldagqylcqagddsnsnkk{**nadlqvlkp**
 241 **epelvyedlr**}{**gsvtfhcalgpevanvak**}flcr{**qssgencdvvvntlglk**}rapafegrilln
 301 pqdk{**dgsfsvvitglr**}kedagr{**ylcgahsdgqlqegspiqawqlfvneestipr**}sptvvk
 361 gvaggsavavlcypnrkesksik{**ywclwegaqngr**}{**cpllvdsegwvk**}aqyegrsllepeg
 421 ngftvilnqltsrdagfywcltngdtlwrvtveikiiegepnlkvpgnvtavlgetlkv
 481 pchfpckfssykywckwnntgcqalpsqdegpskafvncdensr{**lvsltlnlvtr**}{**adeg**
 541 **wywcgvk**}{**qghfygetaavyvaveer**}kaagsrdvslakadaapdekvlidsgfreienkaiq
 601 dprlfaeekavadtrdqadgsrasvdsgsseeqggssr{**alvstlvplglvavgavavgv**
 661 **ar**}arhrknvdrvsirsyrtdismsdfensrefgandnmgassitqetslggk{**eefvatte**
 721 **sttetk**}epkkakrsskeeaemaykdflqsstvaeaqdgpqea (**C-terminus**)

Unique peptides identifying REG-4 and immunogen sequence of the used anti-REG-4 antibody

As a representative example the sequence of the AAH 17089 variant (158 aa protein) of REG-4 is shown below (taken from PubMed, numbers indicate numbers of first amino acids of each block). REG-4 was identified by 8 unique peptides (Tab. 2.5), which are marked by bold letters in brackets in the amino acid sequence (the unique peptide **sqpiwighdpqkr** comprises the unique peptide **sqpiwighdpqk** of which both sequences served for identification of the protein and only 7 peptides are marked in the amino acid sequence below). As immunogen to raise the used anti-REG-4 antibody (Abcam, ab89917) served recombinant human full length REG-4 protein.

1 masrsmrllllsclaktgvlgdii**r{pscapgwfyhk}{sncygyfr}klr{nwsdaelecqs**
61 **ygngahlasilsk}{eastiaeyisgyqr}{sqpiwighdpqkr}{qqwqwidgamylyr}**swsg
121 ksmggnk**{hcaemssnnnftwssnecnk}**rqhflckyrp

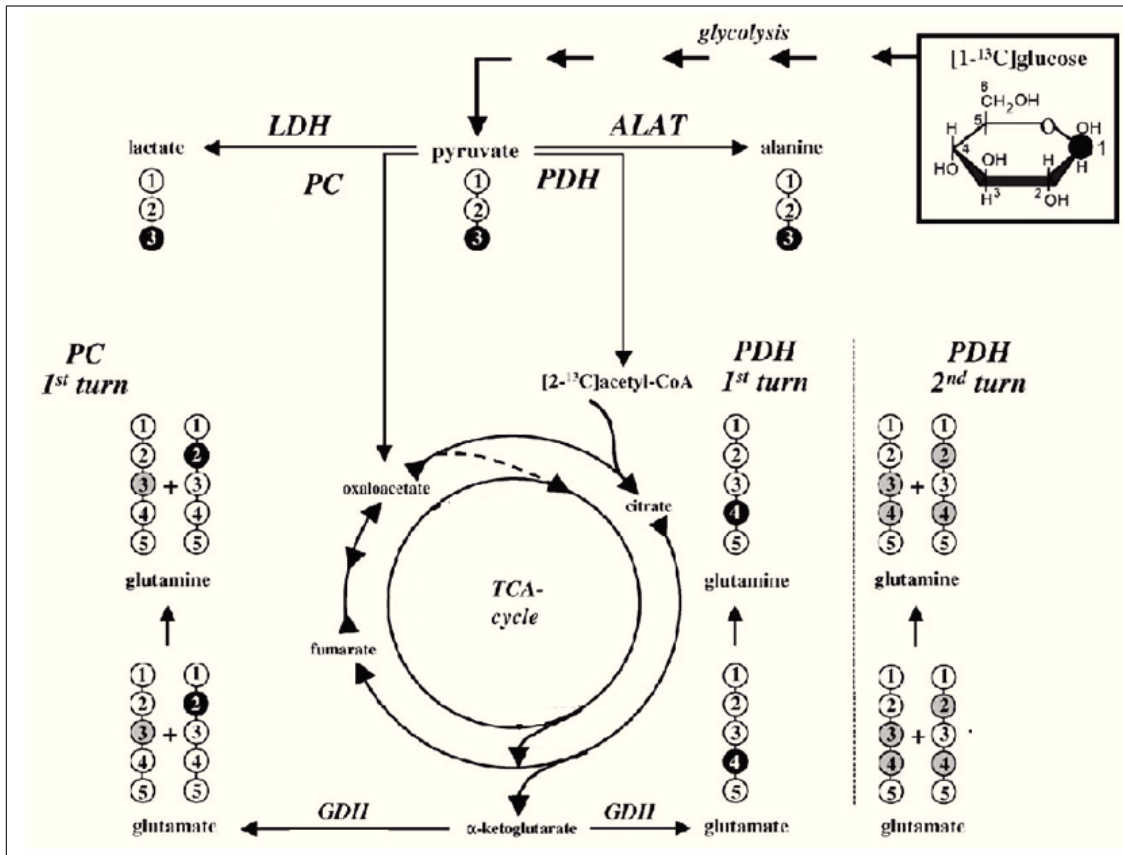


Fig. 4.32: Metabolic fate of the ^{13}C label of $[1-^{13}\text{C}]$ glucose. Label distribution in glycolytic and TCA cycle intermediates during metabolism of $[1-^{13}\text{C}]$ glucose. For label distribution via PC into glutamine and glutamate only one TCA cycle turn is considered, for metabolism via PDH label distribution after one and two TCA cycle turns are presented. The fate of the ^{13}C label from $[1-^{13}\text{C}]$ glucose is indicated by circles; black circles: ^{13}C -label position in glycolytic products (lactate and alanine synthesized via LDH and ALAT, respectively) and in TCA cycle-related metabolites synthesized via PC and PDH during the first TCA cycle turn (for other isotopomers, please see Table 2.17); gray circles: ^{13}C -label position due to equilibration of PC-derived oxaloacetate with fumarate and ^{13}C -label positions within the second TCA cycle turn via PDH. ALAT: alanine aminotransferase, GDH: glutamate dehydrogenase, LDH: lactate dehydrogenase, PC: pyruvate carboxylase, PDH: pyruvate dehydrogenase. Graph and caption taken from [102], modified.

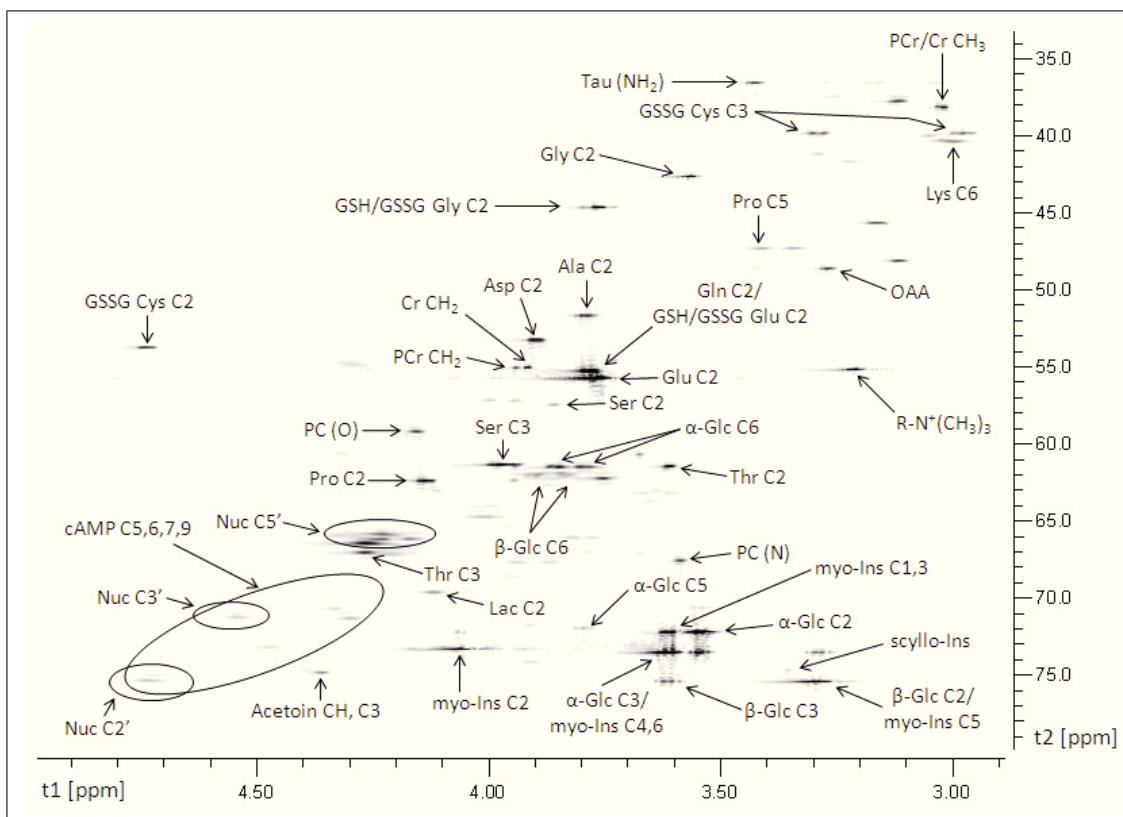


Fig. 4.33: ^1H - ^{13}C HSQC spectrum of ppm regions 2.9-5.0 (t_1) and 33-80 (t_2) of an LS180 cell extract. Compounds were identified using published databases [349, 350] and were compared to ^1H and ^{13}C NMR spectra of cell extracts of same experimental conditions (controls). Amino acid abbreviations are based on IUPAC nomenclature. cAMP: cyclic adenosine monophosphate, Cr: creatine, Glc: glucose, GSH: reduced glutathione, GSSG: oxidized glutathione, Ins: inositol, Nuc: nucleotides, OAA: oxaloacetate, PC: phosphocoline, PCr: phosphocreatine, $\text{R-N}^+(\text{CH}_3)_3$: trimethyl ammonium compounds, Tau: taurine. ppm regions 0.0-3.0 (t_1)/10-40 (t_2) and 4.0-6.5 (t_1)/80-110 (t_2) of the same ^1H - ^{13}C HSQC spectrum are shown in Figure 2.58 and Figure 4.34.

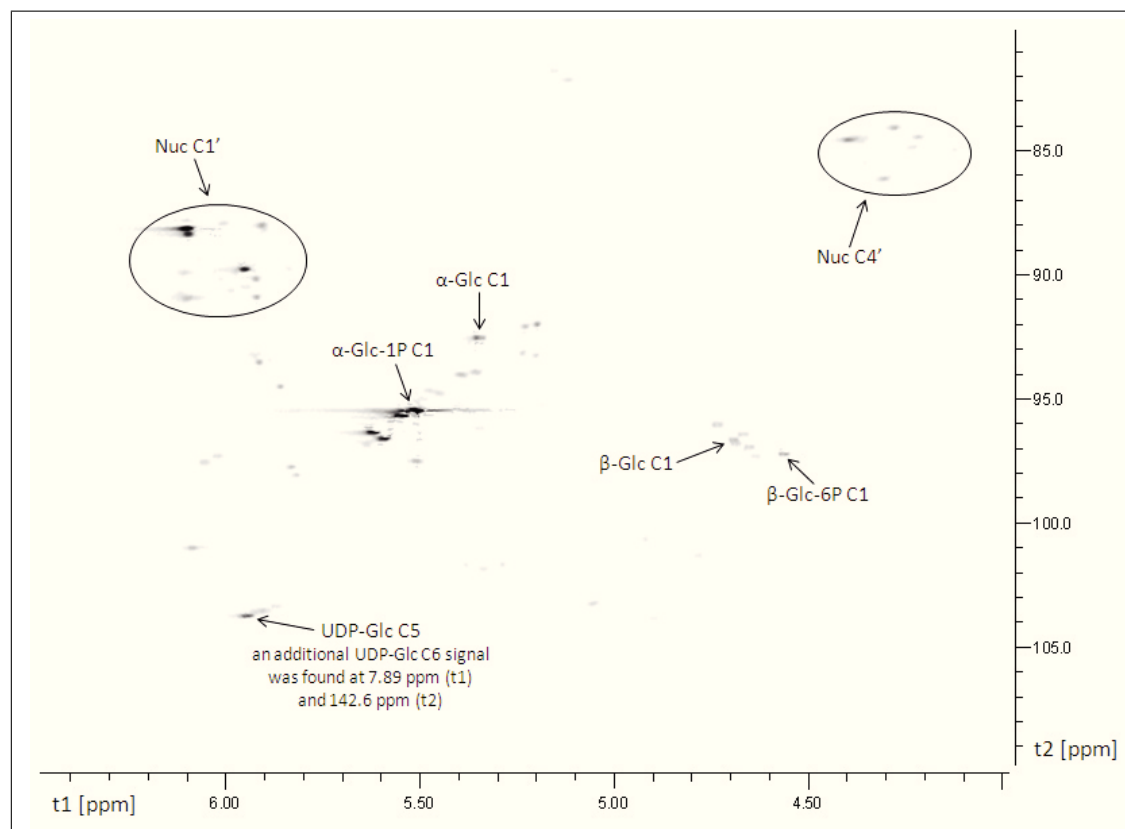


Fig. 4.34: ^1H - ^{13}C HSQC spectrum of ppm regions 4.0-6.5 (t_1) and 80-110 (t_2) of an LS180 cell extracts. Compounds were identified using published databases [349, 350] and were compared to ^1H and ^{13}C NMR spectra of cell extracts of same experimental conditions (controls). Glc: glucose, Nuc: nucleotides, UDP: uridine diphosphate. ppm regions 0.0-3.0 (t_1)/10-40 (t_2) and 2.9-5.0 (t_1)/33-80 (t_2) of the same ^1H - ^{13}C HSQC spectrum are shown in Figure 2.58 and Figure 4.33.

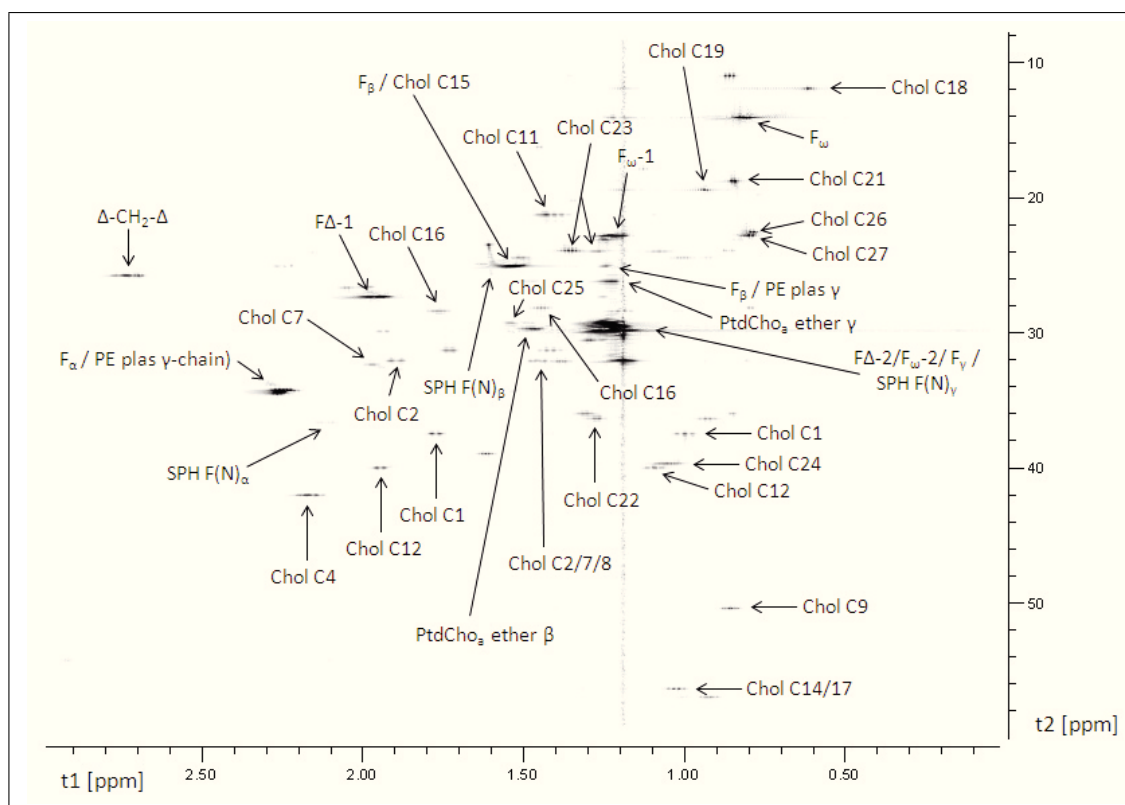


Fig. 4.35: ^1H - ^{13}C HSQC spectrum of ppm regions 0.0-3.0 (t_1)/10-60 (t_2) of a lipophilic LS180 cell extract. Compounds were identified using published databases [349, 350] and were compared to ^1H and ^{13}C NMR spectra of lipid extracts of same experimental conditions (controls). Chol: cholesterol/cholesterolester, F: fatty acid, F_α/β : carbon atom in α/β -position to carboxyl carbon atom, F_Δ : carbon atom at a double bond, F_ω : terminal carbon atom, PE: phosphatidylethanolamine, PtdCho: phosphatidylcholine, SPH: sphingomyeline. ppm regions 3.0-5.5 (t_1)/40-75 (t_2) and 5.0-5.5 (t_1)/120-135 (t_2) of the same ^1H - ^{13}C HSQC spectrum are shown in Figure 4.36.

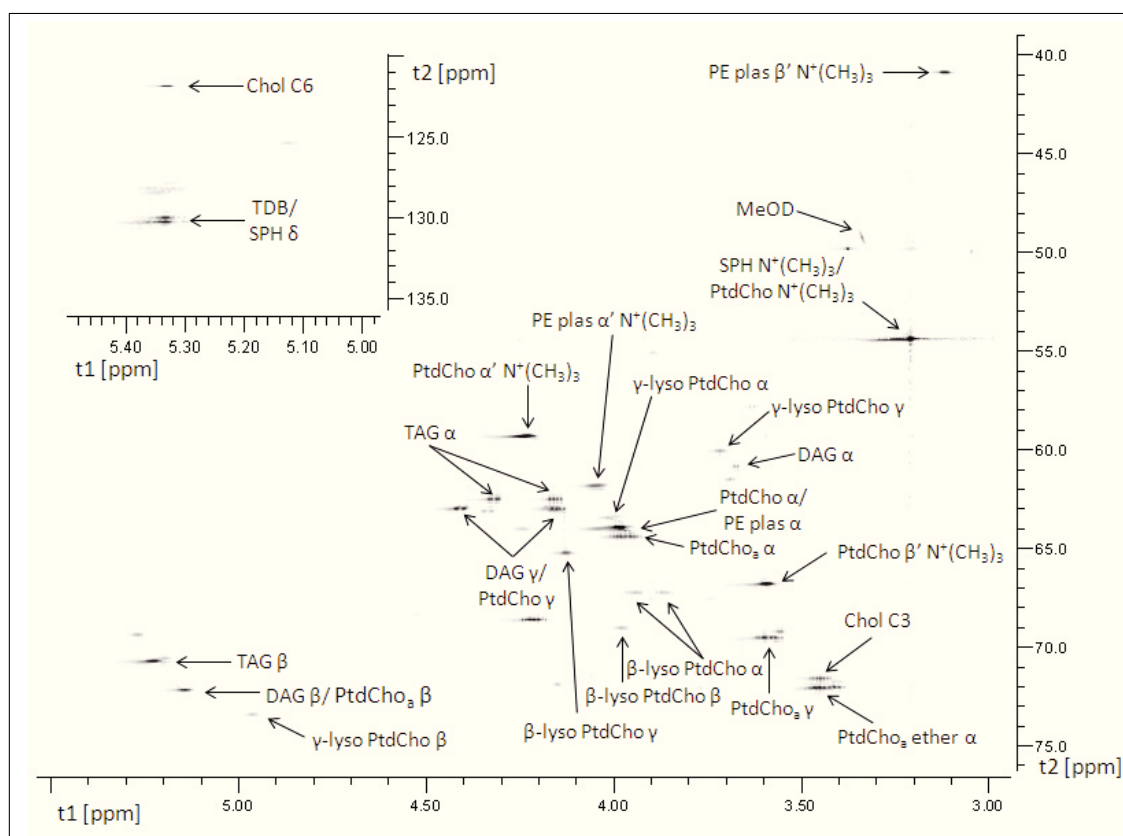


Fig. 4.36: ^1H - ^{13}C HSQC spectrum of ppm regions 3.0-5.5 (t1)/40-75 (t2) and 5.0-5.5 (t1)/120-135 (t2) of a lipophilic LS180 cell extract. Compounds were identified using published databases [349, 350] and were compared to ^1H and ^{13}C NMR spectra of lipid extracts of same experimental conditions (controls). Chol: cholesterol/cholesterolester, DAG: diacylglycerols, $R\text{-N}^+(\text{CH}_3)_3$: trimethyl ammonium compounds, PE: phosphatidylethanolamine, plas: plasmalogen, PtdCho: phosphatidylcholine, SPH: sphingomyeline, TAG: triacyl glycerols, TDB: total number of double bonds. ppm regions 0.0-3.0 (t1)/10-60 (t2) of the same ^1H - ^{13}C HSQC spectrum are shown in Figure 4.36.

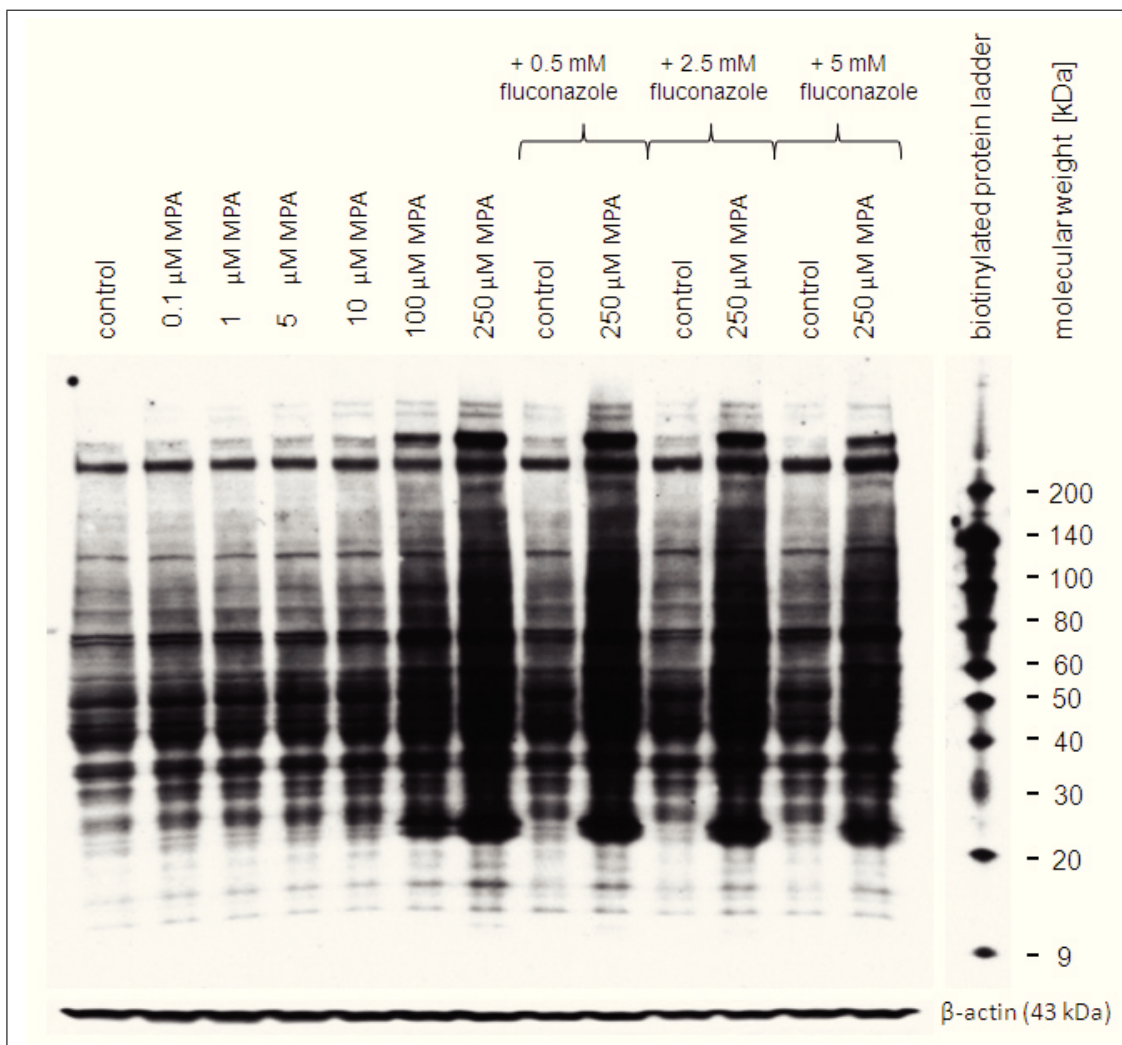


Fig. 4.37: Western blot of LS180 cell lysates after 72h of MPA and/or fluconazole treatment in FBS-free media and incubation with an anti-MPA/AcMPAG antibody. A film developed after a shorter exposure time is shown in Figure 2.46 to facilitate visualization of proteins at the medium molecular weight range. A western blot of the same experiment run with FBS is shown in Figure 2.45.

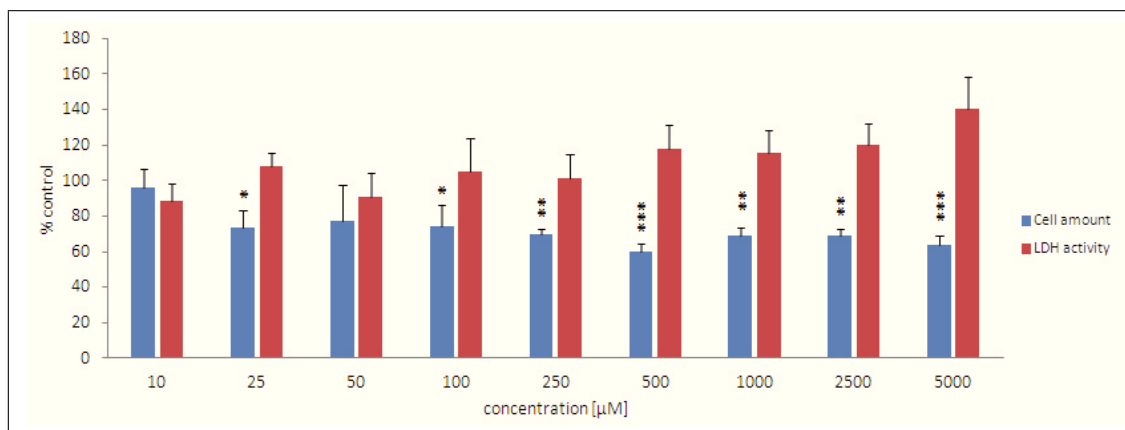


Fig. 4.38: Effects of fluconazole treatment on LS180 cell number and LDH activity in LS180 cell culture media after 72h (redosed every 24h). Values are given as means of % of controls with standard deviations ($N=6$). Significance was determined using one-way ANOVA combined with Scheffe's post – hoc test with *: $p<0.05$; **: $p<0.01$; ***: $p<0.001$ versus controls. Values were calculated from fluorescence intensities using the CyQUANT® NF Cell Proliferation Assay for assessment of cell number and calculated from LDH activities and normalized to fluorescence intensities using the CyQUANT® NF Cell Proliferation Assay for assessment of extracellular LDH. LDH activities represent only the incubation time of 48h to 72h (24h total) due to media renewal every 24h.